The genesis and evolution of Makarov Basin, Arctic Ocean

by

John Evangelatos

Submitted in partial fulfilment of the requirements
for the degree of Doctor of Philosophy

at

Dalhousie University
Halifax, Nova Scotia
April 2018

DEDICATION

A conspicuous element of Western civilization is the selfless pursuit of knowledge. As beneficiaries of its achievements, we owe a debt of gratitude to the birthplace of this great civilization – Ancient Greece.

I, thus, dedicate this thesis to my forefathers who, through their hardships and sacrifice, I am free to carry on their legacy.

ΑΦΙΕΡΩΣΗ

Ένα ευδιάκριτο στοιχείο του δυτικού πολιτισμού είναι η ανιδιοτελής επιδίωξη της γνώσης. Ως δικαιούχοι των επιτευγμάτων της, οφείλουμε ένα χρέος ευγνωμοσύνης στη γενέτειρα του μεγάλου αυτού πολιτισμού: η Αρχαία Ελλάδα.

Κατά συνέπεια, αφιερώνω αυτή την διατριβή στους προγόνους μου που, εξαιτίας τις κακουχίες και θυσίες τους, είμαι ελεύθερος να συνεχίσω το κληροδότημα τους.

LIST OF TABLES

LIST OF FIGURES

viii

ABSTRACT

Plate tectonic theory commenced with the observation that continental margins fit together like pieces of a puzzle. No such fit is readily apparent to the margins of Amerasia Basin of the Arctic Ocean, resulting in a stubborn outlier to global plate-reconstructions. This problem persists partly because of a paucity of data in the perennial ice-covered seas. Makarov Basin is well-positioned to address this problem, situated at the northern margin of Amerasia Basin, adjacent to Lomonosov Ridge. This study tests the hypothesis that this segment is a transform margin that resulted from rotational opening of Amerasia Basin. For this purpose, this study analyses the seismic stratigraphy, geomorphology, potential field and seismic velocity data of Makarov Basin and surrounding areas. The data are mainly from a unique seismic line that transects Makarov Basin and onto Lomonosov Ridge.

The sedimentary cover averages 1.9 km-thick in Makarov Basin, with a maximum thickness of ~5 km in a northern deep subbasin. The deeper successions within the subbasin host interbedded volcanic and/or volcaniclastic material. A shift in sedimentary supply, from proximal to distal, is recorded after the onset of Cenozoic rifting that separated Lomonosov Ridge from the Barents–Kara Shelf and formed Eurasia Basin. Thereafter, sedimentation is largely pelagic to hemipelagic.

The crust of Makarov Basin is typically 9 to 11 km thick, except beneath the subbasin where it is 5 km thick. The crust abruptly thickens to >20 km from Makarov Basin to central Lomonosov Ridge. Results from gravity modelling reveal that the tectonic style of the Amerasian margin of Lomonosov Ridge varies from passive rifting to strike-slip along its length. The rhomboid shape of Makarov Basin, the straight and steep morphology of the Amerasian flank of Lomonosov Ridge, the presence of numerous sub-parallel ridges created by splay faulting and the abrupt crustal transition between the two provinces is evidence of transverse/transtensional tectonics along the central segment of the ridge. This result supports a rotational model of opening for Amerasia Basin, at least for its initial stages, and is a critical element to understanding the larger tectonic framework of the Arctic Ocean.

LIST OF ABBREVIATIONS USED

ACEX   Arctic Coring Expedition
AMLIP MD   Alpha-Mendeleev Large Igneous Province Magnetic Domain
ARTA   Alpha Ridge Test of Appurtenance
AWI   Alfred Wagner Institute
CTD   Conductivity, Temperature, Depth
CESAR   Canadian Expedition to Study the Alpha Ridge
ECS   Extended Continental Shelf
FAA   Free-air anomaly
HALIP   High Arctic Large Igneous Province
HAMH   High Arctic Magnetic High domain
HLY   Healy
IBCAO   International Bathymetric Chart of the Arctic Ocean
IODP   Integrated Ocean Drilling Program
LC   Lower Crust
LIP   Large Igneous Province
LOREX   Lomonosov Ridge Experiment
LORITA   Lomonosov Ridge Test of Appurtenance
NP-28   North Pole-28
TRA   TransArctic
TWTT   Two-way traveltime
UC   Upper Crust

ACKNOWLEDGEMENTS

Also, I would like to mention the many colleagues that have aided me in a variety of ways. Amongst them are Drs. Francky St-Ange and Calvin Campbell, Aaron Farkas, Jena Higgins and Irena Schulten.

Finally, I am deeply grateful to Laura Avila, my wife, who agreed to move to Dartmouth, Nova Scotia, at my behest and who endured many hardships alongside me while I laboured on my thesis.

CHAPTER 1: INTRODUCTION

Global plate tectonic reconstructions require geometric elements of Earth to balance, since Earth is neither expanding nor shrinking. For example, to accommodate extension in one region, requires compression in another. It is necessary to know the tectonic history of each region of the earth, therefore, in order to ensure this balance. The Arctic Basin is one of the last regions on Earth where the tectonic history is uncertain.

The Arctic Ocean is the smallest of the world's five major oceans. It comprises two major basins – the Amerasia and Eurasia basins (Fig. 1.1). These two basins are separated by the Lomonosov Ridge, a narrow submarine high that extends from the Canadian Polar margin off of Ellesmere Island and Northwest Greenland to the East Siberian Shelf. The evolution of Eurasia Basin is well understood due to the presence of an active mid-ocean ridge and conjugate seafloor spreading magnetic anomalies (Vogt et al., 1979; Srivastava, 1985; Brozena et al., 2003). The evolution of Amerasia Basin, on the other hand, is not as well understood.

Geoscientific data in the Arctic Ocean was sparse until about 2006, owing largely to operational challenges. Its remoteness and perennial sea ice cover made surveying difficult and expensive. There has been a significant increase in the number of marine geoscientific surveys in the central Arctic Ocean to address the need for bathymetric and geological data by Arctic coastal States for Extended Continental Shelf (ECS) purposes (Coakley et al., 2016). These surveys were facilitated by the decline in sea ice cover and thickness (Comiso et al., 2008). Extensive mapping of Canada Basin and surrounding areas has been a result (Fig. 1.2). This mapping has led to development of robust tectonic

models for southern Amerasia Basin (e.g., Chian et al., 2016). Knowledge of the formation of northern Amerasia Basin, however, has lagged (Alvey et al., 2008). Data are extremely limited in these northernmost areas. Additionally, the area is underpinned by a large igneous province (LIP) – the Alpha-Mendeleev ridge complex. This LIP dominates the seafloor geology and potential field anomalies, making it difficult to image potential tectonic elements.

Makarov Basin is a small sedimentary basin that lies between the Alpha-Mendeleev ridge complex and Lomonosov Ridge (the northern limit of Amerasia Basin). This basin provides a window into the underlying structure of the basin and thereby is critical to unraveling the tectonic history of the Amerasia Basin. It is hypothesized that Makarov Basin formed by transtensional tectonics as Amerasia Basin formed. The basin should record, therefore, elements of transform and extensional tectonics.
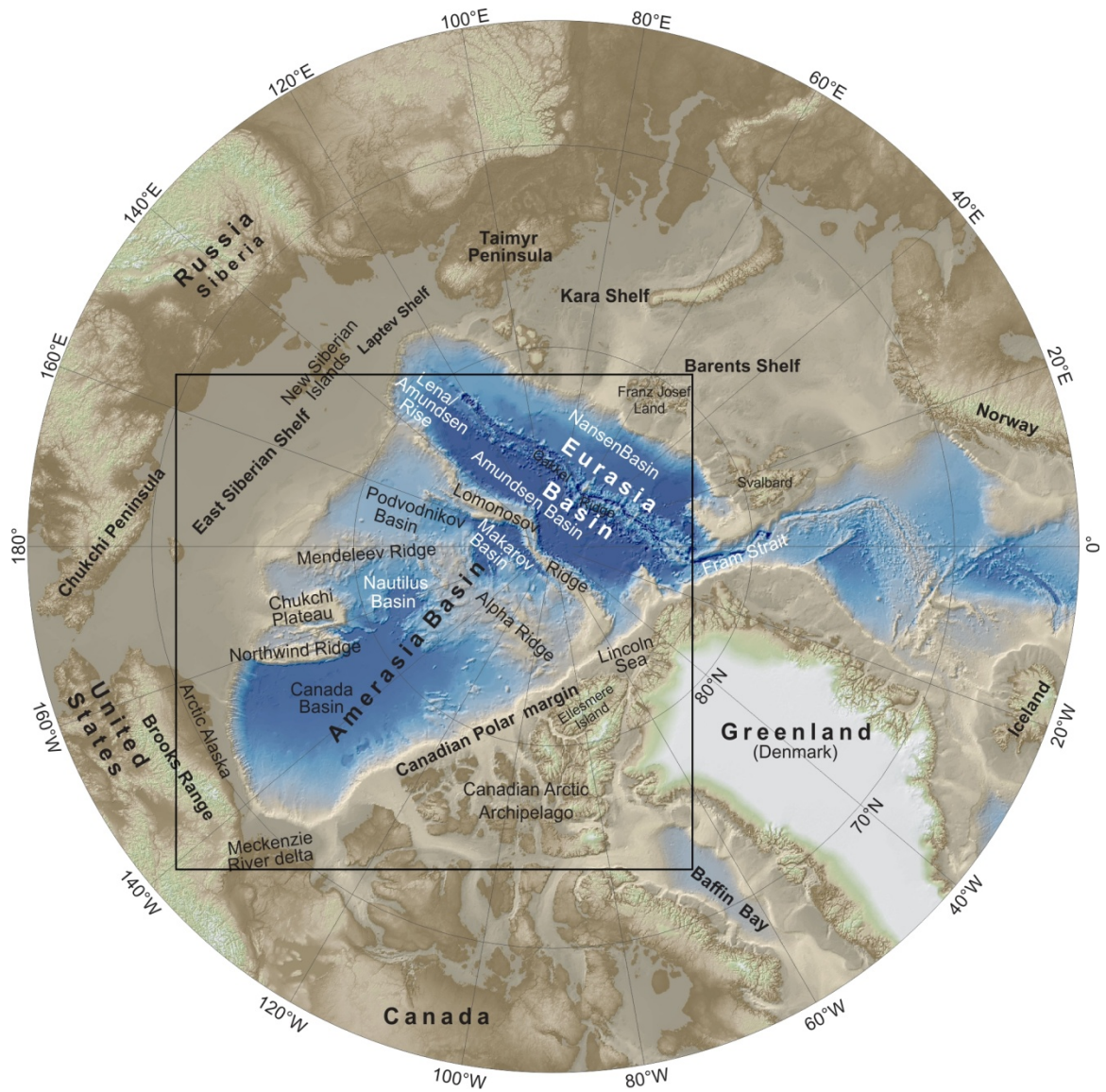
Fig. 1.1. Topographic/bathymetric map of the Arctic region. The rectangle outlines the geographic extent of Figs. 1.2 to 1.5. Map projection is North Pole Stereographic (latitude of origin of 90° N, central meridian of 90° W). Bathymetry and topography are from the International Bathymetric Chart of the Arctic Ocean (IBCAO) version 3.0 grid (Jakobsson et al., 2012).
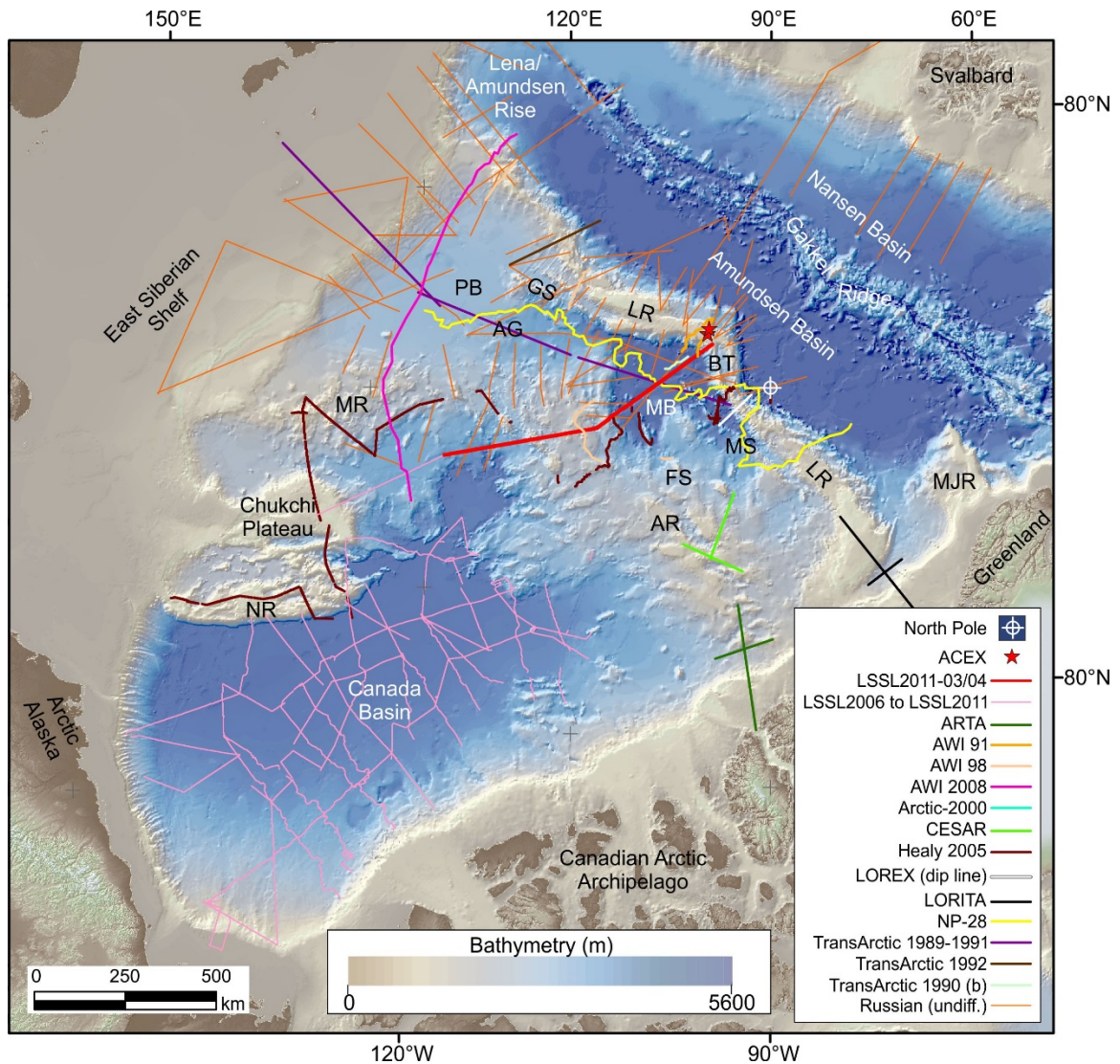
Fig. 1.2. Coloured bathymetric map of the Arctic Ocean. Map projection is North Pole Stereographic (latitude of origin of 75° N, central meridian of 90° W). Acronyms are: AG – Arlis Gap, Belov Trough, FS – Fedotov Seamount, GS – Geophysicists Spur, LR – Lomonosov Ridge, MB – Makarov Basin, MR – Mendeleev Ridge, Morris Jesup Spur – MJS, MS – Marvin Spur, NR – Northwind Ridge and PB – Podvodnikov Basin. Seismic transects shown in this figure are: LSSL2011-03/04 (Evangelatos and Mosher, 2016; Evangelatos et al., 2017), LSSL2006 to LSSL2011 (Mosher et al., 2016), ARTA (Funck et al., 2011), AWI 91 (Jokat et al., 1992, 1995), AWI 98 (Jokat 2003; 2005), AWI 2008 (Weigelt et al., 2014; Jokat and Ickrath, 2015), Arctic-2000 (Lebedeva-Ivanova et al., 2006), CESAR (Jackson et al., 1985), Healy 2005 (Bruvoll et al., 2010; 2012; Dove et al., 2010), LOREX (Forsyth and Mair, 1984), LORITA (Jackson et al., 2010), TransArctic 1989–1991 (Lebedeva-Ivanova et al., 2011), TransArctic 1992 (Poselov et al., 2011), NP-28, TransArctic 1990 (b) (Langinen et al., 2009) and other undifferentiated Russian lines (Kaminsky, 2017). ACEX refers to drill sites of IODP Expedition 3002 (Backman et al., 2006). Bathymetry and topography are rendered from the IBCAO version 3.0 grid (Jakobsson et al., 2012).

1.1. Statement of the Problem

Uncertainties regarding the evolution of the Arctic Ocean, particularly Amerasia Basin, prohibit an accurate and complete plate-tectonic reconstruction model for the entire globe. These uncertainties enable multiple palaeo-reconstruction models for the formation of Amerasia Basin, which often conflict (cf. Miller and Verzhbitsky, 2009; Grantz et al., 2011; Doré et al., 2016). For example, models must account for the tectonic style of the Amerasian margin of Lomonosov Ridge; however, whether this margin formed by passive rifting or by a strike-slip system is under debate (e.g., Cochran et al., 2006). In addition, it is important to constrain the relative timing of the Alpha-Mendeleev large igneous province as this problem bears on the cause of opening of Amerasia Basin (e.g., Døssing et al., 2013). A greater understanding of the tectonic history and geology of Makarov Basin, situated between Alpha and Lomonosov ridges, is the objective of this thesis as it is of prime importance for resolving these two problems. The basin sits at the northern extent of the margin of Amerasia Basin and offers the opportunity to image through its depths to interpret the nature of its crust and sedimentary successions. Marine seismic reflection and wide angle/refraction seismic data, recently acquired by the Geological Survey of Canada, are the main sources of information used to support the objectives of the thesis. In addition, potential fields (i.e., gravity and magnetic) data were analyzed to supplement seismic interpretations and extrapolate findings regionally.

1.2. Thesis Objectives

The overarching objective of this thesis is to advance knowledge on the geological framework of Makarov Basin and adjacent areas. This objective is addressed by focusing specifically on:

- determination of the style of deformation that occurred between Makarov Basin and adjacent Lomonosov Ridge by analyzing morphology and geological structure.

- establishment of the seismic stratigraphy of Makarov Basin and identifying major geological events that impacted the basin.

- determination of the connection between the Alpha-Mendeleev LIP and Makarov Basin using wide-angle seismic and potential fields data.

- extension of the study beyond the main seismic line by investigating nearby geological provinces using potential field data.

Success in these efforts will improve understanding of the geological history of northern Amerasia Basin and, thus, constrain tectonic models for the formation of the entire basin and, indeed, the globe.

1.3. Background

The Arctic Ocean is almost entirely landlocked, like the Mediterranean Sea (Coachman and Aagaard, 1974) or the Gulf of Mexico (Lundin and Doré, 2017). The only deep-water exchange occurs with the North Atlantic Ocean via Fram Strait, situated between Northeast Greenland and Svalbard (Fig. 1.1). Continental shelves and submarine ridges of the Arctic Ocean encompass a much greater area than its abyssal plains (Jakobsson et al., 2003). There are two principal basins in the Arctic Ocean: the Cenozoic Eurasia Basin and the Late Jurassic (?) to Cretaceous Amerasia Basin (Fig. 1.3). Below, prominent morphological features within the Arctic Ocean and their respective geological histories are summarized (Figs. 1.1 and 1.2).
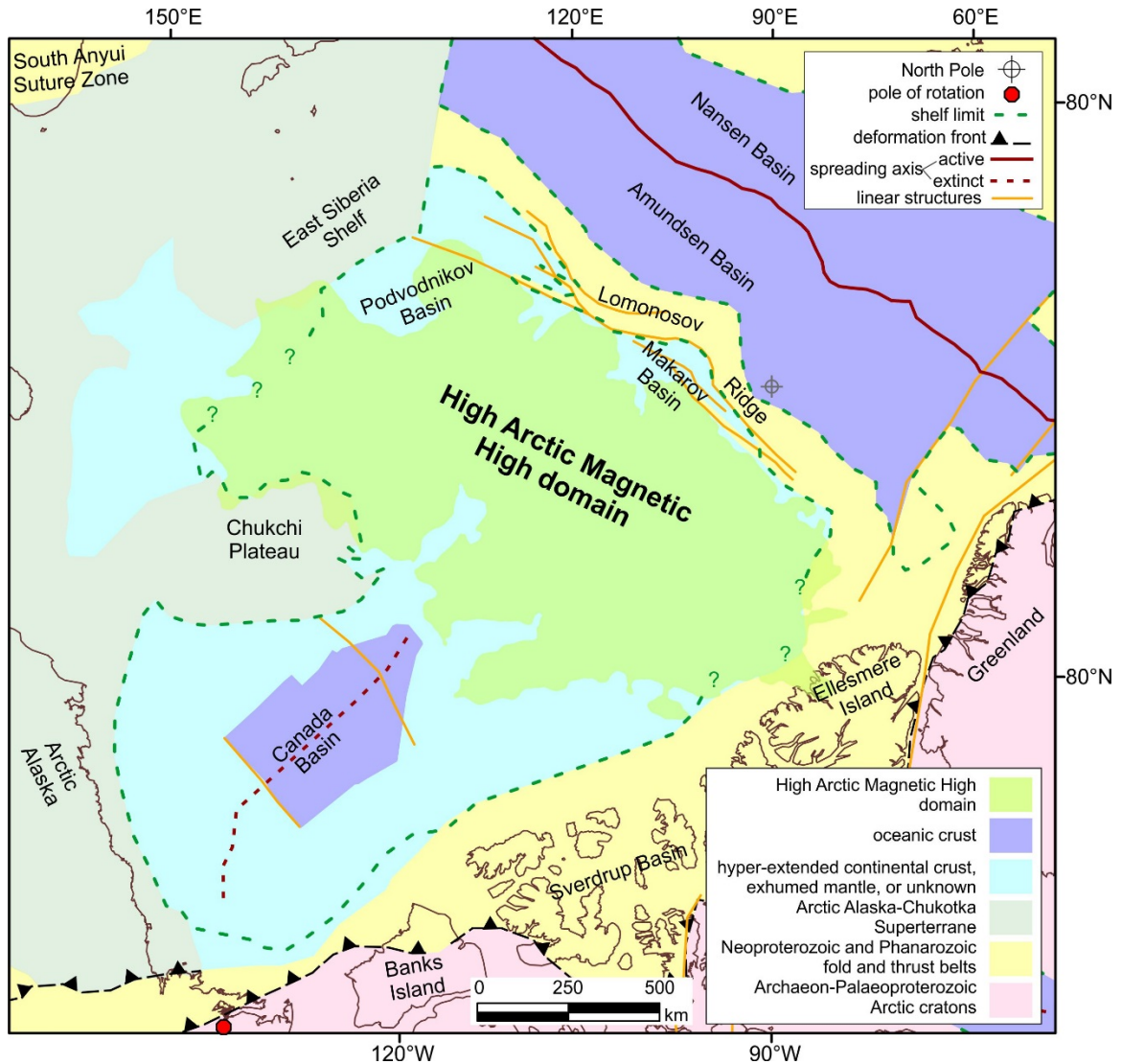
Fig. 1.3. Simplified tectonic map of the Arctic Ocean (after Pease et al., 2014). Additional elements shown in the figure are: pole of rotation for opening of Amerasia Basin (Grantz et al., 1979), linear structures on the Amerasian flank of Lomonosov Ridge (Evangelatos and Mosher, 2016), High Arctic Magnetic High domain (Oakey and Saltus, 2016) and oceanic crust in Canada Basin (Chian et al., 2016).

1.3.1. Lomonosov Ridge

Lomonosov Ridge is 1800 km long, stretching between the East Siberian Shelf and the Greenland/Canadian Archipelago shelf. It varies between 50 and 100 km in width between the 2000 m isobaths on its two flanks. Near the North American shelf, however, the ridge broadens into a plateau (220 km wide at the 1000 m depth contour) and shallows to <320 m. At this location, the trend of Lomonosov Ridge bends sharply such

that its axis is sub-parallel to the continental shelf margin. It has a generally flat-lying crest, at this location, that lies between 500 to 1600 m water depth. Bends (i.e., deviations) along the strike length of Lomonosov Ridge are evident near the North Pole. These bends are viewed as offsetting the top of Lomonosov Ridge from a straight-line projection by more than 100 km. At this location, Lomonosov Ridge hosts an intra-ridge basin known as Belov Trough. Towards Siberia, the ridge shoals to as little as 700 m and deepens to 1700 m in a trough (part of the Lena-Amundsen Rise) before joining the East Siberian Shelf (Fig. 1.1). With respect to the gravity field, free-air gravity anomalies observed at Lomonosov Ridge are moderate to high (20–90 mGal; Fig. 1.4), and resemble anomalies observed at shelf margins. The magnetic signal at Lomonosov Ridge is subdued relative to adjacent areas (Fig. 1.5), except for a ~1000 nT anomaly on the Amerasian flank of the ridge near the Canadian Polar margin.

The continental origin of Lomonosov Ridge is confirmed by various investigations (Karasik et al., 1971; Sweeney et al., 1982; Backman et al., 2008; Jackson et al., 2010). Lomonosov Ridge was once part of the palaeo-Barents–Kara Shelf, but rifted and drifted away from the shelf due to opening of Eurasia Basin in the early Palaeogene (Heezen and Ewing, 1961; Wilson, 1963; Weber and Sweeney, 1985; Jokat et al. 1992; Brozena et al., 2003).

1.3.2. Eurasia Basin

The deep sea part of Eurasia Basin is crudely trapezoidal in shape and bounded by the Lomonosov Ridge, Siberian Shelf (Laptev Sea area), Barents-Kara Shelf and Greenland Shelf. In addition, the basin is connected to the North Atlantic Ocean via Fram

Strait and Nansen Sound. The Gakkel Ridge, formerly Nansen Ridge (e.g., Kristoffersen, 1982; Kristoffersen et al., 1982), is an active oceanic spreading ridge that bisects Eurasia Basin. The trend of Gakkel Ridge changes along its axis, mirroring the shape of the Barents-Kara Shelf and Lomonosov Ridge, which are conjugate margins. This observation implies that the ridge inherited its shape upon opening of Eurasia Basin (Vogt et al., 1979). Volcanism along the ridge is localized and possibly related to mantle heterogeneity (Cochran et al., 2003). The modern spreading rates along Gakkel Ridge are the slowest in the global mid-ocean ridge system (DeMets et al., 1994). Analysis of the magnetic spreading anomalies indicates that Eurasia Basin expanded at ultra-slow spreading rates throughout its history (Fig. 1.5; Coakley and Cochran, 1998; Jokat and Schmidt-Aursch, 2007). Amundsen Basin lies between Lomonosov Ridge and Gakkel Ridge. The abyssal plain of this basin is fairly deep and flat with depths exceeding 4300 m (Jakobsson et al., 2012). Between Gakkel Ridge and the Barents-Kara Shelf is Nansen Basin. The seafloor in this basin is comparatively shallower with depths ranging from 3600 to 4000 m. The Nansen Basin has a shallower seafloor because it is supplied sediments from the Barents-Kara Shelf. In contrast, sediments from the Barents-Kara Shelf are obstructed from reaching Amundsen Basin by the Gakkel Ridge. The age of oceanic crust underlying Eurasia Basin is inferred based on well-defined seafloor spreading magnetic anomalies (Fig. 1.5; Vogt et al., 1979; Srivastava, 1985; Brozena et al., 2003). The recognition of chron 25 in Amundsen Basin, however, is under debate (Brozena et al., 2003; Langinen et al., 2009). Plate-tectonic reconstruction of the Eurasian rift margins using chron 25 directly juxtaposes linear magnetic anomalies from Lomonosov Ridge and the Barents Shelf, according to Døssing et al. (2013). Relying on

potential fields and seismic lines from the Barents Shelf margin, Minakov et al. (2012) concluded that "minor shearing or oblique extension prior to breakup is needed to restore the conjugate margins of Eurasia Basin".

1.3.3. Amerasia Basin

Amerasia Basin is separated from Eurasia Basin by Lomonosov Ridge. This ridge, Arctic Alaska, East Siberia and the Canadian Arctic Archipelago surround the basin. Prominent morphological features within Amerasia Basin include Canada Basin, the Chukchi Borderland, the Alpha and Mendeleev ridges, and the Makarov and Podvodnikov basins. Relative to Eurasia Basin, the geological evolution of Amerasia Basin is not well constrained.

Published plate-reconstructions of Canada Basin are inconsistent due to the absence of well-defined magnetic chron anomalies (Vogt et al., 1982; Grantz et al., 2011; Chian et al., 2016; Fig. 1.5). Many tectonic models pertaining to the origin of Amerasia Basin have been advanced; however, the "rotational" model is the most widely accepted (pole of rotation shown in Fig. 1.3). There are different versions of the rotational model (e.g., Carey, 1958; Tailleur, 1973; Grantz et al., 1979, 1998, 2011). These variants share the concept that Arctic Alaska rifted and drifted away from the Canadian Polar margin in a counter-clockwise "fan-like" motion (Lawver and Scotese, 1990). Returning Arctic Alaska to the Canadian Polar margin is achieved by aligning the 1000 m isobaths (Grantz et al., 1979), the hinge lines beneath the inner or middle shelf (Grantz et al., 1990) or Triassic sediment facies (Embry, 1990) from opposing margins. Associated poles of rotation are located within the Mackenzie River delta region (Tailleur, 1973; Grantz et

al., 1979) and the angle of rotation is 66–70° (Grantz et al., 1990). Halgedahl and Jarrard (1987) analyzed the palaeomagnetic response from oriented drill cores derived from two wells on the North Slope, Alaska. These data are from the lower member of the Kuparuk River Formation, which has a Berriasian to Valanginian age (145.0–134.7 Ma). These authors concluded that "[t]he only pre-existing model which is compatible with the Kuparuk River paleomagnetic pole is that for approximately 70° of counter-clockwise rotation of the Arctic Alaska Plate away from the Canadian Arctic about a finite rotation pole in the Mackenzie Delta". Furthermore, the timing of opening for Canada Basin, or the entire Amerasia Basin, is constrained between 130 Ma and no later than 100 Ma, according to their interpretations. Embry and Dixon (1994) proposed a Hauterivian age (134.7–130.8 Ma) for opening of Amerasia Basin based on identification of breakup unconformities from Arctic Alaska and Sverdrup Basin (conjugate margins). These authors also correlate the end of spreading with a regional Cenomanian unconformity (100.5–93.9 Ma).

A gravity low that bisects Canada Basin (Laxon and McAdoo, 1994; Fig. 1.4), and is shown in seismic reflection profiles to coincide with a negative relief structure along basement (Mosher et al., 2012), is interpreted as an extinct spreading centre. The position of this hypothetical spreading centre supports the rotation model. A recent study by Chian et al. (2016) concluded that the extent of oceanic crust beneath Canada Basin is significantly narrower than previously assumed (cf. Grantz et al., 2011). More recent variations on the rotational model invoke a more complex multi-phase evolution for Amerasia Basin (e.g., Grantz et al., 1998, 2011). In addition, recent models present the Chukotka and Arctic Alaska terranes as a single microplate that moved jointly during

opening of Amerasia Basin (e.g., Pease, 2011). Collision of this microplate with Siberia

due to closing of the South Anyui Ocean formed the South Anyui Suture (Rowley and

Lottes, 1988; Lawver et al. 2002; Fig. 1.3). The timing of this event and, indeed, the

origin of this suture, however, are not confirmed (e.g., Miller et al., 2008; Kuzmichev,

2009).

1.3.4. Alpha and Mendeleev Ridges

Alpha and Mendeleev ridges form a distinct physiographic entity that spans 1800

km from the Siberian Shelf to the Canadian Polar margin offshore Ellesmere Island. The

Alpha-Mendeleev ridge complex is characterized by elevations up to 2000 m above the

adjacent Canada and Makarov basins, and its width varies from 200 to 600 km along its

length. The ridge complex and surrounding areas exhibit a distinct pattern of alternating

high amplitude, positive and negative magnetic anomalies (Fig. 1.5). Oakey and Saltus

(2016) relied on a pseudo-gravity transformation to redefine the High Arctic Magnetic

High domain (HAMH). These authors conclude that the ridge complex has a "deep

magnetic root". The gravity field at these ridges correlates strongly with seafloor

topography (Weber, 1986; Dove et al., 2010; Fig. 1.4).

The interpretation of the Alpha-Mendeleev ridge complex as a large igneous

province (LIP) is supported by basalt and other volcanic rocks recovered in dredges,

cores and drilling (Van Wagoner et al., 1986; Andronikov et al., 2008; Mayer and

Armstrong, 2012; Jokat et al., 2013; Mayer et al., 2016; Petrov et al., 2016), its magnetic

signature (Vogt et al., 2006) and the seismic velocity structure of its crust (e.g., Funck et

al., 2011). Mineral textures from volcaniclastic samples dredged from the Alpha Ridge

during the CESAR (Jackson et al., 1985) and HEALY0805 (Mayer and Armstrong, 2008) expeditions indicate shallow-water eruptions (<800 m; VanWagoner et al., 1986). The hypothetical extinct spreading centre in Canada Basin does not extend into the HAMH (Oakey and Saltus, 2016). Either this spreading centre simply terminates near the fringes of the LIP (e.g., model 2 from Alvey et al. [2008]), or pre-existing basement structures were overprinted by later magmatism related to the Alpha–Mendeleev ridge complex (e.g., Grantz et al., 2011). Consequently, the northern extent of oceanic spreading and, thus, the position of a dextral transform boundary, as required by the rotational model, are unclear.

1.3.5. Makarov and Podvodnikov Basins

The Makarov and Podvodnikov basins are situated in northern Amerasia Basin between the Alpha-Mendeleev ridge complex and Lomonosov Ridge. Seafloor depths in Makarov Basin can reach down to 4000 m. Although data coverage is limited, there is general consensus in the scientific literature that Makarov Basin is, at least partially, floored by oceanic crust (e.g., Langinen et al., 2009; Lebedeva-Ivanova et al., 2011; Nikishin et al., 2014). Makarov Basin hosts Marvin Spur, a linear ridge that trends sub-parallel to Lomonosov Ridge.

The name "Podvodnikov Basin" is not officially recognized by the Marine Gazetteer (2017). This name, however, is not only common in the Russian scientific literature (e.g., Sorokin et al., 1999; Petrov et al., 2016), but also in Western literature (Alvey et al., 2008; Dove et al., 2010; Grantz et al., 2011; Pease et al., 2014). As such, the name Podvodnikov Basin is used throughout this thesis in reference to the basin

adjacent to the Siberian Shelf between Lomonosov and Mendeleev ridges (Fig. 1.2).

Seafloor depths are a minimum at ~2000 m at the base of the East Siberian continental

slope, and attain a maximum at ~3900 m in northern Podvodnikov Basin. Arlis Gap

refers to a section of northern Podvodnikov Basin where a structure (sub-)perpendicular

to adjacent Mendeleev Ridge and Lomonosov Ridge is buried (Jakobsson et al., 2012).

Seafloor depths abruptly increase from 2800 m to 3800 m across this structure (Sorokin

et al., 1999; Jakobsson et al., 2012). Seismic imaging shows the Arlis Gap is indeed

underlain by a basement high (Arlis Ridge) that has obstructed sedimentation into

Makarov Basin from the Podvodnikov Basin and East Siberian Shelf (Kutschale, 1966;

Sorokin et al., 1999; Fig. A.4). The Arlis Ridge is genetically tied to the Alpha-

Mendeleev ridge complex based on its high amplitude magnetic signature (~800 nT

anomaly; Fig. 1.5), which is consistent with the character of the High Arctic Magnetic

High domain (Sorokin et al., 1999). Approximately half of the crust beneath

Podvodnikov Basin is a thinned part of the Lomonosov Ridge crust, and the other half is

made of thick igneous crust tied to Mendeleev Ridge (Jokat and Ickrath, 2015). Based on

gravity inversion, Alvey et al. (2008) presented tectonic models that include entrapped

oceanic crust of Jurassic age, a remnant of the South Anyui Ocean, beneath northern

Podvodnikov Basin.

The gravity signal at Makarov and Podvodnikov basins is generally depressed;

however, distinct positive free-air anomalies are associated with small ridges and

seamounts (e.g., Marvin Spur and Fedotov Seamount; Fig. 1.4). The HAMH partly

overlaps with the Makarov and Podvodnikov basins. Past authors identified seafloor

spreading anomalies in these basins (Taylor et al., 1981; Kovacs et al., 1999; Døssing et al., 2017). Their interpretations are, however, inconclusive.

1.3.6. High Arctic Large Igneous Province (HALIP)

The circum-Arctic region hosts Cretaceous-Palaeogene mafic volcanic suites with ages spanning ~70 Ma (Tegner et al., 2011) and are collectively known as the High Arctic Large Igneous Province or HALIP (Maher, 2001). The older suites (130–80 Ma) consist of volcanic beds, sills and dykes from Sverdrup Basin (Embry and Dixon, 1990; Estrada and Henjes-Kunst, 2004), Svalbard (Bailey and Rasmussen, 1997), Franz Josef Land (Dibner, 1998) and the East Siberian Shelf (Drachev et al., 1999; Drachev and Saunders 2006) that have a tholeiitic signature. Presently, these suites are scattered throughout the circum-Arctic region; however, they were presumably once contiguous and fed by a plume that triggered the opening of Amerasia Basin and dispersed the magmatic provinces (Buchan and Ernst, 2006; Døssing et al., 2013). Offshore linear magnetic anomalies near Ellesmere Island are linked to mafic dykes observed on Franz Josef Land (Døssing et al., 2013). Unlike the older magmatic suites, younger ones (85–60 Ma) from Ellesmere Island (Estrada et al., 2010) and northern Greenland are more alkaline (Tegner et al., 2011). The relationship between these differing suites and their association with North Atlantic magmatism is debated (Estrada, 2015). Funck et al. (2011) noted that the compositional transition from tholeiitic to alkaline is consistent with observations from other LIPs and may reflect late-stage low temperature melting. Lawver and Müller (1994) proposed that these HALIP suites form a hotspot track linked to early expressions of the Iceland mantle plume. Tegner et al. (2011) countered, however, that

the appearance of an age progression from the HALIP to the North Atlantic LIP results from plate reconfiguration around 60 Ma.
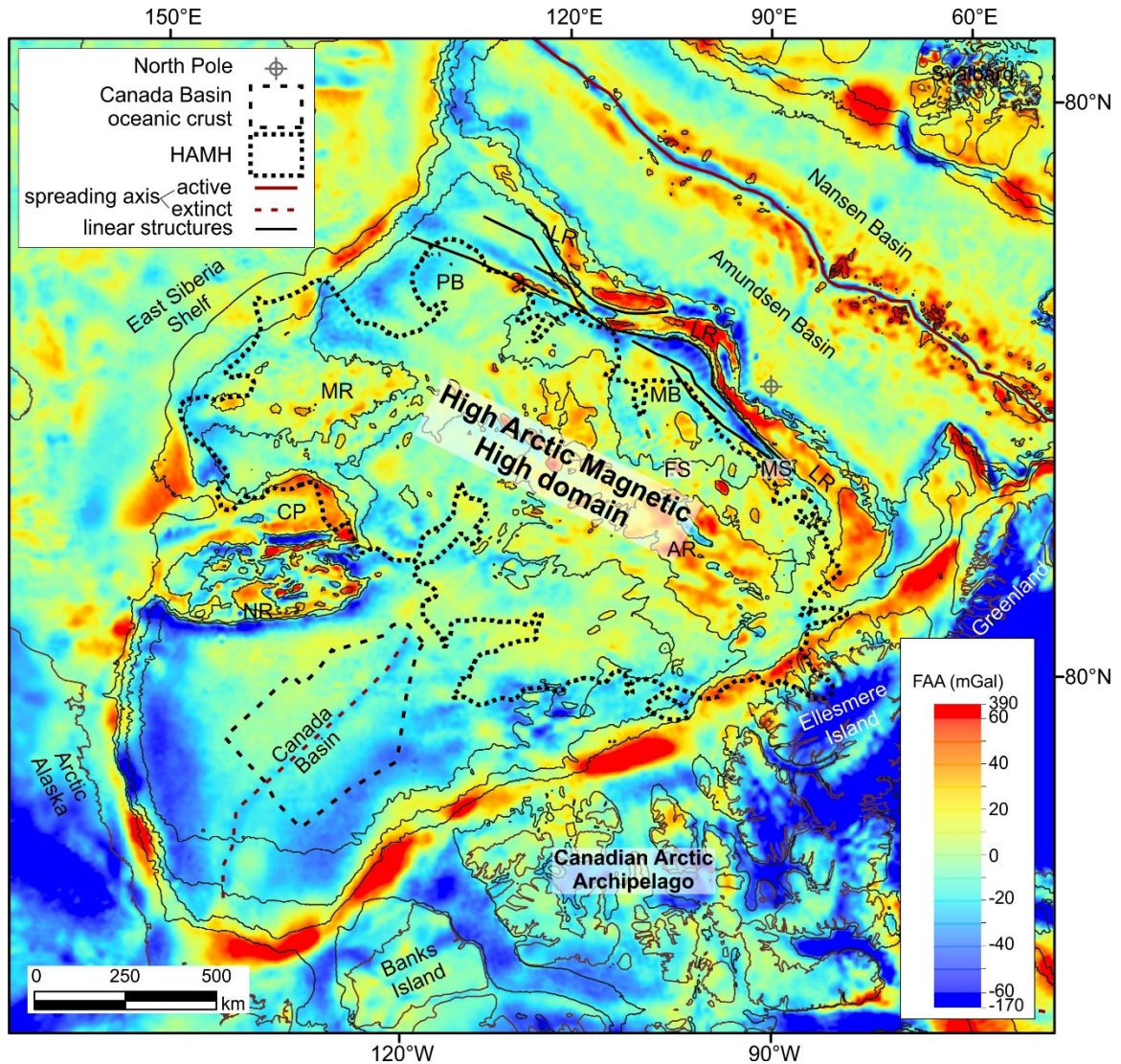
Fig. 1.4. Free-air anomaly (FAA) map of the Arctic Ocean. Acronyms are defined in Fig. 1.2. Gravity grid is from Andersen et al. (2010). The outline for the High Arctic Magnetic High domain (HAMH) is from Oakey and Saltus et al. (2016). The outline for oceanic crust in Canada Basin is Chian et al. (2016). Locations of spreading axes were digitized after Pease et al. (2014) and linear structures on the Amerasian flank of Lomonosov Ridge are from Evangelatos and Mosher (2016). Bathymetric contours (200 m, 500 m, 1000 m, 2000 m and 3000 m) are derived from the IBCAO version 3.0 grid (Jakobsson et al., 2012).
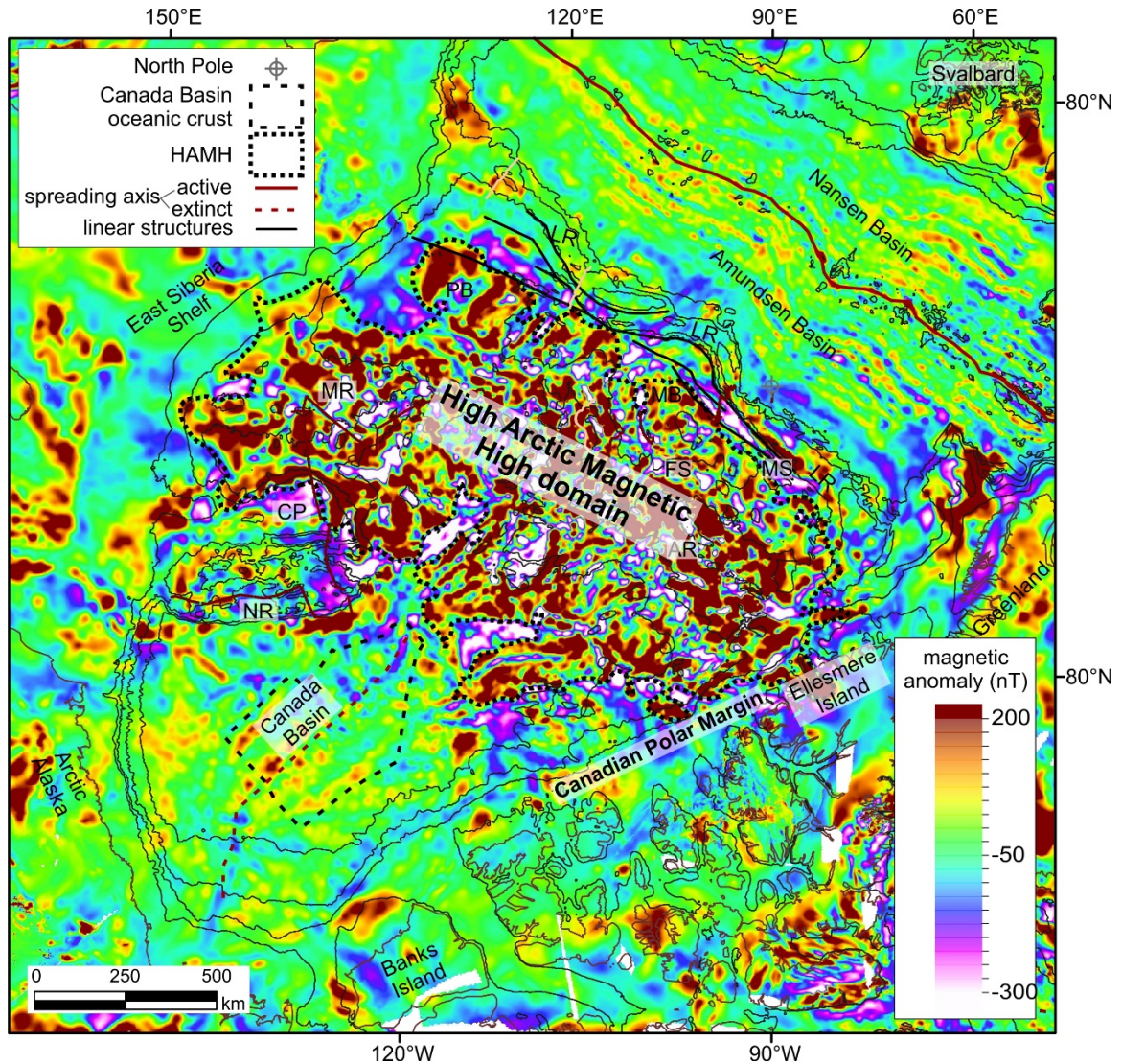
Fig. 1.5. Magnetic anomaly map of the Arctic Ocean. Acronyms are defined in Fig. 1.2. Magnetic grid is from Gaina et al. (2011). The outline for the High Arctic Magnetic High domain (HAMH) is from Oakey and Saltus et al. (2016). The outline for oceanic crust in Canada Basin is Chian et al. (2016). Locations of spreading axes were digitized after Pease et al. (2014) and linear structures on the Amerasian flank of Lomonosov Ridge are from Evangelatos and Mosher (2016). Bathymetric contours (200 m, 500 m, 1000 m, 2000 m and 3000 m) are derived from the IBCAO version 3.0 grid (Jakobsson et al., 2012).

1.4. Thesis Organization

1.4.1. Chapter 2

Chapter 2 is a modified version of "*Evangelatos, J., Mosher, D.C., 2016. Seismic stratigraphy, structure and morphology of Makarov Basin: tectonic implications. Marine Geology 374, 1–13*".

1.4.1.1. Summary

The purpose of this study was to decipher the sedimentary and tectonic history of northern Amerasia Basin by analyzing the seismic stratigraphy, structure and morphology of Makarov Basin and surrounding areas (i.e., Alpha and Lomonosov ridges). This study relies on a ~400 km multi-channel seismic record that extends from Alpha Ridge, across the width of Makarov Basin and onto Lomonosov Ridge, and the Arctic bathymetric chart (Jakobsson et al., 2012). The results show that the sedimentary section within Makarov Basin is thickest near Lomonosov Ridge (~ 5 km thick). The sedimentary section was divided into two broad groups: 1) a lower sedimentary succession consisting of slope and base of slope sediments that were sourced from the Lomonosov Ridge/Barents Shelf, and 2) an upper succession composed primarily of hemipelagic to pelagic sediments. An age model for the upper units was constructed by jump-correlating seismic units to Lomonosov Ridge where ACEX drill core constrains the age of the Cenozoic sedimentary drape. For older units, age was constrained using regional geological events (e.g., crustal age, cessation of Alpha-Mendeleev LIP-related magmatism). The rhomboid shape of the deep subbasin, the straight and steep morphology of the Amerasian flank of Lomonosov Ridge and the presence of numerous sub-parallel ridges interpreted to represent splay faults are evidence of strike-slip tectonics. This interpretation supports the "rotational" model of opening of Amerasia Basin (e.g., Grantz et al., 2011) with a transform to transtensional margin at Lomonosov Ridge.

1.4.1.2. Contributions of Authors

In addition to lead authorship of the publication, the present author conducted the seismic stratigraphic and geomorphological analysis and worked with his co-author on the interpretation of these data. This work mapped prominent seismic horizons and identified seismic facies and facies assemblages, provided a geological interpretation for the seismic units, including the development of an appropriate age model, analyzed bathymetric slope gradients and identified structures related to strike-slip movement along the Lomonosov Ridge margin. Seismic velocities used for estimating the thickness of seismic units were based on preliminary work from coincident sonobuoy records, analyzed by the present author. Analysis of these sonobuoy records is discussed in detail in Chapter 3. The present author produced all of the figures, except for the figure with the Chirp subbottom profiler, created by co-author D. Mosher. D. Mosher was Chief Scientist on the mission that acquired the seismic and sub-bottom data (Mosher, 2012). Early in the formulation of this chapter, D. Mosher recommended that the present author focus on the geomorphology of the Amerasian flank of Lomonosov Ridge, and directed the present author to publications on the theoretical characteristics of transform/transtensional margins. In addition, D. Mosher reviewed the chapter extensively and contributed to the writing. J. Shimeld processed the seismic reflection data (Shimeld, 2011).

1.4.2. Chapter 3

Chapter 3 is a modified version of "Evangelatos, J., Funck, T., Mosher, D.C., 2017. The sedimentary and crustal velocity structure of Makarov Basin and adjacent Alpha Ridge. Tectonophysics 696-697, 99–114".

1.4.2.1. Summary

The purpose of this study was to determine the tectonic origins of Makarov Basin and Alpha Ridge and investigate the geological relationship between these two terrains. To this end, seismic data from sonobuoys distributed along a 650 km-long line that extends from Alpha Ridge and across Makarov Basin to the Lomonosov Ridge were analyzed. Forward modelling of traveltimes, supported by coincident multi-channel seismic reflection and shipborne gravity data, was used to determine the P-wave velocity structure along this line. The results show that the sedimentary cover averages 0.5 km thick on Alpha Ridge and 1.9 km thick in Makarov Basin, but reaches up to 5 km thick at the base of Lomonosov Ridge. Velocities in the lower sedimentary succession near Lomonosov Ridge are interpreted as representing interbedded volcaniclastic or volcanic rock. The shallow basement of Alpha Ridge is characterized by semi-continuous high amplitude reflections and is interpreted as volcanic rock possibly intercalated with sedimentary rock. Velocities do not vary significantly in the upper and mid-crustal layers between Alpha Ridge and Makarov Basin. This result suggests that the basin, at least partly, either formed during or was influenced by Alpha-Mendeleev LIP-related magmatism. Crustal thickness increases from 5 km in Makarov Basin to >20 km as part of Lomonosov Ridge over a short distance of 70 km. This abrupt transition of crustal

thicknesses from Makarov Basin to Lomonosov Ridge supports the interpretation that this section of the ridge as a transform margin. Appendix B includes seismic records from all sonobuoys pertinent to this study.

1.4.2.2. Contributions of Authors

The present author processed the sonobuoy data, forward modelled traveltimes, conducted two-dimensional gravity modelling (after converting velocities to density), interpreted the results within a regional geological context, wrote the chapter and produced all figures. Co-authors T. Funck and D. Mosher contributed to the writing and provided constructive criticism at all stages of the manuscript. T. Funck provided programming scripts fundamental to the velocity and density models. Also, T. Funck contributed to the description and discussion of uncertainty in the data. With respect to the Discussion section, T. Funck steered the analysis of the velocity and gravity results towards geologically feasible tectonic models and suggested comparison of the crustal structure of Makarov Basin to normal oceanic crust of appropriate age. D. Mosher was Chief Scientist on the scientific cruise that acquired the seismic reflection and refraction data (Mosher, 2012). Also, D. Mosher provided direction on the interpretation of velocities from the sedimentary layers. J. Shimeld processed the seismic reflection data, and B. Coakley processed the gravity data.

1.4.3. Chapter 4

The 2-D gravity models were included in a poster presentation and are part of a manuscript that is yet to be submitted. The poster was presented as "*Evangelatos, J.,*

Oakey G., Saltus, R., 2017, Central Arctic Crustal Modeling Constrained by Potential Field data and recent ECS Seismic Data, European Geosciences Union General Assembly 2017".

1.4.3.1. Summary

The purpose of this study was to characterize crustal thickness (to a first order approximation) in northern Amerasia Basin in order to better understanding the structural relationship between the northern basins and Lomonosov Ridge. To this end, thirteen two-dimensional gravity profiles that extend from Alpha Ridge to Amundsen Basin via Makarov Basin and Lomonosov Ridge were modeled. To constrain the detailed geometry of models and derive estimates for density, these profiles overlapped with existing seismic profiles where possible. For simplicity, the Earth models were restricted to one water layer, two layers each for the sedimentary and crustal sections, and a uniform mantle. Additional information from off-line sources, MCS, wide angle/refraction seismic data and the regional magnetic field, were incorporated into the study to estimate layer thicknesses and densities. The results show that, as Alpha Ridge and Lomonosov Ridge converge near the Canadian Polar margin, the crust of Makarov Basin progressively narrows until it is undistinguishable. Gravity models support conclusions from refraction studies that showed a relatively abrupt crustal transition between Makarov Basin and central Lomonosov Ridge. Closer to the East Siberian Shelf, the crustal transition between Podvodnikov Basin and Lomonosov Ridge is more gradual. Appendix C includes all gravity models not presented in Chapter 4.

1.4.3.2. Contributions of Authors

The present author generated the gravity models, interpreted these models, drafted the figures and wrote the paper. Co-author G. Oakey contributed an electronic copy of the gravity grid from Andersen et al. (2010), from which the gravity profiles were extracted. In addition, G. Oakey provided guidance on addressing the problem, extensive feedback on the quality of the gravity modelling and, along with R. Saltus, reviewed the poster presentation and this chapter. The present author generated the gravity models, interpreted these models, drafted the figures and wrote the paper. Co-author G. Oakey contributed an electronic copy of the gravity grid from Andersen et al. (2010), from which the gravity profiles were extracted. In addition, G. Oakey provided guidance on addressing the problem, extensive feedback on the quality of the gravity modelling and, along with R. Saltus, reviewed the poster presentation and this chapter.

1.4.4. Chapter 5

1.4.4.1. Summary

The purpose of this final chapter is to summarize important results and conclusions derived from this thesis. Based on crustal structure, structure and morphology, the Amerasian flank of Lomonosov Ridge is interpreted as a transform/transtensional margin. The age model for Makarov Basin is established by correlation seismic facie assemblages to regional geological events and to the ACEX drill hole. Results from two-dimensional models of the gravity field provided a more regional

context to these constraints. This new information is integrated into the latest Arctic

plate-reconstruction models and presented in palinspastic maps.

1.4.5. Appendices

Appendix A summarizes past seismic experiments that were conducted in

Amerasia Basin and are pertinent to this thesis. Published seismic cross-sections from

these experiments are included.

Appendix B includes the seismic records of sonobuoys deployed along line

LSSL2011-03/04 and are fundamental to Chapter 3. Seismic velocity models with

raypaths for picked phases accompany each respective seismic record.

Appendix C presents the profiles of two-dimensional gravity models excluded

from Chapter 4.

CHAPTER 2: SEISMIC STRATIGRAPHY, STRUCTURE AND MORPHOLOGY OF MAKAROV BASIN AND SURROUNDING REGIONS – TECTONIC IMPLICATIONS

Preface

Chapter 2 is a modified version of publication "*Evangelatos, J., Mosher, D.C., 2016. Seismic stratigraphy, structure and morphology of Makarov Basin: tectonic implications. Marine Geology 374, 1–13*".

Abstract

The tectonic history of Amerasia Basin, Arctic Ocean, is not well known because of a paucity of data and complexities introduced by the Alpha-Mendeleev Ridge large igneous province. Makarov Basin, at the northern limit of Amerasia Basin and adjacent to Lomonosov Ridge, may provide a window into understanding the larger tectonic framework. The objective of this study is to decipher the sedimentary and tectonic history of northern Amerasia Basin by analysing the seismic stratigraphy, structure and morphology of Makarov Basin and surrounding regions (Alpha and Lomonosov ridges) of the central Arctic Ocean. The principal data sources for this study are a 400 km long multi-channel seismic line, extending from Alpha Ridge to the crest of Lomonosov Ridge via central Makarov Basin, and the Arctic bathymetric chart.

The seismic record within Makarov Basin is divided into five seismic units. The first unit overlying basement hosts Late Cretaceous (minimum age) slope to base of slope sediments. Some of these sediments are interbedded with volcanic or volcaniclastic rocks

with a minimum age of 89 Ma. Makarov Basin becomes isolated from proximal sources of sediments after the onset of rifting that separated Lomonosov Ridge from the Barents Shelf, which may have occurred as early as the mid-Late Cretaceous, and led to the creation of Eurasia Basin. Sediments are largely pelagic to hemipelagic as a result of this isolation. This deposition style also applies to the draped sedimentary strata on Alpha and Lomonosov ridges. The uppermost seismic units within Makarov Basin are jump correlated to the stratigraphic record of the ACEX drill site on top of Lomonosov Ridge to provide age control. This correlation shows that the 44.4–18.2 Ma hiatus documented in the drill core is not apparent in the basin. Inter-ridge correlations and the absence of an obvious planate surface on Alpha Ridge also suggest that sedimentation was uninterrupted on this ridge during the hiatus.

Seismic data reveal a deep subbasin (~5 km thick) within Makarov Basin. This subbasin is immediately adjacent to Lomonosov Ridge within major bends in the general strike orientation of the ridge. The rhomboid shape of the deep subbasin, the straight and steep morphology of the Amerasian flank of Lomonosov Ridge and the presence of numerous sub-parallel ridges (e.g. Geophysicists and Marvin spurs) created by splay faulting are evidence of strike-slip (transtensional) tectonics. This interpretation supports the "rotational" model of opening of Amerasia Basin with a transform to transtensional margin at Lomonosov Ridge. As spreading continued, however, the tectonics became increasingly extensional perpendicular to Lomonosov Ridge. There is no evidence of major tectonic deformation in Makarov Basin beyond the late Paleocene.

2.1. Introduction

The Arctic Ocean is the smallest and shallowest of the world's five major oceans. It comprises extensive shallow continental shelves and two major deep-water basins — the Amerasia and Eurasia basins (Fig. 2.1). The two basins are separated by the Lomonosov Ridge, spanning the Arctic Ocean from the North American shelf off of Ellesmere Island and Northwest Greenland to the East Siberian Shelf. The onset of rifting between Lomonosov Ridge and the Barents Shelf may have commenced as early as the mid-Late Cretaceous (Drachev, 2011), and led to seafloor spreading in Eurasia Basin during the late Paleocene (magnetic chron anomaly 25 or 24; Vogt et al., 1979; Srivastava, 1985; Brozena et al., 2003). Amerasia Basin lies on the opposite side of Lomonosov Ridge. This ridge, Arctic Alaska, Siberia and the Canadian Arctic Archipelago surround the basin (Fig. 2.1). Prominent geomorphological features within Amerasia Basin include Canada Basin, the Chukchi Borderland, the Alpha and Mendeleev ridges, and the Makarov and Podvodnikov basins (Rowley and Lottes, 1988; Fig. 2.1). In contrast to Eurasia Basin, the geological history of Amerasia Basin is not well known. This uncertainty results largely from the paucity of data in Amerasia Basin, which is due to its remote location and perennial cover of sea ice, and due to the geological complexity of the region. Furthermore, plate-reconstructions of the basin are hampered by the absence of well-defined magnetic isochron anomalies (Gaina et al., 2011). Consequently, opposing models for the genesis of Amerasia Basin have been advanced (cf. Miller and Verzhbitsky, 2009; Grantz et al., 2011). Unravelling the history of Makarov Basin, which lies in the underexplored northern Amerasia Basin, will support interpretation of the tectonic origin of the entire Amerasia Basin and its post-formation

history. The objective of this study, therefore, is to decipher the tectonic and

sedimentological history of northern Amerasia Basin by analysing the stratigraphy,

structure and morphology of Makarov Basin and surrounding regions using recently

acquired seismic reflection and bathymetric data.
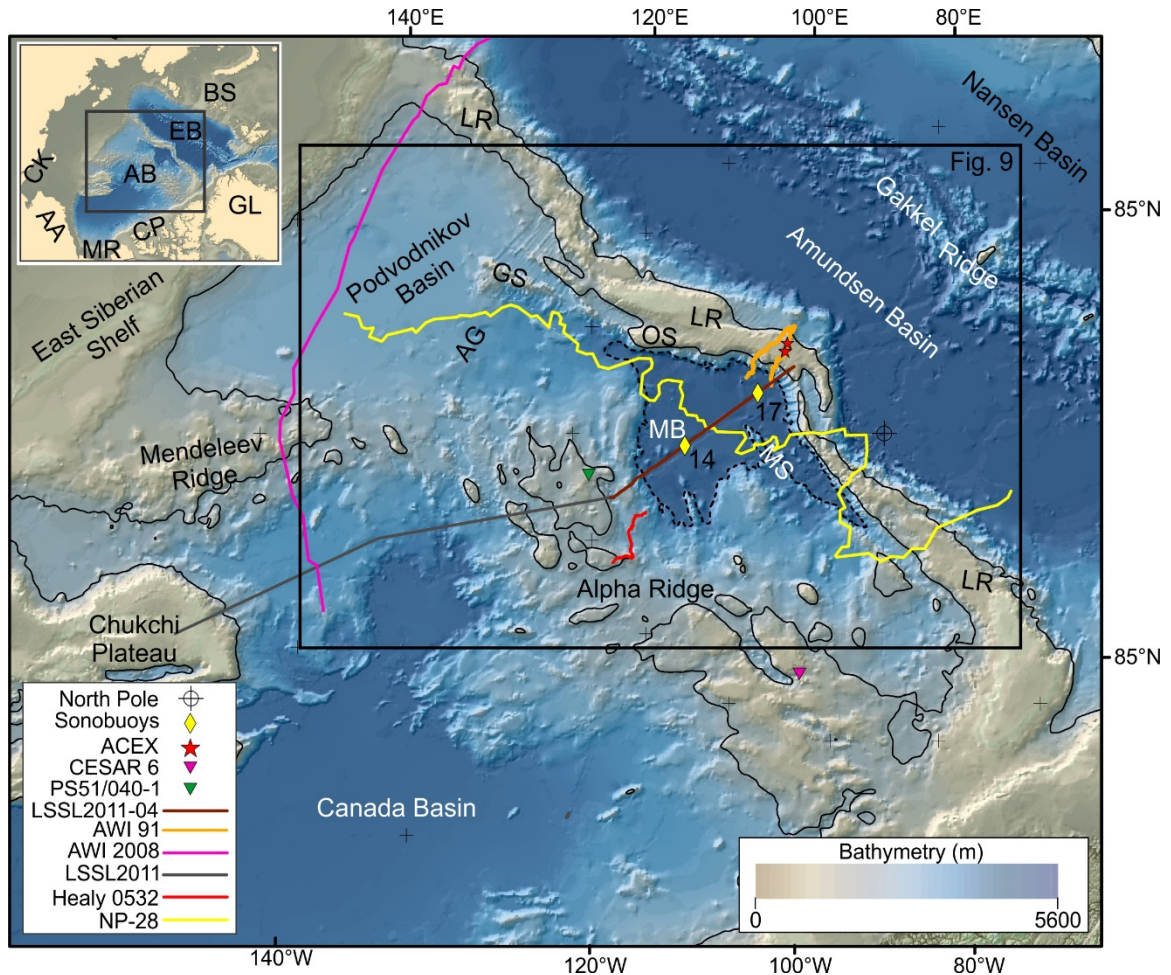
Fig. 2.1. Colour-shaded bathymetric map of northern Amerasia and Eurasia basins. Makarov Basin is delineated by a dashed line representing the 3700mbathymetric contour. The thin black like corresponds with the 2000mbathymetric contour, which is used to describe Lomonosov Ridge. Acronyms used in this figure and others are: AA—Arctic Alaska, AB—Amerasia Basin, AG — Arlis Gap, BS — Barents Shelf, CP — Canadian Polar margin, CK — Chukotka, EB — Eurasia Basin, GL — Greenland, GS — Geophysicists Spur, LR — Lomonosov Ridge, MB — Makarov Basin, MR — Mackenzie River delta, MS — Marvin Spur, OS — Oden Spur. Note, the name Geophysicists Spur is not officially included in the General Bathymetric Chart of the Oceans Gazetteer (http://www.gebco.net/), but we use it as it is common in the Russian literature (e.g. Morozov et al., 2013; Taldenkova et al., 2014). Other studies shown in this figure are: ACEX [drill sites from IODP Expedition 302; Backman et al., 2006], CESAR 6 [piston core; Mudie and Blasco, 1985], PS51/040-1 [sediment core; Jokat, 1999], AWI 91 [MCS; Jokat et al., 1992, 1995], AWI 2008 [MCS; Weigelt et al., 2014], Healy 0532 [MCS; Bruvoll et al., 2010], LSSL2011 [MCS;

Mosher, 2012], NP-28 [seismic reflection from ice-station; Langinen et al., 2009]. Map projection is North Pole Stereographic with a latitude of origin of 75° N and a central meridian of 90° W. Bathymetry and elevation are from the International Bathymetric Chart of the Arctic Ocean (IBCAO) version 3.0 grid (Jakobsson et al., 2012).

2.2. Geological Setting

Makarov Basin lies at the northern extent of Amerasia Basin between Alpha

Ridge and Lomonosov Ridge (Fig. 2.1). The basin encompasses an area of approximately

63,000 km2 and its abyssal plain reaches depths of 4000 m (Fig. 2.1). Lomonosov Ridge

is reasonably well-understood to be a continental fragment isolated by opening of Eurasia

Basin in the Cenozoic (Rowley and Lottes, 1988; Jackson et al., 2010). The Eurasian

margin of Lomonosov Ridge is thus conjugate to the Barents Shelf margin. On the

opposite side, Geophysicists, Oden and Marvin spurs are linear ridges that trend sub-

parallel to Lomonosov Ridge (Fig. 2.1). These features are interpreted as continental

fragments splintered off of Lomonosov Ridge (Cochran et al., 2006). Alpha Ridge forms

the southern border of Makarov Basin. The Alpha and Mendeleev ridges are part of a

large igneous province (LIP), as evidenced by its high amplitude magnetic anomalies

(Weber, 1986; Vogt et al., 2006), velocity structure (Funck et al., 2011), and basalts

recovered in situ (Van Wagoner et al., 1986; Andronikov et al., 2008; Jokat, 1999).

Together with Cretaceous volcanic suites found throughout the circum-Arctic (e.g.,

Hansen Point volcanics on Ellesmere Island; Estrada and Henjes-Kunst, 2004), the
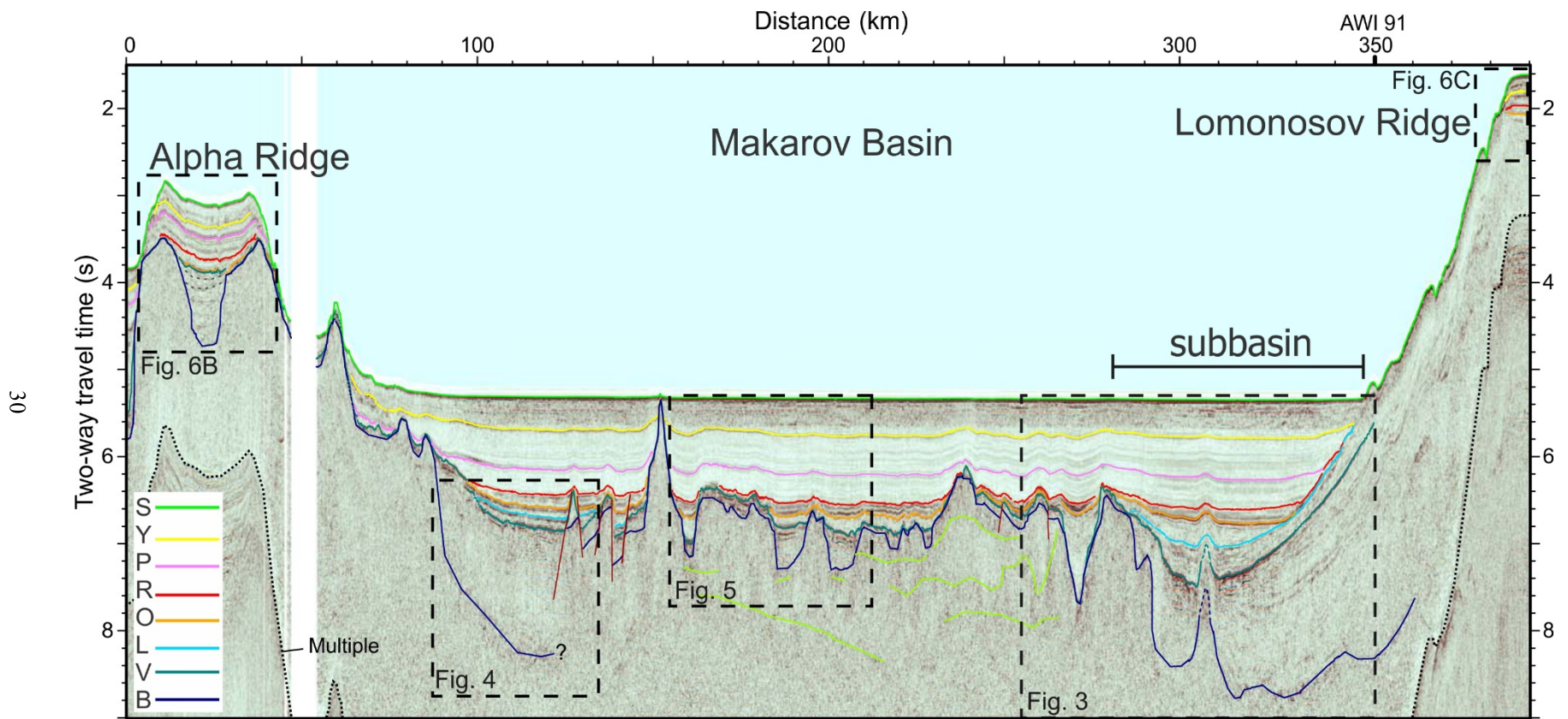
Fig. 2.2. MCS profile of line LSSL2011-04 is shown in the time domain. Seafloor multiple is outlined by dotted black line. Lime green lines represent isolated semi-coherent acoustic signal within acoustic basement. Brown lines are for faults. The trackline of the profile is plotted in Fig. 2.1. Time sections shown in Figs. 2.3–2.6 are outlined by dashed boxes.

Alpha-Mendeleev ridge complex is assumed to be part of the greater High Arctic Large Igneous Province (HALIP) (Maher, 2001; Tegner et al., 2011). The duration of the HALIP and its timing relative to the opening of Amerasia Basin are disputed (Estrada, 2015). There is also current debate about whether the Alpha-Mendeleev ridge complex is an oceanic plateau emplaced on top of oceanic crust (e.g., Funck et al., 2011; Jokat et al., 2013), or stretched continental crust overprinted by later magmatism (e.g., Lebedeva-Ivanova et al., 2006; Døssing et al., 2013). The distinct magnetic character of the Alpha-Mendeleev ridge complex extends under Makarov Basin (Saltus et al., 2011). Isolated bedrock elevations found in the southeastern part of Makarov Basin are considered to be genetically related to Alpha Ridge (Jackson et al., 1986). Although there are many tectonic models explaining the creation of the early Arctic Ocean (i.e., Amerasia Basin), the "rotational" model is the most widely accepted (e.g., Carey, 1958; Tailleur, 1973; Grantz et al., 1979, 1998, 2011). According to this model, the Arctic Alaska–Chukotka microplate rifted and drifted away from the Canadian Arctic continental margin about a pole of rotation located in the Mackenzie River delta region (Lawver et al., 2002). Spreading is thought to have commenced in the Early Cretaceous (Embry and Dixon, 1994), although the age is not well constrained. The rotational model was buoyed by the discovery of a negative gravity anomaly that bisects Canada Basin. It was interpreted as a buried extinct spreading centre (Laxon and McAdoo, 1994) and negative basement relief coincident with this gravity anomaly has since been resolved by seismic reflection (Mosher et al., 2012). The gravity anomaly is not observed within the Alpha-Mendeleev LIP magnetic domain (Saltus et al., 2011), suggesting that any previous existing basement structure is masked by late magmatism related to, the Alpha-Mendeleev ridge

complex. Consequently, the northern extent of spreading and the nature of the margin

between Amerasia Basin and Lomonosov Ridge are ambiguous and the tectonics are not

well constrained.

Table 2.1. Seismic horizons are described from deepest to shallowest. Listed depths are for the abyssal part of Makarov Basin between 80 and 352 km. Abrupt changes due to structural highs along horizon B are excluded.

Horizon	Colour	Description
B	dark blue	Delineates amorphous acoustic signal (Facies 1) from overlying coherent seismic facies, thus defining the top of acoustic basement.
v	dark cyan	A distinct high amplitude reflection easily discerned in Makarov Basin, but less so beneath the ridges. The V horizon clearly demarcates a relatively continuous and stratified section from an underlying section characterized by semi-coherent signal (Facies 2).
L	light blue	Defined by an up section change from Facies 4 to Facies 5 with the latter onlapping against this horizon. It is mapped in two separate locations along the line: 99 to 133 km, and 286 to 329 km.
O	orange	Observed at the base of a band of prominent basin-wide reflections (Facies 6). The depth of this reflection is 6.30–6.74 s TWTT.
R	red	Delineates the top of the band of reflections discussed under the O horizon. The R horizon is not always well constrained due to gradational weakening of amplitude strength with decreasing depth. This reflection is mostly constrained between 6.27–6.60 s TWTT.
P	pink	A high amplitude reflection that parallels the R horizon and spans the length of Makarov Basin at a depth of approximately 5.71–6.26 s TWTT (except where it intersects structural highs or on the flanks of Alpha and Lomonosov ridges).
Y	yellow	Similar to the P horizon, but generally found at approximate depths of 5.28–5.79 s TWTT. This horizon is embedded between relatively disrupted reflections (Facies 8).
S	green	Seafloor reflection.
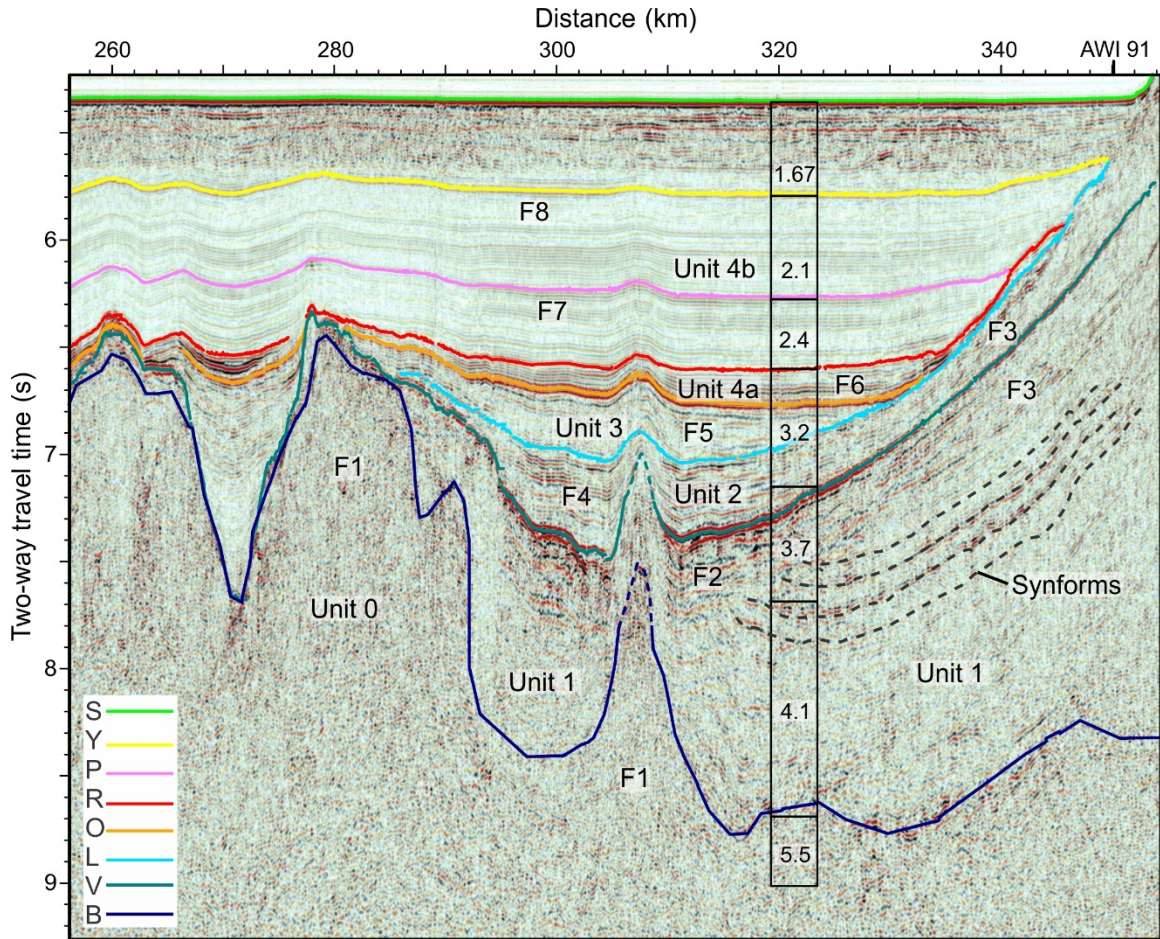
Fig. 2.3. A section of line LSSL2011-04 outlining the deep subbasin. Dashed black lines mark synformal reflections. Data from sonobuoy SB2011-17 are used for calculating the P-wave interval velocities (km·s^{-1}) shown in the column (Chian and Lebedeva-Ivanova, 2015). Seismic facies are described under Section 2.4.2.

2.3. Methodology

2.3.1. Data Acquisition

Multi-channel seismic (MCS) reflection data used in this study were acquired in 2011 as part of a Canadian-American collaboration using two ice breakers: the Canadian Coast Guard Ship *Louis S. St-Laurent* and the US Coast Guard Cutter *Healy* (Mosher, 2012; Mayer and Armstrong, 2011). The *Healy* broke ice ahead of the *Louis S. St-Laurent* during seismic operations. The seismic source consisted of a cluster of three Sercel GI guns with a combined volume of 1150 in^3. The array was towed 11.5 m below

the sea surface (below the depth of sea ice) and tight against the stern of the ship to protect it from ice. The receiver was a 230 m-long hydrophone streamer and the active section consisted of 16 channels spaced 6.25 m apart. Each channel comprised a group of four hydrophones. The signature of the seismic source yielded a peak power frequency at 45 Hz. Assuming a constant water velocity of 1500 m s^{-1}, the corresponding vertical resolution of the seismic data is ~8 m (assuming the Rayleigh criteria of 1/4 wavelength as detectable resolution). Horizontal resolution is limited by the shot interval and post-stack trace interval. The shot interval was variable because firing was based on time, not distance. Post-stack trace spacing is nominally 25 m. Details of the acquisition system are found in Mosher et al. (2009) and Mosher (2012).

2.3.2. *Seismic Processing and Interpretation*

Details of the seismic processing are provided by Shimeld (2009, 2011). Fig. 2.2 shows the final processed version of the seismic reflection data. Processed SEG-Y files, including geographic position data, were imported into IHS Kingdom Suite seismic interpretation software. Seismic reflection horizons were then mapped/picked based on peak amplitudes. Processed seismic data are sampled at 4 ms (i.e., 6 m at 1500 m s^{-1}), thus the best interpretation resolution is close to the Rayleigh resolution of the seismic data. Vertical offsets indicative of faulting were also mapped. Picked seismic horizons were converted to depth using seismic velocities derived from refraction analysis reported in Chian and Lebedeva-Ivanova (2015). These sonobuoys were deployed during acquisition of the seismic reflection data (see Mosher, 2012) and, therefore, coincide precisely with the MCS profile.
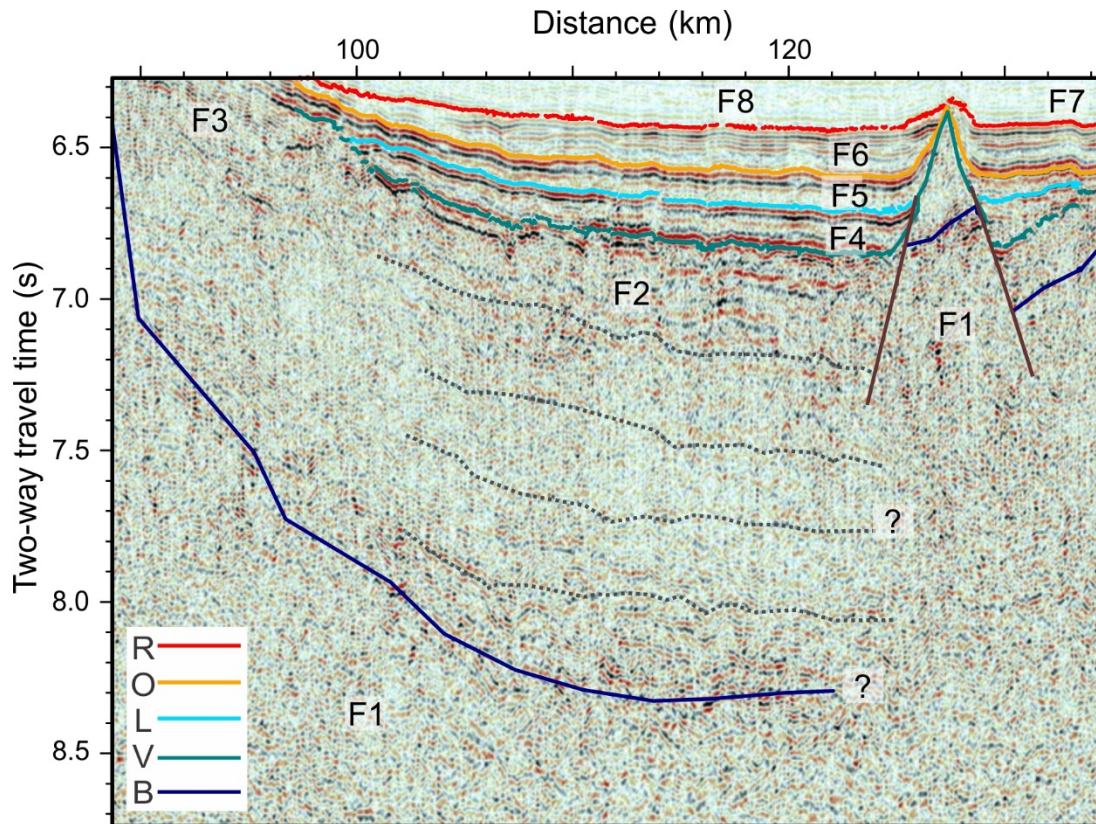
Fig. 2.4. A section of line LSSL2011-04 near Alpha Ridge. Dotted black lines mark semi-coherent reflections in Unit 1. Seismic facies are described under Section 2.4.2.

2.4. Results

The 2011 seismic line LSSL2011-04 is a 400 km-long transect across Makarov Basin from Alpha Ridge in the south to Lomonosov Ridge in the north (Figs. 2.1 and 2.2). The sedimentary section was interpreted by correlating eight seismic reflection horizons and eight seismic facies that were subsequently organized into five seismic units.

2.4.1. Seismic Horizons

The eight picked seismic reflection horizons are labelled B, V, L, O, R, P, Y and S from bottom to top in Fig. 2.2. They represent prominent laterally continuous horizons or horizons of significant change in reflection characteristics (Table 1). With the

exception of horizons P and Y, seismic horizons demarcate boundaries of different seismic facies assemblages.

2.4.2. Seismic Facies

The eight picked seismic reflection horizons are labelled B, V, L, O, R, P, Y and S from bottom to top in Fig. 2.2. They represent prominent laterally continuous horizons or horizons of significant change in reflection characteristics (Table 1). With the exception of horizons P and Y, seismic horizons demarcate boundaries of different seismic facies assemblages.

Seismic facies defined along line LSSL2011-04 are presented in Figs. 2.3, 2.4, 2.5, and 2.6, and described below:

• Facies 1 (F1) represents an amorphous acoustic facies with little coherent energy. Any hint of coherent energy may represent structure, but could also result from multi-path echo returns.

• Facies 2 (F2) consists of bands of reflections with limited lateral continuity (b15 km) featuring medium coherency and low frequencies with high amplitudes that attenuate rapidly with increasing depth. These attributes are highly variable and individual reflections within a specific band may diverge or remain parallel and concordant with an upper boundary.
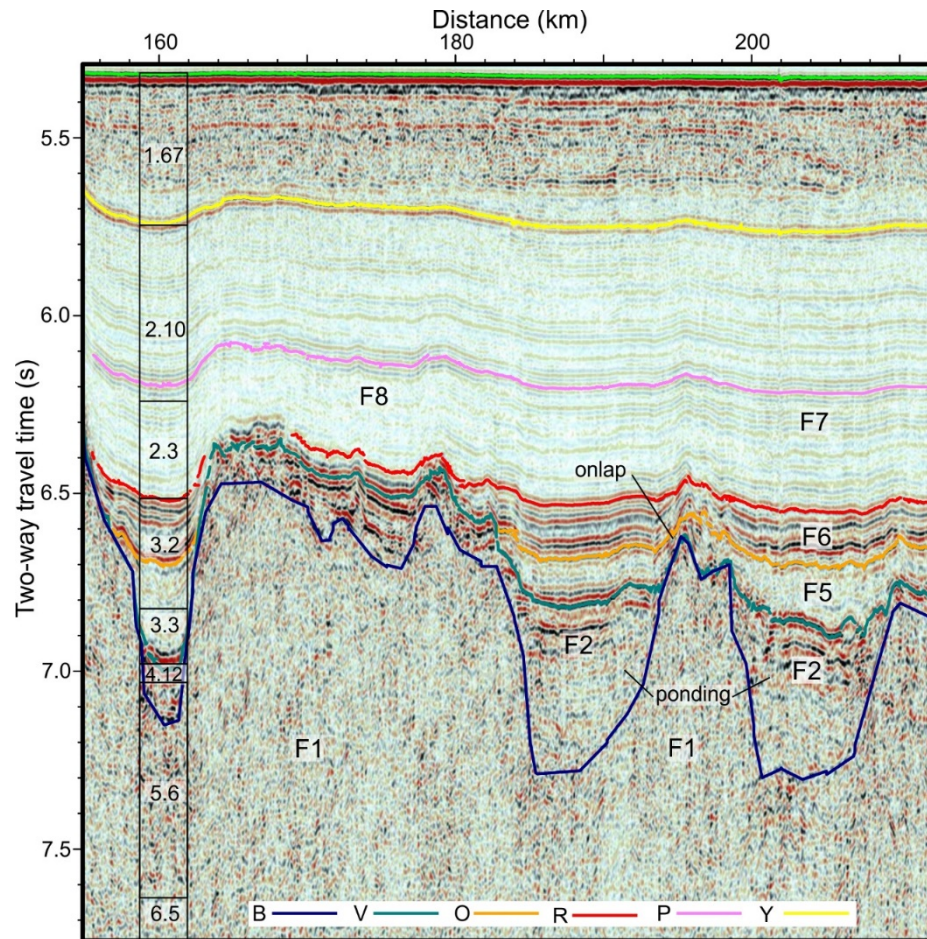
Fig. 2.5. A section of line LSSL2011-04 depicting bands of layered reflections immediately beneath the V horizon. These reflections appear to be ponding in areas of negative relief. Data from sonobuoy SB2011-14 are used for calculating the P-wave interval velocities (km·s^{-1}) shown in the column (Chian and Lebedeva-Ivanova, 2015). Seismic facies are described under Section 2.4.2.

• Facies 3 (F3) comprises low to medium amplitude reflections that dip basinward. The

reflections are moderately coherent and contorted upslope.

• Facies 4 (F4) is defined by stratified reflections with medium to high amplitudes.

Reflections are higher in frequency and are more continuous in comparison with Facies

2. In addition, reflections are crudely concordant with the lower boundary.

• Facies 5 (F5) is represented by stratified reflections with low to medium coherency and amplitude strength. Lateral changes in amplitude characteristics are discerned and reflections are often tilted and/or divergent.

• Facies 6 (F6) consists of a thin band of basin-wide continuous high amplitude reflections with lateral pinch-out terminations. Amplitude strength increases with depth. Reflections are generally concordant with underlying structures.

• Facies 7 (F7) is the most common seismic facies and consists of basinwide continuous high frequency reflections that are stratified and concordant with underlying reflections. Reflection amplitudes are generally low to medium and vary laterally. Lateral coherency also varies.

• Facies 8 (F8) is similar to Facies 7, except that amplitudes are low and continuity is poor. Despite these characteristics, individual horizons trace across Makarov Basin.

2.4.3. Seismo-stratigraphic Units

The eight seismic horizons and eight acoustic facies presented above were used to divide the seismic section into five seismic units. Seismic velocities used for estimating the thickness of units are shown in Figs. 2.3 and 2.4.

2.4.3.1. Unit 0 (Facies 1)

Unit 0 is generally composed of seismic Facies 1,which is incoherent signal. Isolated semi-coherent reflections are, however, distinguishable (Fig. 2.2). The top of the unit, the B horizon, is a rugose surface with excursions in excess of 1 s two-way travel

time (TWTT). Only one of these excursions reaches the seafloor at 152 km along the seismic profile (Fig. 2.2). The base of this unit is undefined.

2.4.3.2. Unit 1 (Facies 2 and 3)

Unit 1 consists of Facies 2 and 3 reflections. The base of the unit, the B horizon, is defined by high-amplitude and semi-coherent reflections that reach depths of 8.2 and 8.8 s TWTT near the Alpha and Lomonosov ridges, respectively (Fig. 2.2). Below the base of slopes, Facies 3 (basinward dipping reflections) grades laterally into Facies 2 or underlies it. Synformal deep reflections also appear truncated by Facies 2 (Fig. 2.3) near Lomonosov Ridge. Unit 1 is as much as 1800 ms TWTT (approximately 2.5–3 km) thick in the deep subbasin (Fig. 2.3) adjacent to the base of slope of this ridge. The dimensions of Unit 1 are not as clearly defined beneath the base of slope of Alpha Ridge, but semi-coherent reflections are identified (Fig. 2.4). Maximum thickness reaches 1400 ms TWTT — seismic velocities that would allow depth conversion are poorly constrained in this region. In Makarov Basin, the B horizon is commonly mapped along the base of bands of semi-coherent reflections (Facies 2) in sections of low relief. Lateral terminations suggest ponding beneath topographic lows of the V horizon (Fig. 2.5).

2.4.3.3. Unit 2 (Facies 3 and 4)

Facies 4 dominates in this unit, except on the flank of Lomonosov Ridge where Facies 3 (dipping reflections) is present. Similar to Unit 1, dipping reflections beneath the slope of Lomonosov Ridge (Facies 3) grade laterally into horizontal reflections (Facies 4). The basal contact shows abrupt truncations of reflectionswhere relief on horizon V is

rugged and downlap/onlap relationships where relief is smooth (Fig. 2.3). The V and L horizons are the bottom and top boundaries of Unit 2, respectively. The thickness of this unit is as much as 450 ms TWTT (750 m).

2.4.3.4. Unit 3 (Facies 5)

Unit 3 lies between the **L** horizon, or **V** if **L** is not present, at its base, and the **O** horizon at its top. It consists mainly of seismic Facies 5. Unit 3 is normally less than 280 ms TWTT (420 m) thick, except in a buried valley located between 266 and 277 km along line LSSL2011-04 (Fig. 2.3), where it reaches 1000 ms TWTT (1500 m). Its thickness strongly correlates with relief along the **B** or **V** horizons. Unit 3 reflections onlap against Unit 1 (where present), and are either truncated or lap against the **V** horizon (Fig. 2.5).

2.4.3.5. Unit 4 (Facies 6, 7 and 8)

The bottom and top boundaries of Unit 4 are horizons **O** and **S** (seafloor), respectively. This unit is further subdivided by the R horizon into a lower Unit 4a and an upper Unit 4b. In addition, horizons P and Y are embedded within the upper subunit. Units 4a and 4b generally range in thickness from 100 to 170 ms TWTT (120 to 200 m) for Unit 4a, and 640 to 920 ms TWTT (780 to 1000 m) for Unit 4b. Thicknesses are substantially less in sections of pronounced relief along the **V** horizon and at the edges of the basin. Seismic facies 6, 7 and 8 consist of stratified continuous reflections— amplitude strength and coherency distinguishing the three facies. Unit 4a consists exclusively of Facies 6. Facies 7 and 8 are interbedded within Unit 4b and also laterally

grade into each other (Fig. 2.5). There is a conformable relationship between units 3 and

4. Reflections in this unit onlap against the edges of the basin. Evidence of major

deformation is absent from this unit.

2.4.4. Alpha and Lomonosov Ridges

Most seismic horizons mapped across Makarov Basin cannot be readily traced to

the top of Alpha and Lomonosov ridges; reflections truncate at the edge of the basin or

onlap and offlap the ridges resulting in pinch-out and condensed sections (Fig. 2.2). As a

result, seismic reflection horizons were correlated between the ridges and Makarov Basin

by matching reflection patterns (Fig. 2.6A).
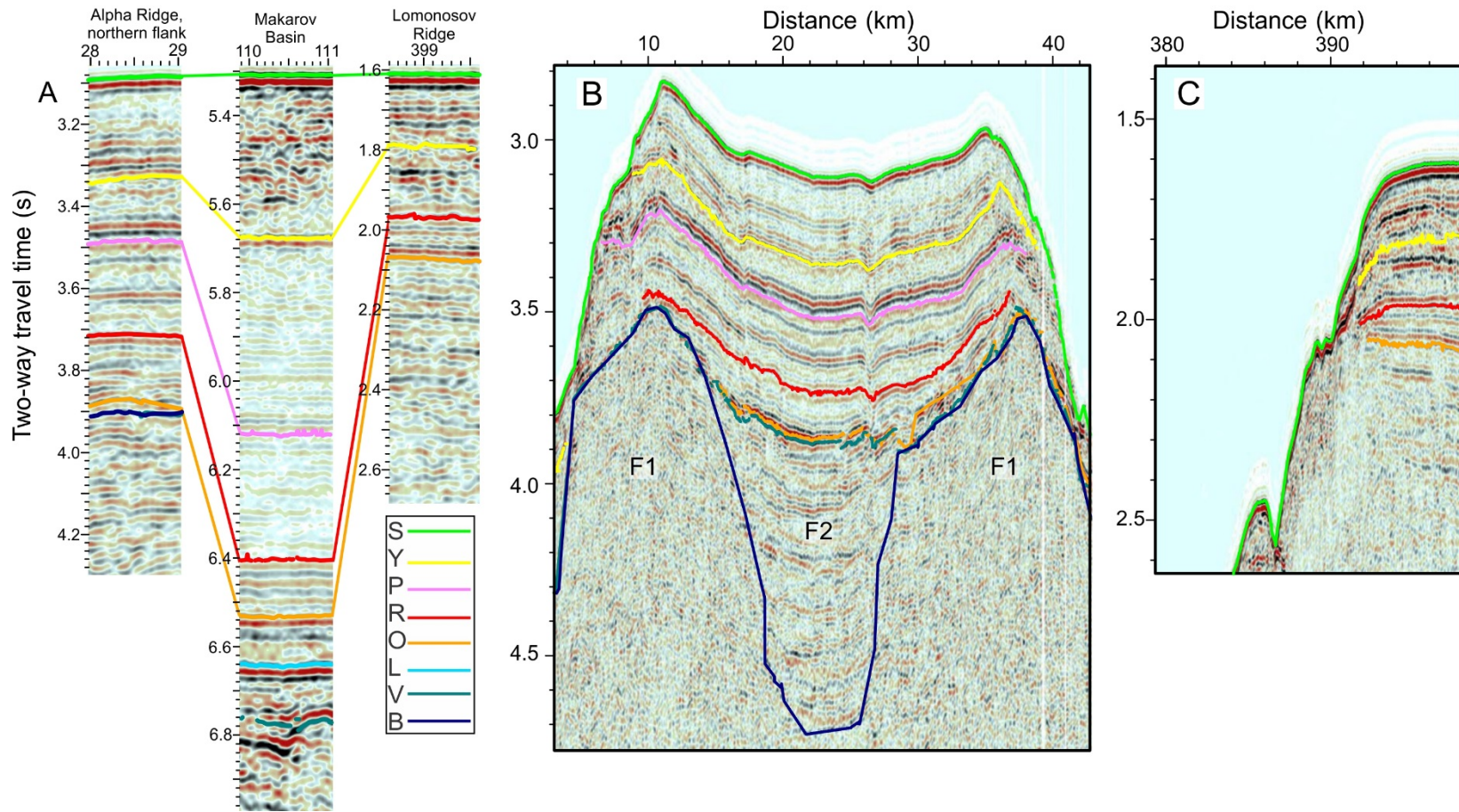
Fig. 2.6. Sections of line LSSL2011-04 showing A) seismo-stratigraphic correlation between Alpha Ridge,Makarov Basin and Lomonosov Ridge, B) and C) the sedimentary drape over Alpha Ridge and Lomonosov Ridge, respectively. Note ponding beneath the V horizon, in B). Seismic facies are described under Section 2.4.2.

On Alpha Ridge, ponding of Facies 2 reflections, beneath the V horizon, is observed between 16 and 30 km along the seismic profile (Fig. 2.6B). Shallow reflections, above the O horizon are concordant with respect to underlying relief similar to Facies 7 and 8 of Makarov Basin. An erosional surface or post-depositional deformation are not observed in the shallow seismic section of Alpha Ridge.

Line LSSL2011-04 extends about 6 km over the crest of Lomonosov Ridge (Fig. 2.6C). Reflections below the O horizon are concordant with overlying reflections. Shallow reflections on Lomonosov Ridge are horizontal, except where they terminate at the ridge flank. The data show a thin drape on Lomonosov Ridge relative to Alpha Ridge.

2.4.5. Physiography

The seafloor of Makarov Basin is almost 4000 m deep, which is typically 200 m deeper than Canada Basin (Jakobsson et al., 2012). As revealed in high resolution subbottom profiler data (Chirp), the seafloor dips gently to the north on average (Fig. 2.7). The basin is about 300 km wide in a north–south direction and 400 km wide in its east to west orientation. Arlis Gap is a restricted connection with Podvodnikov Basin (Fig. 2.1). Unusual bends in the strike of Lomonosov Ridge near the point of the North Pole have long been recognized (Lane, 1997; Cochran et al., 2006). The bends offset the position of the top of Lomonosov Ridge from a straight line projection by more than 100 km and hosts an intra-ridge basin with a length of 140 km and a width of 25 km (Fig. 2.1). The segment of Lomonosov Ridge that is closer to North America appears blocky with a generally flat-lying crest that lies at depths of 500 to 1600 m and plunges

northward. Minimum depths along the Siberian segment of the crest vary from 700 to 1700 m. For most of its length, the width of the Lomonosov Ridge varies from 50 km to 100 km between the 2000 m isobaths. Slopes along the Amerasian flank of Lomonosov Ridge are steep (4 to 8°), straight and laterally continuous (Fig. 2.8), as opposed to slopes on the Amundsen Basin-facing flank that appear segmented (i.e., not a continuous slope).

Marvin Spur is a small ridge feature that sub-parallels Lomonosov Ridge and extends into Makarov Basin. The minimum depth of Marvin Spur is ~1500 m. The spur plunges towards the centre of Makarov Basin where it disappears below sedimentary cover at 87.8° N and 176.1° E. The gap between Marvin Spur and Lomonosov Ridge narrows from 90 km near the centre of Makarov Basin to 30 km close tothe North American shelf. Towards the Siberian Shelf, Oden and Geophysicists spurs and other small ridges are observed fanning out of the Amerasian flank of Lomonosov Ridge (Fig. 2.1). Alpha and Mendeleev ridges are as shallow as 1100 m water depth; nearly 2900 m above the abyssal plain of Makarov Basin. The width of Alpha Ridge is highly variable; in general, it narrows from 600 km near the Canadian Polar margin to less than 200 km near Arlis Gap, where it abuts Mendeleev Ridge. Its length from the Canadian Polar margin to the centre of the depression between Alpha and Mendeleev ridges is 1100 km. The morphology of Alpha Ridge is complex with many irregular ridges and troughs that are short in length (<150 km). The orientations of these features are crudely parallel to the overall trend of Alpha Ridge. Slopes from Alpha Ridge into Makarov Basin are highly variable but generally less steep than those from Lomonosov Ridge (<6°).
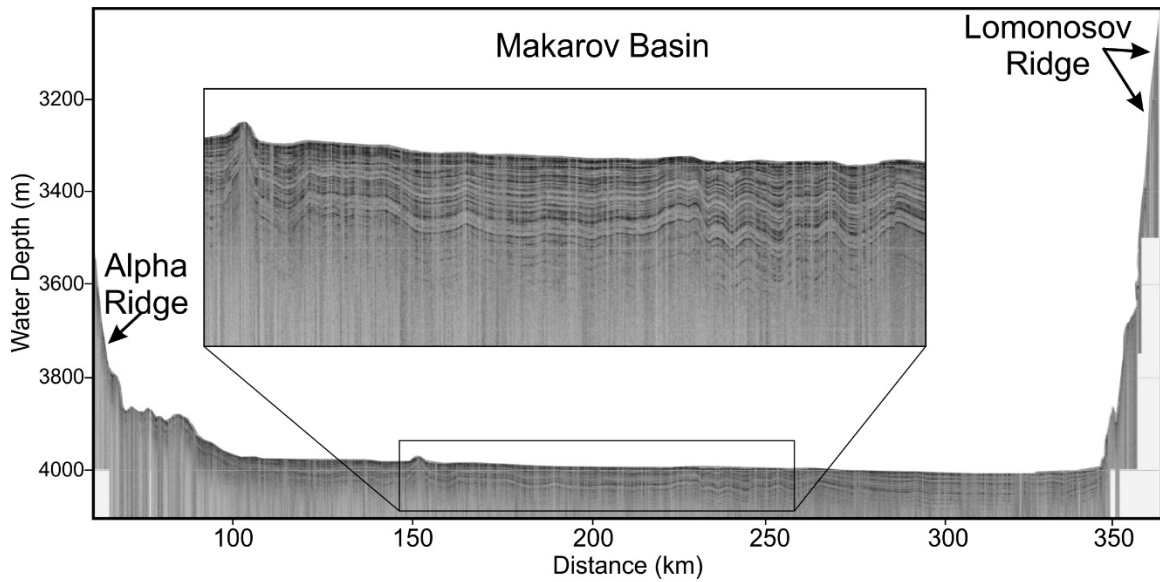
Fig. 2.7. Chirp subbottom profiler across Makarov Basin from Alpha Ridge (left) to Lomonosov Ridge (right). This line is coincident with the seismic line show in Fig. 2.2. Depth conversions were made assuming a water velocity of 1500 m s^{-1}.
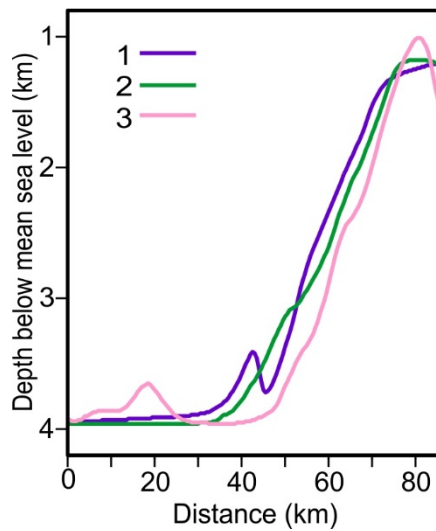
Fig. 2.8. Three bathymetric cross-sections from Makarov Basin (left) to Lomonosov Ridge (right) are shown. Location of lines shown in Fig. 2.9.

45

2.5. Interpretations

2.5.1. Seismic Interpretation

2.5.1.1. Unit 0

Unit 0 is part of the geological basement. This unit includes large volumes of magmatic material based on its acoustic characteristics (Facies 1), rugose nature of the top surface (horizon B) and proximity to the Alpha-Mendeleev ridge complex. Pinnacle-type structures that are part of this unit (e.g., 152 km along line; Fig. 2.2) are interpreted as volcanic edifices similar to those described in northern Canada Basin (Shimeld et al., 2016). We attribute the existence of these edifices to the Alpha-Mendeleev LIP. The nature of isolated semi-coherent energy in this unit is unclear, but we speculate that it represents lithological contacts of igneous origin (e.g., sills or volcanic layering), although it could be due to acoustic artefacts.

2.5.1.2. Unit 1

The stratified, high amplitude and semi-continuous character of Facies 2 reflections suggests that the upper part of this unit is composed of interbedded layers of volcanogenic and sedimentary material. The volcanogenic layers may represent volcanic flows, sills or volcaniclastic sediments, as they appear to infill low areas beneath horizon V (top of volcanics). Alternatively, their high amplitudes may result from post-depositional alteration. Sediment samples from similar acoustic horizons were recovered in 2010 from the top of a seamount in north central Canada Basin by shallow coring (Edwards et al., 2010). Recovered material included hydrothermally altered sediments

with high acoustic velocities. In this case, the high amplitude reflections may be due to hydrothermal alteration by warm fluids emanating from the underlying volcanics. In the deep subbasin (Fig. 2.3), Facies 3 reflections are interpreted as prograding slope sediments, agreeing with conclusions made by Kristoffersen et al. (2007) on the nearby AWI 91 lines (Fig. 2.1). Synformal reflections near the base of Lomonosov Ridge (Fig. 2.3) appear cross-cut by Facies 2 reflections, which suggest that those sediments were deposited during the early stage of opening of Makarov Basin. Unit 1 near Alpha Ridge is interpreted as a thick sequence of volcanic-dominated strata. Any sedimentary layers present are likely minor, as suggested by the poor coherency of corresponding reflections (Fig. 2.4).

2.5.1.3. Unit 2

Facies 3 of Unit 2, on the flank of Lomonosov Ridge, grades into Facies 4 within the deep subbasin adjacent to Lomonosov Ridge. As with Unit 1, these facies represent prograding slope sediments. Upslope contorted reflections of Facies 2 are indicative of slumping along the flank of Lomonosov Ridge, and are equivalent to the slump units that Kristoffersen et al. (2007) describe. Unit 2 is interpreted as being composed of slope and base of slope sediments.

2.5.1.4. Unit 3

Unit 3 infills many of the small basins formed by the dramatic basement relief. Faint reflections terminate laterally against units 0 or 1. Unit 3 reflections do not correlate to the flank of Lomonosov Ridge, but are rather concordant with underlying structure.

These two characteristics suggest that sediments were deposited primarily by hemipelagic or pelagic processes.
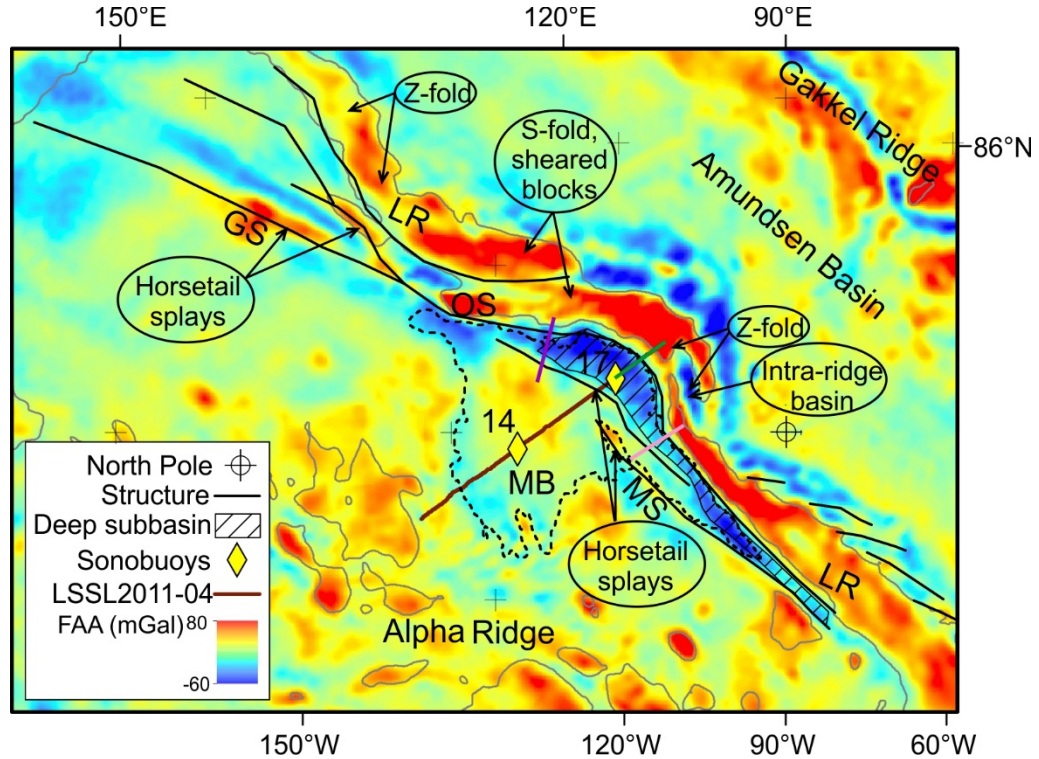
Fig 2.9. Colour-shaded free air anomaly (FAA) gravity map of Makarov Basin and surrounding areas is shown with structural interpretations overlain. Acronyms are defined in Fig. 2.1. The dashed black line and thin solid grey lines are the 3700 m and 2000 m bathymetric contours, respectively. Gravity values are from the compilation of Andersen et al. (2010).

2.5.1.4. Unit 4

Unit 4 is the thickest and most consistent sequence within Makarov Basin, accounting for the majority of the sedimentary stratigraphy. In Unit 4a, the higher amplitudes of Facies 6 reflections are attributed to changes in lithology as a result of possible turbidite deposition, or a siliceous phase of pelagic sedimentation. In Unit 4b, the stratified and concordant character of facies 7 and 8 are inferred to represent hemipelagic to pelagic sediments. The undulating nature of the seafloor and shallow

sediments is also emphasized in the subbottom profiler data (Fig. 2.7), reflecting the topography of deeper structure.

2.5.2. Alpha and Lomonosov Ridges

Based on the interpretation that Alpha Ridge was heavily affected (if not created) by a large igneous province, the basement of the ridge is assumed to be dominantly composed of igneous material. Similar to Makarov Basin, Facies 2 on Alpha Ridge is interpreted as volcanic and/or volcaniclastics. On Lomonosov Ridge, reflections below the **O** horizon (Cenozoic–Mesozoic unconformity; Jokat et al., 1992) were interpreted as sedimentary successions of Mesozoic or older age (Jokat et al., 1992; Grantz et al., 2001). The drape sections of Alpha and Lomonosov ridges correlate with Unit 4 from Makarov Basin, and are similarly interpreted as pelagic to hemipelagic sedimentary strata.

2.5.3. Morphological and Structural Analysis

The flank of Lomonosov Ridge, dropping into Makarov Basin, forms a steep and straight slope (Fig. 2.8). This morphology contrasts with its opposite flank into Amundsen Basinwhich is block-faulted and stepped (Jokat et al., 1995; Cochran et al., 2006). This latter morphology is common to rifted passive margins (e.g., Scotian margin; Keen and Potter, 1995), while the straight steep flank into Makarov Basin is characteristic of transform or strike-slip margins (e.g., Lorenzo and Wessel, 1997; Basile and Allemand, 2002).

Another notable difference between the two flanks of Lomonosov Ridge is the existence of smaller sub-parallel ridges on the Amerasian side that are not present on the

opposite side. A seismic reflection profile acquired along 81° N reveals buried basement horst" structures in Podvodnikov Basin that were interpreted as fragments of continental basement linked to the Lomonosov Ridge margin (Jokat et al., 2013). These structures are probably the buried extensions of Geophysicists Spur and other adjacent marginal ridges (cf. Figs. 2.1 and 2.9). Closer to the Canadian Polar margin, line LSSL2011-04 reveals a buried structural high at ~280 km along the line (Fig. 2.3). Bathymetry, gravity and seismic crossings by ice station NP-28 suggest that this basement structure is a distinct linear ridge between Marvin Spur and Lomonosov Ridge (Figs. 2.1 and 2.9; Figs. 3 and 5 in Langinen et al., 2009). Basile and Brun (1999) show that horsetail splays develop in the vicinity of the intersection between transform and divergent boundaries. Within the horsetail splay, block rotations about vertical and horizontal tilting axes lead to the formation of a surface slope perpendicular to the slope of the divergent basin, explaining the formation of tilted marginal ridges (e.g., Geophysicist Spur) at transform margins. In the context of our study, Geophysicists Spur, and nearby smaller ridges, and Marvin Spur, and its neighbouring ridges, are interpreted as two distinct sets of splay structures.

A distinguishing characteristic of Lomonosov Ridge is its prominent bends along its long axis (Figs. 2.1 and 2.9). The bend about the point of the North Pole forms a Z-fold. The segment of the ridge hosting an intra-ridge basin (Belov Trough) is adjacent to splay structures (Marvin Spur), and is interpreted, therefore, as a releasing bend. Lomonosov Ridge then bends back, forming a S-fold centred on the segment where two flat-topped blocks appear sheared (near Oden Spur). This segment is interpreted as a restraining bend. The ridge then bends again before bending back to resume its original strike orientation. This last part is once more shaped like a Z-fold and is adjacent to splay

structures (Geophysicists Spur and other small ridges), suggesting another releasing bend close to the Siberian Shelf (Fig. 2.9). The sinusoidal form of Lomonosov Ridge and the co-existence of extensional and compressional features along its Amerasian flank imply dextral strike-slip deformation (Christie-Blick and Biddle, 1985; Basile and Brun, 1999; Noda, 2013).

The area between the basement structure (~280 km along line LSSL2011-04) and Lomonosov Ridge forms a deep narrow subbasin on seismic profile — deeper than the remainder of Makarov Basin (Fig. 2.2). The continuation of this subbasin is confirmed by multiple seismic crossings (e.g. Langinen et al., 2009) and its rhomboid shape is outlined by a gravity low (Fig. 2.9). This form is described by Mann et al. (1983); Basile and Brun (1999) and Noda (2013) as characteristic of pull-apart basins (grabens) in a transform margin setting. In addition, sandbox modelling of a transtensional system predicts the development of dual depocentres along the fault zone (Wu et al., 2009), which may be analogous to the deep subbasin and the nearby intra-ridge basin (Fig. 2.9). Basile and Brun (1999) show that horsetail splays are also associated with pull-apart basins in large displacement transform settings.

The complex morphology of Alpha Ridge is (Fig. 2.1) is likely controlled by volcanic edifices (Vogt et al., 2006) and extension (Miller and Verzhbitsky, 2009; Bruvoll et al., 2010; Chernykh et al., 2015). It is not clear, however, if the troughs and ridges that characterize the morphology of Alpha Ridge are related to extensional/transtensional stresses during formation of Makarov Basin, or if Alpha Ridge represents a later magmatic event.

Fig. 2.10. The chrono-stratigraphic chart shows seismo-stratigraphic correlations between ACEX (Backman et al., 2006), Podvodnikov Basin (PB: Weigelt et al., 2014), Makarov Basin (MB1: Langinen et al., 2009; MB2: this study) and Arctic tectonic events. Note that time scales for the Cretaceous and Cenozoic periods differ.

2.6. Discussion

2.6.1. Age Model

Regional Arctic stratigraphies have been advanced for Lomonosov Ridge (Backman et al., 2006, 2008), Alpha and Mendeleev ridges (Bruvoll et al., 2010), Podvodnikov Basin (Weigelt et al., 2014) and Makarov Basin (Langinen et al., 2009) (seismic tracks shown in Fig. 2.1). In order to assign ages to our stratigraphy, we

correlated seismic horizons with regional tectonic events and ACEX cores from the top of Lomonosov Ridge (Backman et al., 2006, 2008; Figs. 2.1 and 2.10). Line LSSL2011-04 crosses the AWI 91 lines, which were used to locate the ACEX drill sites, but only at the base of slope of Lomonosov Ridge. As such, the steep slope and thin sediment cover along the flank of the ridge make direct correlation speculative.

The age and affinity of basement (Unit 0) beneath Makarov Basin is not well constrained. According to the rotational model of Grantz et al. (2011), opening of Amerasia Basin, including Makarov Basin, commenced about 195 Ma and was complete by 127.5 Ma. That would place a minimum age of 127.5 Ma for basement rocks within Makarov Basin, if they are original crust formed during creation of the basin. Alternatively, Døssing et al. (2013) interpreted magnetic anomalies close to the Canadian Polar margin as seafloor spreading anomalies. According to their preferred reconstruction models, the oldest magnetic chrons in Makarov Basin in this area are between M16n and M11An.1n (~138–132 Ma) or M9n and M4n (~129–126 Ma) (Fig. 2.10). Embry and Dixon (1994) correlate the end of spreading with a regional Cenomanian unconformity (100–93.9 Ma), assuming Makarov Basin formed contemporaneously with the rest of Amerasia Basin (Fig. 2.10).

The oldest sedimentary rocks of Makarov Basin are clastic sediments deposited on the slope and base of slope of the Mesozoic Barents Shelf (now Lomonosov Ridge), and preserved in units 1 and 2 (deep subbasin; Fig. 2.3). A network of channels on the Barents Shelf, such as exists today, likely supplied these sediments to the slope and to Makarov Basin prior to separation of Lomonosov Ridge from the Barents Shelf (Fig.

2.1). Indeed, the sedimentary record of the Barents Sea shows a drop in relative sea-level and the emergence of the Barents Shelf during the Late Cretaceous to Early Cenozoic (Faleide et al., 1993), providing a sediment source for the deep subbasin. The rest of Unit 1 is dominated by volcanogenic material, which we assume is related to emplacement of the Alpha-Mendeleev LIP. The minimum age of Unit 1, therefore, should coincide with the age of latest magmatism of the igneous province (Fig. 2.10). For this purpose, we rely on a basaltic sample retrieved at the top of volcanic rocks on adjacent Alpha Ridge (PS51/040-1; Fig. 2.1). Jokat et al. (2013) date this sample at 89 ± 1 Ma using 40Ar/39Ar isotopic dating techniques. This age nearly agrees with the 80 ± 2 Ma Rb/Sr age of Hansen Point volcanics found on nearby Ellesmere Island (Estrada and Henjes-Kunst, 2004).

Unit 2 sediments were also predominantly sourced from the Mesozoic Barents Shelf; thus, this unit predates rifting and formation of the Eurasia Basin. This source of sediment would be eliminated after separation of Lomonosov Ridge. Initial rifting possibly dates to the mid–Late Cretaceous (Drachev, 2011), or as late as 58 Ma (Glebovsky et al., 2006).

The base of Unit 3, horizon L, coincides with the end of the Barents Shelf as a source of sediment for Makarov Basin (Fig. 2.10). Langinen et al. (2009) do not identify the unconformity coincident with the change in sediment supply, probably due to the limited resolution of the NP-28 seismic line. This important marker is interpreted in the AWI 2008 data (Weigelt et al., 2014; Fig. 2.10); however, due to the proximity of the Siberian Shelf with their seismic track, the acoustic character of underlying (MB1) and

overlying (MB2) units are markedly different from contemporaneous units from Makarov Basin.

The band of prominent reflections (Facies 6) that characterize Unit 4a is observed throughout the high Arctic Ocean (Weigelt et al., 2014). In the AWI 91 lines from Lomonosov Ridge (Fig. 2.1), this band of reflections is defined as seismic unit LR 3 (Jokat et al., 1995). The synthetic seismogram representing Unit 3 from the ACEX core matches well with LR 3 (Backman et al., 2008). Lithologically, Unit 3 is described as a silty clay interval hosting warm water microfossils (Moran et al., 2006) and spans from 56.2 to 49.7 Ma (Backman et al., 2008). Similar to the approach of Langinen et al. (2009), we jump-correlate the unit representing the band of prominent reflections with Unit 3 from ACEX (Fig. 2.10). The upper tens of metres of this core interval "contains silica that has been altered to cristobalite" (Moran et al., 2006). The base of ACEX Unit 3 is assumed to correlatewith an erosional unconformity observed in the AWI lines (Jokat et al., 1995). It is not clear, however, if rocks immediately overlying this unconformity (hiatus) were sampled as recovery was not continuous between ACEX units 3 and 4 (Backman et al., 2006; Fig. 2.10). As such, the O horizon, base of Unit 4, is potentially older. Its assigned age does, however, approximately correspond with the initiation of spreading in Eurasia Basin (Glebovsky et al., 2006; Fig. 2.10).

The remaining sequence of Unit 4 is also jump correlated to ACEX units 1 and 2. The R horizon correlates with the base of ACEX Unit 2, which is biostratigraphically dated at 49.7 Ma (Backman et al., 2008). As recorded by the appearance of biosiliceous ooze, ACEX Unit 2 documents the transition to freshwater and relatively cool conditions

in the Arctic Ocean (Moran et al., 2006). ACEX Unit 1 includes an Eocene to early

Miocene hiatus (44.4–18.2 Ma). In Makarov Basin, the absence of a conspicuous basin-

wide erosional surface at the appropriate depths and greater overall thickness of Unit 4

implies that sedimentation was continuous in Makarov Basin during this hiatus. Langinen

et al. (2009) similarly concluded that deposition was at least partly continuous in

Makarov Basin during this period. Material eroded off of Lomonosov Ridge during this

period may have deposited in Makarov Basin. Any contribution, however, would be

relatively minor as there is no evidence of thick slope sequences during that time period.

The **P** horizon is visible in the NP-28 line (see Fig. 10 in Langinen et al., 2009). We make

no attempts to constrain the age of this reflection as the corresponding section in the

ACEX borehole is absent. The **Y** horizon correlates with the base of ACEX Unit 1/5,

indicating the end of the Eocene–early Miocene hiatus (Fig. 2.10). This period also

coincides with the onset of enhanced water circulation and ventilated conditions in the

Arctic Ocean (Jakobsson et al., 2007). Langinen et al. (2009) refer to this marker as "d1".

The undisturbed nature of Unit 4 sediments suggests that this layer was deposited after all

major regional tectonic events ceased. Makarov Basin was, therefore, relatively

tectonically inactive after the late Paleocene.
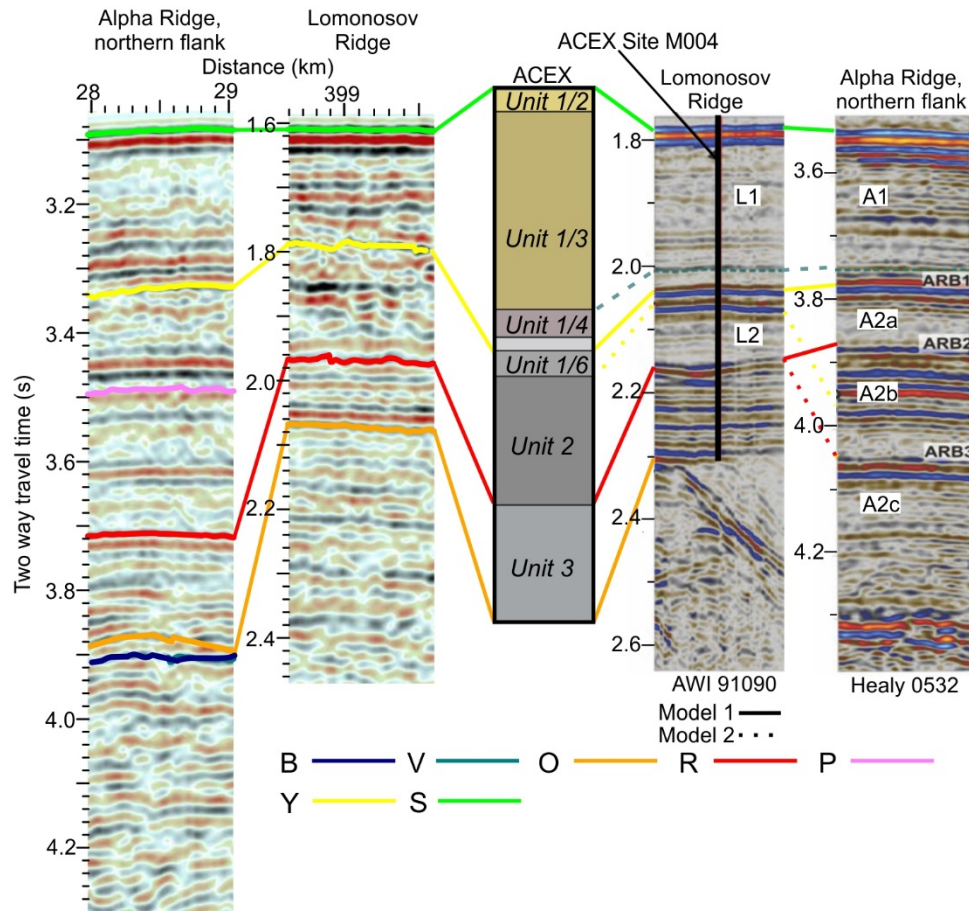
Fig. 2.11. Seismic sections of Alpha Ridge and Lomonosov Ridge from LSSL2011-04 (this study), AWI 91 and Healy 0532 (from Bruvoll et al., 2010) are correlated to ACEX and contrasted. Bruvoll et al. (2010) favoured Model 2 (dotted lines). ACEX column after Backman et al. (2008).

2.6.2. Implications for Amerasia Basin

2.6.2.1. Sedimentary History of Alpha Ridge

Seismic line Healy 0532 was acquired on the northern flank of Alpha Ridge in close proximity to our seismic profile (Bruvoll et al., 2010, 2012; Fig. 2.1). In agreement with our study, Bruvoll et al. (2012) concluded that the high amplitude reflections at or below basement at the Alpha and Mendeleev ridges (horizon V in this study) are caused by volcanic flows, sills and tuff. These layers are inferred to be responsible for the

distinct high amplitude anomalies related to the Alpha-Mendeleev LIP (Vogt et al., 2006; Saltus et al., 2011).

The sedimentary cover over Alpha Ridge must be younger than ~90 Ma based on correlations with Makarov Basin (Fig. 2.6A) and ages from piston core CESAR 6 (Mudie and Blasco, 1985; Fig. 2.1). Unlike with Mendeleev Ridge (Bruvoll et al., 2012) and Lomonosov Ridge (Jokat et al., 1995), a planate surface is not present on Alpha Ridge according to line LSSL2011-04 (Fig. 2.6B) and the contiguous seismic line to the south (Brumley, 2014; Fig. 2.1). As such, the central part of Alpha Ridge was not emergent during the Cenozoic.

The inter-ridge stratigraphic correlation proposed in this study implies that the late Paleocene to early Miocene section (ACEX Unit 3 to base of Unit 1/5) is expanded on Alpha Ridge relative to Lomonosov Ridge. In contrast, the early Miocene to present succession (ACEX units *1/5* to *1/1*) is similar in thickness between the two ridges (Fig. 2.11). The favoured of two age models (Model 2) advanced by Bruvoll et al. (2010) shows the early Eocene marker (base of ACEX *Unit 2*) at similar depths to our study (horizon R). Their Model 2 does not mark the end of the major hiatus (base of ACEX *Unit 1/5*). Both the preferred model of Bruvoll et al. (2010) and the one proposed in this study agree that sedimentation was continuous on Alpha Ridge during the major hiatus (44.4–18.2 Ma) documented in ACEX core.

2.6.2.2. Amerasian Margin of Lomonosov Ridge

Whether the Amerasian margin of Lomonosov Ridge was created by a transform (Cochran et al., 2006) or an Atlantic-style rift system (Langinen et al., 2009; Miller and Verzhbitsky, 2009) is debated. Evidence and interpretations presented above support a transform margin along the Amerasian flank of Lomonosov Ridge, consistent with the rotational model (Grantz et al., 1979, 1998, 2011; Lawver et al., 2002; Shephard et al., 2013). As supported by onshore geological studies in Arctic Russia, however, Miller and Verzhbitsky (2009) asserted that Makarov and Podvodnikov basins formed by rifting of the Lomonosov Ridge/Barents Shelf margin between ~120 and 105 Ma (Albian–Aptian). Also, Gaina et al. (2014) argued that the Late Cretaceous–Cenozoic position of stage poles for opening of the North Atlantic predicts extension perpendicular to Lomonosov Ridge for northern Amerasia Basin. To reconcile opposing explanations for the nature of the Amerasian flank of Lomonosov Ridge, we suggest the margin was initially transform and, as rotation continued, became transtensional and eventually extensional perpendicular to Lomonosov Ridge.

2.7. Conclusions

Makarov Basin of the central Arctic Ocean lies in a critical area to unravel the tectonic and sedimentological history of Amerasia Basin. Newly acquired seismic reflection data and the Arctic bathymetric chart were used to decipher the relationship between Makarov Basin, Alpha and Lomonosov ridges.

Five seismic reflection units describe the basement morphology and sedimentary history of Makarov Basin. The deepest unit (Unit 0) describes geological basement.

Distinction of areas of original basement formed by extension and that formed or magmatically overprinted by the Alpha-Mendeleev LIP is not possible on seismic reflection data alone. Unit 1 is interpreted as mostly volcanogenic material, except in the deep subbasin (~5 km thick) adjacent to Lomonosov Ridge where a mix of volcanic and sedimentary layers is interpreted. The top of Unit 1 is a distinct basin-wide high amplitude reflection which is interpreted as a lithological transition from mixed volcanic and sedimentary rocks to sediment-dominated sequences. This horizon is dated to late-phase magmatism of the Alpha-Mendeleev LIP with a minimum age of ~89 Ma. The primary sediment source for units 1 and 2 is inferred to be the Mesozoic Barents Shelf. This source was disrupted after Lomonosov Ridge rifted from the Barents Shelf. This event may have begun as early as the mid-Late Cretaceous and rifting was complete by 58 Ma. Unit 3 and 4 are composed of hemipelagic to pelagic sediments that infill and drape over underlying structure. Even the topmost sediments reflect deeper surface morphologies indicating pelagic conditions have continued through to the present. These units indicate that Makarov Basin was isolated from sources of sediment by the surrounding Alpha and Lomonosov ridges, with little, if any, sediment sourced from these ridges after the mid-Late Cretaceous. The age of these units was determined by correlation with the ACEX core on Lomonosov Ridge. Similar to the Cenozoic section of Makarov Basin, the drape on Alpha and Lomonosov ridges were formed by pelagic to hemipelagic sedimentation. The significant hiatus in the ACEX core between 44 and 18.2 Ma is not apparent in the seismic reflection records of Makarov Basin or Alpha Ridge. The absence of a planate surface suggests that Alpha Ridge was not emergent during the Cenozoic.

The slope of Lomonosov Ridge into Makarov Basin is steep, straight and laterally continuous. The bend in Lomonosov Ridge forms half of a rhomboid shape adjacent to the deep subbasin within Makarov Basin. A number of ridges (e.g., Geophysicists, Oden and Marvin spurs), found only on the Amerasian side, strike sub-parallel to Lomonosov Ridge. These features are interpreted as splay structures and the bends in Lomonosov Ridge and the deep subbasin are characteristic of pull-apart basins. These features contrast with the stepwise and block-faulted form of the Amundsen Basin-facing flank of Lomonosov Ridge, which is known to be a classic rift margin. Instead, these features are characteristic of a transform/transtensional margin. This interpretation is consistent with the rotational model (e.g., Grantz et al., 2011).We suggest that the initial rotational spreading resulted in a transform/transtensional margin at Lomonosov Ridge (Mesozoic Barents Shelf margin). As spreading continued, the tectonic stress regime became extensional, perpendicular to Lomonosov Ridge. There is no evidence of extension later than the late Paleocene, as implied by the undisturbed character of Cenozoic strata in Makarov Basin.

CHAPTER 3: THE SEDIMENTARY AND CRUSTAL VELOCITY STRUCTURE OF MAKAROV BASIN AND ADJACENT ALPHA RIDGE

Preface

Chapter 3 is a modified version of publication "*Evangelatos, J., Funck, T., Mosher, D.C., 2017. The sedimentary and crustal velocity structure of Makarov Basin and adjacent Alpha Ridge. Tectonophysics 696-697, 99–114*".

Abstract

This study examines the velocity structure of Makarov Basin and the adjacent Alpha Ridge to determine the tectonic origins of these features and link them to the larger Amerasia Basin. Seismic data from sonobuoys distributed along a 650 km-long line extending from Alpha Ridge and across Makarov Basin to the Lomonosov Ridge were analyzed for this purpose. Forward modelling of traveltimes, supported by coincident multi-channel seismic reflection and shipborne gravity data, was used to determine the P-wave velocity structure along the line. The sedimentary cover averages 0.5 km-thick on Alpha Ridge and 1.9 km-thick in Makarov Basin, but reaches up to 5 km-thick at the base of Lomonosov Ridge. Velocities in the sedimentary section range from 1.6 to 4.3 km s^{-1}. As suggested by relatively high velocities, interbedded volcaniclastic or volcanic rock may occur in the deep sedimentary section. The shallow basement of Alpha Ridge (3.3 to 3.6 km s^{-1}) is characterized by semi-continuous high amplitude reflections and is interpreted as volcanic rock possibly intercalated with sedimentary rock. Velocities do not vary significantly in the upper and mid-crustal layers between Alpha Ridge and

Makarov Basin. Total crustal thickness decreases from 27 km beneath Alpha Ridge to 5 km-thick in Makarov Basin then thickens to >20 km over a short distance of 70 km as part of Lomonosov Ridge. The crustal structure of Alpha Ridge is consistent with previous studies suggesting that the Alpha-Mendeleev ridge complex is part of a large igneous province (LIP) with thick igneous crust. The lack of change in crustal velocities between Alpha Ridge and Makarov Basin suggests that the basin, at least partly, either formed during or was influenced by LIP-related magmatism. The rapid transition of crustal thicknesses from Makarov Basin to Lomonosov Ridge supports the interpretation that this section of the ridge is a transform margin.

3.1. Introduction

While recent geophysical studies (e.g., Mosher et al., 2012; Chian et al., 2016; Shimeld et al., 2016) shed light on the evolution of the southern part of Amerasia Basin, the origins of Alpha Ridge and Makarov Basin, in the northernmost part of Amerasia Basin, remain enigmatic (Fig. 3.1). This lack of understanding is in part due to the challenges of data acquisition in this remote ice-covered environment and its complex geology. Attempts at deciphering the crustal affinity of the Alpha-Mendeleev ridge complex have led to contradictory models for its origin. Funck et al. (2011) favour an oceanic origin for the Alpha Ridge based on the apparently homogenous crustal velocity structure of the ridge complex, which is similar to other large igneous provinces. Conversely, Døssing et al. (2013) interpreted sub-linear magnetic anomalies in the southern part of the ridge (near Ellesmere Island) as Late Jurassic–Early Cretaceous dykes intruded into thinned continental crust (Fig. 3.1). The type of crust beneath

63
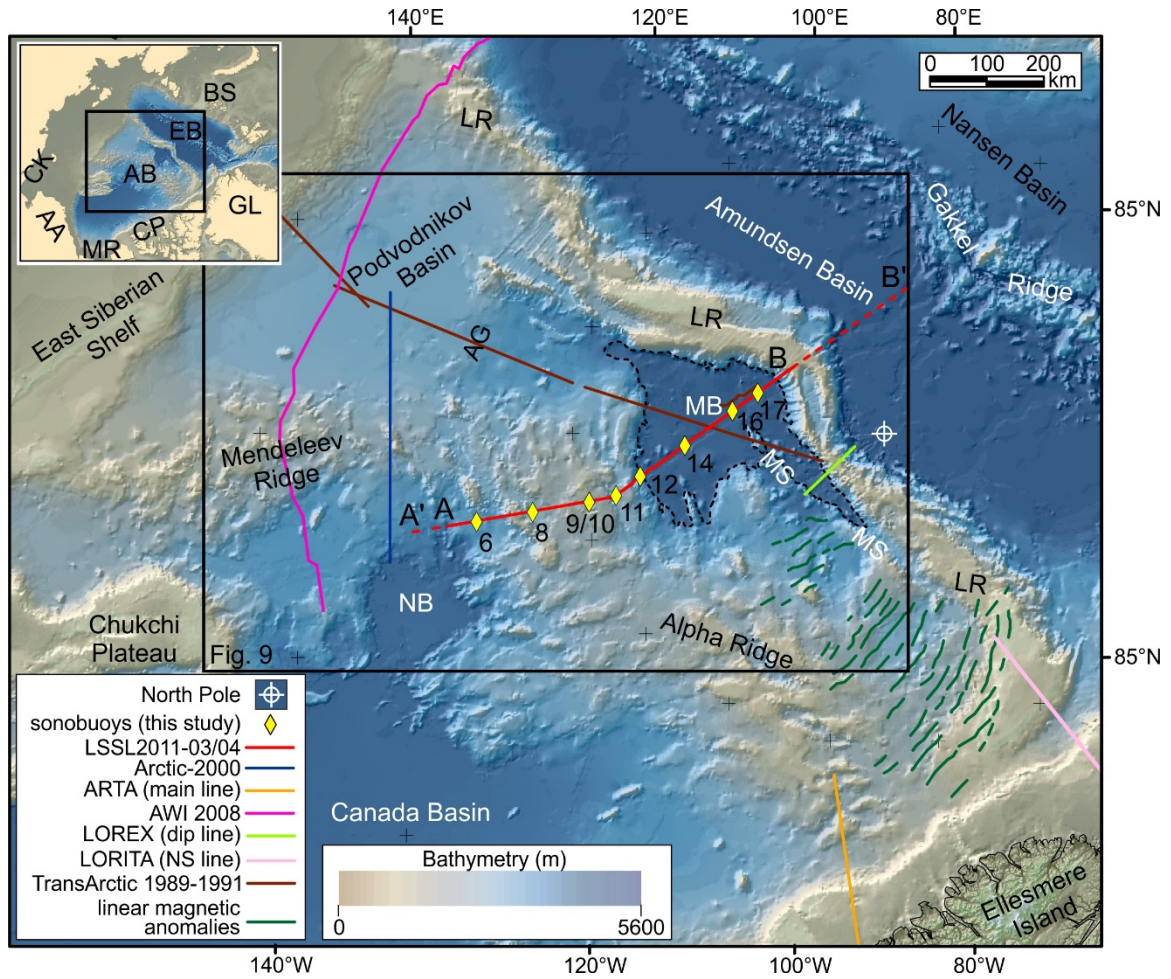
Fig. 3.1. A coloured bathymetric map of northern Amerasia and Eurasia basins. Labels A and B indicate the end points of the seismic profile shown in Figs. 3.4 and 3.5, and labels A′ and B′ are the end points of the gravity model shown in Fig. 3.7. Makarov Basin is delineated by a dashed black line representing the 3700 m bathymetric contour. Acronyms used in this figure and Figs. 3.2 and 3.10 are: AA – Arctic Alaska, AB – Amerasia Basin, AG – Arlis Gap, BS – Barents Shelf, CP – Canadian Polar margin, CK – Chukotka, EB – Eurasia Basin, GL – Greenland, LR – Lomonosov Ridge, MB – Makarov Basin, MR – Mackenzie River delta, MS – Marvin Spur, NB – Nautilus Basin. (Note that several publications, e.g., Jokat and Ickrath (2015), include Podvodnikov Basin as part of Makarov Basin.) Other studies shown in this figure are: Arctic-2000 (Lebedeva-Ivanova et al., 2006), ARTA (Funck et al., 2011), AWI 2008 (Weigelt et al., 2014; Jokat and Ickrath, 2015), LOREX (Forsyth and Mair, 1984), LORITA (Jackson et al., 2010) and TransArctic 1989–1991 (Lebedeva-Ivanova et al., 2011), and linear magnetic anomalies interpreted by Døssing et al. (2013). Bathymetry and elevation are from the International Bathymetric Chart of the Arctic Ocean (IBCAO) version 3.0 grid (Jakobsson et al., 2012). The map projection for this figure and other map figures is North Pole Stereographic with a latitude of origin of 75° N and a central meridian of 90°W.

Makarov Basin is likewise not well known; it may consist of thinned continental crust, as

argued for nearby Podvodnikov Basin (Lebedeva-Ivanova et al., 2011), or of thick

oceanic crust, as argued by Forsyth and Mair (1984). Jokat and Ickrath (2015) concluded

that, along their transect (Fig. 3.1), almost 50% of Podvodnikov Basin is underlain by

extended continental crust of the Lomonosov Ridge. The thinned continental crust terminates against thick igneous crust west of the Mendeleev Ridge.

The objective of this paper is to constrain the origin and relationship between Alpha Ridge and Makarov Basin by studying their sedimentary and crustal structure. To achieve this aim, we rely on new coincident seismic refraction and reflection data supplemented by gravity data. The distribution of data along a line that covers both the Alpha Ridge and Makarov Basin offers the opportunity to address some of the uncertainties regarding the interpretation of these submarine features and thus improve our understanding of the geological history of the Amerasia Basin.

3.2. Geological Setting

Amerasia and Eurasia basins are the two major deep-water basins comprising the Arctic Ocean (Fig. 3.1). Lomonosov Ridge separates the two basins, extending from the North American shelf off Ellesmere Island and Greenland to the Siberian Shelf. The continental origin of Lomonosov Ridge is confirmed by various investigations (Karasik et al., 1971; Sweeney et al., 1982; Backman et al., 2008; Jackson et al., 2010). Lomonosov Ridge was once part of the palaeo-Barents Shelf, but rifted and drifted away from the shelf in the early Palaeogene due to the opening of Eurasia Basin (Lawver et al.,
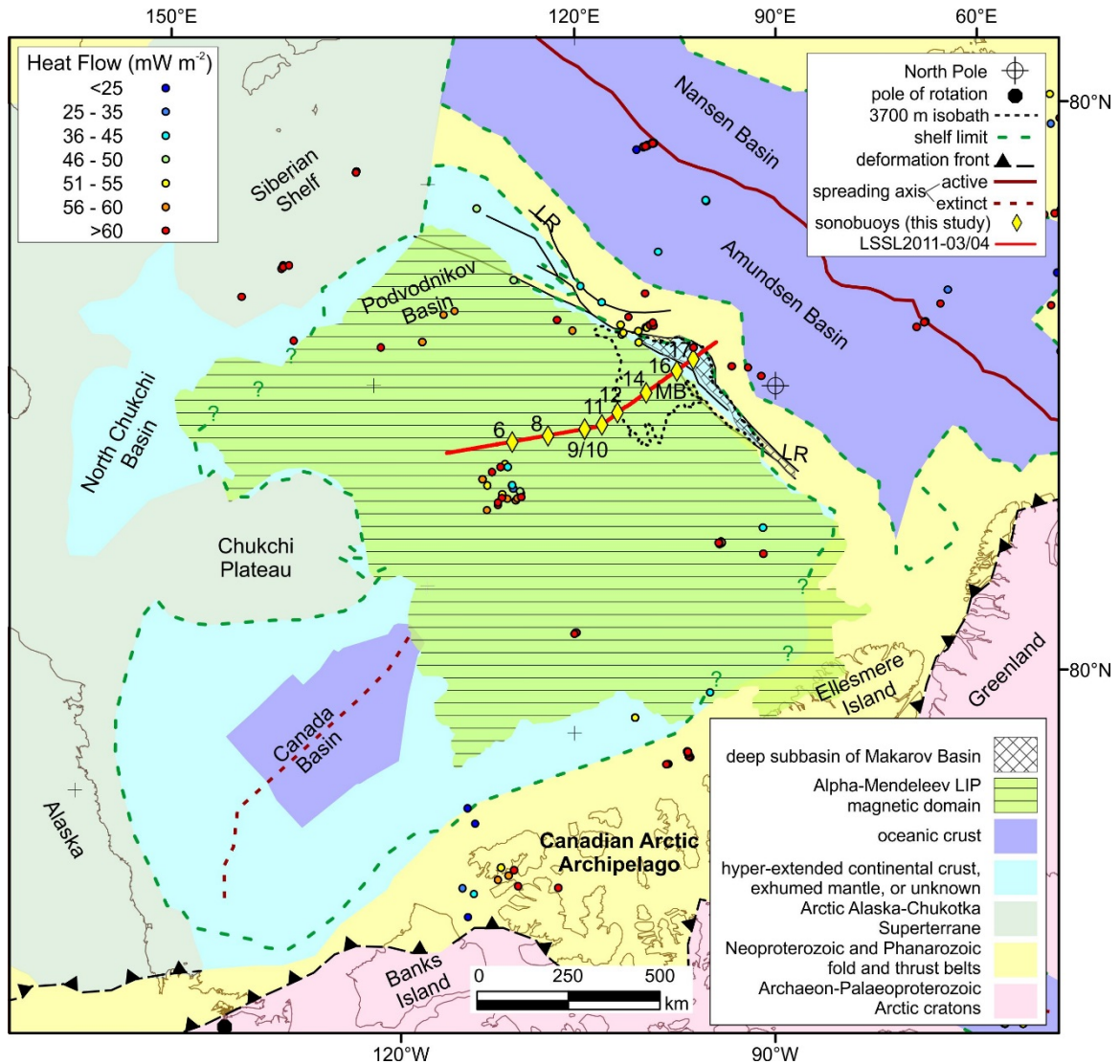
Fig. 3.2. Simplified tectonic map of the Arctic Ocean (after Pease et al., 2014). Other sources shown in the figure are: marine heat flow data (data available at http://www.heatflow.und.edu; see also Pollack et al., 1993), pole of rotation for opening of Amerasia Basin (Grantz et al., 1979), sonobuoys and seismic line LSSL2011-03/04 (this study), 3700 m isobath produced using the IBCAO version 3.0 grid (Jakobsson et al., 2012), deep subbasin of Makarov Basin (Evangelatos and Mosher, 2016), Alpha-Mendeleev LIP magnetic domain (Saltus et al., 2011) and oceanic crust in Canada Basin (Chian et al., 2016).

2002; Pease et al., 2014). The evolution of this basin is documented by well-defined

magnetic reversal anomalies (Brozena et al., 2003) associated with Gakkel Ridge, the

active spreading centre (Fig. 3.2). Analysis of the magnetic spreading anomalies indicates

that Eurasia Basin expanded at ultra-slow spreading rates throughout its history (Coakley

and Cochran, 1998; Jokat and Schmidt-Aursch, 2007).

Amerasia Basin is surrounded by the Canadian Polar margin, the Alaskan and

Siberian shelves, and Lomonosov Ridge (Fig. 3.1). Bathymetric and sedimentary basins

within Amerasia Basin include the Canada, Makarov, Nautilus and Podvodnikov basins.

The Alpha-Mendeleev ridge complex and the Chukchi Plateau are also part of Amerasia

Basin. The Alpha-Mendeleev ridge complex extends from the Canadian Polar margin

near Ellesmere Island to the Siberian Shelf, separating Makarov and Podvodnikov basins

from the rest of Amerasia Basin. Makarov Basin is bounded almost entirely by Alpha and

Lomonosov ridges, and is connected to Podvodnikov Basin through the Arlis Gap (Fig.

3.1). The processes that shaped Amerasia Basin and formed the various physiographic

features within the basin are seemingly complex. Consequently, new geoscientific data

are needed to unravel the details of the geological evolution of Amerasia Basin. For

example, unlike Eurasia Basin, the existence of seafloor spreading in Amerasia Basin, as

evidenced by magnetic isochrons, is contested (Vogt et al., 1982; Grantz et al., 2011;

Chian et al., 2016). Such uncertainty has led to numerous plate-reconstruction models for

the origin of Amerasia Basin (summarized in Lawver and Scotese [1990] and Cochran et

al. [2006]). The widely supported "rotational" model, championed by Grantz et al. (1979,

1998, 2011), amongst others, attributes opening of Amerasia Basin to counter-clockwise

rotation of the Arctic Alaska–Chukotka microplate away from the Canadian Polar margin

about a pole of rotation in the area of the Mackenzie River delta (Fig. 3.2). A linear

gravity low that bisects Canada Basin (Laxon and McAdoo, 1994), and is shown in

seismic reflection profiles to coincide with a negative basement structure (Mosher et al.,

2012), is interpreted as an extinct spreading centre (Fig. 3.2). This interpretation supports

the rotational model. The northern extent of this gravity anomaly terminates at the edge

of the magnetic domain associated with the Alpha-Mendeleev Large Igneous Province (LIP) (Saltus et al., 2011; Fig. 3.2).Whether the spreading centre actually terminates at that location or is masked by the LIP is undetermined. The tectonic model of Grantz et al. (2011), supported by morphological evidence presented by Cochran et al. (2006) and Evangelatos and Mosher (2016), suggests it propagated to Lomonosov Ridge.

Alpha Ridge and Mendeleev Ridge form a distinct physiographic entity that spans 1800 km from the Siberian Shelf to the Canadian Arctic shelf off Ellesmere Island. The Alpha-Mendeleev ridge complex is characterized by elevations up to 2000 m above the adjacent Canada and Makarov basins, and its width varies from 200 to 600 km along its length (Fig. 3.1). The ridge complex and surrounding areas exhibit a chaotic pattern of alternating high and low amplitude and short wavelength magnetic anomalies (Gaina et al., 2011). Saltus et al. (2011) defined this region as the Alpha-Mendeleev LIP magnetic domain. These authors suggested a large magnetic thickness based on a pseudogravity transformation. The interpretation of the Alpha-Mendeleev ridge complex as a LIP is supported by basalt recovered in dredges, cores and drilling (Van Wagoner et al., 1986; Andronikov et al., 2008; Jokat et al., 2013; Petrov et al., 2016), its magnetic signature (Vogt et al., 2006) and the seismic velocity structure of its crust (e.g., Funck et al., 2011). Mineral textures from volcaniclastic samples dredged from the Alpha Ridge during the CESAR (Jackson et al., 1985) and HEALY0805 (Mayer and Armstrong, 2008) expeditions indicate shallow-water eruptions (<800 m; Van Wagoner et al., 1986). The origin of these ridges, however, is still not clear (Dove et al., 2010). The recognition of mafic volcanism of Cretaceous age in the circum-Arctic led researchers to include the ridge complex as part of the greater High Arctic Large Igneous Province (HALIP)

(Maher, 2001). While early HALIP-related magmatic suites are predominantly tholeiitic, later magmatism is more alkaline (Tegner et al., 2011). The genetic relationship between these different suites and their connection to Arctic tectonics is not known (Estrada, 2015). Various authors have proposed that a mantle plume, focused offshore of Ellesmere Island, initiated rifting in Amerasia Basin and sustained over ~50 Myr of circum-Arctic magmatism (Embry and Osadetz, 1988; Buchan and Ernst, 2006; Døssing et al., 2013).

The rhomboid-shaped Makarov basin is approximately 300 by 400 km wide. The abyssal plain of Makarov Basin is well-outlined by the 3700 m bathymetric contour (Fig. 3.1) with seafloor depths reaching down to 4000 m. Marvin Spur is a linear ridge in northern Makarov Basin that trends sub-parallel to Lomonosov Ridge (Fig. 3.1). Isolated basement protrusions also occur near Alpha Ridge in the southern part of the basin. Seismic refraction studies (Forsyth and Mair, 1984; Lebedeva-Ivanova et al., 2011) and interpreted magnetic reversal anomalies near the Canadian Polar margin (Døssing et al., 2013) are compatible with normal oceanic crust in Makarov Basin (Figs. 3.1 and 3.2). Cochran et al. (2006), Doré et al. (2016) and Evangelatos and Mosher (2016) showed evidence that Makarov Basin, at least in part, formed as a result of transtensional tectonics adjacent to the palaeo-Barents Shelf (now Lomonosov Ridge) during opening of Amerasia Basin. Based on studies conducted onshore, Miller and Verzhbitsky (2009)
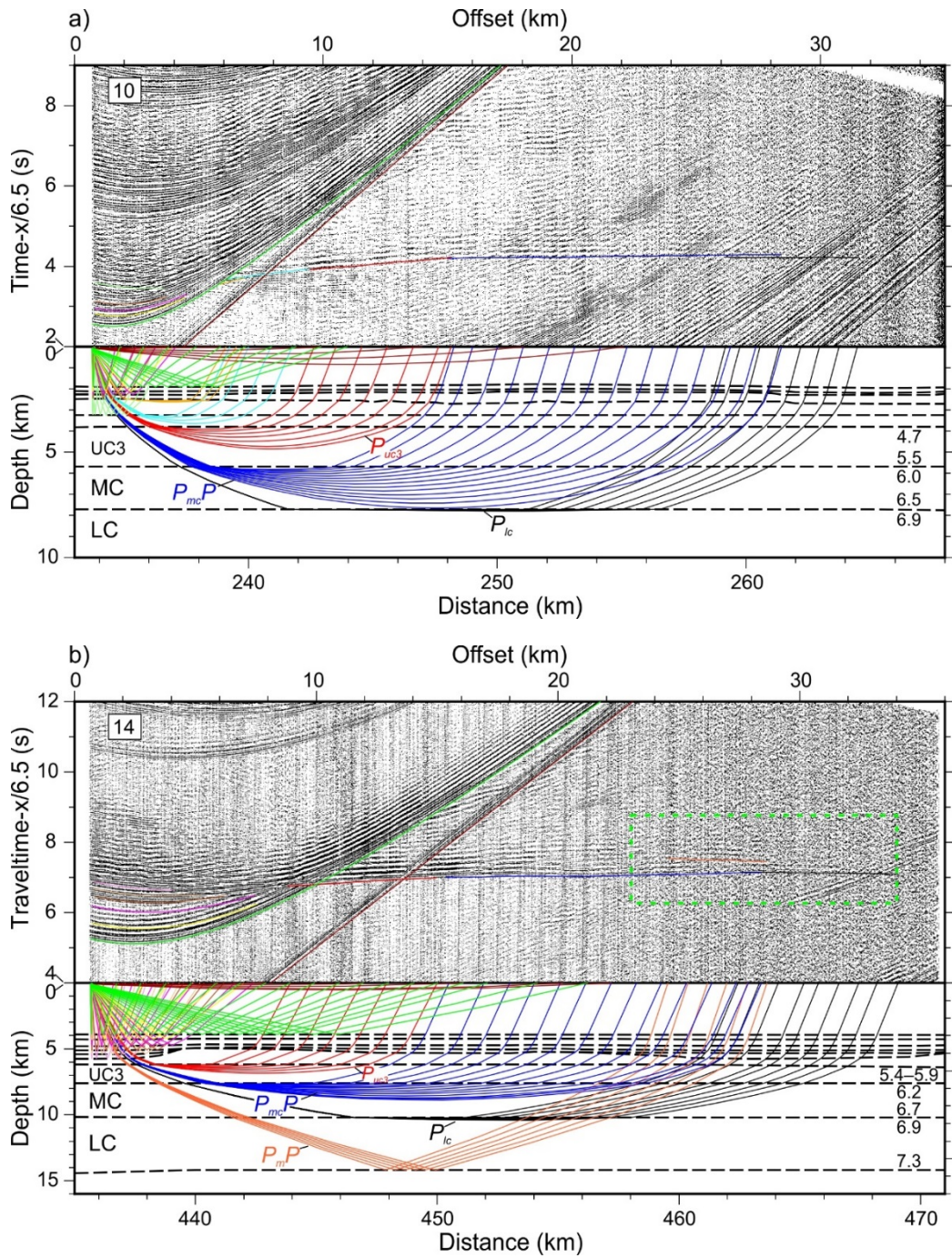
Fig. 3.3. Records and modelling of sonobuoy stations a) 10 (Alpha Ridge), and b) 14 (Makarov Basin) are depicted. The top panels show the seismograms with overlain calculated traveltimes, and the bottom panels outline the raypaths through the velocity model. The green dashed box outlines the portion of station 14 shown in Fig. 3.6. Names and P-wave velocities (km s^{-1}) for select crustal phases and layers are labelled (refer to Section 3.4). Displayed seismic records were band-pass filtered between 4 and 20 Hz. Deployment positions are shown in Fig. 3.1.

argued that the Alpha-Mendeleev ridge complex rifted off the margin of the palaeo-Barents Shelf, thus forming the Makarov and Podvodnikov basins in between these ridges. The results of this study can elucidate the geological connection between these submarine features.

3.3. Methodology

3.3.1. Data Acquisition

Coincident seismic refraction and multi-channel seismic (MCS) data were acquired in Amerasia Basin in 2011 (Mosher, 2012). During seismic operations, data were collected aboard the Canadian Coast Guard Ship *Louis S. St-Laurent*. Meanwhile, the US Coast Guard Cutter *Healy* broke ice ahead of the *Louis S. St-Laurent*. This configuration allowed for continuous seismic acquisition in heavy ice cover (Mayer and Armstrong, 2011; Mosher, 2012; Mosher et al., 2013). Expendable sonobuoys[1] model 53C from Ultra-Electronics, were deployed either off the stern of the *Louis S. St-Laurent* or ahead of the ship via helicopter. Upon deployment, a sonobuoy released a hydrophone that suspended 60m below the water surface. The signals recorded by the hydrophone were transmitted to the vessel by radio and digitally recorded in SEG-Y format. The sonobuoys were not fitted with a navigational device, and, once deployed, drifted freely with the ice pack. The maximum operating time for a sonobuoy is about eight hours, during which the ship generally sailed between 35 and 50 km. Straight lines and a constant ship speed were not possible in heavy ice. Seismic energy was not observed beyond offsets of 27 to 43 km (Fig. 3.3) with the exception of sonobuoy 9 that only had a

---

[1] For brevity, we refer to sonobuoys according to their order of deployment rather than their full name (e.g., SB2011-6 is simply sonobuoy 6; refer to Chian and Lebedeva-Ivanova [2015]).

maximum offset of 19 km. Source energy is inferred to control maximum offsets in Alpha Ridge due to the observation of the direct wave beyond the last recognizable arrival associated with a crustal phase. For Makarov Basin, the maximum offsets for the direct wave and crustal phases are close (<5 km apart), suggesting that radio range is the limiting factor in this case. Fourteen sonobuoys were deployed along a line LSSL2011-03/04 extending from Alpha Ridge and across Makarov Basin to the Amerasian flank of the Lomonosov Ridge (Fig. 3.1). Of those deployments, nine sonobuoy records are included in this study. The five excluded sonobuoys either malfunctioned or returned data only for very short offsets before failing. Water depths along the line range from about 1500 m on Alpha Ridge to almost 4000 m in Makarov Basin.

The MCS data were acquired using a 16-channel digital streamer with a group spacing of 6.25 m. The streamer was 230 m long. The seismic source was arranged as a three-airgun array with a total volume of 1150 in^3 (~19 l). Towed at 11.5 m below sea surface, this configuration yielded a frequency spectrum of 5 to 60 Hz, resulting in a maximum vertical resolution of about 8 m (1/4 wavelength). Firing on distance was not practical in ice. The firing interval was adjusted according to water depth to avoid interference from multiple reflections. This adjustment resulted in a variable firing interval, ranging between 14 and 19 s. Because of the irregular geometry and shot interval, traces were gathered into bins of 25×25 m intervals along a curved line for MCS stacking. Processing of the MCS data is described in Shimeld (2011) and Mosher et al. (2013).
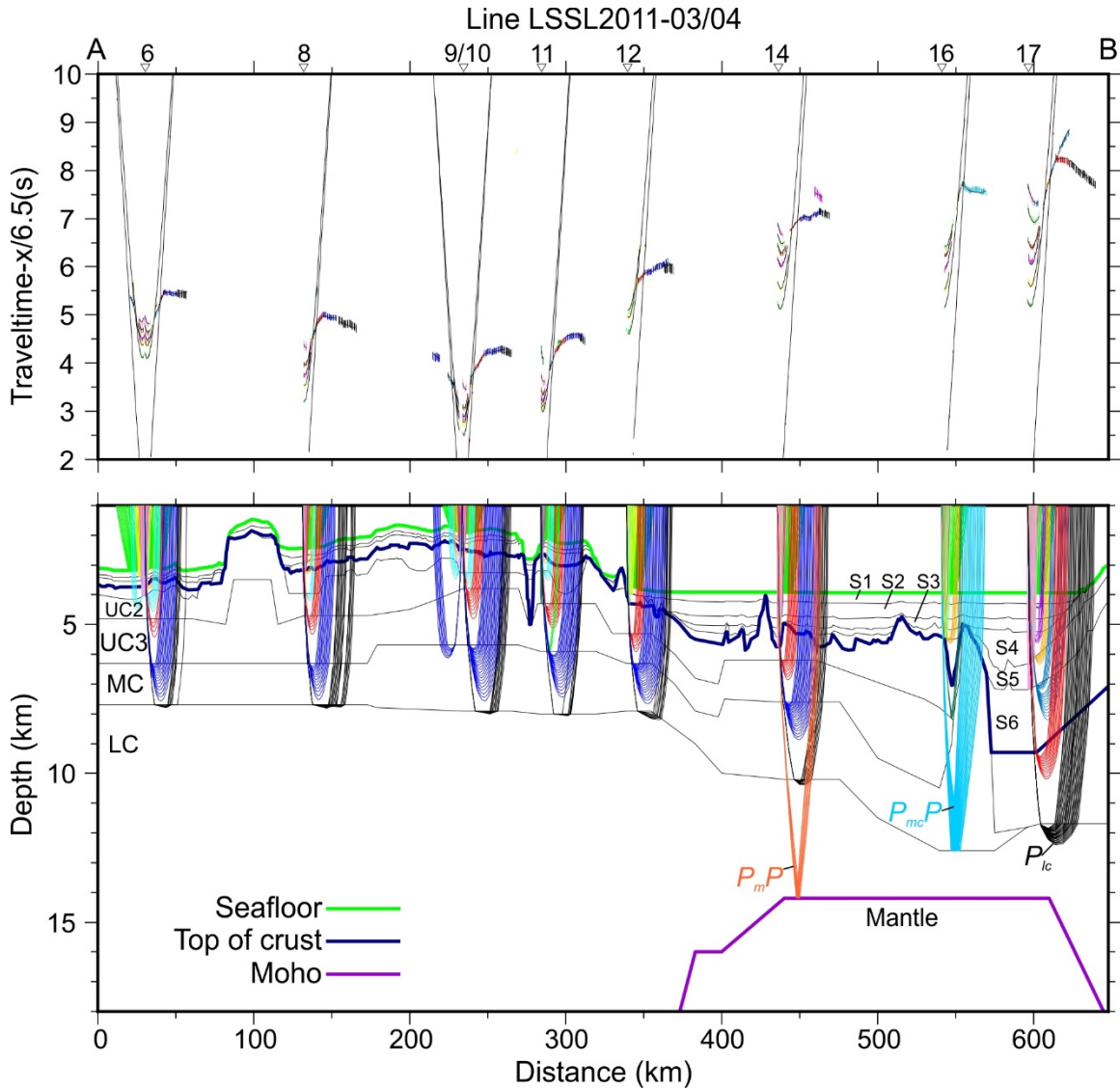
Fig. 3.4. (Top panel) observed traveltime picks are shown with the calculated traveltimes overlain. Traveltime picks are represented by vertical error bars. (Bottom panel) raypath diagrams from velocity modelling. Labels for select phases and layers are shown (refer to Section 3.4).

In addition to the seismic acquisition system, both the *Louis S. St-Laurent* and the *Healy* were equipped with Bell BGM-3 gravimeters. Gravity data recorded on board the *Louis S. St-Laurent* are less affected by noise. This result is because the *Healy* typically broke ice ahead of the *Louis S. St-Laurent*, thus sustaining significantly more accelerations that led to more noise on the gravimeter on board the Healy. Our study primarily uses gravity data from the *Louis S. St-Laurent* (Mosher, 2012). Further details

on geophysical acquisition are provided in Mosher (2012) and Mosher et al. (2013). The seismic reflection data are publicly available through the Geological Survey of Canada (Mosher et al., 2016).

3.3.2. Seismic Refraction and Gravity Data Processing

Static corrections were applied to the seismic data to account for the trigger/gun firing delay. Data were de-spiked using a spike-zeroing filter (Stanghellini and Bonazzi, 2002). As the sonobuoys were not equipped with a navigational device, the source–receiver offsets were derived using the traveltime of the direct wave. For this correction, we applied the following quadratic equation:

$$X = a + bT + cT^2$$

where X is the offset in km, T represents the traveltime of the direct wave in seconds, and coefficients a, b and c are −0.006, 1.441 and 0.00075, respectively (Lebedeva-Ivanova and Lizarralde, 2011). This formula was empirically derived using CTD (Conductivity, Temperature, Depth) measurements in High Arctic waters. Most records from sonobuoys have a high signal-to-noise ratio.

Barring periods of instrument failure, marine gravity data were acquired continuously during the expedition. The raw data were corrected for Eötvös effects and latitude. The data were then filtered with a 2-min Gaussian moving-window to correct for ship heave and re-sampled at 1 min intervals. Long-term instrument drift was addressed by tying back to an absolute gravity station at the end of the cruise (Mosher, 2012).

Finally, the gravity data were de-spiked with an 8-min median filter and reduced to free-air gravity anomalies.
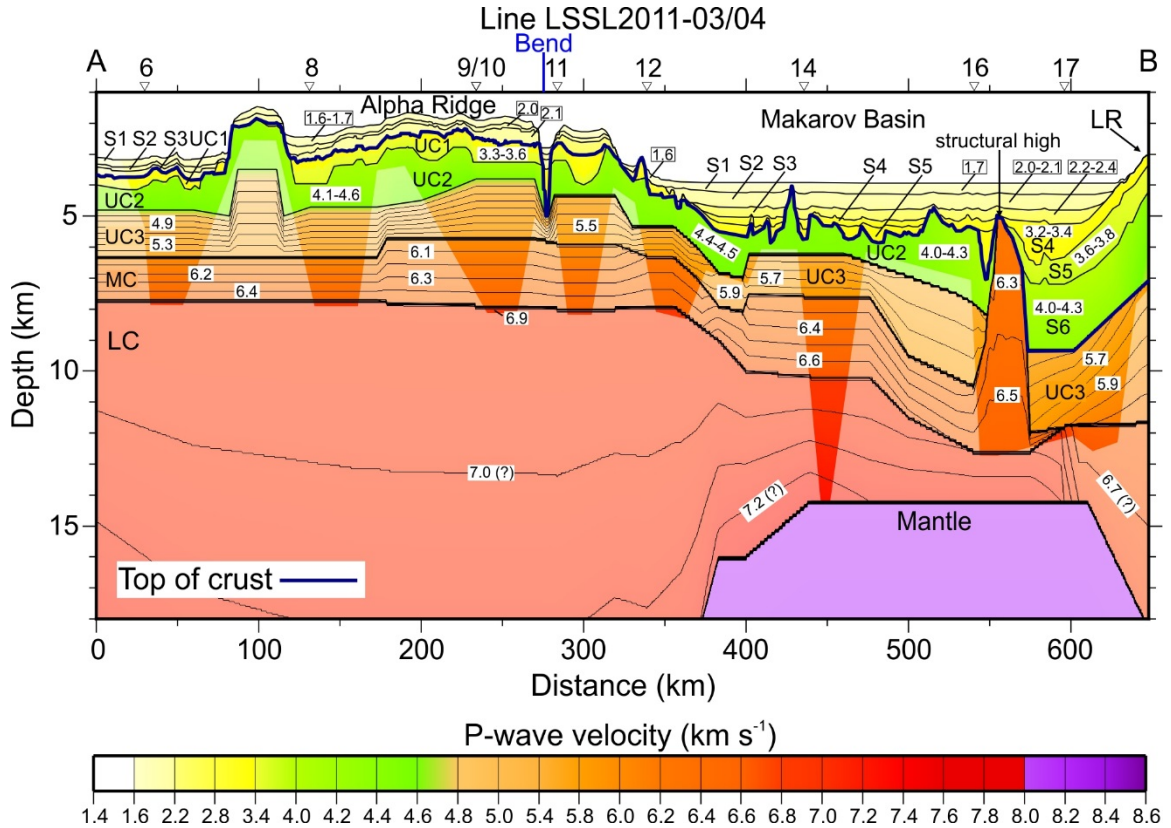
Fig. 3.5. P-wave velocity model for line LSSL2011-03/04. Pale colours indicate sections unconstrained by MCS or data from sonobuoys. Ray coverage is shown in Fig. 3.4. "Bend" marks the location along line LSSL2011-03/04 where the orientation of the line changes (Fig. 3.1). Velocities are specified in km s^{-1}.

3.3.3. Geophysical Modelling

3.3.3.1. Modelling Seismic Velocity

The development of a two-dimensional representation of the subsurface velocity structure requires that the calculated arrival times of reflected and refracted seismic waves, based on the velocity model, match the observed arrival times on wide-angle reflection and refraction data within the range of the data uncertainty. Observed arrival times for the various phases were determined using ZPLOT, a program designed for

interactive picking of traveltimes (Zelt, 1994). Calculated arrival times were derived by forward modelling using RAYINVR, a seismic program developed by Zelt and Smith (1992) that uses the ray-tracing technique. The velocity model divides the subsurface into distinct layers (Figs. 3.4 and 3.5) defined by boundary and velocity nodes. Velocity gradients between nodes are linear.

The sonobuoy position is assumed to be constant; however, variable relief at the seafloor and in subsurface structure can introduce errors as the sonobuoy drifted. If the drift of the buoy is along the shot line, the effects can be corrected by using a variable sonobuoy position in the modelling. However, the drift presumably has an unknown component perpendicular to the line where information on water depth or deeper structures is unavailable. For this reason, only the offset correction between the sonobuoys (source) and the shots (receiver) was applied.

Seismic velocities for a given phase were determined one station at a time and each layer in the velocity model was analyzed in sequence from shallowest to deepest. The final model is the result of multiple iterations (Figs. 3.3, 3.4 and 3.5). Converted shear waves were not included in this study. The depth of the seafloor was measured with a Knudsen 12 kHz echo sounder mounted on the hull of the *Louis S. St-Laurent* (Mosher, 2012). The layer boundaries identified at individual sonobuoys were converted from depth to two-way traveltime (TWTT) to check for correlation with the seismic reflections on the MCS record. Where there is such a correlation, the MCS record was used to define the detailed geometry of these layer boundaries, which would not have been possible with the resolution of the data from sonobuoys alone. Although some coherent signal is

present within basement, seismic reflection imaging was inadequate to resolve upper crustal interfaces. Below the imaging depth of the MCS data, therefore, boundaries were constrained by refraction and wide-angle reflection data and represented as horizontal surfaces. It is difficult to independently assess the geometry of intra-crustal layer boundaries without reversed ray coverage. Near Alpha and Lomonosov ridges, however, relief was added to deeper layer boundaries to fit the free-air gravity anomalies. The crustal velocity structures derived by Funck et al. (2011) (Alpha Ridge), Lebedeva-Ivanova et al. (2011) (Makarov Basin) and Poselov et al. (2012) (Lomonosov Ridge) were used as guides only for early iterations of the velocity structure at deep crustal levels. As there is no overlap in ray coverage between neighbouring stations (Fig. 3.4), the transition in velocity across layer segments is smoothed (Fig. 3.5).

3.3.3.2. Error Analysis of Velocity Model

To quantify the accuracy of the velocity model, a formal error analysis was carried out in which the root-mean-square of the misfit between observed and modelled traveltimes (RMS error) was calculated (Table 1). Uncertainties were assigned to traveltime picks based on visual inspection, which relied on the frequency content of the phase being picked and interfering signal from other phases. Uncertainties ranged from20 ms to 80 mswith an average value of 41 ms. As the signal-to-noise ratio increases with offset, the pick uncertainty increased accordingly. χ^2 quantitatively represents the fit between model and data. The ideal χ^2 is unity (Zelt and Smith, 1992). Values <1 indicate over-fit of the data, but can also be caused by an overestimation of pick uncertainty.

Perfectly fit data have $\chi^2 = 0$. In practice, low values for χ^2 were fairly simple to obtain as the experiment has no reversed ray coverage.

Because uncertainty is not represented entirely by χ^2, uncertainty in velocity and depths to layer boundaries are also estimated by sensitivity analysis. This process involved noting the RMS error of a given phase after systematically varying depth and velocity. This information is used to identify the best values (i.e., pairs with minimum RMS error) for boundary depths and layer velocities and to estimate uncertainty. Table 3.2 lists the uncertainties assigned to the sedimentary and upper crustal layers.
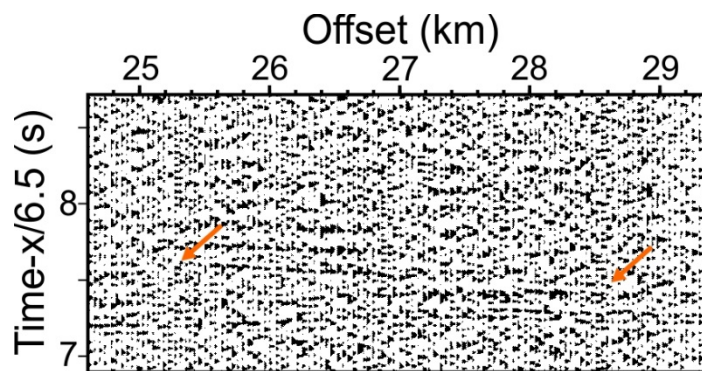
Fig. 3.6. Record from station 14 centred on the *PmP* reflection phase. Orange arrows point to the ends of the phase.

3.3.3.3. Two-dimensional Gravity Modelling

The base of the crust is poorly resolved by the data from sonobuoys (Fig. 3.4). Depth to the Mohorovičić discontinuity (Moho) along line LSSL2011-03/04 is seismically constrained based on P_mP reflections from station 14 (Fig. 3.6). In addition, at the intersection with line TransArctic 1989–1991 (Figs. 3.1 and 3.7), Moho is constrained at a depth of 14.0 ± 1.5 km, as determined by P_mP and P_n phases (Lebedeva-

Ivanova et al., 2011). Elsewhere along the line, Moho depth was adjusted by gravity modelling to fit the long wavelength component of the observed gravity.

Our velocity model was converted to a density model using the empirical relationship derived by Osler (1993) from the work of Ludwig et al. (1970):

$$\rho = -2.83Vp^4 + 70.4Vp^3 - 598Vp^2 + 2230Vp - 700$$

where V_p and ρ are P-wave velocity (in km s^{-1}) and density (in kg m^{-3}), respectively. Mantle density is assumed to be 3300 kg m^{-3}. The gravitational response of the density model is calculated according to the method of Talwani et al. (1959) and then compared with the shipborne gravity (Fig. 7). The density model was extended on either end of the velocity model to account for edge effects (Fig. 1). Seafloor depths were extracted from the International Bathymetric Chart of the Arctic Ocean (IBCAO) version 3.0 (Jakobsson et al., 2012). The observed gravity for the section of the model extending into Nautilus Basin was fit by incorporating seafloor depth, setting sedimentary layer boundaries parallel to the seafloor down to the basement and extending deeper layer boundaries horizontally southward. For the section extending across Lomonosov Ridge and into Amundsen Basin, the model incorporates seafloor depths and seismic data constrain the sedimentary succession and crust (Jokat et al., 1992; Jokat et al., 1995; Weigelt and Jokat, 2001; Jackson et al., 2010; Poselov et al., 2012; Døssing et al., 2014).

3.4. Results and Interpretations

A velocity model representing the earth structure extending from Alpha Ridge through Makarov Basin was developed. It is divided into the sedimentary cover, crust and

mantle (Fig. 5). The distinction between sedimentary cover and crust is largely based on the MCS data. Table 2 lists the velocity range, average thickness and estimated uncertainties of modelled velocity and the top of layer boundaries for sedimentary and upper crustal layers.

Table 3.1. Results of error analysis for the individual phases are listed. n, t_{RMS}, and χ^2 are the number of observed travel-time picks, the root-mean-square difference between observed and calculated travel-times, and normalized χ^2. Column "Identification" describes which stations were defined for a particular phase. P_{water} and $P_{water}P$ are the direct wave (water wave) and seafloor reflection, respectively. All other phases are defined in Section 3.4.

Phase	Identification	N	t_{rms} (s)	χ^2
P_{water}	All	1583	0.022	0.730
$P_{water}P$	All	1685	0.018	0.513
P_{S1}	None	–	–	–
$P_{S1}P$	All	460	0.026	0.460
P_{S2}	17	6	0.026	0.496
$P_{S2}P$	All, except 12	356	0.025	0.284
P_{S3}	8	6	0.037	0.255
$P_{S3}P$	All, except 12	315	0.028	0.337
P_{S4}	17	27	0.030	0.584
$P_{S4}P$	12, 14, 16, 17	183	0.027	0.244
P_{S5}	16, 17	56	0.017	0.152
$P_{S5}P$	14, 17	77	0.027	0.171
P_{S6}	17	74	0.022	0.186
$P_{S6}P$	None	–	–	–
P_{uc1}	6, 8, 9, 10, 11	52	0.032	0.323
$P_{uc1}P$	6, 8, 9, 10, 11	138	0.028	0.260
P_{uc2}	6, 8, 9, 10, 11	177	0.022	0.297
$P_{uc2}P$	11	16	0.026	0.110
P_{uc3}	All, except 9, 16	327	0.025	0.189
$P_{uc3}P$	11	16	0.033	0.318
P_{mc}	All, except 16, 17	649	0.025	0.179
$P_{mc}P$	16	120	0.036	0.372
P_{lc}	All, except 9, 16	471	0.038	0.234
$P_{m}P$	14	37	0.026	0.097
P_{n}	None	–	–	–
All phases	All	6848	0.025	0.436

3.4.1. Sedimentary Layers

MCS reflection data in this study typically recover coherent signals down to 1.5 s TWTT (~1.5 km) below seafloor along Alpha Ridge, and down to 3.5 s TWTT (~5 km) below seafloor in Makarov Basin (Fig. 8). These data clearly resolve the base of the sedimentary cover and the upper parts of the crust. We identify three and six sedimentary layers for Alpha Ridge and Makarov Basin, respectively (Fig. 3.5). Refractive phases for shallow sedimentary layers (P_{s1} to P_{s3}) are typically secondary arrivals. They are difficult to identify because of interference with reverberations of first arrivals. In Makarov Basin, refractive phases for the deep sedimentary layers (P_{s4} to P_{s6}) are first arrivals and, therefore, easier to identify. Layer boundaries constrained by reflective phases ($P_{s1}P$ to $P_{s6}P$) correlate with continuous high amplitude reflections in MCS data.

Velocities in the sedimentary layers range from 1.6 km s^{-1} to 4.3 km s^{-1} (Table 3.2). These velocities are used to convert seismic reflection data from traveltime to depth. Average thickness of the sedimentary cover is 0.5 km for Alpha Ridge and 1.9 km for Makarov Basin with a maximum of up to 5 km near Lomonosov Ridge.

Sedimentary layers S1, S2 and S3 exhibit velocities of 1.6–2.2 kms^{-1} on Alpha Ridge, and 1.6–2.5 km s^{-1} in Makarov Basin. The combined sedimentary thickness for these three layers ranges from 0 to 1.3 km, with the thickest sections found in Makarov Basin. Layers S1 to S3 coincide with seismic reflection facies (Fig. 3.8) that were interpreted as hemipelagic to pelagic deposits (Bruvoll et al., 2010; Evangelatos and Mosher, 2016) and/or distal turbidites (Johnson et al., 1990; Langinen et al., 2009). The drape-like character of these layers supports either of these interpretations.

Table 3.2. General properties of sedimentary layers S1 to S6 and upper crustal layers UC1 to UC3 are listed. Alpha Ridge is from 0 to 340 km along line and Makarov Basin is from 340 to 625 km along line (Fig. 3.5).

Layer	Velocity (km s^{-1})	Average thickness on Alpha Ridge (km)	Average thickness on Makarov Basin (km)	v_{error} (km s^{-1})	d_{error} (km)
S1	1.6–1.8	0.2	0.3	0.1	0.05
S2	2.0–2.2	0.1	0.4	0.1	0.05
S3	2.1–2.5	0.2	0.3	0.1	0.05
S4	2.8–3.4	-	0.3	0.2	0.1
S5	3.1–3.8	-	0.3	0.2	0.1
S6	3.9–4.3	-	0.4	0.2	0.2
UC1	3.3–3.6	0.4	-	0.2	0.1
UC2	4.0–4.6	1.1	1.3	0.2	0.2
UC3	4.8–6.0	1.6	1.5	0.2	0.3

v_{error}: uncertainty of velocity.

d_{error}: uncertainty of top layer boundary.

Sedimentary layer S4 is present only in Makarov Basin (Fig. 3.5). Velocities vary between 2.8 and 3.4 km s^{-1} with an average layer thickness of 0.3 km and a maximum of 1.4 km. The upper part of S4 (above horizon L; Fig. 3.8b) corresponds to units 3 and 4a from Evangelatos and Mosher (2016), who interpreted these units to consist of hemipelagic sediments. The lower part of S4 (below horizon L; Fig. 3.8b) coincides with Unit 2 (Evangelatos and Mosher, 2016) and exhibits basinward dipping reflections that grade into more horizontally stratified reflections at the base of the Lomonosov Ridge. This part of S4 consists mainly of sediments that were deposited in Makarov Basin and on the slope of Lomonosov Ridge while the latter was still connected to the Barents Shelf (Evangelatos and Mosher, 2016).
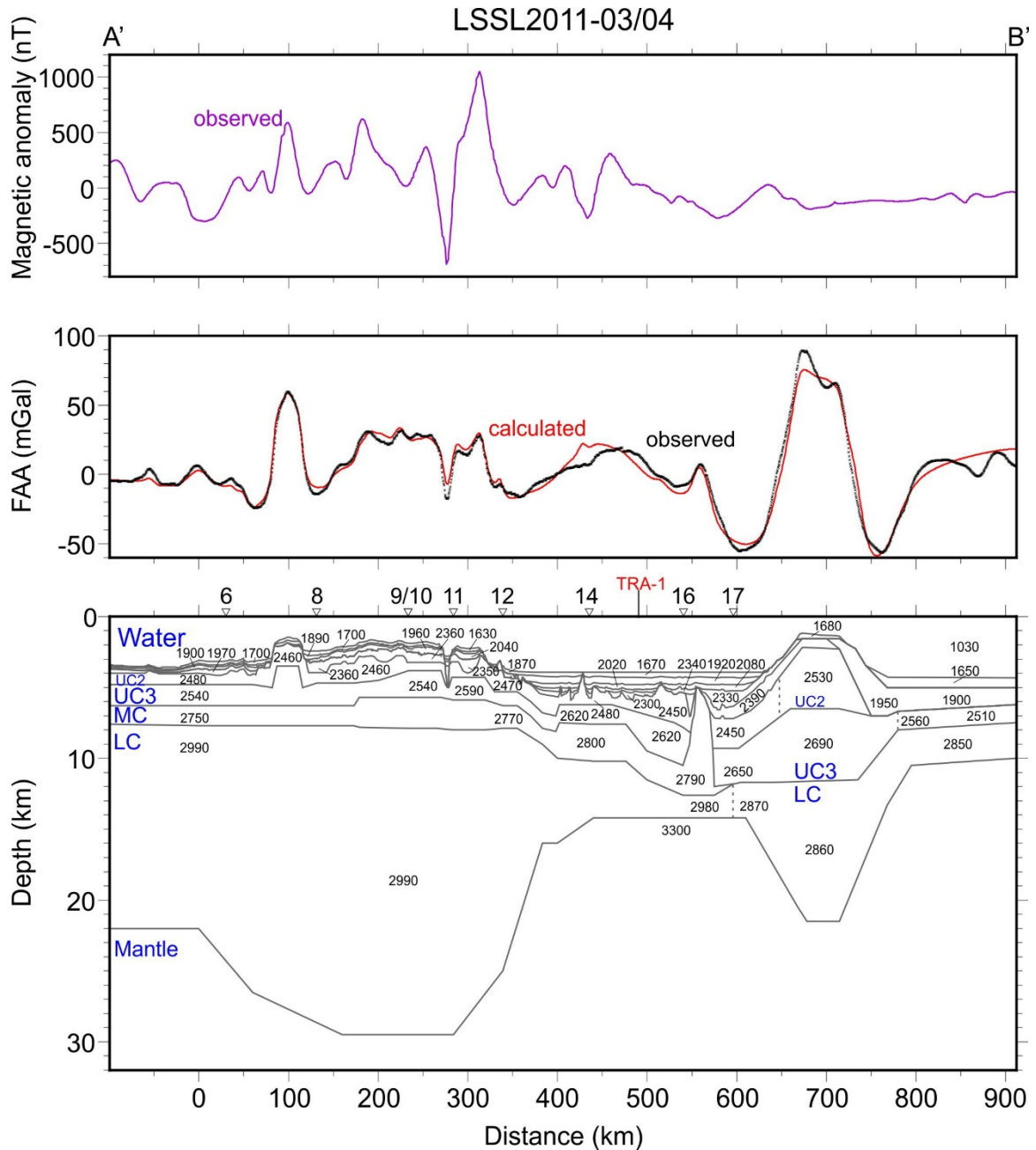
Fig. 3.7. Two-dimensional gravity model for line LSSL2011-03/04. (Top panel) observed magnetic anomaly data extracted from a grid. (Middle panel) observed free-air gravity anomaly (FAA) is compared to calculated gravity. (Bottom panel) subsurface gravity model shown with representative densities specified in kg m^{-3}. "TRA-1" marks the cross-point with line TransArctic 1989–1991 (Fig. 3.10). FAA data are a combination of shipborne gravity (Mosher, 2012) and the compilation of Gaina et al. (2011). Magnetic data are a combination of compilations by Brozena et al. (2003) and Gaina et al. (2011). Refer to Fig. 3.1 for location.

Velocities of 3.1 to 4.3 km s^{-1} were determined for layers S5 and S6 (Fig. 3.5).

These layers are observed mainly in the deep subbasin of Makarov Basin (Fig. 3.8b).

They range in thickness from 0 to 3.4 km with an average of 0.7 km. Layer S5 has high amplitude, semi-continuous and stratified reflections (Fig. 3.8b). Layer S6 is similar, but of lower amplitude and less coherency. The two layers correspond to Unit 1 of Evangelatos and Mosher (2016), and are interpreted as a mix of volcanic and sedimentary material based on their acoustic character.

The base of the sedimentary cover is mapped along a high amplitude reflection that is traceable across line LSSL2011–03/04 (Fig. 3.8). This horizon separates relatively continuous and stratified seismic facies, interpreted as sedimentary layers S1 to S6, from underlying semi-continuous seismic facies that have high amplitudes and poor to moderate coherence (Fig. 3.8). Shallow intra-basement reflections appear offset by faulting.

3.4.2. Upper Crustal Layers

The velocity model of this study distinguishes five crustal layers. Three layers,

UC1, UC2, and UC3, have velocities less than or equal to 6 kms^{-1} and together define the

upper crust. The upper crust is resolved by refractive (P_{uc1}, P_{uc2}, and P_{uc3}) and reflective

($P_{uc1}P$, $P_{uc2}P$ and $P_{uc3}P$) phases.
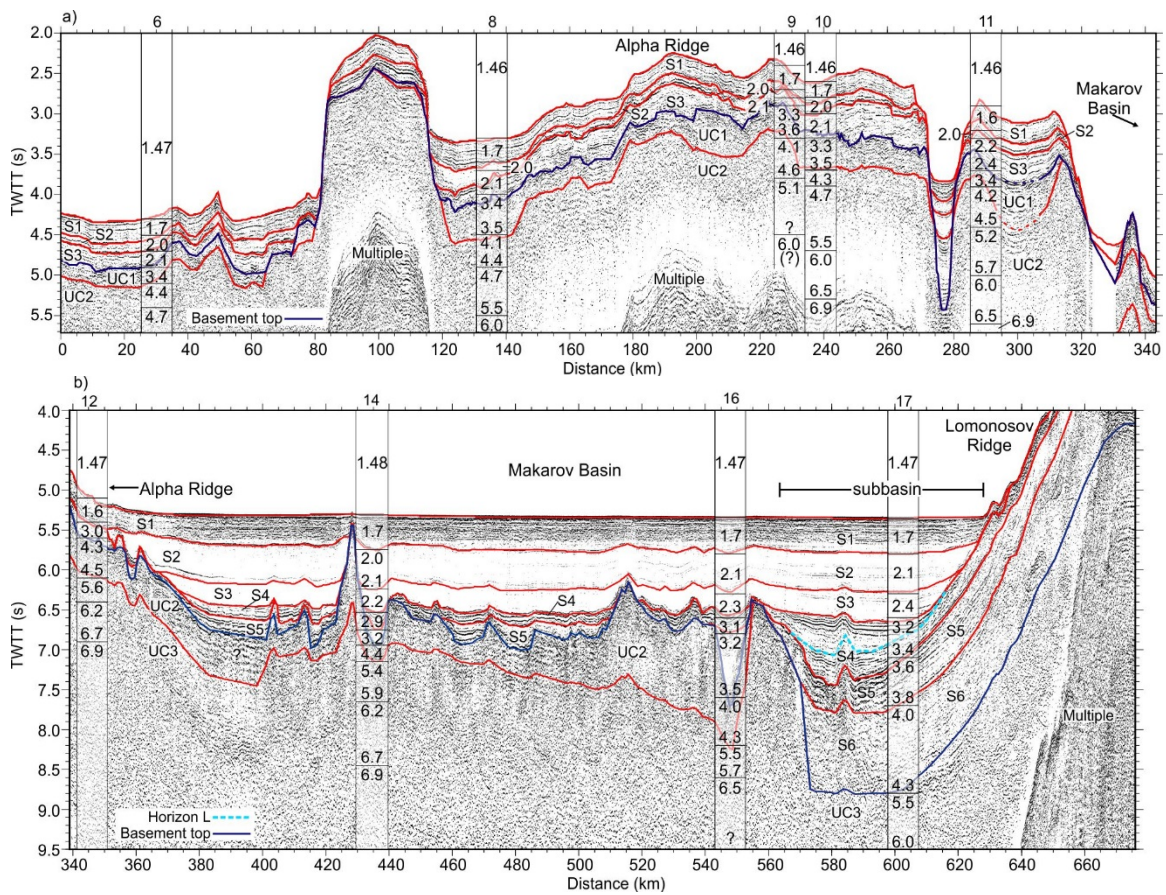
Fig. 3.8. Multi-channel seismic profiles along line LSSL2011-03/04 are shown from a) Alpha Ridge and b) Makarov Basin. Layer boundaries from the velocity model, displayed as red lines, were converted from depth to time. Horizon L demarcates the boundary between units 2 and 3 from Evangelatos and Mosher (2016). Basement top is defined based on changes in acoustic character. Annotations for P-wave velocities are specified in km s^{-1}.

Layer UC1 has an average thickness of 0.4 km and is only observed on Alpha

Ridge. UC2 is present from 0 to 560 km along the line and has a variable thickness of 0.5

to 2.7 km, excluding a filled valley between 272 and 282 km distance along line (Fig.

3.8a). UC3 is the lower part of the upper crust. Its thickness is between 0.8 and 2.8 km.

On Alpha Ridge, velocities for UC1, UC2 and UC3 are 3.3–3.6 km s^{-1}, 4.1–4.6 km s^{-1}

and 4.8–5.6 km s^{-1}, respectively. In Makarov Basin, between 360 km and 560 km along

line (Fig. 3.5), velocities for layers UC2 and UC3 are 4.4–4.5 km s^{-1} and 5.4–6.0 km s^{-1},

respectively. These velocities are derived solely from station 14, as ray coverage in the

upper crust of station 16 is poor. Beneath the deep subbasin (560 to 625 km along line;

Fig. 3.5) and near the slope of Lomonosov Ridge, layer UC3 has a velocity of 5.5–6.0 km

s^{-1}.

Although P-wave velocities for layer UC1 overlap with different types of

sedimentary rock (Sheriff and Geldart, 1995), we suggest that UC1 is composed of

volcaniclastic or volcanic rock possibly intercalated with sedimentary rock. This

interpretation is based on its stratified and semi-continuous seismic character (Fig. 3.8a).

Such seismic facies are interpreted as sills, tuff and/or volcanic flows in other parts of

Alpha Ridge and Mendeleev Ridge (Bruvoll et al., 2012). Recovery of

volcanic/volcaniclastic rocks from shallow coring (Jokat et al., 2013) and dredging

(Mayer and Armstrong, 2012; Mayer et al., 2016) from disparate locations corroborate

this interpretation. Correlation between basement topography and high amplitude

magnetic anomalies at Alpha Ridge (Vogt et al., 1979; Kovacs and Vogt, 1982) implies

that the upper crust is composed of mafic rock, which is typically more magnetic than

felsic rock (Hunt et al., 1995). High porosity in the basalts (Wilkens et al., 1991) may

also contribute to the lower than expected velocities.
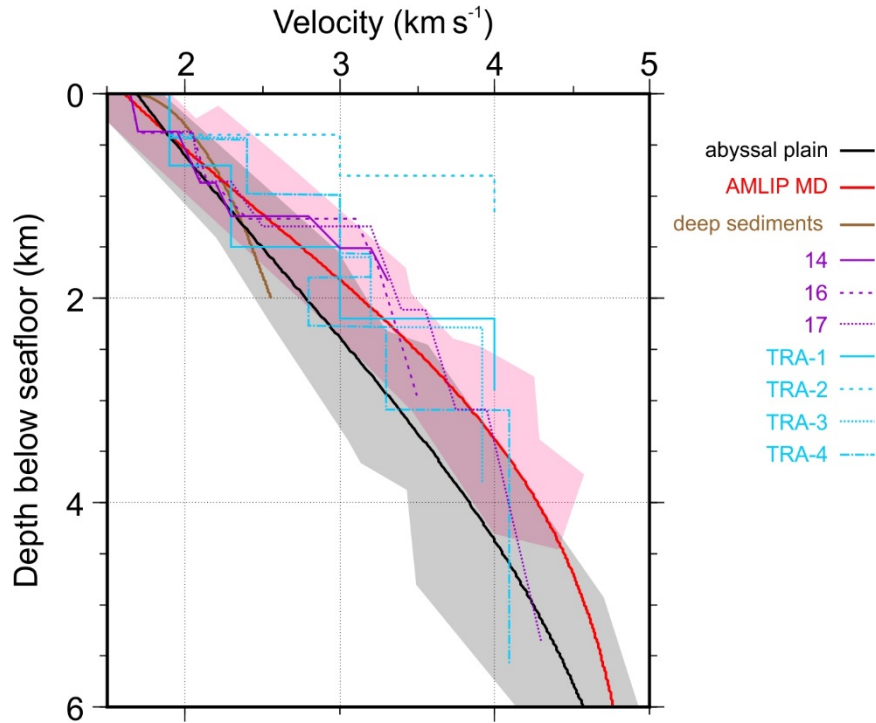
Fig. 3.9. Data from sonobuoys 14, 16 and 17, deployed in Makarov Basin, are plotted against regional velocity-depth curves calculated by Shimeld et al. (2016). The "abyssal plain" curve (black line) represents central Canada Basin, while the "AMLIP MD" curve (red line) is for sonobuoy locations enclosed by the area defined by the Alpha-Mendeleev LIP magnetic domain (Saltus et al., 2011; Fig. 3.2). The grey and pink shaded areas illustrate the range in data points (from Chian and Lebedeva-Ivanova [2015]) used to calculate the curves for the abyssal plain and AMLIP MD regions, respectively. The brown curve labelled "deep sediments" is a square root function derived from seismic refraction measurements made in deep-sea sediments (N ~3.6 km water-depth) from the Gulf of Mexico and North Atlantic (Nafe and Drake, 1961). TRA-1, -2, -3 and -4 are extracted from the velocity model of line TransArctic 1989–1991 (Lebedeva-Ivanova et al., 2011) at the points shown in Fig. 3.10. TRA-3 and TRA-4 were converted to the depth domain using interval velocities derived by Langinen et al. (2006).

The acoustic signature of UC2 is amorphous, possibly due to lithological change

or lack of acoustic energy at this imaging depth. We interpret the upper crust of Alpha

Ridge and part of Makarov Basin (360 to 560 km along line; Fig. 3.5) as a thick

magmatic succession (with possible intercalated sedimentary rock in the shallow parts).
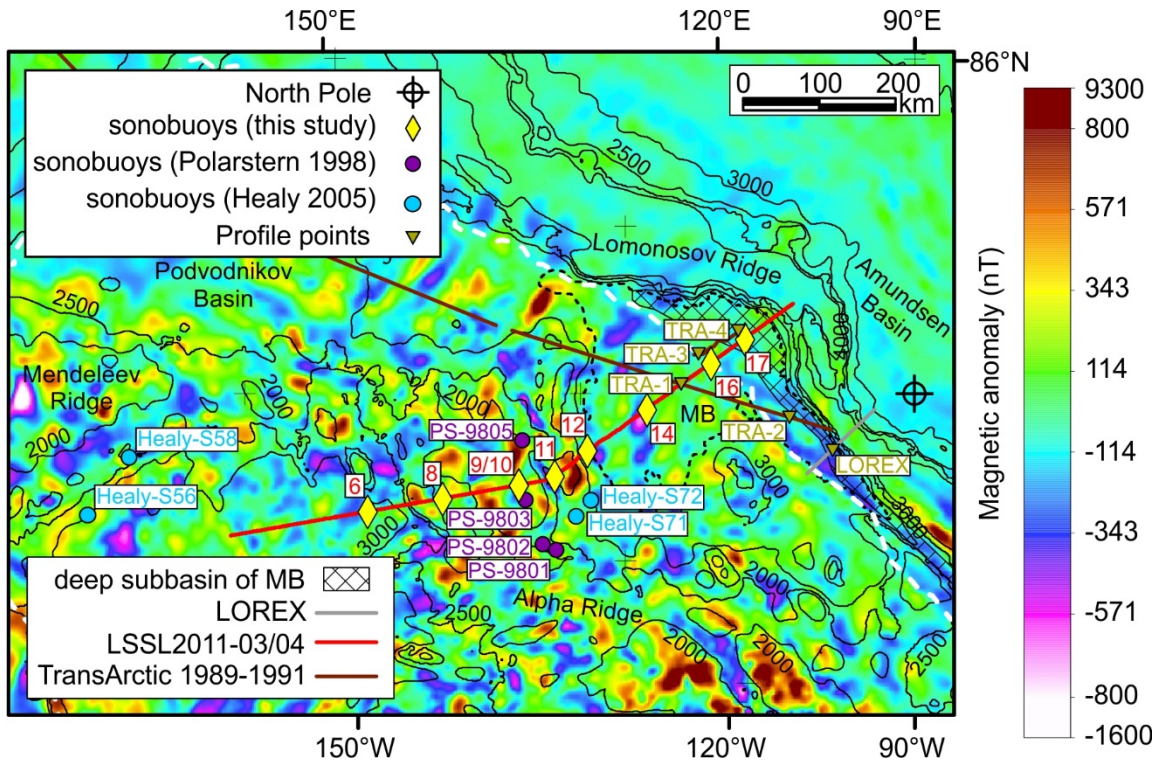
Fig. 3.10. A coloured magnetic map of northern Amerasia and Eurasia basins. Makarov Basin is delineated by a dashed black line representing the 3700m bathymetric contour. Thin black lines are bathymetric contours for 1000, 2000, 2500, 3000 and 4000 m. The white dashed line delineates the Alpha-Mendeleev LIP magnetic domain (Saltus et al., 2011). Other studies shown in this figure are: sonobuoys from Healy 2005 (Bruvoll et al., 2012), sonobuoys from Polarstern 1998 (Jokat, 2003), LOREX (dip line) (Forsyth and Mair, 1984), the TransArctic 1989–1991 line (Lebedeva-Ivanova et al., 2011) and the deep subbasin of MB (Makarov Basin) (Evangelatos and Mosher, 2016). The magnetic compilation is from Gaina et al. (2011) and the isobaths were produced using the IBCAO version 3.0 grid (Jakobsson et al., 2012). Values above 800 nT and below −800 nT are monochromatic.

3.4.3. Mid- and Lower Crustal Layers

The middle (MC) and lower (LC) crustal layers are constrained by refractions P_{mc} and P_{lc}, respectively. On Alpha Ridge, the mid-crustal layer (6.0–6.5 km s^{-1}) has a thickness of 1.4–2.1 km. In Makarov Basin, from 360 to 540 km, these values are 6.2–6.7 km s^{-1} and 1.1–2.6 km, respectively. Uncertainties in mid-crustal velocities are estimated to be ± 0.3 km s^{-1}. The base of layer MC has an uncertainty of ± 0.4 km. Layer MC pinches out beneath the slope of Lomonosov Ridge (575 to 605 km along line; Fig. 3.5).

The rays associated with the observed P_{lc} arrivals sample only the uppermost part of the LC layer (Fig. 3.4). The velocity at the top of the lower crust is estimated at 6.9 ± 0.4 km s^{-1}. The Moho is constrained by P_mP reflections (Figs. 3.4 and 3.6) at station 14 at a depth of about 14 km. This depth corresponds well with a cross-tie between lines LSSL2011-03/04 and TransArctic 1989–1991 (Fig. 3.7). Gravity modelling was used to define the Moho for the remainder of the profile. The Moho depth ranges from >30 km at Alpha Ridge to 14 km beneath Makarov Basin (Fig. 3.7). Interpretations of the MC and LC layers are discussed in Section 3.5.

3.4.4. Mantle

Seismic energy was not observed on any sonobuoy beyond an offset of 43 km– a limitation imposed by radiowave transmission of the received signal back to the ship and/or due to the seismic source energy. In comparison, along the ARTA line (Funck et al., 2011), the minimum offset for the mantle refraction P_n beneath Alpha Ridge is ~70 km. Along the TransArctic 1989–1991 profile, the P_n phase was observed at a minimum offset of 35 km in Makarov Basin (Lebedeva-Ivanova et al., 2011). No P_n phases were noticed in our sonobuoy data. As such, this study provides no information on upper mantle velocities.

3.5. Discussion

3.5.1. Sedimentary Succession of Makarov Basin

The sedimentary history of Makarov Basin appears distinct from that of Canada Basin. Initial sediment input to Makarov Basin came from the Lomonosov Ridge/Barents

Shelf (Evangelatos and Mosher, 2016), while in Canada Basin first sedimentary deposition on basement originated from the Alaskan margin (Mosher et al., 2012). After the separation and subsequent subsidence of Lomonosov Ridge from the Barents Shelf, topographic barriers (Alpha and Lomonosov ridges) hindered sedimentation into Makarov Basin from proximal sources. Consequently, mid-Upper Cretaceous to present sedimentary deposits in Makarov Basin are largely hemipelagic to pelagic (Evangelatos and Mosher, 2016), while turbidite deposition dominates in Canada Basin (Mosher et al., 2012).

Fig. 3.9 shows velocity-depth profiles of sedimentary layers from Makarov Basin plotted against the velocity-depth functions derived by Shimeld et al. (2016) for the Alpha-Mendeleev LIP magnetic domain and the abyssal plain of Canada Basin. In addition, a curve representing deep-sea sediments from the Gulf of Mexico and North Atlantic (Nafe and Drake, 1961) is also plotted in this figure. For depths of burial corresponding with layers S1–S3 (from 0 to ~1–1.3 km depth below seafloor; Fig. 3.9), velocities do not discriminate between the different functions. For the deeper succession (> ~1.3 km depth below seafloor), velocities from Makarov Basin best match the function for the Alpha-Mendeleev LIP magnetic domain (Fig. 3.9). This function is characterized by a high velocity gradient. Shimeld et al. (2016) argued that this trend cannot be readily explained by likely lithological variations and proposed enhanced chemical compaction due to "episodic high palaeo-heat flow" as an alternative. In their model, the anomalous heat flow values were caused by late magmatism related to the Alpha-Mendeleev LIP. The latest confirmed age of such magmatism is ~89 Ma, constrained by ^{40}Ar/^{39}Ar isotopic dating of basalt recovered in situ (Jokat et al., 2013). Assuming that its

sedimentary succession consists of "siliciclastic sediments and sedimentary rocks" (Shimeld et al., 2016) typical of deep-water marine basins, this process could hypothetically explain the high velocities in Makarov Basin. Existing heat flow data is sparse and unevenly distributed (Fig. 3.2); hence, it cannot be used to validate the possibility that the deep succession was influenced by late magmatism. We thus prefer to attribute the high velocity of sedimentary layers to lithological factors including possible cementation/lithification. Volcanic or volcaniclastic material such as tuff that is cemented as part of its process of formation, intercalated with sediments, might also explain the higher than expected velocities. Such a relationship is suggested by high amplitude and semi-continuous reflections from these intervals (Evangelatos and Mosher, 2016; Fig. 3.8b). Volcanogenic material is plausibly related to mid-Late Cretaceous to Palaeocene volcanism on Ellesmere Island and northern Greenland (Estrada et al., 2010; Tegner et al., 2011). Diagenetic biosiliceous units may be a contributing factor. Biosiliceous ooze was identified in dredge samples from Alpha Ridge (CESAR; Mudie and Blasco, 1985) and in core from Lomonosov Ridge (IODP 302; Backman et al., 2006, 2008).
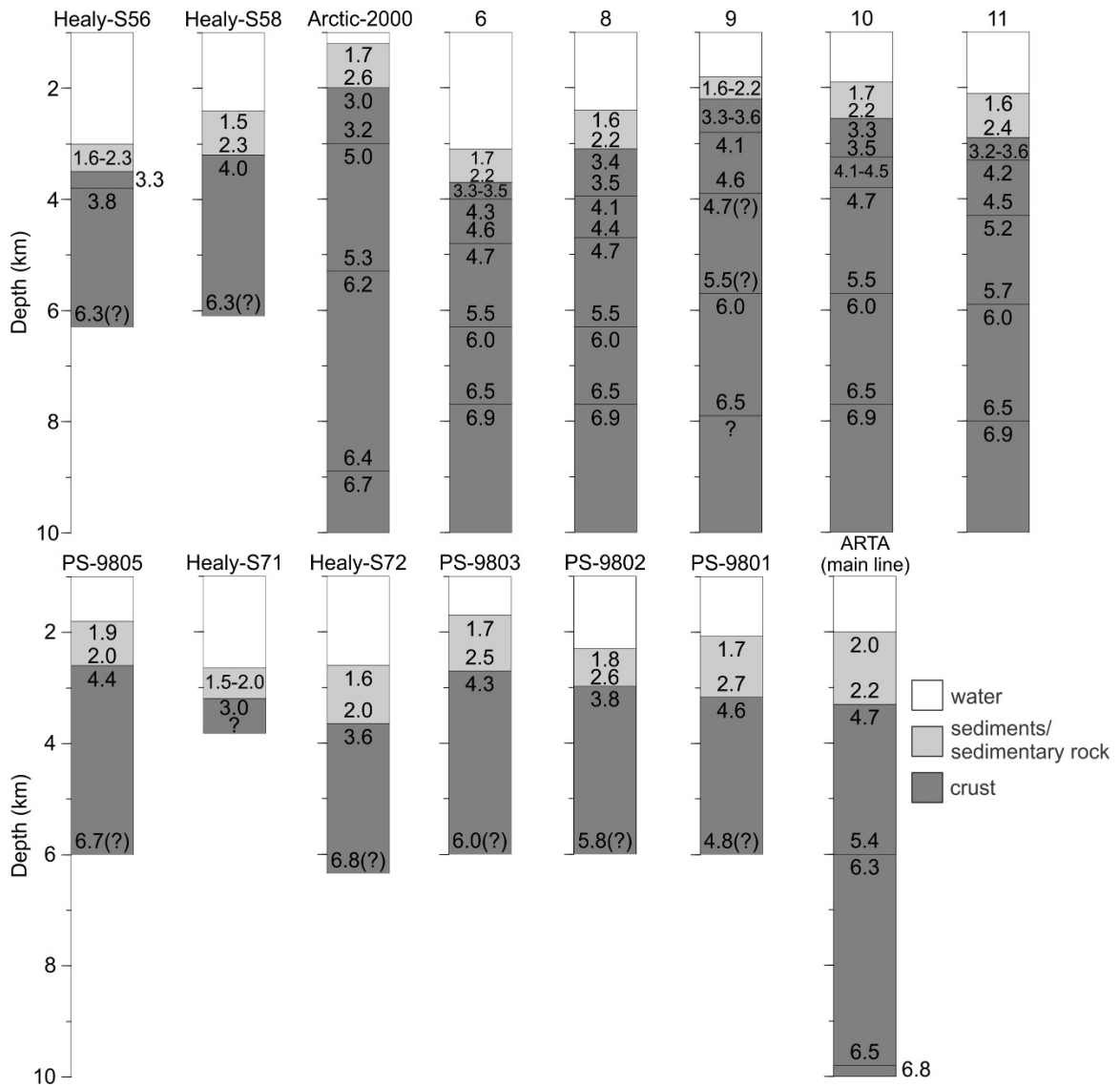
Fig. 3.11. Comparison of P-wave velocities from this study with other experiments from the Alpha and Mendeleev ridges. ARTA (main line) is from Funck et al. (2011), Arctic-2000 is from Lebedeva-Ivanova et al. (2006), Healy-S56, -S58, -S71, -S72 are from Bruvoll et al. (2012), PS-9801, -9802, -9803, -9805 are from Jokat (2003), and labels 6, 8, 9, 10 and 11 are stations from this study. Velocities for the Arctic-2000 and ARTA columns are extracted from 265 km and 80 km distance along their respective lines (Fig. 3.1). Note, we re-interpret layers III (3.0–3.2 km s^{-1}) and IV (5.0–5.3 km s^{-1}) from Arctic-2000 as part of the crust (refer to Section 3.5.2). Velocities are specified in km s^{-1}.
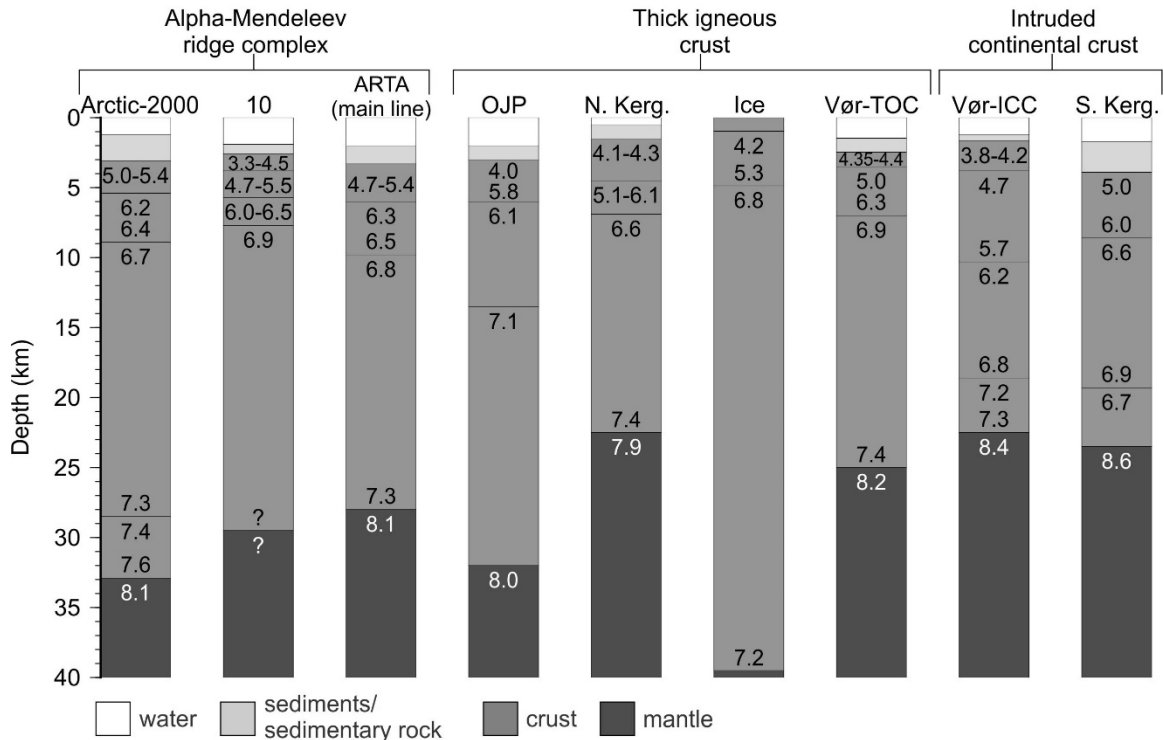
Fig. 3.12. P-wave velocities from the Alpha-Mendeleev ridge complex and other LIPs are compared. Vertical profiles extracted for Mendeleev Ridge: Arctic-2000 (Lebedeva-Ivanova et al., 2006); Alpha Ridge: ARTA (main line) (Funck et al., 2011) and station 10 (this study); Ontong Java Plateau: OJP (Gladczenko et al., 1997), Iceland: Ice (Darbyshire et al., 1998), North and South Kerguelen Plateau: N. Kerg. (Charvis et al., 1995) and S. Kerg. (Operto and Charvis, 1995), respectively; Thick Oceanic Crust and Intruded Continental Crust of VøringMarign: Vør-TOC and Vør-ICC (Mjelde et al., 2005), respectively. Velocities are specified in km s^{-1}. For station 10, Moho depth is based on gravity modelling (refer to Section 3.3.3.3).

3.5.2. Crust of Alpha Ridge

In our study, the velocity of the uppermost volcanic crust ranges from 3.3 to 3.6 km s^{-1}. The location and results from other studies are shown in Figs. 3.10 and 3.11, respectively. Funck et al. (2011) reported velocities of up to 4.7 km s^{-1}, while Bruvoll et al. (2012) showed it to be as low as 3.0 km s^{-1}. Two possibilities are offered to explain the variation in velocities for the uppermost crust shown in Fig. 3.11:

1) The resolution of the various data sets is different depending on acquisition parameters, processing and data quality. For example, a velocity layer similar to UC1was not identified in the ARTA experiment (Funck et al., 2011; Fig. 3.11), yet the seismic

reflection data from their study show intra-basement acoustic facies similar to that described here for UC1. We assume that a layer similar to UC1 is unresolved in the ARTA experiment due to the difference in seismic trace spacing between our study (20–30 m; Mosher, 2012) vs. ARTA (1200–1500 m; Funck et al., 2011). For the Polarstern 1998 (Jokat, 2003) and Healy 2005 experiments (Bruvoll et al., 2012) (Fig. 3.11), modelling did not resolve crustal velocity structures below shallow basement as seismic energy was generally only recorded to offsets <15 km.

2) Variation in seismic velocities may reflect lithological heterogeneity in the composition of shallow basement. Seismic patterns and facies in layer UC1 resemble basement as identified by Jokat (2003) and Bruvoll et al. (2012) in their respective studies of seismic reflection profiles over the Alpha-Mendeleev ridge complex. Jokat (2003) reported that a basaltic fragment recovered at the base of a sediment core (Jokat, 1999) is representative of basement. Dredging on the Canada Basin-facing flank of Alpha Ridge recovered tuff (Mayer et al., 2016). Bruvoll et al. (2012) interpreted basement at the Alpha-Mendeleev ridge complex as composed of massive lava flows, tuff and pillow basalts. They attributed the presence of relatively low P-wave velocities to intercalated sedimentary rock between volcanic beds. Intra-basement seismic facies and P-wave velocities from the Alpha and Mendeleev ridges (Jokat, 2003; Bruvoll et al., 2012; this study) resemble results from Manihiki Plateau (Pietsch and Uenzelmann-Neben, 2015). Hochmuth (2015) assigned P-wave velocities as low as 3.0 to 4.3 $km\,s^{-1}$ for the upper crust at the western part of Manihiki Plateau. At the eastern part of this feature, basalts, intercepted near the top of basement in drill core (DSDP Leg 33 Site 317; Schlanger et

al., 1976), correspond with interval velocities of 3.5–4.0 s^{-1} (Pietsch and Uenzelmann-Neben, 2015).
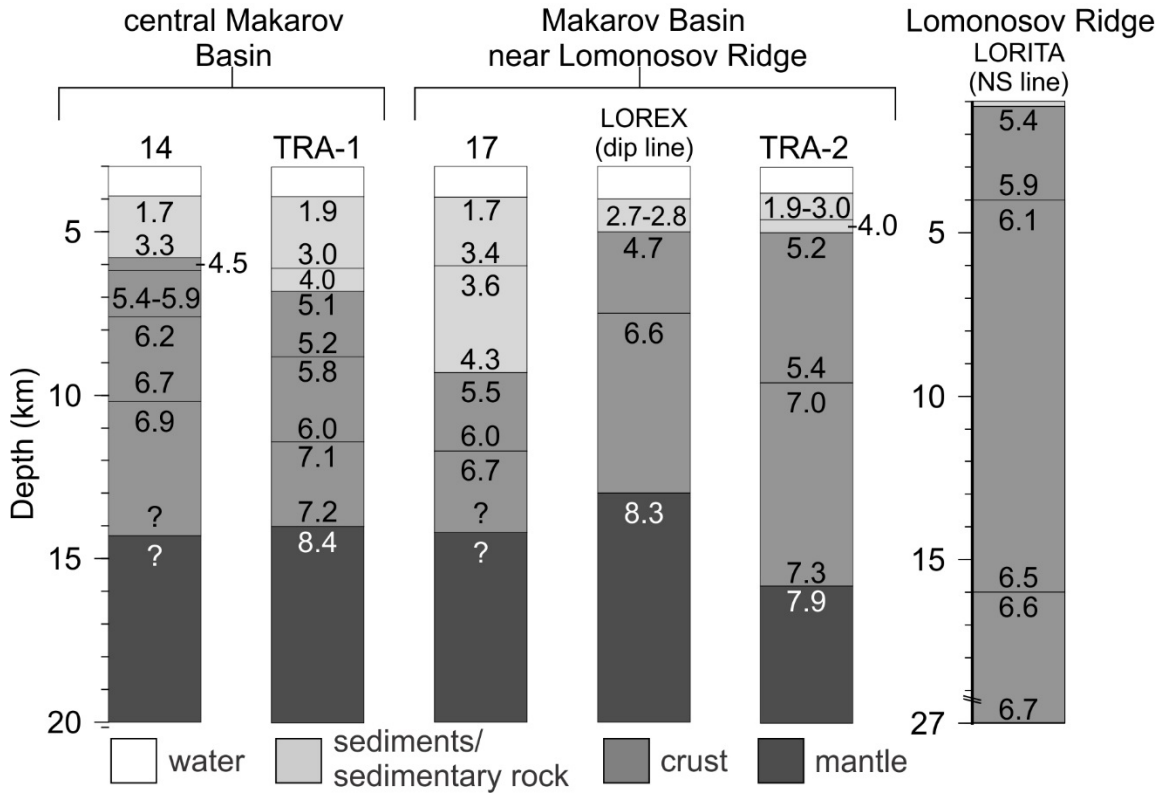
Fig. 3.13. P-wave velocities from this study and other experiments from Makarov Basin are compared. LOREX (dip line) is from Forsyth and Mair (1984), LORITA (NS line) is from Jackson et al. (2010), TRA-1 and TRA-2 are extracted along line TransArctic 1989–1991 from Lebedeva-Ivanova et al. (2011), and stations 14 and 17 are from this study (locations shown in Fig. 3.10). Velocities are specified in km s^{-1}. For stations 14 and 17, Moho depth is based on gravity modelling (refer to Section 3.3.3.3).

The MCS record mostly shows incoherent noise in layer UC2 (Fig. 3.8). Based on previous studies, Alpha Ridge formed or was significantly altered as a result of a LIP. The upper crust of Alpha Ridge is, therefore, interpreted as a magmatic succession with a combined average thickness of 3.2 km and a velocity range of 3.3–5.6 km s^{-1} (Fig. 3.5). The thick successions of basalt at the Faroe Islands, at least 6.6 km (Passey and Bell, 2007), present a plausible analogue to the magmatic upper crust of Alpha Ridge. Along line Arctic-2000 (Fig. 12), Lebedeva-Ivanova et al. (2006) interpreted layers with P-wave

velocities of 5.0–5.4 km s^{-1} (their layer *IV*) as "dominated by carbonate and terrigenous sedimentary rocks, with some igneous intercalations". This interpretation is based on the assumption that recovered dredge samples of such rock types in the vicinity of the line are in situ (Kaban'kov et al., 2004). Coincident seismic reflection data are available; however, layer *IV* is inadequately resolved (Lebedeva-Ivanova et al., 2006). During the more recent Arctic-2012 expedition, a mix of carbonate (dominant), terrigenous, metamorphic and igneous rock types were recovered along steep slopes of the Mendeleev Ridge (Morozov et al., 2013; Gusev et al., 2014), which Petrov et al. (2016) interpreted as evidence in support of the continental affinity of this ridge. Assuming that Alpha and Mendeleev ridges represent a single geological entity, as suggested by studies of potential fields and seismic refraction modelling (e.g., Dove et al., 2010; Funck et al., 2011), then layer *IV* in the model of Lebedeva-Ivanova et al. (2006) and our layer UC3 are stratigraphically equivalent. We question, however, the interpretation of these layers as chiefly sedimentary. Shallow drilling (<2 m) through basement confirmed only the presence of basalt from Mendeleev Ridge (Petrov et al., 2016). With respect to this study, the MCS data do not show seismic facies consistent with carbonates or terrigenous sedimentary rock (e.g., stratification, progradation structures, carbonate platforms), but imaging is admittedly limited at these depths.
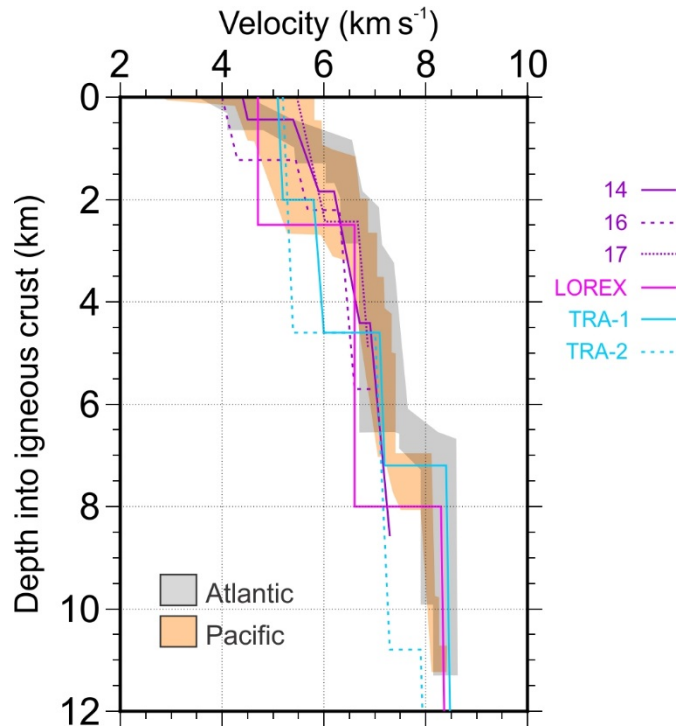
Fig. 3.14. P-wave velocity profiles of stations 14, 16 and 17 (this study), LOREX (dip line) (Forsyth and Mair, 1984), and TRA-1 and TRA-2 were extracted along line TransArctic 1989–1991 (Lebedeva-Ivanova et al., 2011). Locations are shown in Fig. 10. Grey and orange shaded areas illustrate the range in data points for normal oceanic crust from the Atlantic (59–127 Ma) and Pacific (29–140 Ma) oceans (White et al., 1992), respectively.

Velocities for theMC layer (6.0–6.5 km s^{-1}) are fast relative to fresh basalts.

Grevemeyer et al. (1998) modelled layer 2A oceanic crust using P-wave velocities of

2.9–4.3 km s^{-1} and Bourbié et al. (1987) lists the maximum value for basalt at 6 km s^{-1}.

The velocities for the MC layer are also slower than those reported for mid-crustal

gabbros (6.95 ± 0.22 km s^{-1}; Holbrook et al., 1992). Such intermediate values (6.0–6.5

km s^{-1}) are more consistent with metabasalts and metadolerites (≤6.25 km s^{-1}) measured

from rock samples from the Bay of Islands ophiolite complex in Newfoundland, Canada

(Salisbury and Christensen, 1978). These lithologies represent the sheeted dykes that

define oceanic layer 2C (Becker et al., 1989; Carlson and Herrick, 1990), where

velocities of 5.8–6.5 km s^{-1} are reported (Ewing, 1976). Alternatively, Lebedeva-Ivanova

et al. (2006), who favoured a continental origin for Mendeleev Ridge, interpreted their

layer V (5.9–6.5 km s^{-1}) as magmatically altered crystalline basement. Their interpretation is based on correlations with the TransArctic 1989–1991 line and similarities to velocities derived from outcropping granite at Henrietta Island on the Siberian Shelf. If the continental model is correct, the Alpha-Mendeleev ridge complex is similar to the southern Kerguelen Plateau, which is inferred to represent stretched continental crust overprinted by plume-related magmatism (Operto and Charvis, 1995).

The thickness of the LC layer is based on gravity modelling calibrated at a single station (Fig. 3.6). Despite this limitation, even by the most conservative estimate, the lower crust constitutes a large fraction of the total crustal thickness of Alpha Ridge (Fig. 3.12). The thickness of the lower crust, and overall crustal thickness (25–30 km; Fig. 3.12), is consistent along the length of Alpha and Mendeleev ridges (Lebedeva-Ivanova et al., 2006; Funck et al., 2011; this study). It should be noted, however, that deep seismic studies of Alpha and Mendeleev ridges are few relative to the size of the ridge complex. As such, the apparently homogeneous structure of those ridges may be due to aliasing and/or data resolution.

In summary, the internal crustal velocity structure of Alpha Ridge consists of a 2.3–4.5 km-thick succession of magmatic rock (chiefly extrusive rock) lying above a 1.4–2.1 km-thick middle layer with intermediate velocities (6.0–6.5 km s^{-1}) that, in turn, overlies a relatively thick lower crust with high velocities (>6.9 kms^{-1}). Together with the basement pattern from the MCS data and its magnetic character, Alpha Ridge is consistent with other LIPs with thick igneous crust (Fig. 3.12). This velocity structure differs from magmatically overprinted thinned continental crust (e.g., intruded

continental crust on the Vøring margin; Mjelde et al., 2005) (Fig. 3.12). This interpretation suggests that the Alpha-Mendeleev ridge complex initially formed as an Iceland-type structure during seafloor spreading in Amerasia Basin (Vogt et al., 1979; Forsyth et al., 1986; Jackson et al., 1986; Asudeh et al., 1988; Weber, 1990; Lane, 1997); or at a later stage in the history of the basin (Grantz et al., 2011). With respect to an Iceland-type model, Brumley (2009) argued that the stress field implied by the extinct spreading centre in Canada Basin (Fig. 3.2) is inconsistent with the general orientation of rift structures (troughs and ridges) on the Alpha-Mendeleev ridge complex (Fig. 3.1). Aside from discriminating large scale crustal types based on velocity structure, the seismic and gravity data cannot resolve possible continental fragments entrained within predominantly magmatic crust or if magma intruded original continental material.

3.5.3. Crust of Makarov Basin

Based on their interpretation of the TransArctic 1989–1991 seismic refraction data, Lebedeva-Ivanova et al. (2011) concluded that Makarov Basin was probably underlain by oceanic crust, except for continental fragments or slivers that rifted off Lomonosov Ridge (e.g., Marvin Spur; Fig. 3.1). Models of the crustal velocity structure for Makarov Basin differ between this study and the TransArctic 1989–1991 profile (Fig. 3.13). Discrepancies are attributed to resolution of the data sets. Specifically, the TransArctic 1989–1991 experiment involved a receiver spacing of 7–14 km (Lebedeva-Ivanova et al., 2011). Consequently, some of the layer boundaries for the upper and mid-crustal layers for the TransArctic 1989–1991 line are modelled based on only a few seismic traces and, therefore, are not well constrained. In comparison, the seismic trace

spacing for our experiment was 20–30 m (Mosher, 2012), thereby resulting in denser ray coverage in the vicinity of the sonobuoy stations.

In Makarov Basin, between 360 and 560 km along line (Fig. 3.5), velocities for layers UC2, UC3 and MC are similar or slightly faster relative to layers from Alpha Ridge. We propose that the absence of significant lateral variations in velocity structure between Alpha Ridge and part of Makarov Basin (from 360 to 560 km; Fig. 3.5) is due to lithological homogeneity. If the Alpha-Mendeleev LIP was emplaced late in the history of Amerasia Basin, lithological homogeneity results from significant magmatic overprinting of the crust of Makarov Basin. A large part of Makarov Basin closest to Alpha Ridge is, indeed, included within the Alpha-Mendeleev LIP magnetic domain (Saltus et al., 2011; Oakey and Saltus, 2016; Figs. 3.2 and 3.10), which corroborates this tectonic model. The change in crustal thickness from the foot of Alpha Ridge to central Makarov Basin (360 to 560 km along line; Fig. 3.7) is gradual, thinning from 10 km to 8–9 km over a distance of 200 km. Such a relationship is noted between the Manihiki Plateau and the adjacent Samoan Basin (Hochmuth, 2015). Passive rift margins may also exhibit gradual transitions from shallow shelves to deep basins, but lateral changes in velocity structure are much more apparent in such cases (e.g., southeast Greenland margin; Korenaga et al., 2000). The tectonic model of Grantz et al. (2011) shows Makarov Basin forming during the initial phases of opening of Amerasia Basin. According to this model, the Alpha-Mendeleev ridge complex was emplaced later on oceanic crust. Velocity-depth profiles indicate that crustal layers for Makarov Basin are generally thick relative to normal oceanic crust of comparable age (Fig. 3.14). Assuming that the crust is oceanic in origin, thickening is attributed to magmatism related to the

Alpha-Mendeleev LIP. Alternatively, the LIP extruded through and on top of stretched continental crust, as Chian et al. (2016) described extensive regions of thinned continental crust within Canada Basin. Døssing et al. (2013) proposed that linear magnetic anomalies close to the Canadian Polar margin (Fig. 3.1) are caused by an Upper Jurassic–Lower Cretaceous dyke swarm related to initial rifting of the Amerasia Basin. Assuming this rift zone extends farther west and away from the Canadian Polar margin, the implication is that the crust of Makarov Basin is continental in origin. The general orientation of the stress field responsible for the dyke swarm, however, is at odds with the observed extensional fabric of Alpha Ridge (Fig. 3.1).

The top of a basement structure at 550–570 km along line (Fig. 3.8b) is resolved by the MCS data. The velocity structure of this feature (6.2–6.6 km s^{-1}) is constrained by the $P_{mc}P$ phase (Figs. 3.4 and 3.5). Evangelatos and Mosher (2016) suggested that this structure splayed off of Lomonosov Ridge as a result of transtension, similar to Marvin Spur (Cochran et al., 2006). As shown in Fig. 3.7, the lack of a corresponding magnetic response, as one would expect if this feature was magmatic, supports a continental origin for this structure. The TransArctic 1989–1991 line resolves a similar basement structure between Marvin Spur and Lomonosov Ridge (Lebedeva-Ivanova et al., 2011; TRA-2 in Fig. 10). Modelled velocities for this feature resemble upper crustal velocities (5.8–6.5 km s^{-1}) from the LORITA line on Lomonosov Ridge (Jackson et al., 2010; refer to Fig. 3.1 for location).

In the deep subbasin of Makarov Basin, bounded by Lomonosov Ridge and the pronounced basement structure at 550–570 km along line (Fig. 3.8b), there is

disagreement in velocity structure between station 17, the TransArctic 1989–1991 profile

and the LOREX line (Fig. 3.13). Again, the deviations are attributed to differences in

resolution due to inconsistent acquisition methods. Morphological evidence (horsetail

splays and a rhomboid shape) suggests that the subbasin is a pull-apart basin formed by

transtension (Evangelatos and Mosher, 2016). If this interpretation is correct, the narrow

width of the subbasin (Figs. 3.2 and 3.10) favours highly stretched continental crust

beneath this part of Makarov Basin. Assuming a genetic tie between the subbasin and the

Lomonosov Ridge, velocities for layer UC3 (5.4–6.0 km s^{-1}) are plausibly equivalent to

pre-Cenozoic (meta-)sedimentary rock from the ridge where P-wave velocities of ~3.7–

5.9 km s^{-1} (Jokat, 2005) and 5.4–5.9 km s^{-1} (Jackson et al., 2010) are reported.

Alternatively, the subbasin may be underlain by oceanic crust, as proposed by Forsyth

and Mair (1984) for the LOREX line. As shown in Fig. 3.14, velocities for station 17 are

compatible with normal oceanic crust; however, results from LOREX and the

TransArctic 1989–1991 line (TRA-2) are less consistent.

 In contrast to the gradual transition between Alpha Ridge and Makarov Basin, the

crust thins over a lateral distance of 70 km from 20 km at Lomonosov Ridge to 5 km in

Makarov Basin (Fig. 3.7). This abrupt transition is also noted in the LOREX line (Forsyth

and Mair, 1984) and is consistent with crustal studies at transform margins (e.g.,

southwest Newfoundland margin; Todd et al., 1988). This interpretation corroborates

previous work that concluded that the Makarov Basin-facing side of Lomonosov Ridge is

part of a strike-slip system (e.g., Cochran et al., 2006; Evangelatos and Mosher, 2016).

Lateral changes in lower crustal velocities are also more apparent from Makarov Basin to

Lomonosov Ridge (Fig. 3.13) compared to the transition from Alpha Ridge to Makarov

Basin (Fig. 3.5). The properties of the LC layer are, however, principally constrained by gravity modelling.

3.6. Conclusions

From a geological perspective, the northern Amerasia Basin in the Arctic Ocean is amongst the least understood regions on Earth. To gain insight on the tectonic history of this region, nine seismic records from sonobuoys spanning almost 650 km from Alpha Ridge and across Makarov Basin to Lomonosov Ridge were analyzed. Velocities from the upper sedimentary layers of Makarov Basin do not deviate significantly from velocity-depth curves for typical siliciclastic deep-sea sediments. Deeper sedimentary layers have velocities that are similar to those of equivalent burial depth found within the Alpha-Mendeleev LIP magnetic domain in northern Canada Basin. We attribute the high velocities of this section to interbedded volcanic/volcaniclastic rock. Biosiliceous sediments may have also contributed to the high velocities.

The shallow part of the upper crust for Alpha Ridge and part of Makarov Basin (360 to 560 km along line; Fig. 3.5) is interpreted as volcaniclastic/volcanic rock, possibly intercalated with minor sedimentary rock. Overall, however, the upper crust of Alpha Ridge is a thick succession (2.5–3.5 km) of magmatic (primarily extrusive) rock. The mid-crustal layer is 1.4–2.1 km thick with velocities intermediate between those of fresh basalts and gabbro. Gravity modelling suggests that the lower crust constitutes more than half of the total thickness of the crust beneath Alpha Ridge. These characteristics of the crustal structure of Alpha Ridge are consistent with a tectonic and magmatic origin

similar to other LIPs with thick igneous crust. The presence of continental crust in Alpha Ridge, however, cannot be ruled out.

The crustal velocity structure of Alpha Ridge and Makarov Basin (between 360 and 560 km distance) is similar with deviations <0.3 km s^{-1} (Fig. 3.5), which is within the uncertainties of the velocity model. The implication is that these two features share a common geological origin, or that the emplacement of Alpha-Mendeleev LIP modified the crust of Makarov Basin to such extent that it resembles a condensed version of the crust of Alpha Ridge. Crustal thickening towards Alpha Ridge is also attributed to the emplacement of the LIP.

The results from density modelling suggest that the transition from Lomonosov Ridge to Makarov Basin is characterized by a 15 km decrease in crustal thickness over a distance of only 70 km. Such a sharp transition is consistent with past interpretations of the Amerasian flank of Lomonosov Ridge as a transform/transtensional margin. A non-magnetic basement structure in Makarov Basin, previously interpreted as a splay structure related to transtension, is genetically tied to the upper crust of Lomonosov Ridge by similarities in seismic velocity structure.

CHAPTER 4: INSIGHTS ON NORTHERN AMERASIA BASIN, ARCTIC OCEAN, FROM TWO-DIMENSIONAL FORWARD MODELLING OF THE GRAVITY FIELD

Preface

Material included in Chapter 4 were presented in "*Evangelatos, J., Oakey G., Saltus, R., 2017, Central Arctic crustal modeling constrained by potential field data and recent ECS Seismic Data, European Geosciences Union General Assembly 2017*".

Abstract

Understanding the crustal structure that underpins the northern part of Amerasia Basin of the Arctic Ocean is critical to determination of the tectonic evolution of the entire basin. For this purpose, 13 two-dimensional density models were generated to analyze the regional Arctic gravity field. These profiles trend perpendicular the main submarine ridges of Amerasia Basin (i.e., Alpha, Mendeleev and Lomonosov ridges) while crossing Makarov and Podvodnikov basins. Rock densities were calculated from published seismic velocities. Seismic records, where available, were used to constrain the gravity models. In the absence of constraints on boundary depths for crustal layers, the observed gravity field was simulated by changing boundary depths while maintained constant layer densities for specific geological provinces. The transition from Makarov and Podvodnikov basins to Lomonosov Ridge is divided into three zones that differ based on the rate of change of crustal thickness. Where Alpha Ridge abuts Lomonosov Ridge, adjacent to the Canadian Polar margin (Zone 1), modelling reveals that the density for the crustal root of Lomonosov Ridge (2900 kg m^{-3}) differs from that of Alpha Ridge (3000

kg m^{-3}). The implication is that Lomonosov Ridge was not significantly affected by LIP-related magmatism. Within Makarov Basin (Zone 2), the crustal transition with Lomonosov Ridge is abrupt. This result is consistent with models that interpret the Amerasian margin of Lomonosov Ridge as a strike-slip boundary. In contrast, the crustal transition between Podvodnikov Basin and Lomonosov Ridge (Zone 3) is relatively gradual, indicating extension perpendicular to Lomonosov Ridge. Evidence thus suggests that the style of deformation changes along the strike of Lomonosov Ridge.

4.1. Introduction

Recent seismic investigations in the Arctic Ocean provide new constraints on the crustal composition and character of Makarov and Podvodnikov basins and adjacent areas of the northern Amerasia Basin (e.g., Jokat and Ickrath, 2015; Evangelatos et al., 2017). The progress in data acquisition, however, has not yet resulted in significant advancements in reconstructing the evolution of Amerasia Basin. Conflicting models exist in even the most recent plate-reconstructions (e.g., Shephard et al., 2013; Doré et al., 2016; Døssing et al., 2017).

This study aims to better define the structural relationship between the northern Amerasia Basin and Lomonosov Ridge, by modelling the gravity field to provide evidence of possible tectonic underpinnings. Additionally, this study investigates lateral variability in the depth of the Mohorovičić discontinuity (Moho) within particular geological provinces.

4.2. Background

4.2.1. Geological Setting

Lomonosov Ridge separates Amerasia and Eurasia basins– the two basins of the large Arctic Ocean. The Amerasia Basin is enclosed by the Canadian Polar margin, Arctic Alaska and eastern Siberia. Lomonosov Ridge is reasonably well-understood to be a continental fragment isolated by opening of Eurasia Basin in the Cenozoic (Rowley and Lottes, 1988; Jackson et al., 2010). The Eurasian margin of Lomonosov Ridge is thus conjugate to the Barents margin. Geophysicists, Oden and Marvin spurs are linear ridges that trend sub-parallel to Lomonosov Ridge on its Amerasia flank (Fig. 4.1). These features are interpreted as continental fragments splintered off of Lomonosov Ridge (Cochran et al., 2006; Evangelatos and Mosher, 2016). Oakey and Saltus (2016) proposed that Marvin Spur is a volcanic ridge, due to its deep-rooted magnetic source. The free-air gravity anomalies observed at Lomonosov Ridge are generally between 20–90 mGal. Particularly high anomalies are observed along the central segment of the ridge (>60; Fig. 4.2).

Makarov and Podvodnikov basins are situated in the northern part of Amerasia Basin between Lomonosov Ridge and Alpha and Mendeleev ridges (Fig. 4.1). Discounting basement highs, seafloor depths in Makarov Basin range from ~3000 m to almost 4000 km in the abyssal plain (Fig. 4.1). For Podvodnikov Basin, the seafloor dips northward from the foot of the Siberian Shelf towards Makarov Basin, deepening from ~2800 m to ~4000 m water depths. There appears to be a bathymetric step across Arlis Gap where the seafloor depth drops from 2860 m to 3210 m over a short distance of ~70

km (Fig. 4.1). This morphology mimics basement topography (Sorokin et al., 1999). Isolated protrusions of bedrock found in the southeastern part of Makarov Basin (e.g., Fedotov Seamount; Fig. 4.1) are genetically tied to Alpha Ridge (Jackson et al., 1986). Positive free-air gravity anomalies in Makarov and Podvodnikov basins generally coincide with bathymetric highs (e.g., Marvin and Geophysicists spurs) (Fig. 4.2). Evangelatos and Mosher (2016) used the gravity low adjacent to Lomonosov Ridge to define the "deep subbasin" of Makarov Basin.

The width of the Alpha-Mendeleev ridge complex ranges from 200 to 600 km. Water depths reach less than 1100 m on Alpha Ridge and less than 800 m on Mendeleev Ridge (Fig. 4.1). There is a strong correlation between the gravity field and bathymetry of the ridges (Weber, 1986; Dove et al., 2010; Fig. 4.2). Furthermore, gravity corrected for bathymetry (i.e., marine Bouguer correction) reveals a subdued anomaly along the Alpha-Mendeleev ridge complex, suggesting minimal lateral variability (Oakey and Saltus, 2016). The magnetic expression of the Alpha-Mendeleev ridge complex and adjacent abyssal plains is characterized by short wavelength anomalies with alternative high and low amplitudes (Fig. 4.3). This region defines the High Arctic Magnetic Domain (HAMH) presented by Oakey and Saltus (2016). In situ rock sampling from various points along the ridge complex recovered basaltic fragments (Van Wagoner et al., 1986; Andronikov et al., 2008; Jokat et al., 2013; Morozov et al., 2013; Mayer et al., 2016). These rock types, in combination with the seismic velocity structure of the ridge (Funck et al., 2011) and its magnetic pattern (Vogt et al., 2006; Saltus et al., 2011; Oakey and Saltus, 2016), suggest that the ridge complex was formed by, intruded with, and/or overprinted by extensive magmatism related to a large igneous province (LIP). This LIP

is referred to as the Alpha-Mendeleev LIP in this study. The greater High Arctic Large

Igneous Province (HALIP) includes the Alpha-Mendeleev LIP (Maher, 2001); however,

the genetic relationship between the magmatic suites that comprise HALIP and their

connection to Arctic tectonics is not well understood (Estrada, 2015).

Funck et al. (2011) favour a predominantly oceanic origin for the Alpha-

Mendeleev ridge complex, based on similarities in velocity structure to other LIPs. This

model contrasts with the interpretation of sub-linear magnetic anomalies in the southern

part of the ridge (near Ellesmere Island) as Late Jurassic–Early Cretaceous dykes

intruded into thinned continental crust (Fig. 4.3; Døssing et al., 2013).
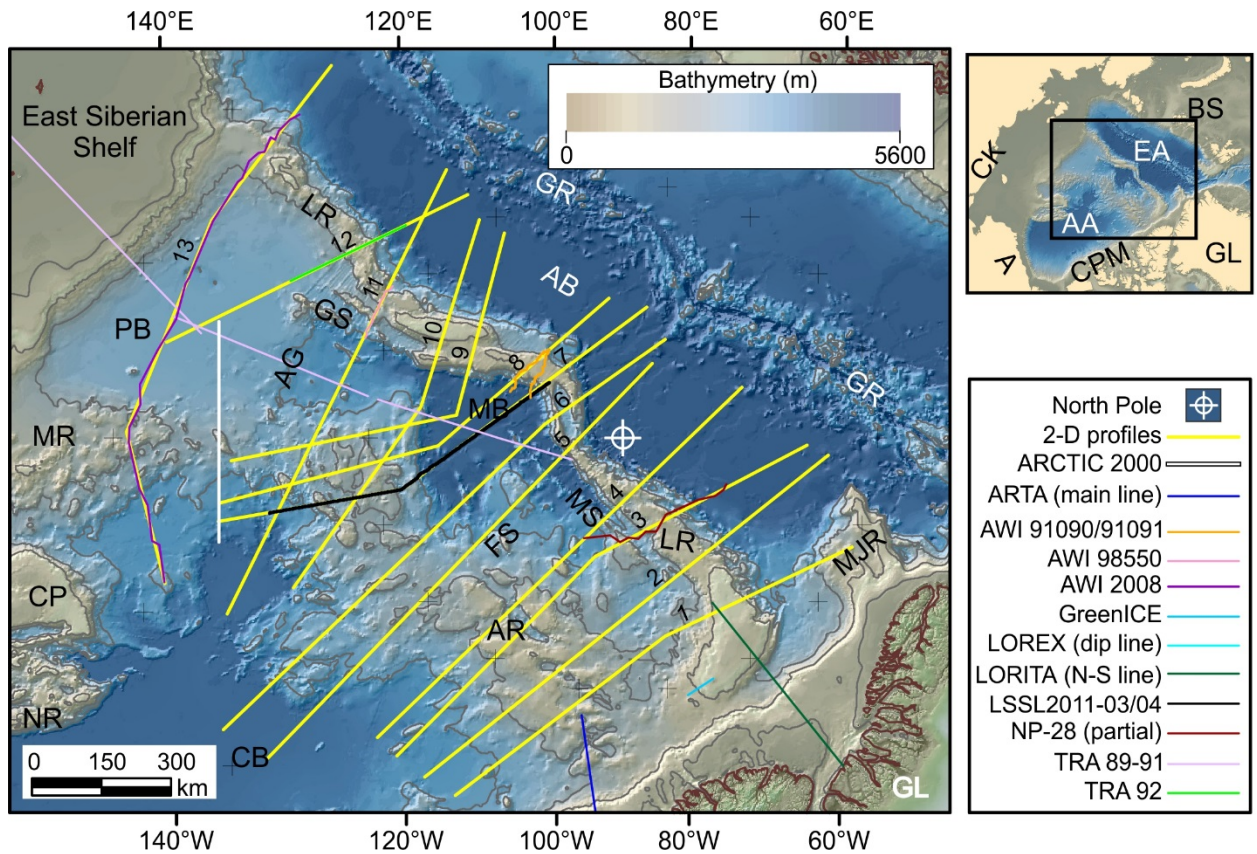
Fig. 4.1. The bathymetric map of northern Amerasia and Eurasia basins. Acronyms used in this figure and others are: A – Alaska, AA – Amerasia Basin, AB – Amundsen Basin, AG – Arlis Gap, BS – Barents Shelf, CPM – Canadian Polar margin, CB – Canada Basin, CK – Chukotka, CP – Chukchi Plateau, EA –

Eurasia Basin, FS – Fedotov Seamount, GL – Greenland, GR – Gakkel Ridge, GS – Geophysicists Spur, LR – Lomonosov Ridge, MB – Makarov Basin, MR – Mendeleev Ridge, Morris Jesup Rise – MJS, MS – Marvin Spur, NR – Northwind Ridge, OS – Oden Spur and PB – Podvodnikov Basin. The locations of profiles used for 2-D potential field modelling are shown yellow lines that are numbered from 1 to 13. Seismic profiles from other studies are: Arctic-2000 (Lebedeva-Ivanova et al., 2006), ARTA (Funck et al., 2011), AWI 91090/91091 (Jokat et al., 1992), AWI 98550 (Jokat, 2005), AWI 2008 (Weigelt et al., 2014; Jokat and Ickrath, 2015), GreenICE (Kristoffersen and Mikkelsen, 2006), LOREX (Forsyth and Mair, 1984), LORITA (Jackson et al., 2010), LSSL2011-03/04 (Evangelatos et al., 2017), NP-28 (Langinen et al., 2009), TransArctic 1989-1991 (TRA 89-91; Lebedeva-Ivanova et al., 2011) and TransArctic 1992 (TRA 92; Poselov et al., 2012). Top right panel shows the location of the study area relative to the North Polar region. Map projection used for this figure and others is North Pole Stereographic with a latitude of origin of 75° N and a central meridian of 90° W. Bathymetry and elevation are from the International Bathymetric Chart of the Arctic Ocean (IBCAO) version 3.0 grid (Jakobsson et al., 2012).
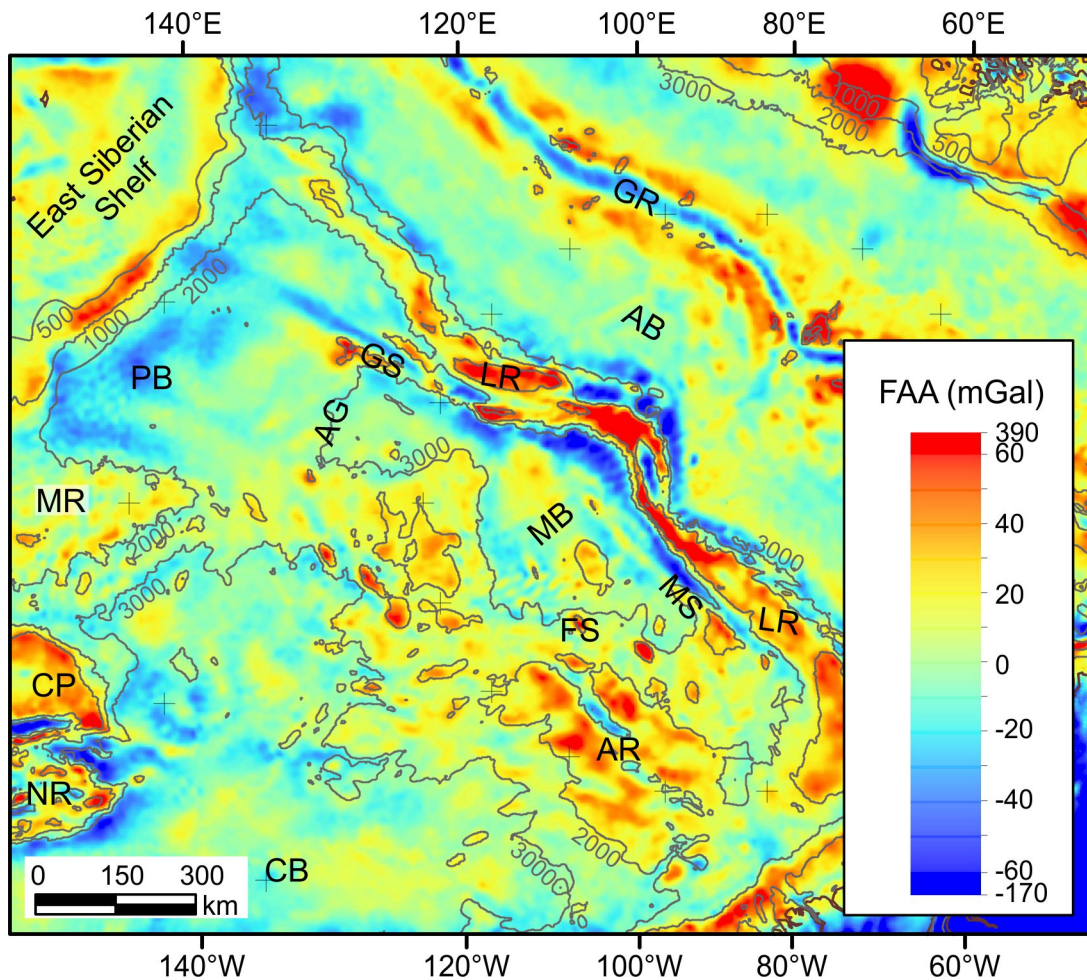
Fig. 4.2. Coloured free-air anomaly map of northern Amerasia and Eurasia basins. Acronyms used in this figure are defined in Fig. 4.1. The gravity compilation is from Anderson et al. (2010) and selected isobaths (200 m, 500 m, 1000 m, 2000 m and 3000 m) were produced using the IBCAO version 3.0 grid (Jakobsson et al., 2012). Colours for values above 60 mGal and below -60 mGal are monochromatic.
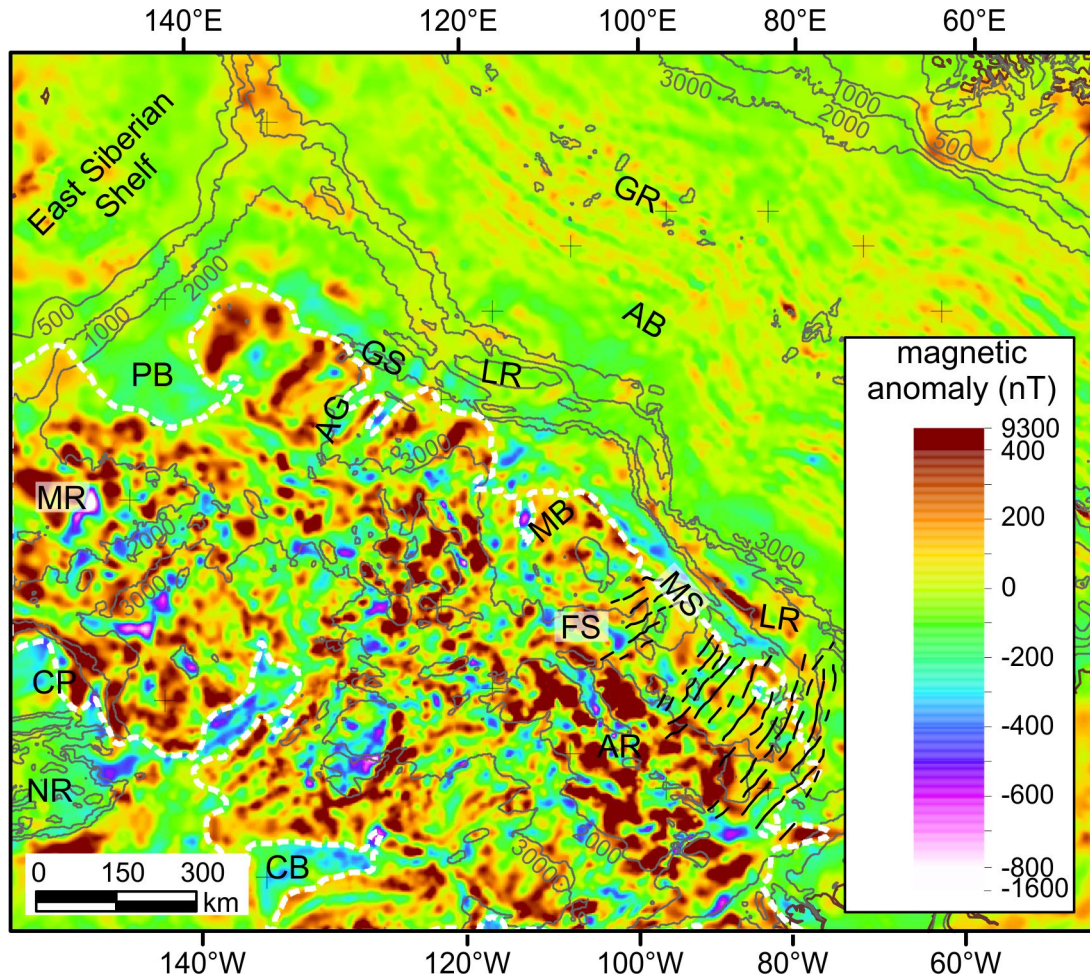
Fig. 4.3. Coloured magnetic anomaly map of northern Amerasia and Eurasia basins. Acronyms used in this figure are defined in Fig. 4.1. The High Arctic High Magnetic domain defined by Oakey and Saltus (2016) is outlined by a dashed white line. The black lines trace magnetic lineations interpreted by Døssing et al. (2013). The magnetic compilation is from Gaina et al. (2011) and selected isobaths (200 m, 500 m, 1000 m, 2000 m and 3000 m) were produced using the IBCAO version 3.0 grid (Jakobsson et al., 2012). Colours for values above 400 nT and below -800 nT are monochromatic.

4.3. Methodology

4.3.1. Seismic Constraints

Seismic reflection and refraction data were used to constrain the gravity models where applicable (Table 4.1). Lines NP-28 (partial), AWI 91091, AWI 98550 and AWI 2008 are seismic reflection records constrain the detailed geometry of the sedimentary layers. Their locations are shown of Figure 4.1. Profile 7 is constrained by LSSL2011-03/04 – a high resolution seismic reflection record with coincident sonobuoy data that

sample down to the uppermost parts of the lower crust. The density model developed using the TransArctic 1992 wide-angle reflection and refraction record (Poselov et al., 2012) forms the basis of Profile 12. The locations of these seismic surveys are shown in Fig. 4.1. Summaries of their acquisition parameters are discussed below. Note the substantial differences in experimental methodology, and resolution, amongst these surveys.

The ARTA experiment was a refraction survey carried out on sea ice off of Ellesmere Island in Spring 2008 (Funk et al., 2011). The "main" line from ARTA extends onto Alpha Ridge perpendicular to the margin. The northern end of the ARTA line is ~30 km away from the 336 km mark along Profile 1. The LORITA "NS" line, another refraction survey, extends from Ellesmere Island/Greenland to Lomonosov Ridge (Jackson et al., 2010). The LORITA line crosses Profile 1 at 708 km distance.

The North Pole-28 (NP-28) line is the track from a Soviet ice station active from 1987-1989 (Langinen et al. 2009). The ice station began its mission in Podvodnikov Basin and was eventually abandoned ~400 km southeast of the Morris Jesup Rise, after having traversed between Amundsen Basin and the Makarov-Podvodnikov basins several times. Profile 3 coincides with the NP-28 track over a length of ~280 km. Seismic reflection data acquired from this experiment resulted in a data spacing of approximately 0.5–1 km and an imaging depth of 1–2.5 s two-way travel time (TWTT). The TransArctic 1992 line is another Soviet/Russian refraction survey that extended 280 km from Podvodnikov Basin, across Lomonosov Ridge and into Amundsen Basin (Poselov et al., 2012).

In 2011, a joint US-Canada survey in the Arctic Ocean acquired lines LSSL2001-01 to -04 (Mosher et al., 2015). This 1210 km composite line spans from the Chukchi Plateau, into Nautilus Basin and across Alpha Ridge and Makarov Basin to the crest of Lomonosov Ridge (Fig. 4.1). Coincident refraction records were acquired (Chian and Lebedeva-Ivanova, 2015; Evangelatos et al., 2017). Brumley (2014) analyzed a segment of the MCS record that extends from the Chukchi Plateau to Alpha Ridge. Evangelatos and Mosher (2016) focused on the portion that crosses Makarov Basin to establish the seismic stratigraphy of that basin. Their interpretation is incorporated into Profile 7.

Table 4.1. Overlapping seismic lines used to constrain the density models are listed. Layer boundaries from seismic reflection records were converted from traveltime to depth using seismic velocities provided in the reference.

Profile	Line	Reference
1*	ARTA LORITA	Funck et al. (2011) Jackson et al. (2010)
2	None	
3	NP-28 (partial)	Langinen et al. (2009)
4	None	
5	None	
6	None	
7	LSSL2011-03/04	Evangelatos et al. (2017)
8	AWI-91091	Jokat et al. (1992)
9	None	
10	None	
11	AWI-98550	Jokat (2005)
12	TRA-92	Poselov et al. (2012)
13	AWI-2007	Jokat and Ickrath (2015)

*The ARTA and LORITA lines constrain Profile 1 at 336 km and 708 km, respectively.

Additional seismic surveys pertinent to this study include Jokat et al., (1992, 1995, 2013), Jokat (2003, 2005), Weigelt et al, (2014), and Jokat and Ickrath, (2015). Refraction records from these studies provide information on the velocity structure of

sedimentary basins and the upper crust of Alpha and Lomonosov ridges. Associated seismic reflection records resolve the base of Cenozoic drape and image reflections down to ~3 s TWTT in the basins. Seismic lines AWI-91091 and AWI-98550 constrain gravity models of profiles 8 and 9, respectively. Jokat and Ickrath (2015) modelled the density structure along AWI 2008 (Fig. 4.1); however, they used a density of 2.67 kg m^{-3} for the water layer (Fig. 4.4). In this paper, the gravity signal along line AWI 2008 was re-modeled while honouring the seismic constraints (Profile 13).
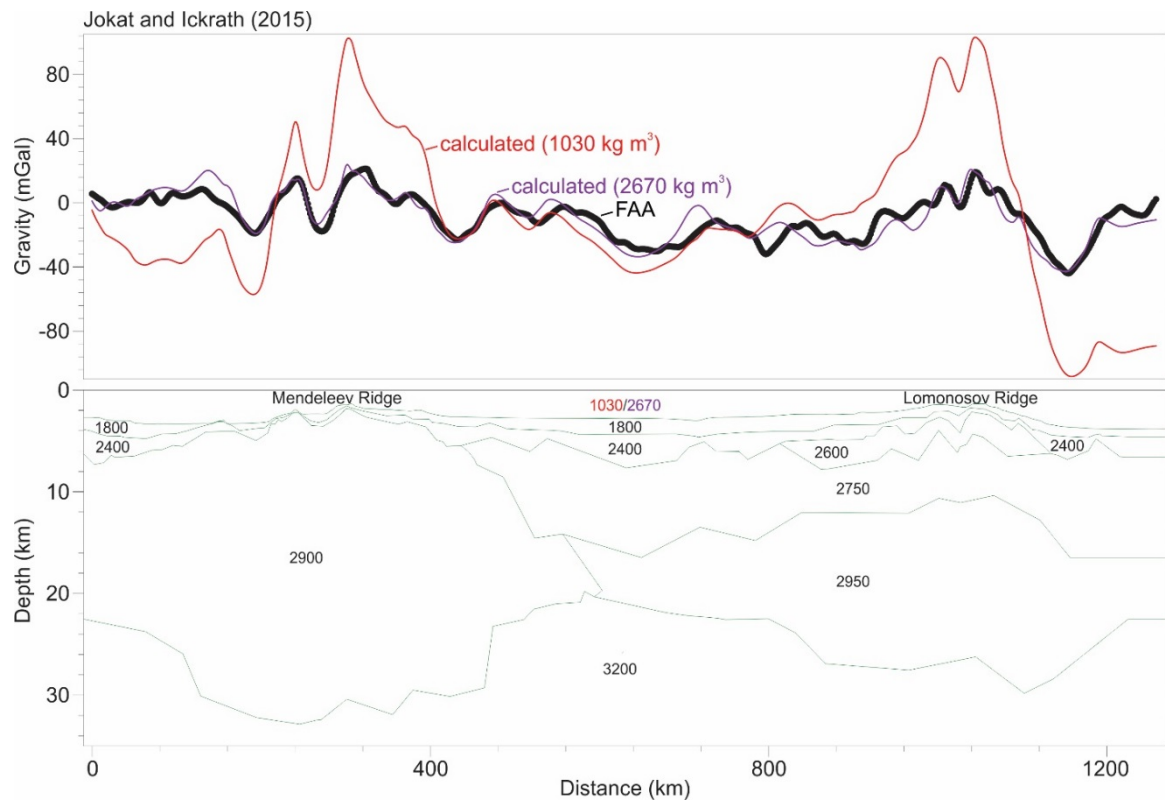
Fig. 4.4. Two-dimensional gravity models for line AWI 2008 modified from Jokat and Ickrath (2015). The top panel shows the observed free-air gravity anomaly compared to the calculated gravity assuming densities of 1030 kg m^{-3} (red) and 2670 kg m^{-3} (purple) for the water layer. Jokat and Ickrath (2015) used the latter value for their gravity model. The bottom panel shows the subsurface gravity model with densities specified in kg m^{-3}.

4.3.2. Gravity Modelling

The goal of gravity modelling was to produce a geologically credible subsurface density model that is consistent with the observed gravity field. To analyze the crustal structure of the various submarine features in northern Amerasia Basin, the gravity signature of thirteen profiles oriented perpendicular to Lomonosov Ridge were analyzed (locations shown in Fig. 4.1). As measured along the crest of Lomonosov Ridge, the profiles are 50 to 300 km apart. The lengths of the profiles range from approximately 700 to 1300 km. Seafloor depths along the profiles were extracted from the International Bathymetric Chart of the Arctic Ocean (IBCAO) version 3.0 grid (Jakobsson et al., 2012). Node spacing in the bathymetry grid is 0.5 km. Potential field data were extracted from gravity and magnetic compilations produced by Anderson et al. (2010) and Gaina et al. (2011), respectively. Node spacings for the gravity and magnetic grids are 5 km and 2 km, respectively. For the profiles, the spacing between these data points is approximately 1.5 km.

The calculated gravity field was computed using the geophysical modelling package *GM-SYS*. The software calculates the gravity field for every point along a given line according to the technique of Rasmussen and Pedersen (1979), which is a generalized form of the two-dimensional (2-D) technique developed by Talwani et al. (1959).

For modelling purposes, the following was assumed:

- The water column has a uniform density of 1030 kg m^{-3}.

- Modelled blocks are 2-D (i.e., project to infinity in the out-of-plane direction). Exceptions were made for certain bathymetric highs that were modelled as 2.5-D blocks.

- The assigned densities were based on values from the scientific literature or calculated from published velocities. "Gardner's rule" (Gardner et al., 1974) was used for estimating densities of sedimentary rocks from P-wave velocities (Vp). Crustal densities were derived using the formula of Osler (1993), which is based on the velocity-density relationship established by Ludwig et al. (1970). The relationship between V_p and density is shown graphically in Fig. 4.5.

- The sedimentary cover in Amerasia Basin and Lomonosov Ridge was divided into upper and lower layers. The breakup unconformity for Eurasia Basin (~56 Ma; Brozena et al., 2003) defines the boundary between these two layers. This event lies at the base of a band of prominent high amplitude reflections and was identified in seismic reflection profiles from the Alpha-Mendeleev ridge complex (Bruvoll et al., 2010; Brumley, 2014; Evangelatos and Mosher, 2016), Lomonosov Ridge (Jokat et al., 1995; Jokat 2005; Langinen et al., 2009; Weigelt et al., 2014), Podvodnikov Basin (Weigelt et al., 2014) and Makarov Basin (Langinen et al., 2009; Evangelatos and Mosher, 2016). This unconformity was also reported in drill core (IODP Expedition 302; Backman et al., 2006, 2008).

- As with the sedimentary section, the underlying crust was modelled using an upper and lower part. For simplicity, layers with meta-sedimentary rocks (e.g., Jackson et al., 2010; Poselov et al., 2012) and mid-crustal layers are included in the upper crust. P-wave velocities for upper crustal layers were generally <6.2 km s^{-1}, but did include some velocities up to 6.2 km s^{-1}.

- This study did not consider layers of high velocity lower crust (e.g., Funck et al., 2011) as entities separate from the lower crust.

- The depth of the Mohorovičić discontinuity (Moho) is largely unconstrained in the models. Crustal densities are, therefore, kept uniform while relief along the Moho is introduced to simulate the long wavelength signal of the gravity field.

- The mantle is assigned a uniform density of 3300 kg m^{-3}.

4.3.3. Lithostatic Pressure

Pressure at point x along profile is calculated by summing all pressure induced by every element from depth z to the surface, and is expressed mathematically as:

$$p(x, z) = \sum_{j=0}^{z} p_{xj} = g * \Delta z * \sum_{j=0}^{z} \rho_{xj}$$

where g is the acceleration due to gravity, which is assumed to be constant at 9.81 m s^{-2}, ρ is density of rock and derived from the Earth models generated by gravity modelling. The Earth models are discretized into cells with dimensions $\Delta x \times \Delta z$. where Δx is 1.5 km long in the x direction (distance along profile) and Δz is 0.1 km long in the z direction (depth).
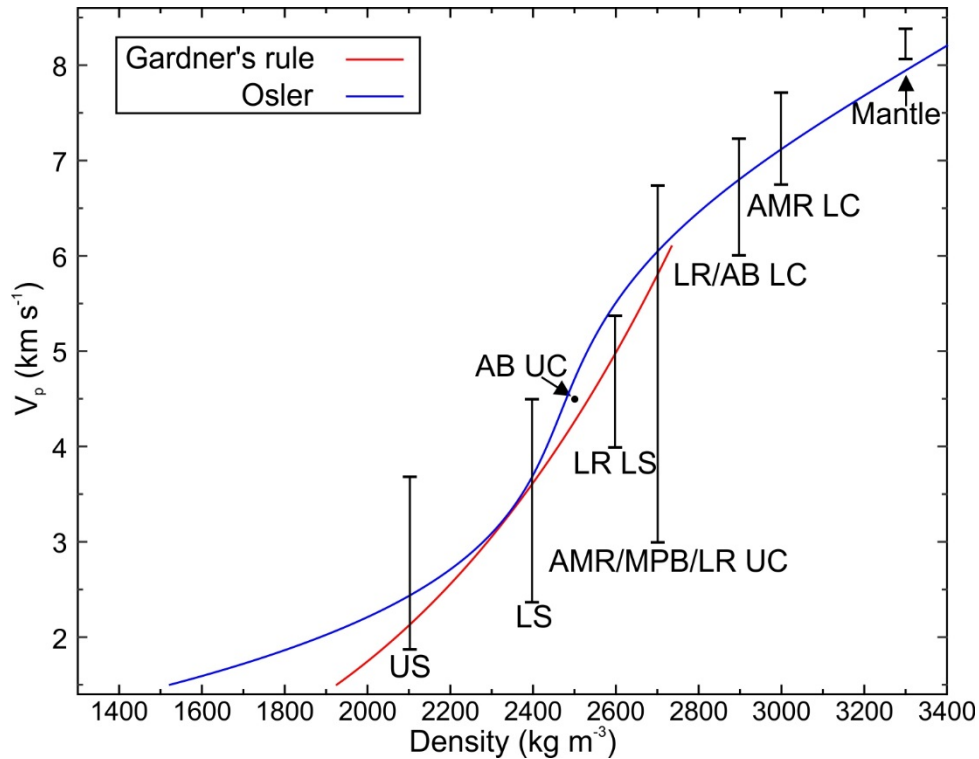
Fig. 4.5. The P-wave velocity-density relationship shown was used to estimate densities for gravity modelling. The curves for Gardner's rule and Osler are published in Gardner et al. (1974) and Osler (1993), respectively. Acronyms used in this figure are: US – upper sediments, LS – lower sediments (excludes the lower sedimentary layer at Lomonosov Ridge), LR LS – Lomonosov Ridge lower sediments, AMR/MPB/LR UC – Alpha-Mendeleev ridge complex/Makarov and Podvodnikov basins/Lomonosov Ridge upper crust, AB UC – Amundsen Basin upper crust, LR/AB LC – Lomonosov Ridge/Amundsen Basin lower crust, AMR LC – Alpha-Mendeleev ridge complex lower crust. Sources for constructing the variation in *Vp* for each density used are referenced under Section 4.4.

4.4. Density structure

The subsurface density structure for the thirteen models were based on seismic studies from the Arctic Ocean. These studies offered constraints on the geometry and density of sedimentary and crustal layers for the Alpha-Mendeleev ridge complex, Makarov and Podvodnikov basins, Lomonosov Ridge and Amundsen Basin.

4.4.1. Alpha-Mendeleev Ridge Complex

A thin hemi-pelagic sedimentary drape covering the Alpha-Mendeleev ridge complex was assigned a representative density of 2100 kg m^{-3} based on velocities of 1.6

to 3.4 km s^{-1} (Jokat, 2003; Funck et al., 2011; Bruvoll et al., 2012; Jokat and Ickrath, 2015; Evangelatos et al., 2017). The thickness of this layer varies from 0.5 to 1.2 km (Bruvoll et al., 2012; Jokat and Ickrath, 2015; Evangelatos et al., 2017).

On Alpha Ridge, seismic reflection records show draped sediments overlying syn-rift deposits present in grabens or deep valleys (Weber and Sweeney, 1990; Brumley, 2014; Evangelatos et al., 2017). Although sonobuoys were deployed on Alpha Ridge, the raypaths from these experiments did not appear to sample this layer. On Mendeleev Ridge, Jokat and Ickrath (2015) describe Palaeocene and older sedimentary successions filling basement lows. These lower successions exhibit velocities of 4.8 km s^{-1}. In contrast, the Arctic 2000 (Lebedeva-Ivanova et al., 2006) line provided more moderate velocities of 3.5–3.8 km s^{-1} for the lower sedimentary successions. Based on trial and error, a density of 2400 kg m^{-3} was assigned to this layer, which is at the lower end of the velocity range. The thickness of the lower sedimentary layer along AWI 2008 (Profile 13) varies from to 0.5 to 1.2 km (Weigelt et al., 2014). For simplicity and consistency, this density was also applied to the equivalent layer on Alpha Ridge. Its 2-D geometry was inferred based on seismic reflection data, where available (e.g., Profile 7; Evangelatos et al., 2017).

The crust of the Alpha-Mendeleev ridge complex was divided into upper and lower parts. The upper crust was assigned an average value of 2700 kg m^{-3} based on P-wave velocities of 3.0–6.5 km s^{-1} from the upper and mid-crustal layers (Asudeh et al., 1988; Jokat, 2003; Lebedeva-Ivanova et al., 2006; Funck et al., 2011; Bruvoll et al., 2012; Jokat and Ickrath, 2015; Evangelatos et al., 2017). The thickness of this layer is estimated at 5 to 8 km (Asudeh et al., 1988; Lebedeva-Ivanova et al., 2006; Funck et al.,

2011; Evangelatos et al., 2017). A lower crustal density of 3000 kg m^{-3} was used for gravity modelling. This estimate agrees with gravity modelling from other studies (Weber, 1986; Funck et al., 2011; Oakey and Saltus, 2016; Evangelatos et al., 2017). For comparison, Dove et al. (2010) used 2860 kg m^{-3} as an average density for the entire crust of Mendeleev Ridge. Moho for the Alpha-Mendeleev ridge complex is seismically constrained at 30 to 33 km depth by the Arctic 2000 (Lebedeva-Ivanova et al., 2006) and ARTA (Funck et al., 2011) lines.

4.4.2. Podvodnikov and Makarov Basins

The upper sedimentary layer exhibits velocities of 1.6 to 3.9 km s^{-1} (Weigelt et al., 2014; Evangelatos et al., 2017). A corresponding density of 2100 kg m^{-3} was assigned to this layer. The thickness of this layer is 3 km near the East Siberian Shelf, thins across the Arlis Gap, and then thickens again to ~1.5 km in Makarov Basin (Lebedeva-Ivanova et al., 2011; Weigelt et al., 2014; Evangelatos et al., 2017).

P-wave velocities of 3.3 to 4.3 km s^{-1} were determined for the lower sedimentary succession in Makarov Basin (Langinen et al., 2009; Evangelatos et al., 2017). Within Podvodnikov Basin, these sedimentary velocities increase to 5.9 km s^{-1} (Weigelt et al., 2014). These high velocities may result from a high degree of consolidation/compaction due to burial depth or caused by a lithological change. A density of 2400 kg m^{-3} was chosen for this layer. The thickness of the lower sedimentary succession thins from ~11 km at the base of the slope of the Siberian Shelf to less than 1 km over Arlis Gap, and then thickens to ~4 km in Makarov Basin (Lebedeva-Ivanova et al., 2011; Evangelatos et al., 2017).

The upper crust has P-wave velocities of 4.0–6.7 km s^{-1} from which a representative density of 2700 kg m^{-3} was derived. The thickness of this layer ranges from 3 to 7 km (Forsyth and Mair, 1984; Lebedeva-Ivanova, 2011; Evangelatos et al., 2017). Wide-angle reflection and refraction experiments indicate lower crustal P-wave velocities of 6.6–7.3 km s^{-1} (Forsyth and Mair, 1984; Lebedeva-Ivanova et al., 2011, Evangelatos et al., 2017). A density of 3000 kg m^{-3}, similar to the value of 2950 kg m^{-3} used by Sweeney et al. (1982), was assigned to this layer. Lower crustal thickness varies between 2.5 and 6 km, as suggested by velocity modelling.

4.4.3. Lomonosov Ridge

The thin hemi-pelagic sedimentary drape over Lomonosov Ridge was assigned a density of 2100 kg m^{-3} based on P-wave velocities of 1.6 to 3.4 km s^{-1} (Jokat et al., 1992; Jokat, 2005; Jokat and Ickrath, 2015). Due to the wide spacing of traces, the LORITA study poorly resolves the sedimentary section (Jackson et al., 2010). Excluding segments of significant basement highs and lows, the thickness of this layer varies from ~0.5 km at higher latitudes (Jokat et al., 1992) to ~3.5 km near the Siberian Shelf (Jokat and Ickrath, 2015). Evidence from the NP-28 data (Langinen et al., 2009) suggests that these upper successions thin to ~0.4 km (or 400 ms TWTT) at 88° N (on the North American side of Lomonosov Ridge). On the western flank of Lomonosov Ridge near the Canadian Polar Margin (Fig. 4.1), the GreenICE single channel section shows the upper sedimentary package with a thickness of 0.4–0.6 s TWTT (Kristoffersen and Mikkelsen, 2006).

Sedimentary deposits from the Cretaceous–lower Palaeocene period underlie the breakup unconformity. The thickness of this layer is variable relative to the overlying layer. Moreover, seismic reflection facies indicate syn-rift or pre-rift deposition (Jokat,

2005). This layer is 0.5–1 km thick near the East Siberian Shelf (Weigelt et al., 2014) and 0.4–1.5 km thick near the North Pole (Jokat et al., 1992; Jokat, 2005). Converting the NP-28 ice station data from TWTT to depth yields estimates of 0.4 to 1.7 km thick closer to the Canadian-Greenland margin (Profile 3; Langinen et al., 2009). P-wave velocities for these successions vary from 4.0 to 5.4 km s^{-1} (Jokat et al., 1992; Jokat, 2005; Jokat and Ickrath, 2015). Adjacent to the Canadian Polar Margin, the lower succession, demarcated at the top by "a Late Cretaceous or younger unconformity" (base of Unit D; Kristoffersen and Mikkelsen, 2006), is typically 0 to 0.4 ms TWTT thick, but is locally thicker beneath grabens. This layer was assigned a density of 2600 km s^{-1}.

As with the Alpha-Mendeleev ridge complex, the crust of Lomonosov Ridge was separated into two layers. P-wave velocities for the upper crust range from 5.2 to 6.5 km s^{-1} (Jokat et al., 1992; Jackson et al., 2010; Poselov et al., 2012; Jokat and Ickrath, 2015). Lithologically, the lower velocities may represent meta-sedimentary rocks, as interpreted by Jackson et al. (2010) and Poselov et al. (2012). The density of the upper crust was approximated using a uniform density of 2700 km s^{-1}. The maximum thickness of this layer is ~11 km directly beneath the axis of Lomonosov Ridge (Jackson et al., 2010; Poselov et al., 2012). The upper crust thins beneath the flanks of the ridge.

A density of 2900 km s^{-1} was determined for the lower crust based on P-wave velocities of 6.6–6.7 km s^{-1} (Jackson et al., 2010; Poselov et al., 2012). The thickness of this layer is estimated at 8–9 km (Jackson et al., 2010; Poselov et al., 2012).

4.4.4. Amundsen Basin

The sedimentary section in Amundsen Basin is split between upper successions (Vp = 1.9–2.2 km s^{-1}) that exhibit seismic reflection patterns that are mostly concordant with underlying structure, and lower successions (Vp = 2.2–4.5 km s^{-1}) that dip towards Gakkel Ridge (Jokat et al., 1995). Thicknesses for the upper and lower successions at the base of slope of Lomonosov Ridge are 0.5 and 2.7 km, respectively (Weigelt and Jokat, 2001). Assigned densities for these two sedimentary layers are 2100 kg m^{-3} for the top layer and 2400 kg m^{-3} for the bottom layer.

The crustal section is described as having a thin oceanic layer 2 (Vp = 4.5 km s^{-1}) with a thickness of 0.5 km and a layer 3 (Vp = 6.0–7.2 km s^{-1}) that is 2.5–6 km thick (Duckworth et al., 1982; Duckworth and Baggeroer, 1985). Oceanic layer 2 and 3 were assigned densities of 2500 kg m^{-3} and 2900 kg m^{-3}, respectively.

4.5. Results

The thirteen 2-D gravity models are shown in Figs. 4.6, 4.7, 4.8 and Appendix C. The depths to basement and Moho along the profiles were extracted from these models and interpolated into grids with 12.5 by 12.5 km cell spacing. Based on the Moho grid shown in Fig. 4.9, the depth of Moho in the region of study varies from approximately 10 km in Amundsen to 32 km beneath Alpha Ridge. To test the validity of estimating Moho depth from this grid, results of this study are compared to 2-D gravity models from Oakey and Saltus (2016). While these authors used a mid-crustal density of 2900 kg m^{-3} for Alpha Ridge and an upper crustal density 2800 kg m^{-3} for Lomonosov Ridge, the results from the two studies are similar (Fig. 4.10). Minor discrepancies between the two

methods are attributed to differences in assumed rock densities. Additionally, Moho depths from this study largely agree with results from Glebovsky et al. (2013).

The difference between the depth-to-top of basement and depth-to-Moho grids is crustal thickness (Fig. 4.11). In Makarov and Podvodnikov basins, crustal thickness ranges from slightly over 4 to 16 km. The crust within these basins is thinnest in the northern subbasin area (Fig. 4.11), as defined by Evangelatos and Mosher (2016).The difference between the depth-to-basement and depth-to-Moho grids is crustal thickness (Fig. 4.10). In Makarov and Podvodnikov basins, crustal thickness ranges from slightly over 4 to 16 km. The crust within these basins is thinnest in the subbasin area (Fig. 4.11), as defined by Evangelatos and Mosher (2016).
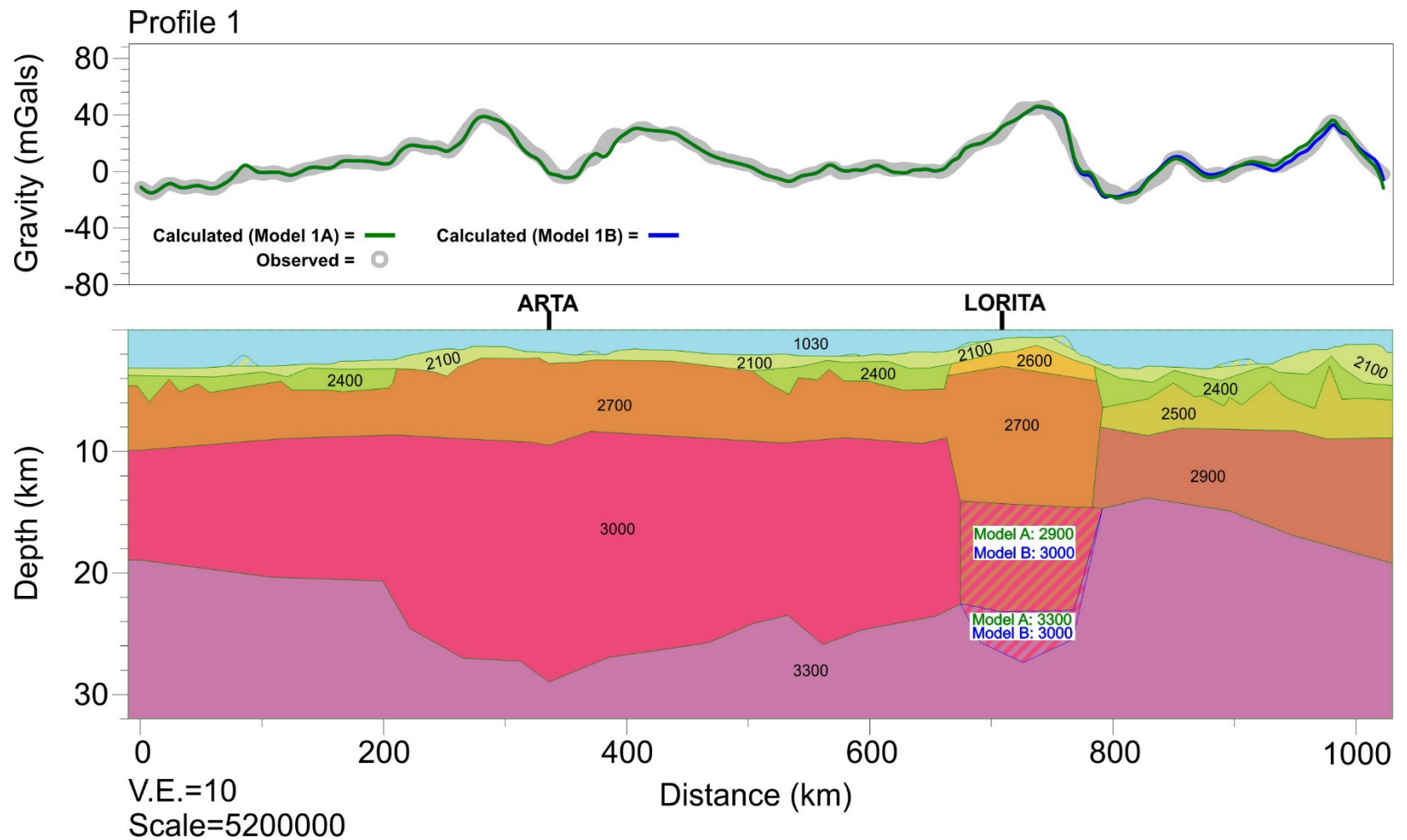
Fig. 4.6. Profile 1. The top panel depicts the observed free-air gravity anomaly compared to calculated gravity (models 1A and 1B). The observed data were extracted from the compilation of Anderson et al. (2010). The bottom panel depicts the subsurface gravity model with densities specified in kg m^{-3}. Note that the lower crust of Lomonosov Ridge is 2900 kg m^{-3} for Model A and 3000 kg m^{-3} for Model B– all other layer densities are unchanged. The depth of Moho beneath Lomonosov Ridge is only boundary layer that differs between models A and B. Refer to Section 4.2.2 for descriptions of seismic data used to constrain this profile. The location of this profile is shown in Fig. 4.1.
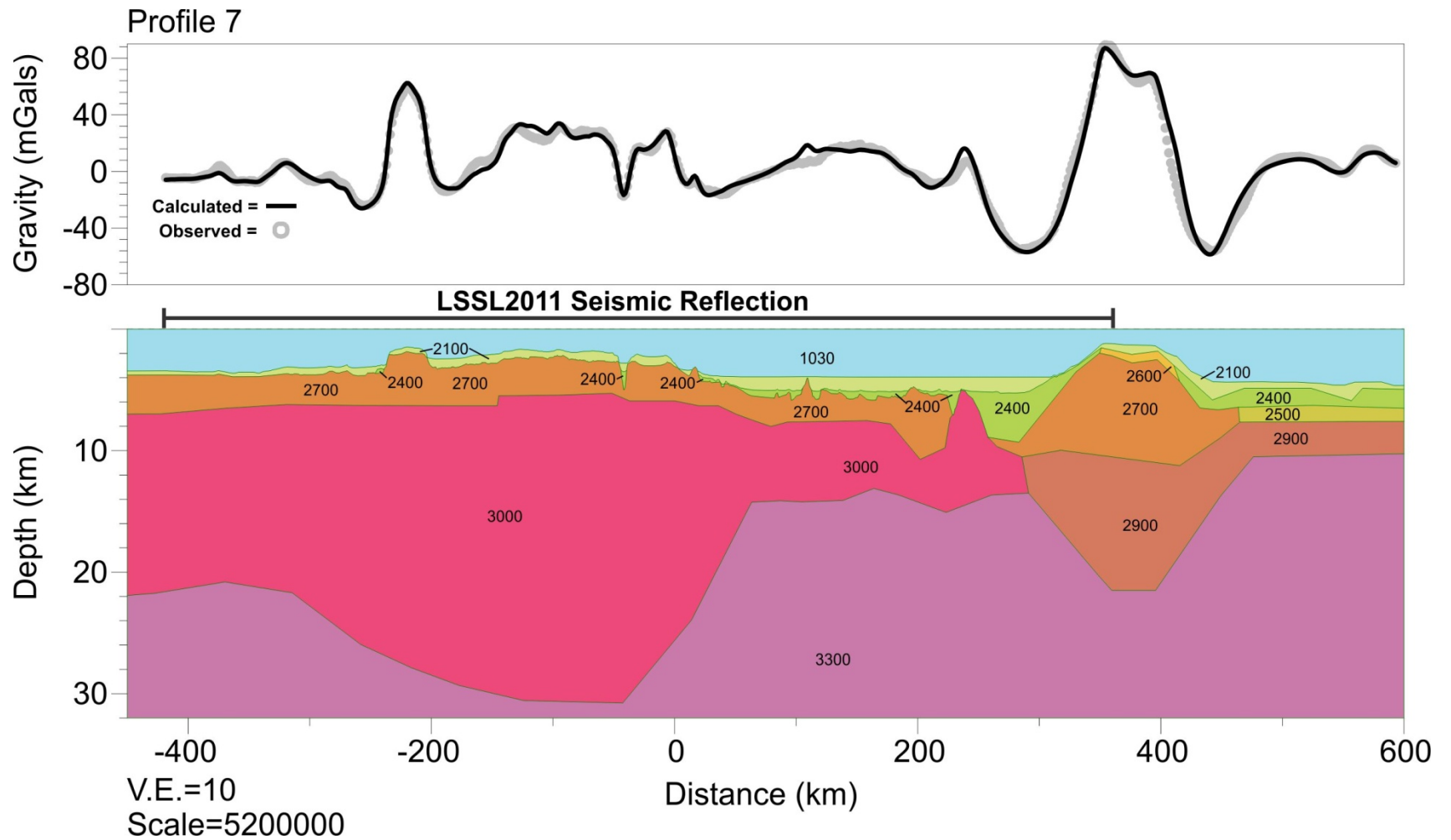
Fig. 4.7. Profile 7. The top panel depicts the observed free-air gravity anomaly compared to calculated gravity. The observed data are a combination of shipborne gravity (Mosher, 2012) and data extracted from the compilation of Anderson et al. (2010) . The bottom panel depicts the subsurface gravity model with densities specified in kg m^{-3}. Refer to Section 4.2.2 for descriptions of seismic data used to constrain this profile. The location of this profile is shown in Fig. 4.1.

Profile 13

High Arctic Magnetic Domain

Observed = ○

Calculated =
Observed = ○

AWI-2008 Seismic Reflection
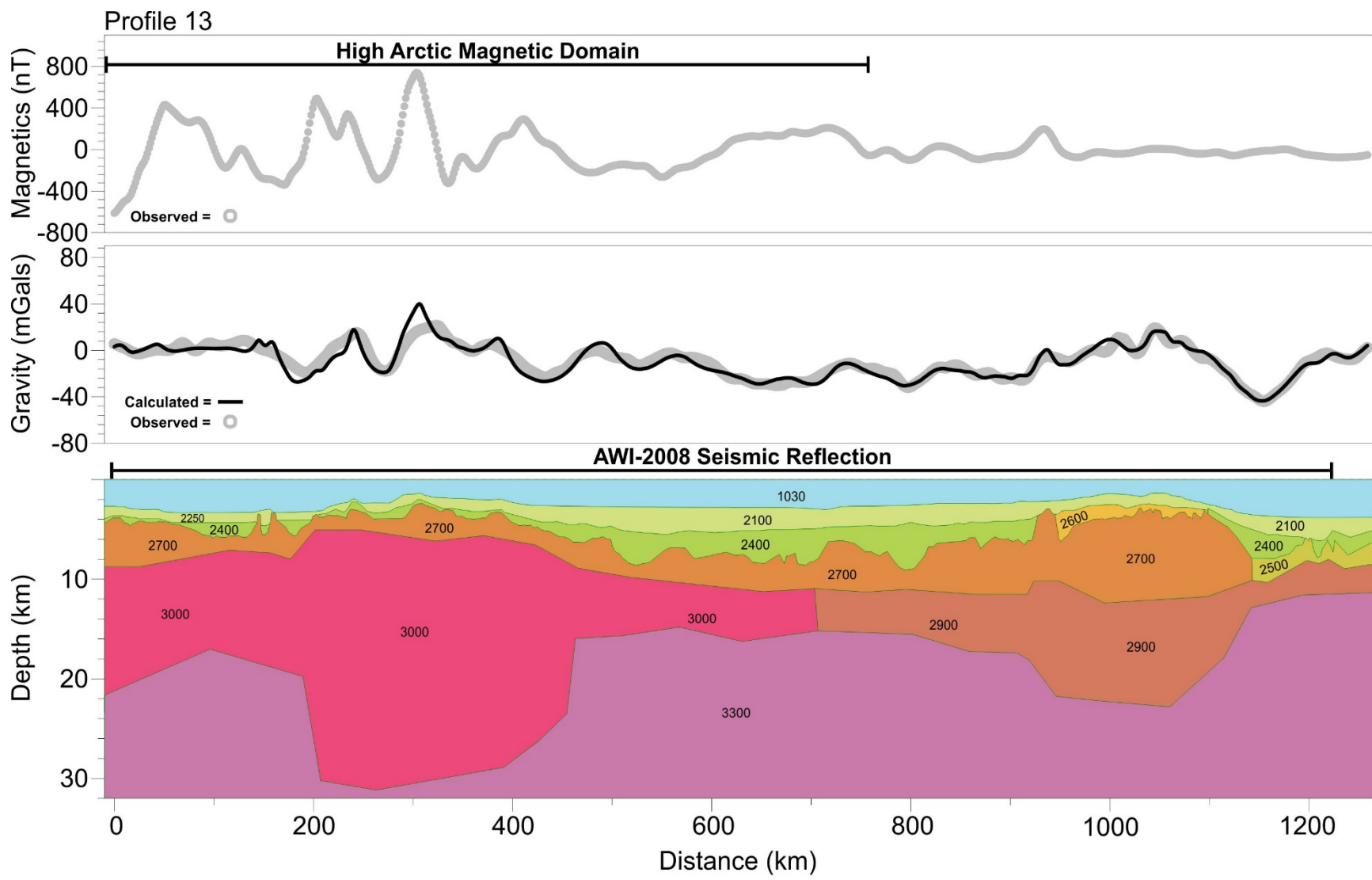
Fig. 4.8. Profile 13. The top panel depicts the observed magnetic anomaly data. The middle panel depicts the observed free-air gravity anomaly compared to calculated gravity. The observed potential field data were extracted from the compilations of Anderson et al. (2010) for gravity and Gaina et al. (2011) for magnetic data. The bottom panel depicts the subsurface gravity model with densities specified in kg m^{-3}. Refer to Section 4.2.2 for descriptions of seismic data used to constrain this profile. The location of this profile is shown in Fig. 4.1.
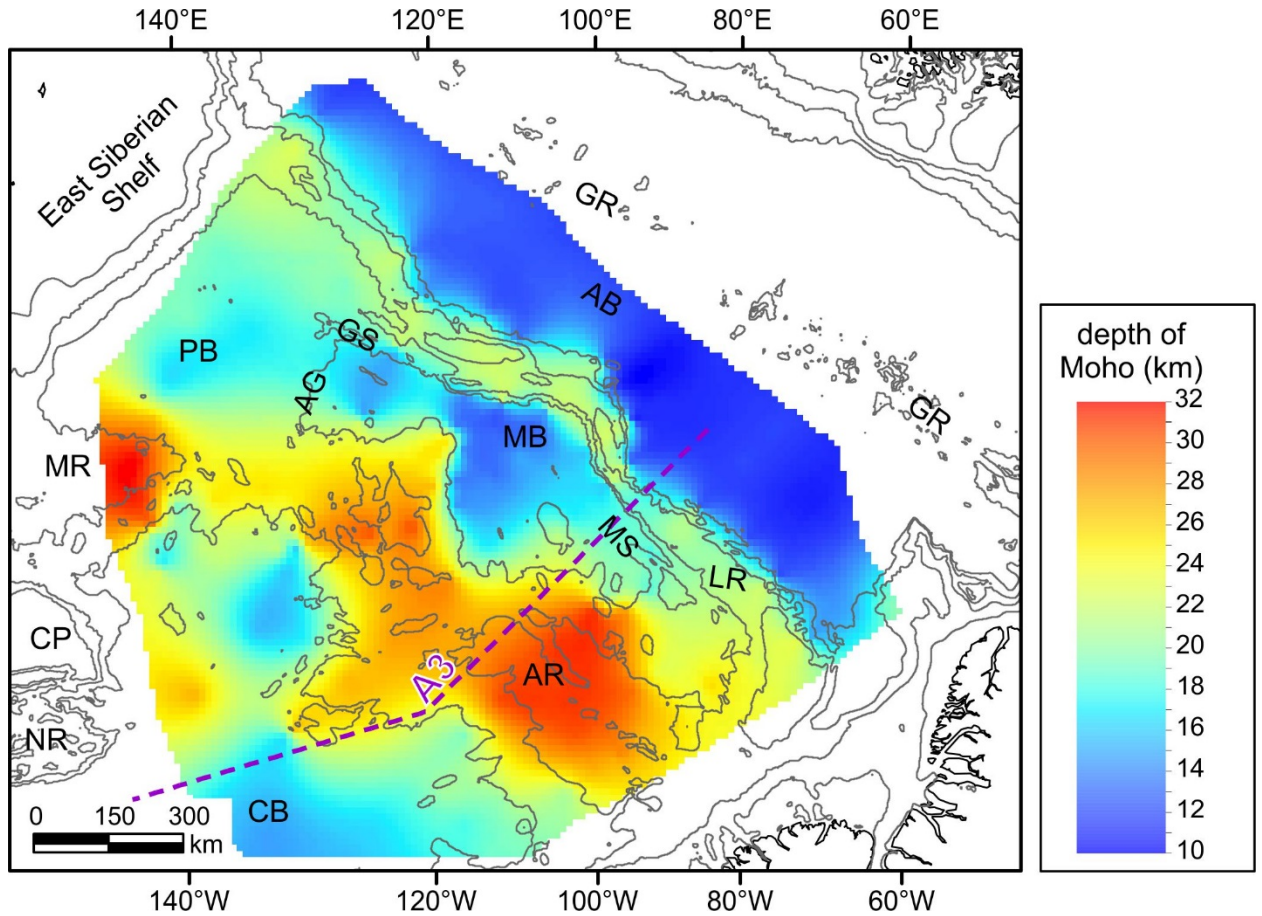
Fig. 4.9. Coloured map of the depth-to-Moho grid. The dashed purple line (A3) shows the location of a gravity model from Oakey and Saltus (2016). Acronyms are defined in Fig. 4.1. Selected isobaths isobaths (200 m, 500 m, 1000 m, 2000 m and 3000 m) were produced from the IBCAO version 3.0 grid (Jakobsson et al., 2012) to provide a geographic reference for the model results.
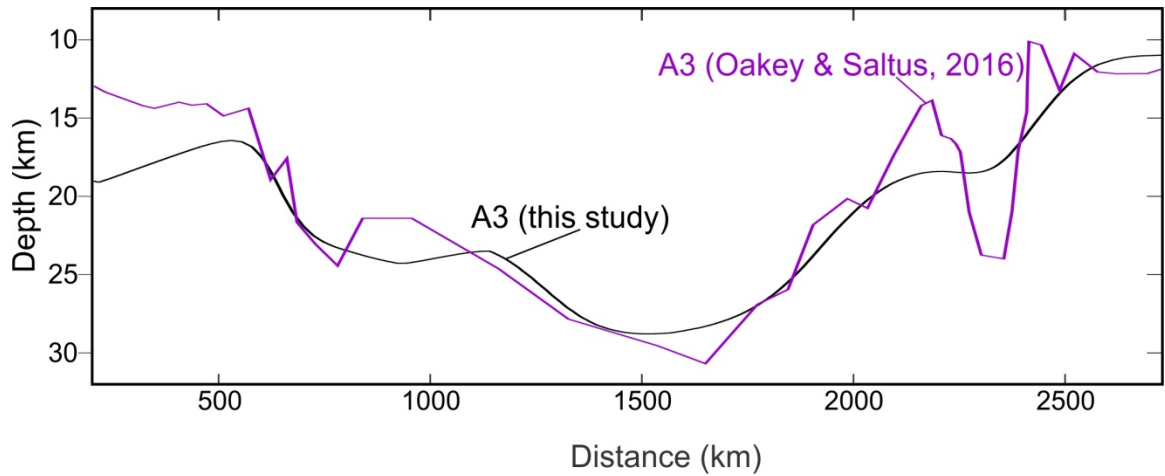
Fig. 4.10. The Moho depths along line A3 from Oakey and Saltus (2016) are compared to Moho depths calculated in this study and extracted from the grid shown in Fig. 4.9.
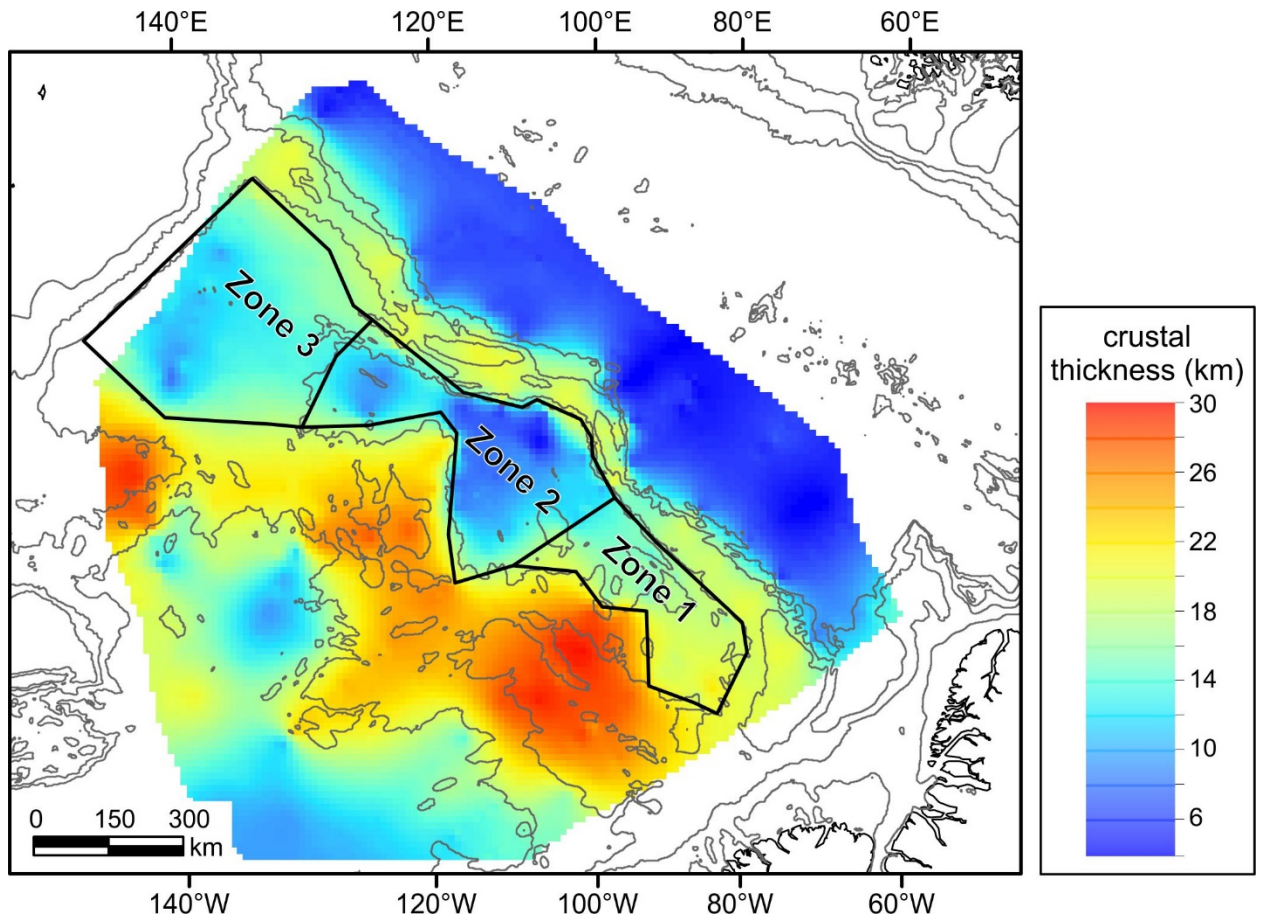
Fig. 4.11. Coloured map of crustal thickness grid. Selected isobaths isobaths (200 m, 500 m, 1000 m, 2000 m and 3000 m) were produced from the IBCAO version 3.0 grid (Jakobsson et al., 2012) to provide a geographic reference for the model results.

4.6. Discussion

4.6.1. The Amerasian Margin of Lomonosov Ridge

The principal aim of this study is to define the structural relationship between the northern Amerasia Basin and Lomonosov Ridge, thus the following discussion focuses on this geographic region. The crustal thickness gradient (rate of change) from the Lomonosov Ridge to the Makarov and Podvodnikov basins varies along the length of the ridge margin. The basins are thus divided into three zones based on this variation. The crustal thickness gradient and topographic gradient, which are linked by isostasy, are used to define these zones (Fig. 4.11). The character of each zone and its tectonic implication are discussed below.

Zone 1: Marvin Spur to the Canadian Arctic Archipelago

Zone 1 centres on the part of the margin closest to the Canadian Polar Shelf. Morphologically, Alpha and Lomonosov ridges converge towards the Canadian Polar margin. The gravity models indicate that the crust of Makarov Basin progressively narrows towards the Canadian Polar margin until it is no longer resolvable (Fig. 4.6). In Model 1A of Profile 1, the crusts of Alpha and Lomonosov ridges are juxtaposed and Moho is ~4–6 km shallower in the latter versus the former. According to one possible model submitted by Døssing et al. (2013), magnetic lineations between Alpha and Lomonosov ridges near the Canadian Polar margin represent magnetic dykes (Fig. 4.3). This interpretation is based on the apparent alignment of these anomalies with NW-trending Early Cretaceous dykes documented on Franz Josef Land (133.8 ± 3.4–125.2 ± 5.5 Ma; Dibner, 1998) upon the restoration of Lomonosov Ridge to the Barents–Kara Shelf (i.e., closing Eurasia Basin). The possibility that the Alpha-Mendeleev LIP impacts

Lomonosov Ridge is considered by assuming identical densities of 3000 kg m^{-3} for the lower crust of Alpha Ridge and Lomonosov Ridge (Model 1B; Fig. 4.6). The Moho beneath Lomonosov Ridge in Model 1B is lowered to a maximum of 27 km depth (versus ~23 km for Model 1A; Fig. 4.6) in order to compensate for the added mass and fit the gravity. The shallower Moho is more compatible with the depth of Moho from the cross-tie with the LORITA refraction line (Jackson et al., 2010). Furthermore, the maximum depth of Moho, according to the TransArctic 1992 model in Zone 3, is also slightly less than 23 km. In addition, the HAMH domain does not overlap with the Lomonosov Ridge (Fig. 4.3), suggesting that "deep-rooted HALIP volcanism did not affect the bulk crustal structure [of Lomonosov Ridge]" (Oakey and Saltus, 2016). As such, Model 1A is considered more geologically viable. The results of this effort imply that Early Cretaceous magmatism on Franz Josef Land is unrelated to the Alpha-Mendeleev LIP.

Zone 2: Makarov Basin

Zone 2 encompasses the central part of the margin of Lomonosov Ridge. The crust is thinnest in this zone compared to other parts of the study area (Fig. 4.11). The crustal thickness decreases from 19–21 km thick beneath Lomonosov Ridge to 5–10 km thick beneath the deep subbasin of Makarov Basin over distances of 10–70 km (based on profiles 5–11; Fig. 4.7 and Appendix C). This relatively abrupt change in crustal thickness from Lomonosov Ridge to Makarov Basin is noted in LOREX data (Forsyth and Mair, 1984), and is typical of transform margins (e.g., Lorenzo and Wessel, 1997; Basile and Allemand, 2002). The steep bathymetric slopes, splay structures and bends along the strike orientation of Lomonosov Ridge along this segment of the margin further support this interpretation (Cochran et al., 2006; Evangelatos and Mosher, 2016). The

existence of a transform margin along the Amerasian side of Lomonosov Ridge is consistent with opening of Amerasia Basin as per the *rotational* model (e.g., Grantz et al., 2011). It has been proposed by various authors that oceanic crust underlies the area encompassed by Zone 2 (Alvey et al., 2008; Lebedeva-Ivanova et al., 2011). A negative relief basement structure was imaged by recent seismic reflection surveys (Kaminsky, 2017). Chernykh et al. (2015) claimed that this buried feature is an extinct spreading centre responsible for opening Makarov Basin in the Upper Cretaceous. Evangelatos et al. (2017), however, concluded that crust beneath Makarov Basin (excluding the deep subbasin) along line LSSL2011 (Fig. 4.6) was thicker than normal oceanic crust of comparable age.

Zone 3: Podvodnikov Basin

Zone 3 is closest to the East Siberian Shelf. Bathymetry within Zone 3 (i.e., Podvodnikov Basin) is smooth (Fig. 4.1) as a consequence of a relatively high sedimentary influx originating from the Siberian landmass (Jakobsson et al., 2003). As evidenced by seismic reflection profiles (e.g., AWI 2008; Jokat and Ickrath, 2015) and regional geoscientific studies (Gaina et al., 2014; Petrov et al., 2016), sedimentary thickness is also greater relative to other zones. Based on seismic reflection record AWI-2008, Jokat and Ickrath (2015) concluded that horst and graben structures beneath the western half of Podvodnikov Basin are due to extension of continental crust similar to that of Lomonosov Ridge. The remainder overlaps with the HAMH of Oakey and Saltus (2016) and is considered part of the crust of Mendeleev Ridge (Fig. 4.8). Interestingly, the preferred model of Alvey et al. (2008) shows Jurassic oceanic crust trapped in the northern part of Podvodnikov Basin. In this case, the Arlis Gap may represents a

boundary between adjacent crustal domains. Doré et al. (2016) and Lundin and Doré (2017) and proposed that Canada Basin and the Makarov and Podvodnikov basins did not open synchronously and were never tectonically linked, which contrasts with the regional rotational model of Grantz et al. (1979, 2011). As discussed in Lundin and Doré, 2017, while Canada Basin was opening (125–80 Ma), a "proto-Makarov–Podvodnikov Basin" was developing due to right-lateral shearing opposite of a hypothetical transform margin located on the northern margin of Canada Basin. Thereafter, Podvodnikov Basin continued to expand from 80 to 60 Ma due to extension oriented perpendicular to Lomonosov Ridge, causing Podvodnikov Basin to widen further relative to Makarov Basin. Extension is also in evidence via surficial structures of Mendeleev Ridge and northern Alpha Ridge (Brumley, 2014; Nikishin et al., 2017).

4.6.2. Is Lomonosov Ridge Undercompensated?

Fig. 4.12 shows lithostatic pressure curves for profiles 1 and 7 (Figs. 4.6 and 4.7), calculated from the assumed rock densities and their thicknesses. In both cases, the signature of Lomonosov Ridge is noticeably higher than adjacent geological provinces. As such, it appears that Lomonosov Ridge is undercompensated or regionally compensated. This anomaly is possibly linked to a middle Eocene to lower Miocene hiatus (Backman et al., 2008). The reason for this hiatus is unclear. Minakov and Podladchikov (2012) proposed that a mineral phase change in the mantle and associated lithospheric heating led to uplifting of the ridge. If true, the apparent undercompensated state of Lomonosov Ridge is a relic signature.
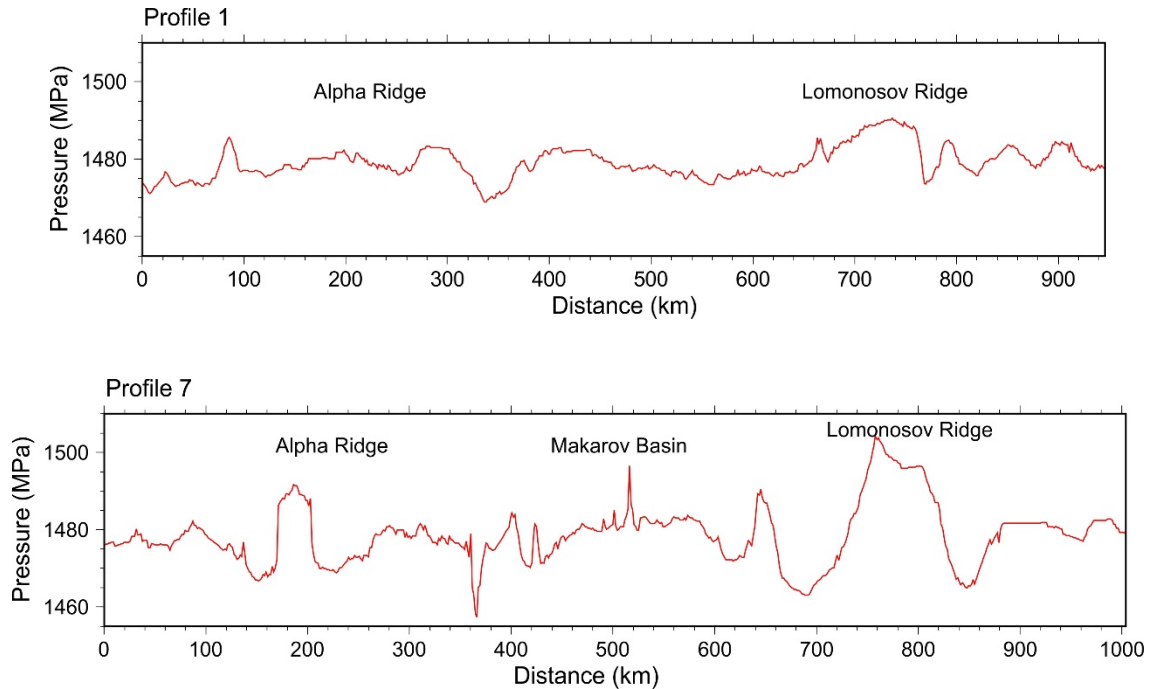
Fig. 4.12. The lithostatic pressure at 50 km depth for profiles 1 and 7 (Figs. 4.6 and 4.7, respectively).

4.7. Conclusions

Thirteen synthetic gravity profiles were modelled to provide insight on the relationship between Makarov and Podvodnikov basins and the adjacent Lomonosov Ridge. Northern Amerasia Basin is divided into three zones based on the difference in the gradient of crustal transition between these basins and Lomonosov Ridge. In Zone 1, close to the Canadian Arctic Archipelago margin, there is no distinct gravity signature between Alpha Ridge and Lomonosov Ridge. This result suggests that there is no tectonic separation of the two domains. In Zone 2, there is an abrupt crustal transition between Makarov Basin and Lomonosov Ridge, according to their respective gravity signatures. This result is consistent with transform or transtensional deformation along this segment of the margin of Lomonosov Ridge. In turn, this interpretation supports a rotational style of opening of Amerasia Basin. In Zone 3, crustal transition between Podvodnikov Basin

and Lomonosov Ridge is more gradual, according to the gravity modelling, suggesting that the basin was formed predominantly by extension.

Other lines of evidence support conclusions presented in this study. In the first case, there is no morphological separation between Alpha and Lomonosov ridges. There is also evidence in the rock record from the adjacent Ellesmere Island, and from dredge samples that the two entities were adjacent. In the second instance, seismic reflection and refraction data also suggest a rapid transition from Lomonosov Ridge to Makarov Basin, with a significant change in crustal velocities and presence of a narrow deep basin infilled with progradational sediments (Evangelatos and Mosher, 2016; Evangelatos et al., 2017). Also, this conclusion is supported by morphological evidence (e.g., Cochran et al., 2006; Evangelatos and Mosher 2016). In the third zone, extensional structures are notable even in a morphological assessment of Mendeleev Ridge and northern Alpha Ridge, as well as in the seismic reflection records of Podvodnikov Basin.

CHAPTER 5: CONCLUSIONS

The tectonic and stratigraphic relationship between Makarov Basin and Lomonosov Ridge is reviewed in this chapter in light of results presented in previous chapters, including seismic reflection stratigraphy, velocities derived from seismic refraction analysis and gravity modelling. These new constraints and the new age model (Chapter 2) are incorporated into the latest Arctic plate-reconstructions.

5.1. The relationship Between Makarov Basin and Lomonosov Ridge

It was widely assumed that *in situ* oceanic crust underlies Amerasia Basin (Carey, 1958; Tailleur 1973; Grantz et al., 1979, 1998, 2011; Lawver and Baggeroer, 1983; Embry and Dixon, 1994; Laxon and McAdoo, 1994; Lawver et al., 2002), as opposed to old entrapped oceanic crust. This assumption was recently confirmed using seismic refraction analysis (Chian et al., 2016). Considering that four shelf margins enclose Amerasia Basin (Fig. 5.1), and assuming that either passive rifting or strike-slip movement forms each margin, there is a finite number of permutations for describing the margins of Amerasia Basin (Lawver and Scotese, 1990). With respect to the Makarov Basin-facing flank of Lomonosov Ridge, there is still disagreement as to the type of margin that applies. According to one hypothesis, the Amerasian flank of Lomonosov Ridge is an extensional rift margin (e.g., Miller and Verzhbitsky, 2009). Hypothetically, Arctic Alaska can serve as the conjugate margin to Lomonosov Ridge (e.g., Dutro, 1981). A wealth of evidence, however, ties Arctic Alaska to the Canadian Arctic margin (Embry, 1990; Grantz et al., 2011; Gottlieb et al., 2014). Also, there is growing support for the notion that the Alpha-Mendeleev ridge complex did not form late, but rather

magmatism related to the Alpha-Mendeleev large igneous province (LIP) triggered opening of Amerasia Basin (e.g., Døssing et al., 2013). As such, the Alpha-Mendeleev ridge complex results from hyperextension of the Lomonosov Ridge/Barents-Kara margin. Tectonic models that promote this hypothesis include Crane (1987), Smith (1987), Dickinson (2009), Miller and Verzhbitsky (2009) and Doré et al. (2016). Jokat and Ickrath (2015) remarked that seismic reflection records from the western part of Podvodnikov Basin show horsts and grabens. These features are interpreted as extended continental crust linked to the Lomonosov Ridge. Such features are evidence of stress oriented perpendicular to Lomonosov Ridge (at least adjacent to Podvodnikov Basin), in compliance with the *extensional rift margin* hypothesis. Such stress is predicted by the relative motions of the Eurasian and North American plates prior to opening of Eurasia Basin, according to Gaina et al. (2002).

In opposition to the *extensional rift margin* hypothesis, the Amerasian margin of Lomonosov Ridge has been interpreted as a strike-slip boundary (e.g., Cochran et al., 2006). As the rotational model requires the existence of such a boundary, Grantz et al. (1979) proposed that the Amerasian side of Lomonosov Ridge formed by transform (Lomonosov Transform). Cochran et al. (2006) noted that Marvin Spur and other small linear ridges that are parallel or sub-parallel to Lomonosov Ridge align along small circles about a pole of rotation in the area of the Mackenzie River delta. These marginal ridges are argued to have formed by splay faulting due to transform and/or transtensional stress during early opening of Amerasia Basin (Cochran et al., 2006). The results from this thesis supports the latter hypothesis or a combination of the two. The relatively abrupt crustal transition from Makarov Basin to Lomonosov Ridge is consistent with a

transform margin (refer to Chapter 3). As demonstrated in chapters 2 and 4, the orientation of the implied stress fields documented along the Amerasian margin of Lomonosov Ridge changes. Specifically, while the central part of Lomonosov Ridge is consistent with a strike-slip system (Chapter 2), the presence of horst and grabens underlying Podvodnikov Basin and adjacent to Lomonosov Ridge favours extension perpendicular to the margin (Jokat and Ickrath, 2015). Closer to the Canadian Polar margin, marginal ridges, like Marvin Spur, are interpreted as splay structures having formed by transtension (Cochran et al., 2006) or, alternatively, passive rifting (Langinen et al., 2009).

Below, the tectonic evolution of Amerasia Basin is explored. Palinspastic figures of this evolution incorporating the recent findings of this study are included.
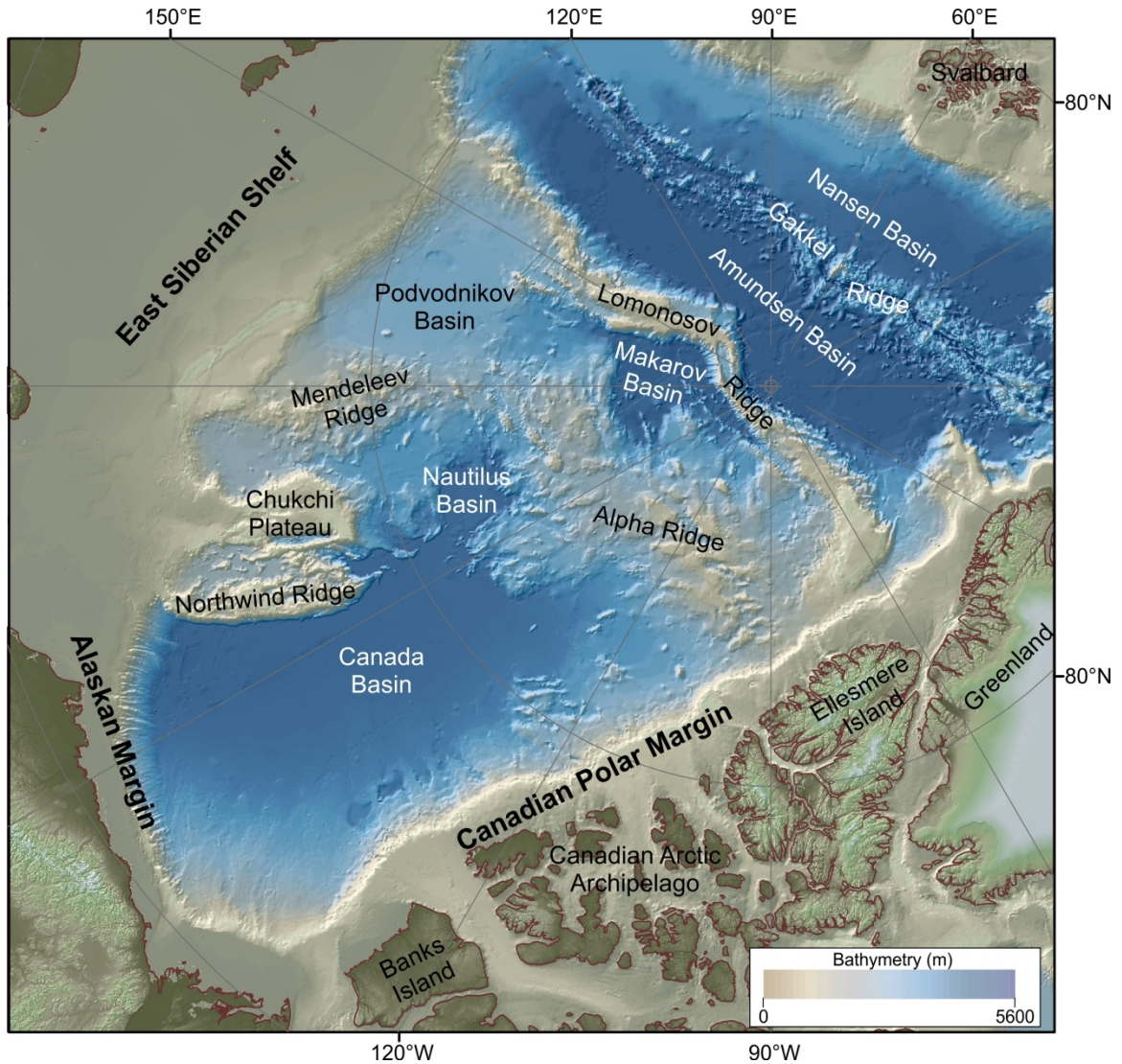
Fig. 5.1. Sun-shaded elevation map of the Arctic Ocean. Bathymetry and topography are rendered from the IBCAO version 3.0 grid (Jakobsson et al., 2012).

5.2. The Origin and Evolution of Makarov Basin

5.2.1. Initiation of Continental Rifting Leading to Amerasia Basin (pre-135 Ma)

Miller et al. (2017) compiled a map of basement geology for the circum-Arctic region (Fig. 5.2). According to this map, continental crust beneath Makarov Basin (where present) is underlain by Caledonide basement adjacent to the North American craton, while the remainder is composed of Timanide basement. As suggested by results

presented in Chapter 3, the upper crust underlying the deep subbasin between Marvin

Spur and Lomonosov Ridge is thinned continental crust. This crust is tied to meta-

sedimentary rocks of the lower Paleozoic Franklinian Basin reported along the coast of

Ellesmere Island and Greenland (Trettin, 1991; Henriksen and Higgins, 2000; Jackson et

al., 2010).
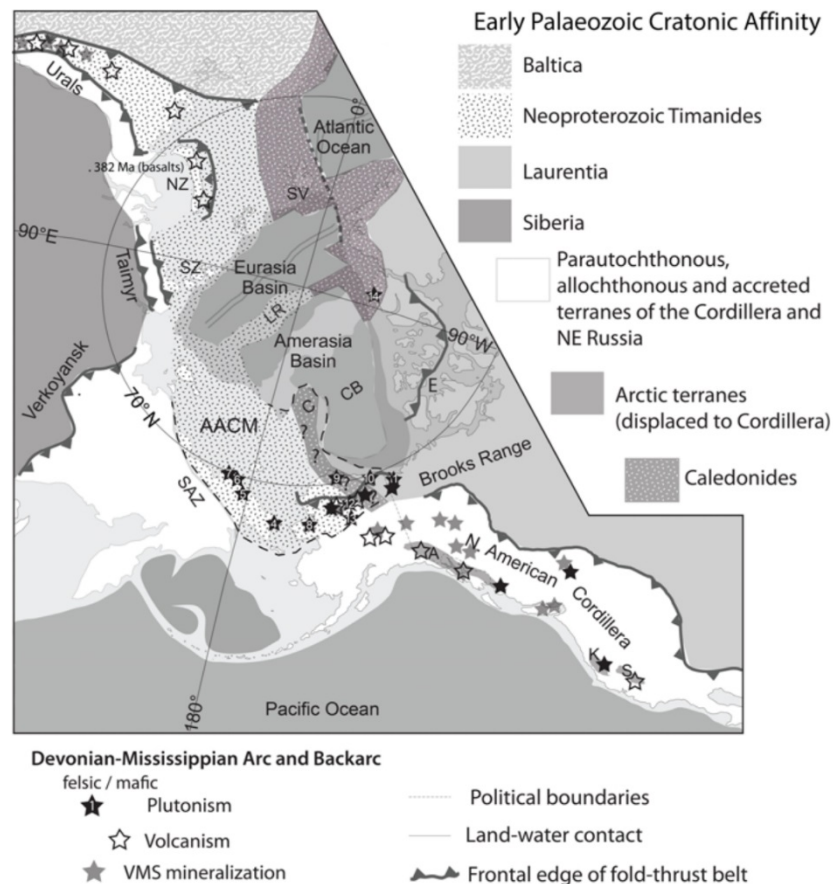
Fig. 5.2. Basement geology map of the Arctic region (from Miller et al., 2017). Acronyms: AACM – Arctic Alaska–Chukotka microplate; C – Chukchi Borderland; CB – Canada Basin; LR – Lomonosov Ridge; NZ – Novaya Zemlya; SAZ – South Anyui Suture Zone; SV – Severnaya Zemlya; SV – Svalbard.

Embry and Dixon (1994) interpreted a regional unconformity from the lower part

of the Middle Jurassic as the beginning of continental rifting that led to the formation of

the early Arctic Ocean based on dating of normal faults offshore Arctic Alaska (Hubbard et al., 1987) and Sverdrup Basin (Embry, 1991). Buchan and Ernst (2006) proposed that High Arctic dyke swarms of Cretaceous age are associated to a regional LIP (i.e., HALIP) and predicted that the centre of the plume was located northwest of Ellesmere Island. Building on these concepts, Døssing et al. (2013) proposed that the HALIP plume caused crustal-scale doming, which eventually led to continental breakup and hence seafloor spreading in Amerasia Basin. In addition, they suggested that an annular magnetic anomaly (Fig. 5.3A) over Alpha Ridge represents the centre of the HALIP plume. Alternatively, opening of Amerasia Basin resulted from horizontal tectonics. The South Anyui Ocean was a large embayment of the Mesozoic–upper Palaeozoic Panthalassa Ocean that was subducted in the Upper Jurassic–Lower Cretaceous (Shephard et al., 2013). Its closure attached the Arctic Alaska–Chukotka microplate to Eurasia along the South Anyui Suture (Figs. 5.3B and 5.3C; e.g., Kuzmichev, 2009; Drachev et al., 2010; Amato et al., 2015). Lundin and Doré (2017) proposed that closure of the South Anyui Ocean in the Upper Jurassic (Kimmeridgian) caused oblique back-arc rifting which led to opening of Canada Basin in the Lower Cretaceous (Fig. 5.3A). To discriminate between these two hypotheses would require analysis of regional geochemical data and plate-kinematic constraints. Such extensive research is beyond the scope of this study.

Doré et al. (2016) presented a variant of the rotational model with the northern transform situated along the southern flank of Alpha and Mendeleev ridges (i.e., facing Canada Basin). Fig. 5.3A is a modified version of this plate-reconstruction model that

includes the Lomonosov Transform. The zone between these transform boundaries is sheared and stretched under oblique extension.

5.2.2. Early Opening of Amerasia Basin (135–90 Ma)

Direct constraints on the maximum age of Makarov Basin are limited. Identification of magnetic chron anomalies can constrain the style of opening and its progression. Taylor et al. (1981) interpreted chrons 34 through to 21 (~80 to 53 Ma) mirrored about a spreading centre that crudely corresponds with the 87°N. Kovacs et al. (1999) described spreading anomalies at the middle part of Makarov Basin. Their best fit model assumes an age of ~128 Ma (M7 anomaly) for the spreading centre. More recent potential field compilations by Gaina et al. (2011) improved the resolution of the High Arctic magnetic grid while further raising doubt on the interpretations of Taylor et al. (1981) for Makarov Basin. Relying on a newer aeromagnetic dataset, Døssing et al. (2013) described linear magnetic anomalies near the Canadian Polar Margin between and perpendicular to Alpha and Lomonosov ridges. These authors interpreted these anomalies as representing seafloor spreading anomalies and/or Lower Cretaceous magnetic dykes. Seafloor anomalies were fit assuming ages of ~138–126 Ma. The interpretations of Døssing et al. (2013) should be viewed with caution, however, as the linearity of the magnetic anomalies identified as dykes and/or magnetic chrons are artificially enhanced by shading and directional filtering. Regardless, based on evidence that this region is underlain by thick magmatically overprinted crust (i.e., gravity modelling, overlap with magnetic domain), any preservation of a magnetic signal related to seafloor spreading is unexpected. Furthermore, as remarked by Sorokin et al. (1999), interpretations of

magnetic chron anomalies from the northern Amerasian basins have not properly considered the effect of (basement) topography.

The tectonic reconstruction model by Grantz et al. (2011) shows Canada and Makarov basins opening contemporaneously as a single large basin. Embry and Dixon (1994) argued that a Hauterivian unconformity (135–131 Ma) represents continental breakup, heralding the beginning of seafloor spreading in Amerasia Basin. Recent studies of Canada Basin (e.g., Chian et al., 2016) agree with the timing. Alternatively, based on onshore geological studies in Arctic Russia, Miller and Verzhbitsky (2009) asserted that Makarov and Podvodnikov basins formed by rifting of the Lomonosov Ridge/Barents Shelf margin between ~120 and 105 Ma (Albian–Aptian). Embry and Dixon (1994) correlated a regional Cenomanian unconformity (100–93.9 Ma) with the end of seafloor spreading in Canada Basin. Strike-slip tectonics in northern Amerasia Basin correspondingly abated approximately during this period.

Analysis of seismic line LSSL2011-03/04 across Makarov Basin has provided important new constrains on the evolution of the basin (refer to chapters 2 and 3). Dextral shearing created splay structures (e.g., Marvin Spur) and small pull-apart basins along the Amerasian margin of Lomonosov Ridge, and possibly the Alpha Ridge margin, that served as depositional centres for sediments supplied by the Mesozoic Barents-Kara Shelf (Fig. 5.3B). The zone underlying these transtensional basins is shown as Phase 1 crust (Fig. 5.3B–5.3F), which is interpreted as thinned continental crust.

5.2.3. Widening of Makarov and Podvodnikov Basins (90–65 Ma)

The deeper sedimentary successions of Makarov Basin host interbedded volcanogenic material, as discussed in Chapter 2, suggesting that Makarov Basin existed while the Alpha-Mendeleev LIP was active (Fig. 5.3C). The end of magmatism related to the Alpha-Mendeleev LIP is uncertain. The $^{40}Ar/^{39}Ar$ age of tholeiitic basalt (89 ± 1 Ma; Jokat et al., 2013) retrieved from Alpha Ridge is, therefore, correlated to the end of major magmatism related to this LIP. In contrast, the tectonic model of Doré et al. (2016) shows seafloor spreading in Makarov and Podvodnikov basins commencing at ~80 Ma with spreading axes oriented parallel to Lomonosov Ridge and offset by transform faults (en echelon). This system proceeded to widen the Makarov and Podvodnikov basins until 60 Ma (Doré et al., 2016). The orientation of stress fields predicted for this region during the Upper Cretaceous–Cenozoic (Gaina et al., 2014) are consistent with this model. This model is, however, inconsistent with the sedimentary structure and the seismic stratigraphies for Makarov Basin (Evangelatos and Mosher, 2016) and Podvodnikov Basin (Weigelt et al., 2014), which imply the existence of lower Upper Cretaceous successions. It is worth noting that upper Cretaceous sediments younger than Cenomanian are not present on Franz Josef Land (Embry, 1994). If the absence of such strata is the result of compressional uplift, extension within Makarov and Podvodnikov basins during the uppermost Cretaceous may be unsupported by stratigraphy.

Seafloor spreading was active in Markarov Basin between ~69 and 57 Ma, according to magnetic modelling of Døssing et al. (2017), and rifting may have initiated as early as ~80 Ma. Their plate-reconstruction model invokes the presence of strike-slip

faults that offset the western part of Alpha Ridge. The conclusions of Døssing et al. (2017) contradict the preferred model of Døssing et al. (2013), which included seafloor spreading prior to the Cretaceous Normal Superchron (~120–83 Ma; Gee and Kent, 2007). It should be noted, however, that the subsurface model along line LSSL2011-03/04 presented by Døssing et al. (2017) is superseded by the study presented in Chapter 3 (i.e., Evangelatos et al., 2017), which includes more refined constraints from coincident sonobuoy data. As discussed in Chapter 3, the lack of lateral variation in crustal seismic velocities between Alpha Ridge and Makarov Basin suggests that the latter "either formed during or was influenced by LIP-related magmatism" (Fig. 3.5). In addition, crustal layers beneath Makarov Basin are thick relative to normal oceanic crust of similar age (Fig. 3.14). Furthermore, Døssing et al. (2017) suggested that a buried pinnacle (150 km along line; Fig. 2.2) is an inactive spreading ridge. This interpretation implies that this feature should have a reasonable strike length (~150–200 km according to their model). As shown in the shipborne gravity data (Fig. 4.7), however, there is no corresponding gravity response to this pinnacle as predicted by two-dimensional forward gravity modelling. Consequently, the claim that this feature represents a spreading centre is rejected.

Fig. 5.3C shows adjustments to the model of Doré et al. (2016) that account for evidence that the Makarov and Podvodnikov basins existed as marginal subbasins prior to these hypothetical latest Cretaceous spreading centres. This figure shows that latest Cretaceous extensional rifting could indeed have occurred within Makarov Basin, as advocated by Gaina et al. (2014). Evidence for seafloor spreading after the Cretaceous Normal Superchron, however, is lacking. Crust produced by extension during this period

is shown as Phase 2 crust (Figs. 5C–5F). In addition, Fig. 5.3C shows the location of two strike-slip faults, presented by Døssing et al. (2017) and referred to here as T_1 and T_2. The sense of relative motion, however, is reversed to accommodate the aforementioned claim that northern Amerasia Basin underwent extension during the latest Cretaceous.

The Lomonosov Ridge/Barents-Kara Shelf continued to dominate supply of siliciclastic sediments to the early Makarov and Podvodnikov basins until Lomonosov Ridge broke away from the Barents–Kara Shelf (Fig. 5.3D). Most of the pre-rift sediment was deposited near the Lomonosov Ridge margin with isolated sedimentary sections possibly present in basement troughs in the rest of Makarov Basin.

5.2.4. Quiescent Period 65–0 Ma

Initial rifting that led to the opening of Eurasia Basin commenced in the latest Cretaceous–early Palaeocene (Glebovsky et al., 2006; Drachev, 2011) with breakup occurring closer to the Palaeocene–Eocene boundary (Brozena et al., 2003). Figs. 5.3E and 5.3F illustrate the development of Eurasia Basin. Opening of this basin ends a major source of sedimentation into Makarov Basin (refer to Chapter 2). Consequently, the Cenozoic sedimentary succession of Makarov and Podvodnikov basins is principally composed of hemipelagic to pelagic deposits (Bruvoll et al., 2010; Chapter 2) and/or distal turbidites (Johnson et al., 1990; Langinen et al., 2009). In addition, two hiatuses (44.4–18.2 Ma and 11.6–9.4 Ma) are documented in the ACEX core from the central Lomonosov Ridge records (Backman et al., 2008), which raise the possibility that middle Eocene to middle Miocene deposits in Makarov Basin originate in part from material eroded off of Lomonosov Ridge (Fig. 2.2). Their contribution, however, would be

relatively minor as there is no evidence of thick slope sequences during that period. Seismic line LSSL2011-03/04 shows a 0.9–1.2 km thick Cenozoic section concordant with the underlying basement structure (Fig. 2.3). Bruvoll et al. (2010) interpreted a "chaotic reflection pattern" along the eastern slope of Mendeleev Ridge (facing Nautilus Basin) as evidence of igneous activity. This event may be local, however, as no major deformation is noted in the Cenozoic sedimentary section along seismic line LSSL2011-03/04, which crosses adjacent Alpha Ridge (Fig. 2.2).

125 Ma

100 Ma

B

Siberian Craton

Kolyma-Omolon

South Anyui
Ocean

Barents-Kara Shelf/
Lomonosov Ridge

Mendeleev Ridge

Marvin
Spur

Arctic Alaska–Chukotka
microplate

Alpha
Ridge

Chukchi
Borderlands

Amerasia Basin

proto-Canada
Basin

Canadian Polar margin

Sverdrup Basin

Greenland

80 Ma

C

Kolyma-Omolon

East Siberian Shelf

?

PB

Mendeleev Ridge

North Chukchi Basin

Chukchi Borderlands

Arctic Alaska

Amerasia Basin

Canada Basin

?

Barents-Kara Shelf/ Lomonosov Ridge

T₂

MB

T₁

Alpha Ridge

Sverdrup Basin

Greenland

60 Ma

D

Kolyma-Omolon

East Siberian Shelf

Barents-Kara Shelf

Lomonosov Ridge

PB

AG

MB

Mendeleev Ridge

North Chukchi Basin

Chukchi Borderlands

Alpha Ridge

Amerasia Basin

Canada Basin

Arctic Alaska

Brooks Range

Sverdrup Basin

Greenland

33 Ma

E

Kolyma-Omolon

?

Barents-Kara Shelf

East Siberian Shelf

Eurasia Basin

Lomonosov Ridge

PB

AG

Mendeleev Ridge

MB

North Chukchi Basin

Chukchi Borderlands

Alpha Ridge

Arctic Alaska

Amerasia Basin

Canada Basin

Eurekan orogeny

Greenland

Canadian Arctic Archipelago

Baffin Bay

0 Ma

F

Russia

East Siberian Shelf

Barents-Kara Shelf

Nansen Basin

Eurasia Basin

Amundsen Basin

Lomonosov Ridge

Podvodnikov Basin

Mendeleev Ridge

MB

North Chukchi Basin

Chukchi Borderlands

Alpha Ridge

Amerasia Basin

Canada Basin

Ellesmere Island

Greenland

Alaska

Canadian Arctic Archipelago

Baffin Bay

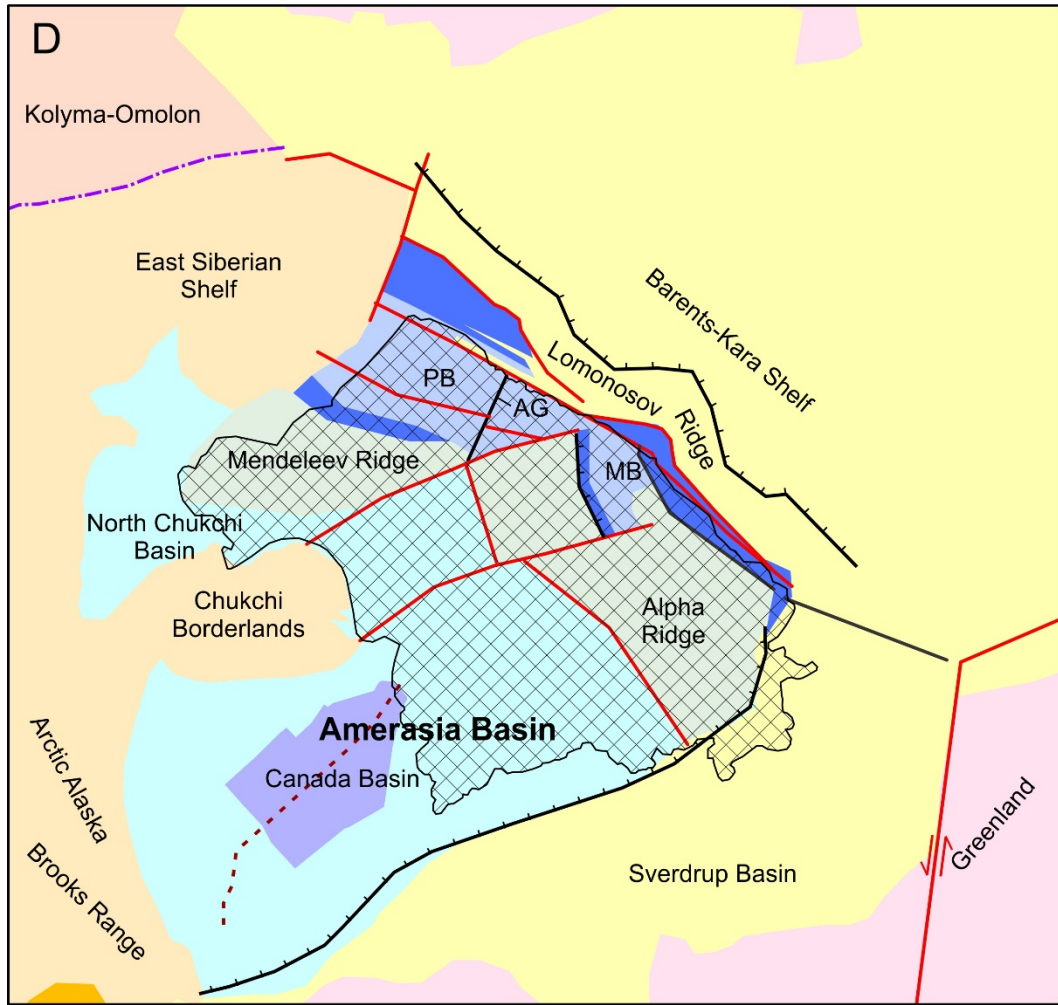|	High Arctic Magnetic High domain		Neoproterozoic and Phanarozoic fold and thrust belts		North Pole
	oceanic crust		Archaeon-Palaeoproterozoic Arctic cratons		sense of strike-slip
	hyper-extended continental crust, exhumed mantle, or unknown		Arctic Alaska-Chukotka Superterrane		transform/transtension
					extensional rifting
	Phase 1 crust		Alpha-Mendeleev ridge complex with sheared continental crust		subduction
					active
	Phase 2 crust		Cordillera		spreading axis — extinct
	donut-shaped anomaly		Kolyma-Omolon superterrane		South Anyui Suture
					convergence
					extension

152
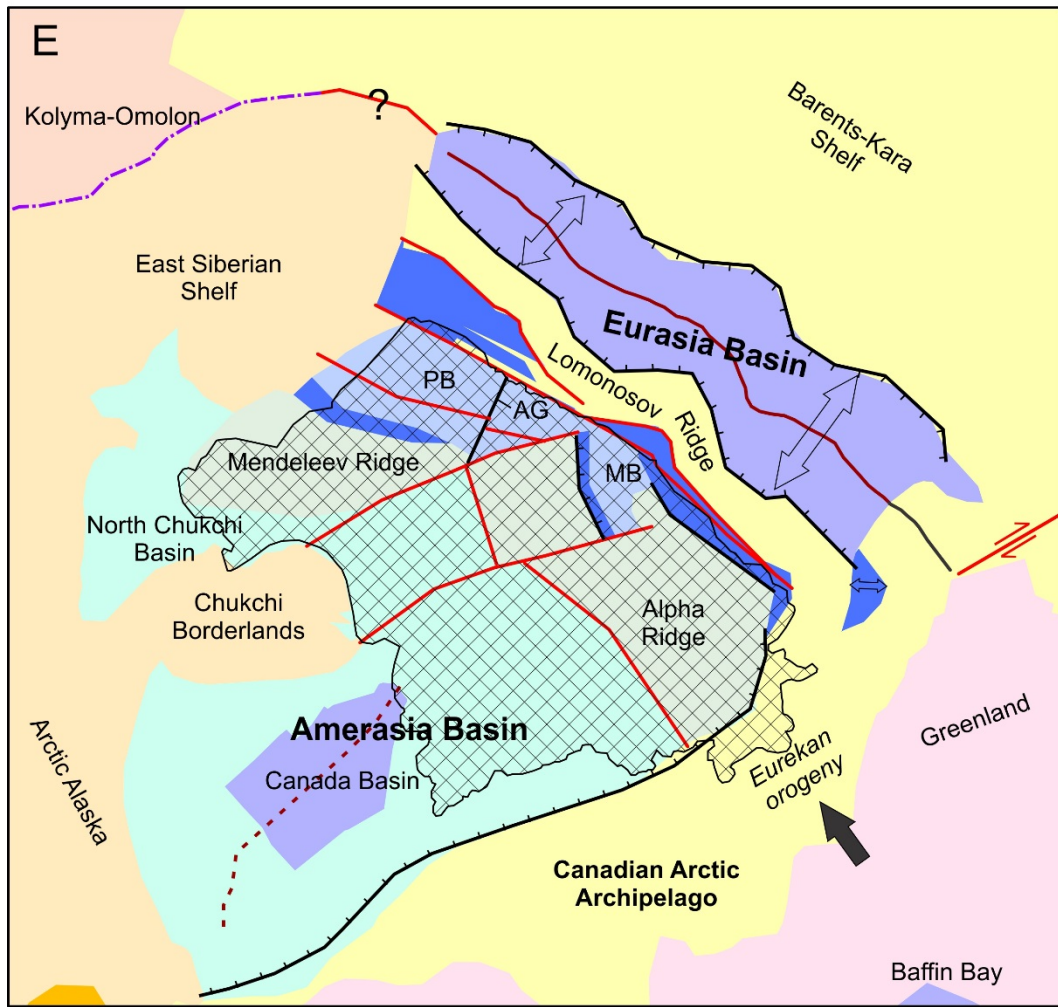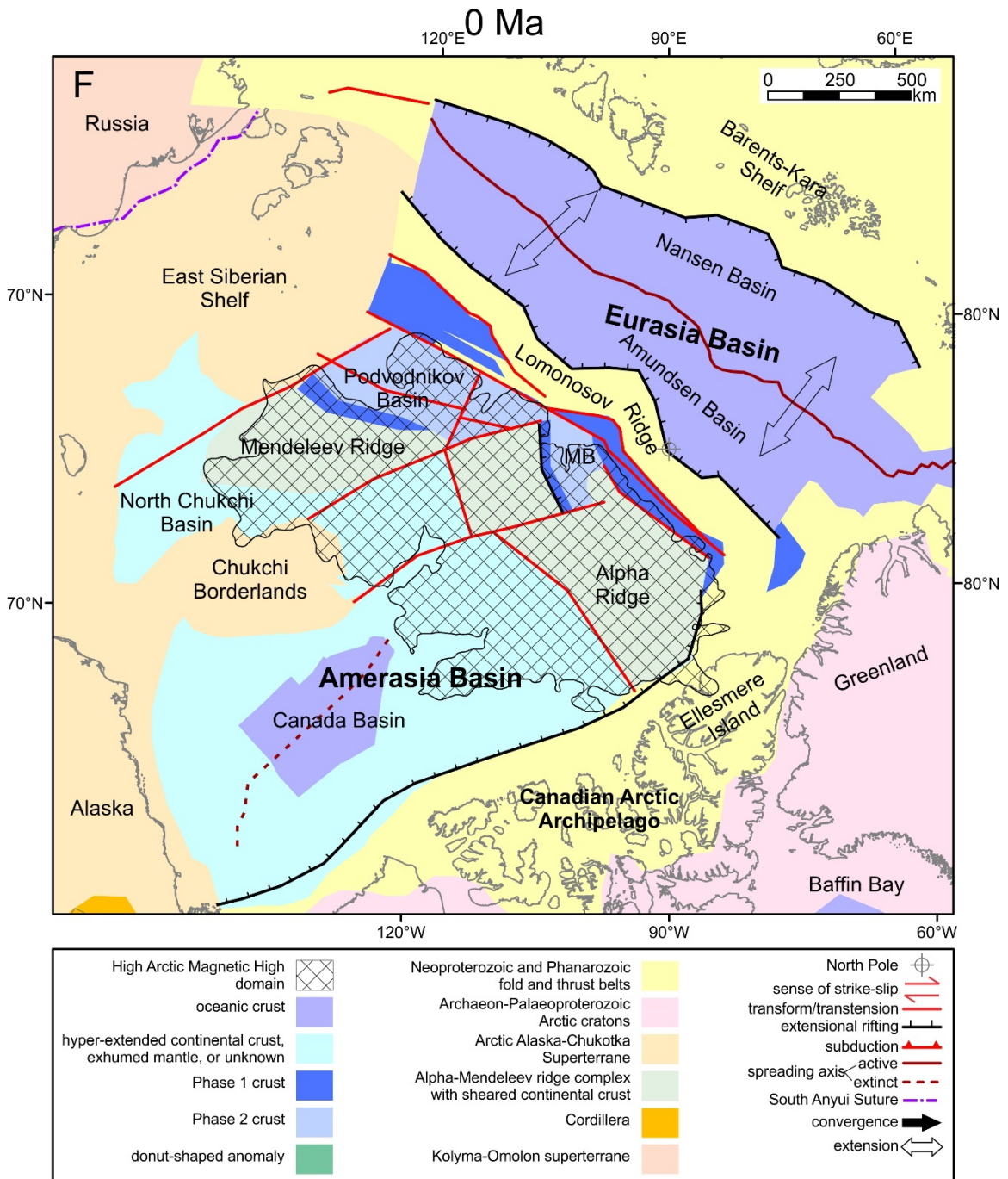
Fig. 5.3. Simplified tectonic plate-reconstruction maps at A) 125 Ma, B) 100 Ma, C) 80 Ma, D) 60 Ma, E) 33 Ma and F) 0 Ma. Phase 1 crust refers to thinned continental crust formed adjacent to Lomonosov Ridge (and possibly Alpha and Mendeleev ridges) by transtension during the initial stage of the opening of Amerasia Basin (~135–90 Ma). Phase 2 crust refers to additional stretching of crust underlying Makarov and Podvodnikov basins that occurred later due to extension perpendicular to Lomonosov Ridge. Additional elements are the Alpha-Mendeleev LIP magnetic domain (Oakey and Saltus, 2016), donut-shaped magnetic anomaly (Døssing et al., 2013), gravity low anomaly (Laxon and McAdoo, 1994) and location of oceanic crust in Canada Basin (Chian et al., 2016). Tectonic plates drift over time relative to a fixed North American craton. Acronyms: AG – Arlis Gap; MB – Makarov Basin; PB – Podvodnikov Basin. Figures adapted from Doré et al. (2016) and Pease et al. (2014).

5.3. Thesis conclusions

Based on the interpretation of new and previous multi-channel seismic and wide-angle reflection and refraction data and consideration of previous conceptual models for regional tectonics, the following conclusions have been made:

- The Amerasian margin of Lomonosov Ridge is a transverse/transtensional margin.

- Makarov Basin formed, at least in part, as a pull-apart basin.

- Within Makarov Basin, a deep subbasin adjacent to Lomonosov Ridge hosts deep sedimentary successions that are interpreted to be of lower Upper Cretaceous age.

- The upper successions of Makarov Basin do not exhibit evidence of major deformation.

- The crustal transition from Makarov Basin to central part of Lomonosov Ridge is relatively abrupt, consistent with the Lomonosov Transform model.

- The crustal thickness in Makarov Basin is greater than normal for oceanic crust of comparable age. The crust flooring Makarov Basin is, thus, interpreted as magmatically overprinted oceanic crust and/or thinned continental crust.

- The lack of significant lateral variability in crustal P-wave velocities between Alpha Ridge and Makarov Basin suggests lithological homogeneity. The two

geological provinces either formed coevally or were both significantly affected by the Alpha-Mendeleev LIP.

- The crustal transition from Makarov or Podvodnikov basins to Lomonosov Ridge varies along the axis of the ridge from: a) no distinguishable basin between Alpha and Lomonosov ridges near the Canadian Polar Margin, b) an abrupt transition from Makarov Basin to central Lomonosov Ridge, and c) a gradual transition from Podvodnikov Basin to Lomonosov Ridge near the East Siberian Shelf.

The formation of the Amerasia Basin consisted, therefore, of a complex set of tectonic factors. The rotational model appears to be responsible for part of its initial opening. Evidence of a transform segment between Makarov Basin and Lomonosov Ridge is consistent with this model. Extension and transform/strike-slip movements orthogonal to Lomonosov Ridge are also apparent, suggesting that the orientation of regional stress fields has also shifted over time. Amerasia Basin has been tectonically inactive from the upper Palaeocene to the present.

REFERENCES

Alvey, A., Gaina, C., Kusznir, N.J., Torsvik, T.H., 2008. Integrated crustal thickness mapping and plate reconstructions for the high Arctic. Earth Planet. Sci. Lett. 271, 310–321.

Amato, J.M., Toro, J., Akinin, V.V., Hampton, B.A., Salnikov, A.S., Tuchkova, M.I., 2015. Tectonic evolution of the Mesozoic South Anyui suture zone, eastern Russia: a critical component of paleogeographic reconstructions of the Arctic region. Geosphere 11, 1530–1564.

Andersen, O.B., Knudsen, P., Berry, P., 2010. The DNSC08GRA global marine gravity field from double retracked satellite altimetry. J. Geod. 84, 191–199. http://dx.doi.org/10.1007/s00190-009-0355-9.

Andronikov, A., Mukasa, S., Mayer, L.A., Brumley, K., 2008. First recovery of submarine basalts from the Chukchi Borderland and Alpha/Mendeleev Ridge, Arctic Ocean. Eos 89 (53), V41D–2124.

Astafurova, E., Glebovsky, V., Fedorov, V., 2006. Results of density modeling of the major structural elements of the Arctic Ocean. In: Scott, R. A. & Thurston, D. K. (Eds.), 2003 Proceedings of the Fourth International Conference on Arctic Margins. US Department of the Interior Minerals Management Service Alaska Outer Continental Shelf Region (OCS Study MMS 2006-003), pp. 165–172.

Asudeh, I., Green, A.G., Forsyth, D.A., 1988. Canadian expedition to study the Alpha-Ridge complex — results of the seismic refraction survey. Geophys. J. 92, 283–301.

Backman, J., Moran, K., McInroy, D.B., Mayer, L.A., Expedition 302 Scientists, 2006. Proceedings of the Integrated Ocean Drilling Program 302. doi:10.2204/iodp.proc.302.101.2006.

Backman, J., Jakobsson, M., Frank, M., Sangiorgi, F., Brinkhuis H., et al., 2008. Age model and core-seismic integration for the Cenozoic Arctic Coring Expedition sediments from the Lomonosov Ridge. Paleoceanography 23, PA1S03, doi:10.1029/2007PA001476.

Bailey, J.C., Rasmussen, M.H., 1997. Petrochemistry of Jurassic and Cretaceous tholeiites from Kong Karls Land, Svalbard, and their relation to Mesozoic magmatism in the Arctic. Polar Res. 16, 37–62.

Basile, C., Allemand, P., 2002. Erosion and flexural uplift along transform faults. Geophysical Journal International 151, 646–653.

Basile, C., Brun, J.P., 1999. Transtensional faulting patterns ranging from pull-apart basins to transform continental margins: an experimental investigation. Journal of Structural Geology 21, 23–37.

Becker, K., Sakai, H., et al., 1989. Drilling deep into young oceanic crust, Hole 504B, Costa Rica Rift. Rev. Geophys. 27, 79–102.

Bourbié, T., Coussy, O., Zinszner, B., 1987. Acoustics of Porous Media, Ed. Technip, 334 p.

Brozena J.M., Childers V.A., Lawver L.A., Gahagan L.M., Forsberg R., Faleide J.I., Eldholm O., 2003. New aerogeophysical study of the Eurasia Basin and Lomonosov Ridge: implications for basin development. Geology 31, 825–828.

Bruvoll, V., Kristoffersen, Y., Coakley, B.J., Hopper, J.R., 2010. Hemipelagic deposits on the Mendeleev and northwestern Alpha submarine Ridges in the Arctic Ocean: acoustic stratigraphy, depositional environment and an inter-ridge correlation calibrated by the ACEX results. Mar. Geophys. Res. 31, 149–171.

Bruvoll, V., Kristoffersen, Y., Coakley, B.J., Hopper, J.R., Planke, S., Kandilarov, A., 2012. The nature of the acoustic basement on Mendeleev and northwestern Alpha ridges, Arctic Ocean. Tectonophysics 514, 123–145.

Brumley, K., 2014. Geologic nature of the Chukchi Borderland, Arctic Ocean. Unpublished Ph.D. thesis, Stanford University, Stanford, California, United States, 251 pp.

Buchan, K.L., Ernst, R., 2006. Giant dyke swarms and the reconstruction of the Canadian Arctic islands, Greenland, Svalbard and Franz Josef Land. In: Hanski, E., Mertanen, S., Ramo, T., Vuollo, J. (Eds.), Dyke Swarms: Time Markers of Crustal Evolution. Taylor & Francis, London, pp. 27–48.

Carey, S.W., 1958. A tectonic approach to continental drift. In: Carey, S.W. (Ed.), Continental Drift; a Symposium. Hobart, Tasmania, pp. 177–355.

Carlson, R.L., Herrick, C.N., 1990. Densities and porosities in the oceanic crust and their variations with depth and age. J. Geophys. Res. 95, 9153–9170.

Charvis, P., Recq, M., Operto, S., Brefort, D., 1995. Deep structure of the northern Kerguelen Plateau and hotspot-related activity. Geophys. J. Int. 122, 899–924.

Chernykh, A. A., Glebovsky, V. Y., Egorova, A.V., Redko, A.G., Suhanov R.A., 2015. Tectonic structure and evolution of the Alpha-Mendeleev Fracture Zone. Abstract, The 7th International Conference on Arctic Margins, ICAM VII, Trondheim, Norway.

Chian, D., Lebedeva-Ivanova, N.N., 2015. Atlas of sonobuoy velocity analyses, Canada Basin, Geological Survey of Canada, Open File 7661, 55 pp. doi:10.4095/295857.

Chian, D., Jackson, H.R., Hutchinson, D.R., Shimeld, J.W., Oakey, G.N., Lebedeva-Ivanova, N., Li, Q., Saltus, R.W., Mosher, D.C., 2016. Distribution of crustal types in Canada Basin, Arctic Ocean. Tectonophysics 691, 8–30 http://dx.doi.org/10.1016/j.tecto.2016.01.038.

Christie-Blick, N., Biddle, K.T., 1985. Deformation and basin formation along strike-slip faults. In: Biddle, K.T., Christie-Blick, N. (Eds.), Strike-slip Deformation, Basin Formation, and Sedimentation. Society of Economic Paleontologists and Mineralogists, Special Publication 37, pp. 1–35.

Coachman, L.K., Aagaard, K., 1974. Physical oceanography of the arctic and subarctic seas. In: Herman, Y. (Ed.), Marine geology and oceanography of the arctic seas. Springer Verlag, New York, pp. 1–72.

Coakley, B.J., Cochran, J.R., 1998. Gravity evidence of very thin crust at the Gakkel Ridge (Arctic Ocean). Earth Planet. Sci. Lett. 162, 81–95.

Coakley, B., Kristoffersen, Y., Hopper, J., Arthun, T., Berge, H., Brass, G., Breien, H., Bruvoll, V., Dove, D., Grindheim, E., Henkart, P., Ivanova, N., Ludvigsen, F., Monsen, K., Reynoso-Peralta, W., White, D., 2005, A Cross-Arctic Geophysical Transect Collected from US Coast Guard Icebreaker Healy, Eos Trans. AGU 86 (52), Fall Meet., Suppl. Abstract T13D-0510.

Coakley B., Brumley, K., Lebedeva-Ivanova, N., Mosher, D. 2016. Exploring the geology of the central Arctic Ocean; understanding the basin features in place and time. J. Geol. Soc., London 173, 967–987. http://doi.org/10.1144/jgs2016-082

Cochran, J.R., M.H. Edwards, Coakley B.J., 2006. Morphology and structure of the Lomonosov Ridge, Arctic Ocean. Geochemistry Geophysics Geosystems 7, Q05019. doi:10.1029/2005GC001114.

Comiso, J.C., Parkinson, C.L., Gersten, R., Stock, L., 2008. Accelerated decline in the Arctic sea ice cover. Geophys. Res. Lett. 35, L01703.

Crane, R.C., 1987. Arctic reconstruction from an Alaskan Point of View. In: Tailleur, I., Weimer, P. (Eds.), Alaskan North Slope Geology. Pac. Sect. Soc. Econ. Paleontol. Mineral. and Alaskan Geol. Soc., Bakersfield, California, pp. 769–783.

Dahl-Jensen, T., Jackson, H.R., Deping, C., Shimeld, J., 2007. Crustal Structure from the Lincoln Sea to the Lomonosov Ridge – Wide-angle and single channel normal incident seismic and ancillary data from LORITA, Danmark og Grønlands Geologisake Undersøgelse Rapport 2007/75, 53 pp.

Darbyshire, F.A., Bjarnason, I.T., White, R.S., Flóvenz, Ó.G., 1998. Crustal structure above the Iceland mantle plume imaged by the ICEMELT refraction profile. Geophys. J. Int. 135, 1131–1149.

Davies, A., Kemp, A., Pike, J., 2009. Late Cretaceous seasonal ocean variability from the Arctic. Nature 460, 254–258.

DeMets, C., Gordon, R.G., Argus, D.F., Stein, S., 1994. Effect of recent revisions to the geomagnetic reversal time scale on estimates of current plate motions. Geophys. Res. Lett. 21, 2191–2194.

Dibner, V.D., 1998. Geology of Franz Josef Land. Norsk Polarinstitutt, 190 pp..

Dickinson, W.R., 2009. Anatomy and global context of the North American Cordillera. Geological Society of America Memoir 204, 1–29.

Doré, A.G., Lundin, E.R., Gibbons, A., Sømme, T.O., Tørudbakken, B.O., 2016. Transform margins of the Arctic: a synthesis and re-evaluation. In: Nemčok, M., Rybár, S., Sinha, S.T., Hermeston, S.A., Ledvényiová , L. (Eds.), Transform margins: development, controls and petroleum systems: Geol. Soc. London, Special Publications 431, 63–94.

Døssing, A., Jackson, H.R., Matzka, J., Einarsson, I., Rasmussen, T.M., Olesen, A.V., Brozena, J.M., 2013. On the origin of the Amerasia Basin and the high Arctic large igneous province – results of new aeromagnetic data. Earth Planet. Sci. Lett. 363, 219–230.

Døssing, A., Hansen, T.M., Olesen, A.V., Hopper, J.R., Funck, T., 2014. Gravity inversion predicts the nature of the Amundsen basin and its continental borderlands near Greenland. Earth Planet. Sci. Lett. 408, 132–145.http://dx.doi.org/10.1016/j.epsl.2014.10.011.

Døssing, A., Gaina, C., Brozena, J.M., 2017. Building and breaking a large igneous province: An example from the High Arctic. Geophys. Res. Lett. 44, 6011–6019.

Dove, D., Coakley, B., Hopper, J., Kristoffersen, Y., the HLY0503 Geophysics Team, 2010. Bathymetry, controlled source seismic and gravity observations of the Mendeleev ridge: implications for ridge structure, origin, and regional tectonics. Geophys. J. Int. 183, 481–502. http://dx.doi.org/10.1111/j.1365-246X.2010.04746.x.

Drachev, S.S., 2011. Tectonic setting, structure and petroleum geology of the Siberian Arctic offshore sedimentary basins. In: Spencer, A. M., Embry, A. F., Gautier, D. L., Stoupakova, A. V., Sørensen, K. (Eds.), Arctic Petroleum Geology: Geol. Soc. London, Memoirs 35, pp. 364–394.

Drachev, S., Saunders, A., 2006. The early Cretaceous Arctic LIP: its geodynamic setting and implications for Canada Basin opening. In: Scott, R.A., Thurston, D. (Eds.), ICAM IV Proceedings, U.S. Dept. of the Interior, Anchorage, pp. 216–223.

Drachev, S., Johnson, G., Laxon, S., McAdoo, D., Kassens, H., 1999. Main Structural Elements of Eastern Russian Arctic Continental Margin Derived from Satellite Gravity and Multichannel Seismic Reflection Data. Kassens, H., Bauch, H.A., Dmitrenko, I.A., Eicken, H., Hubberten, H.-W., Melles, M., Thiede, J., Timokhov, L.A. (Eds.), Land-Ocean Systems in the Siberian Arctic: Dynamics and History. Springer, pp. 667–682.

Duckworth, G.L., Baggeroer, A.B., 1985. Inversion of refraction data from the Fram and Nansen Basins of the Arctic Ocean. Tectonophysics 114, 55–102.

Duckworth, G.L., Baggeroer, A.B., Jackson, H.R., 1982. Crustal structure measurements near FRAM II in the Pole Abyssal Plain. Tectonophysics 89, 173–215.

Dutro, J.T., 1981. Geology of Alaska bordering the Arctic Ocean. In: Nairn, A., Churkin, M., Stehli, F. (Eds.), The Ocean Basins and Margins, Vol. 5, The Arctic Ocean. Plenum, New York, pp. 21–36.

Edwards, B.D., Saint-Ange, F., Pohlman, J., Higgins, J., Mosher, D.C., Lorenson, T.D., Hart, P., 2010. Sedimentology of cores recovered from the Canada Basin of the Arctic Ocean. In AGU Fall Meeting (Abs.) Vol. 1, p. 1915.

Embry, A.F., 1990. Geological and geophysical evidence in support of the hypothesis of anticlockwise rotation of northern Alaska. Mar. Geol. 93, 317–329.

Embry, A.F., 1991. Middle–Upper Devonian clastic wedge of the Arctic islands. In: Trettin, H.P. (Ed.), Geology of the Innuitian Orogen and Arctic Platform of Canada and Greenland, Geological Survey of Canada, Ottawa, Vol. 3, pp. 263–279.

Embry, A.F., Osadetz, K.G., 1988. Stratigraphy and tectonic significance of Cretaceous volcanism in the Queen Elizabeth Islands, Canadian Arctic Archipelago. Can. J. Earth Sci. 25, 1209–1219.

Embry, A.F., Dixon, J., 1990. The breakup unconformity of the Amerasia Basin, Arctic Ocean: Evidence from Arctic Canada. Geol. Soc. Am. Bull. 102, 1526–1534

Embry, A., Dixon, J., 1994. The age of Amerasia Basin. In: Thurston, D., Fujita, K. (Eds.), 1992 Proceedings of the International Conference on Arctic Margins. U.S. Department of the Interior Minerals Management Service Alaska Outer Continental Shelf Region (OCS Study MMS 94-0040), pp. 289–294.

Estrada, S., 2015. Geochemical and Sr–Nd isotope variations within Cretaceous continental flood-basalt suites of the Canadian High Arctic with a focus on the Hassel Formation basalts of northeast Ellesmere Island. Int. J. Earth Sci. 104, 1981–2005.

Estrada, S., Henjes-Kunst, F., 2004. Volcanism in the Canadian High Arctic related to the opening of the Arctic Ocean. Z. Dtsch. Geol. Ges. 154, 579–603.

Estrada, S., Henjes-Kunst, F., Melcher, F., Tessensohn, F., 2010. Paleocene alkaline volcanism in the Nares Strait region: evidence from volcanic pebbles. Int. J. Earth Sci. 99, 863–890.

Evangelatos, J., Mosher, D.C., 2016. Seismic stratigraphy, structure and morphology of Makarov Basin: tectonic implications. Mar. Geol. 374, 1–13.

Evangelatos, J., Funck, T., Mosher, D.C., 2017. The sedimentary and crustal velocity structure of Makarov Basin and adjacent Alpha Ridge. Tectonophysics 696–697, 99–114.

Evangelatos, J., Oakey G., Saltus, R., 2017, Central Arctic crustal modeling constrained by potential field data and recent ECS Seismic Data, European Geosciences Union General Assembly 2017, Vienna, Austria.

Faleide, J.I., Vågnes, E., Gudlaugsson, S.T., 1993. Late Mesozoic-Cenozoic evolution of the south-western Barents Sea in a regional rift-shear tectonic setting. Mar. Pet. Geol. 10, 186–214.

Forsyth, D.A., Mair, J.A., 1984. Crustal structure of the Lomonosov Ridge and the Fram and Makarov Basins near the North Pole. J. Geophys. Res. 89 (B1), 473–481.

Forsyth, D.A., Asudeh, I., Green, A.G., Jackson, H.R., 1986. Crustal structure of the northern Alpha Ridge beneath the Arctic Ocean. Nature 322, 349–352.

Forsyth, D.A., Morel-A-L'Huissier, P., Asudeh, I., Green, A., Jackson, H., 1986. Alpha ridge and Iceland—products of the sample plume? J. Geodyn. 6, 197–214.

Funck, T., Jackson, H.R., Shimeld, J., 2011. The crustal structure of the Alpha Ridge at the transition to the Canadian Polar Margin: Results from a seismic refraction experiment. J. Geophys. Res. 116, B12101, doi:10.1029/2011JB008411.

Fütterer, D.K. (Ed.), 1992. Arctic '91: The Expedition ARKVIII/3 of RV "Polarstern" In 1991. Rep. Polar Res. 107. Alfred Wegener Institute, Bremerhaven, Germany, 267 pp.

Gaina, C., Roest, W.R., Müller, R.D., 2002. Late Cretaceous–Cenozoic deformation of northeast Asia. Earth Planet. Sci. Lett. 197, 273–286.

Gaina, C., Werner, S.C., Saltus, R., Maus, S., 2011. Circum-Arctic mapping project: new magnetic and gravity anomaly maps of the Arctic. In: Spencer, A. M., Embry, A. F., Gautier, D. L., Stoupakova, A. V., Sørensen, K. (Eds.), Arctic Petroleum Geology: Geol. Soc. London, Memoirs 35, pp. 39–48.

Gaina, C., Medvedev, S., Torsvik, T.H., Koulakov, I., Werner, S. C., 2014. 4D Arctic: A glimpse into the structure and evolution of the Arctic in the light of new geophysical maps, plate tectonics and tomographic models. Surv. Geophys. 35, 1095–1122.

Gardner, G.H.F., Gardner, L.W., Gregory, A.R., 1974. Formation velocity and density — the diagnostic basis for stratigraphic traps. Geophysics 39, 770–780.

Gee, J., Kent, D., 2007. Source of oceanic magnetic anomalies and the geomagnetic polarity timescale. In: Kono, M. (Ed.), Geomagnetism, Treatise on Geophysics, vol. 5, pp. 455–507.

Gladczenko, T.P., Coffin, M.F., Eldholm, O., 1997. Crustal structure of the Ontong Java Plateau: modeling of new gravity and existing seismic data. J. Geophys. Res. 102, 22711–22729.

Glebovsky, V.Y., Kaminsky, V.D., Minakov, A.N., Merkur'ev, S.A., Childers, V. A., Brozena, J.M., 2006. Formation of the Eurasia Basin in the Arctic Ocean as inferred from geohistorical analysis of the anomalous magnetic field. Geotectonics 40, 263–281.

Glebovsky, V.Yu., Astafurova, E.G., Chernykh, A.A., Korneva, M.A., Kaminsky,V.D., Poselov, V.A., 2013. Thickness of the Earth's crust in the deep Arc-tic Ocean: Results of a 3D gravity modeling. Russ. Geol. Geophys. 54, 247–262.

Gottlieb, E.S., Meisling, K.E., Miller, E.L., Mull, C.G., 2014. Closing the Canada Basin: detrital zircon geochronology relationships between the North Slope of Arctic Alaska and the Franklinian mobile belt of Arctic Canada. Geosphere 10, 1366–1384.

Grantz, A., Eittreim, S., Dinter, D.A., 1979. Geology and tectonic development of the continental margin north of Alaska. Tectonophysics 59, 263–291.

Grantz, A., May, S.D., Taylor, P.T., Lawver, L.A., 1990. Canada Basin. In: Grantz, A., Johnson, G.L., Sweeney, J.F. (Eds.), The Geology of North America, The Arctic Ocean Region, Vol. L. The Geological Society of America, pp. 379–402.

Lawver, L.A., Scotese, C.R., 1990. A review of tectonic models for the evolution of Canada Basin. In: Grantz, A., Johnson, L., Sweeney, J.F. (Eds.), The Geology of North America, The Arctic Ocean Region, Vol. L. The Geological Society of America, pp. 593–618.

Grantz, A., Clark D.L., Phillips R.L., Srivastava S.P., Blome C.D., Gray L.B., Haga H., Mamet B.L., McIntyre D.J., Mcneil D.H., Mickey M.B., Mullen M.W., Murchey B.I., Ross C.A., Stevens C.H., Silberling N.J., Wall J.H., Willard D.A., 1998. Phanerozoic stratigraphy of Northwind Ridge, magnetic anomalies in the Canada basin, and the geometry and timing of rifting in the Amerasia basin, Arctic Ocean. GSA Bull. 110, 801–820.

Grantz, A., Pease, V.L., Willard, D.A., Phillips, R.L., Clark, D.L., 2001. Bedrock cores from 89° North: implications for the geologic framework and Neogene paleoceanogragraphy of the Lomonosov Ridge and a tie to the Barents shelf. GSA Bull. 113, 1272–1281.

Grantz, A., Hart, P.E., Childers, V.A., 2011. Geology and tectonic development of the Amerasia and Canada Basins, Arctic Ocean. In: Spencer, A. M., Embry, A. F., Gautier, D. L., Stoupakova, A. V., Sørensen, K. (Eds.), Arctic Petroleum Geology: Geol. Soc. London, Memoirs 35, pp. 771–799.

Grevemeyer, I., Weigel, W., Jennrich, C., 1998. Structure and ageing of oceanic crust at 14°S on the East Pacific Rise. Geophys. J. Int. 135, 573–584.

Gusev, E.A., Lukashenko, R.V., Popko, A.O., Rekant, P.V., Mirolyubova, E.S. and Pyatkova, M.N., 2014. New data on the structure of slopes of the Mendeleev ridge seamounts (Arctic Ocean). Dokl. Earth Sci. 455, 250–253.

Halgedahl, S., Jarrard, R., 1987. Paleomagnetism of the Kuparuk River Formation from oriented drill core: evidence for rotation of the North Slope block. In: Tailleur, L., Weimer, P. (Eds.), Alaskan North Slope Geology: Pacific Section. Society of Economic Paleontologists and Mineralogists, Vol. 50, pp. 581–620.

Heezen, B., Ewing, M., 1961. The mid-oceanic ridge and its extension through the Arctic Basin. In: Raasch, G. (Ed.), Geology of the Arctic, vol. 1. University of Toronto Press, Toronto, pp. 622–642.

Henriksen, N., Higgins, A.K., 2000, Early Palaeozoic basin development of North Greenland—Part of the Franklinian Basin. Polarforschung, 68, 131–140.

Hochmuth, K., 2015. From crustal structure to plate kinematics - the role of Large Igneous Provinces in the Pacific Ocean. Unpublished Ph.D. thesis, Universität Bremen, Bremen, Germany, 176 pp.

Holbrook, W.S., Mooney, W.D., Christensen, N.I., 1992. The seismic velocity structure of the deep continental crust. In: Fountain, D.M., Arculus, R., Kay, R.W., (Eds.), Continental lower crust, Developments in Geotectonics, 23. Elsevier, New York, pp. 1–42.

Houtz, R., Ewing, J., 1976. Upper crustal structure as a function of plate age. J. Geophys. Res. 81, 2490–2498.

Hubbard, R.J., Edrich, S.P., Rattey, R.P., 1987. Geologic evolution and hydrocarbon habitat of the "Arctic Alaska Microplate". Marine and Petroleum Geology 4, 2–45.

Hunt, C., Moskowitz, B.M., Banerjee, S.K., 1995. Magnetic properties of rocks and minerals. In: Ahrens, T.J. (Ed.), Rock Physics and Phase Relations: A Handbook of Physical Constants. American Geophysical Union.

Ivanova, N. N., Zamansky, Y. Y., Langinen, A.E., Sorokin, M.Y., 2002. Seismic researches of the earth's crust on the Lomonosov Ridge, Arctic Ocean. Investigation and Protection of Bowels 9, 7–9 (in Russian).

Jackson, H.R., 1985. Seismic reflection results from CESAR. In: Jackson, H.R., Mudie, P., Blasco, S.M. (Eds.), Initial geological Report on CESAR — the Canadian Expedition to Study the Alpha Ridge, Arctic Ocean: Geological Survey of Canada, Paper 84–22, pp. 19–23.

Jackson, H.R., Dahl-Jensen, T., 2007. Field report for LORITA (Lomonosov Ridge Test of Appurtenance). Geological Survey of Canada, Open File 5391, 187 pp.

Jackson, H. R., Potter, P. (Eds.), 2011. Expedition report for the Alpha Ridge Test of Appurtenance (ARTA) 2008. Geological Survey of Canada, Open File 6842, 124 pp.

Jackson, H.R., Mudie, P.J., Blasco, S.M. (Eds.), 1985. Initial geological report on CESAR—The Canadian Expedition to study the Alpha Ridge, Arctic Ocean. Geological Survey of Canada Paper 84–22, 177 pp.

Jackson, H., Forsyth, D., Johnson, G., 1986. Oceanic affinities of the Alpha Ridge, Arctic Ocean. Mar. Geol. 73, 237–261.

Jackson, H.R., Forsyth, D.A., Hall, J.K., Overton, A., 1990. Seismic reflection and refraction. In: Grantz, A., Johnson, L., Sweeney, J.F. (Eds.), The Geology of North America, The Arctic Ocean Region, Vol. L. The Geological Society of America, Boulder, pp. 153–170.

Jackson, H.R., Dahl-Jensen, T., the LORITA Working Group, 2010. Sedimentary and crustal structure from the Ellesmere Island and Greenland continental shelves onto the Lomonosov Ridge, Arctic Ocean. Geophys. J. Inter. 182, 11–35, http://dx.doi.org/10.1111/j.1365-246X.2010.04604.x.

Jakobsson, M., Grantz, A., Kristoffersen, Y., Macnab, R., 2003. Physiographic provinces of the Arctic Ocean. Geol. Soc. Am. Bull. 115, 1443–1455.

Jakobsson, M., Backman, J., Rudels, B., Nycander, J., Frank, M., Mayer, L., Jokat, W., Sangiorgi, F., O'Regan, M., Brinkhuis, H., King, J., Moran, K., 2007. The early Miocene onset of a ventilated circulation regime in the Arctic Ocean. Nature 447, 986–990. doi:10.1038/nature05924.

Jakobsson, M., Mayer, L., Coakley, B., Dowdeswell, J.A., Forbes, S., et al. 2012. The International Bathymetric Chart of the Arctic Ocean (IBCAO) Version 3.0. Geophys. Res. Lett. 39, L12609. doi:10.1029/2012GL052219.

Johnson, L., Grantz, A., Weber, J.R., 1990. Bathymetry and physiography. In: Grantz, A., Johnson, L., Sweeney, J. (Eds.), The Geology of North America, The Arctic Ocean Region, vol. L,. The Geological Society of America, pp. 63–75.

Jokat, W. (Ed.), 1999. ARCTIC '98: The Expedition ARK-XIV 1a of RV "Polarstern" in 1998. Rep. Polar Res. 308. Alfred Wegener Institute, Bremerhaven, Germany, 159 pp.

Jokat, W., 2003. Seismic investigations along the western sector of Alpha Ridge, Central Arctic Ocean. Geophys. J. Int. 152, 185–201.

Jokat, W., 2005. The sedimentary structure of the Lomonosov Ridge between 88°N and 80°N. Geophys. J. Int. 163, 698–726.

Jokat, W., Schmidt-Aursch, M.C., 2007. Geophysical characteristics of the ultra-slow spreading Gakkel ridge, Arctic Ocean. Geophys. J. Int. 168, 983–998.

Jokat, W. (Ed.), 2009. The Expedition of the Research Vessel "Polarstern" to the Arctic in 2008 (ARK-XXIII/3). Rep. Polar Res. 597. Alfred Wegener Institute, Bremerhaven, Germany, 221 pp.

Jokat, W., Ickrath M., 2015. Structure of ridges and basins off East Siberia along 81 degrees N, Arctic Ocean. Mar. Petrol. Geol. 64, 222–232.

Jokat, W., Uenzelmann-Neben, G., Kristoffersen, Y., Rasmussen, T., 1992. ARCTIC'91: Lomonosov Ridge—a double sided continental margin. Geology 20, 887–890.

Jokat, W., Weigelt, E., Kristoffersen, Y., Rasmussen, T., Schöne, T., 1995. New insights into the evolution of the Lomonosov Ridge and the Eurasian Basin. Geophys. J. Inter. 122, 378–392.

Jokat, W., Ickrath, M., O'Connor, J., 2013. Seismic transect across the Lomonosov and Mendeleev Ridges: Constraints on the geological evolution of the Amerasia Basin, Arctic Ocean. Geophysical Research Letters 40, 5047–5051.

Kaban'kov, V.Ya., Andreeva, I.A., Ivanov, V.N., Petrova V.I., 2004. The geotectonic nature of the Central Arctic morphostructures and geological implications of bottom sediments for its interpretation. Geotectonics 38, 430–442.

Kaminsky, V.D. (Ed.), 2017. The Arctic Ocean (geology and morphology). VNIIOkeangeologia, Saint-Petersburg, 291 pp (in Russian).

Karasik, A.M., Gurevich, N.I., Masolov, V.N. & Schelovanov, V.G., 1971. Some features of a deep structure and an origin of Lomonosov Ridge on the aeromagnetic data, Geofiz. Metody razvedki v Arktike 6, 9–19 (in Russian).

Keen, C.E., Potter, P., 1995, Formation and evolution of the Nova Scotian rifted margin: Evidence from deep seismic reflection data. Tectonics 14, 918–932.

Korenaga, J., Holbrook, W.S., Kent, G.M., Kelemen, P.B., Detrick, R.S., Larsen, H.-C., Hoppes, J.R., Dahl-Jenssen, T., 2000. Crustal structure of the southeast Greenland margin from joint refraction and reflection seismic tomography. J. Geophys. Res. 105, 21,591–21,614.

Kovacs, L.C., Vogt, P.R., 1982. Depth-to-magnetic source analysis of the Arctic Ocean region. Tectonophysics 89, 255–294.

Kovacs, L., Glebovsky, V., Sorokin, M., Mashenkov, S., Brozena, J., 1999. New evidence for seafloor spreading in the Makarov Basin. Eos, Trans. AGU 80 (Abs.) 80.

Kristoffersen, Y., 1982. The Nansen Ridge, Arctic Ocean; some geophysical observations of the rift valley at slow spreading rate. Tectonophysics 89, 161–172.

Kristoffersen, Y., Mikkelsen, N. (Eds.), 2004. Scientific drilling in the Arctic Ocean and the site survey challenge: tectonic, paleoceanographic and climatic evolution of the Polar Basin. JEODI Workshop, Copenhagen, Denmark, January 13–14, 2003, Geological Survey of Greenland, Special Publication, 85 pp.

Kristoffersen, Y., Mikkelsen, N., 2006. On sediment deposition and nature of the plate boundary at the junction between the submarine Lomonosov Ridge, Arctic Ocean and the continental margin of Arctic Canada/North Greenland. Mar. Geol. 225, 265–278.

Kristoffersen, Y., Husebye, E.S., Bungum, H., Gregersen, S., 1982. Seismic investigations of the Nansen Ridge during the FRAM-I experiment. Tectonophysics 82, 57–68.

Kristoffersen, Y., Coakley, B.J., Hall, J.K., Edwards, M., 2007. Mass wasting on the submarine Lomonosov Ridge, central Arctic Ocean. Mar. Geol. 243, 132–142.

Kroenke, L.W., Berger, W.H., Janecek, T.R., et al., 1991. Proc. ODP, Init. Repts. 130. College Station, TX (Ocean Drilling Program). doi:10.2973/odp.proc.ir.130.1991.

Kutschale, H., 1966. Arctic Ocean geophysical studies: the southern half of the Siberian Basin. Geophysics 21, 683–709.

Kuzmichev, A.B., 2009. Where does the South Anyui suture go in the New Siberian islands and Laptev Sea? Implications for the Amerasia basin origin. Tectonophysics 463, 86–108.

Lane, L.S., 1997. Canada Basin, Arctic Ocean: evidence against a rotational origin. Tectonics 16, 363–387.

Langinen, A.E., Gee, D.G., Lebedeva-Ivanova, N.N., Zamansky, Yu.Ya., 2006. Velocity structure and correlation of the sedimentary cover on the Lomonosov Ridge and in the Amerasian Basin, Arctic Ocean. In: Scott, R.A., Thurston, D.K. (Eds.), Proceedings of the Fourth International Conference on Arctic Margins, OCS Study MMS 2006-003. U.S. Department of the Interior, pp. 179–188.

Langinen, A.E., Lebedeva-Ivanova, N.N., Gee, D.G., Zamansky, Y.Y., 2009. Correlations between the Lomonosov Ridge, Marvin Spur and adjacent basins of the Arctic Ocean based on seismic data. Tectonophysics 472, 309–322.

Lawver, L.A., Baggeroer, A., 1983. A note on the age of the Canada Basin. J. Alsk. Geol. Soc. 2, 57–66.

Lawver, L.A., Scotese, C.R., 1990. A review of tectonic models for the evolution of Canada Basin. In: Grantz, A., Johnson, L., Sweeney, J.F. (Eds.), The Geology of North America, The Arctic Ocean Region, Vol. L. The Geological Society of America, pp. 593–618.

Lawver, L.A., Müller, R.D., 1994. Iceland hotspot track. Geology 22, 311–314.

Lawver, L.A., Grantz A, Gahagan L.M., 2002. Plate kinematic evolution of the present Arctic region since the Ordovician. Special Paper-Geol Soc Am, 360, 333–358.

Laxon, S., McAdoo, D., 1994. Arctic Ocean gravity field derived from ERS-1 satellite altimetry. Science 265, 621–624.

Lebedeva-Ivanova N., Lizarralde D., 2011. An empirical direct-wave traveltime equation for Arctic sonobuoy data. Abstract. Sixth International Conference on Arctic Margins, ICAM VI, Geophysical Institute, University of Alaska Fairbanks, Fairbanks, AK, USA.

Lebedeva-Ivanova, N.N., Zamansky, Y., Langinen, A., Sorokin, M., 2006. Seismic profiling across the Mendeleev Ridge at 82°N: Evidence of continental crust. Geophys. J. Int. 165, 527–544.

Lebedeva-Ivanova, N.N., Gee, D.G., Sergeyev, M. B. 2011. Crustal structure of the East Siberian continental margin, Podvodnikov and Makarov basins, based on refraction seismic data (TransArctic 1989–1991). Geological Society, London, Memoirs, 35, 395–411.

Lorenzo, J.M., Wessel, P., 1997. Flexure across a continent–ocean fracture zone: the northern Falkland/Malvinas Plateau, South Atlantic. Geo-Marine Letters 17, 110–118.

Ludwig, W.J., Nafe, J.E., Drake, C.L., 1970. Seismic refraction. In: Maxwell, A.E. (Ed.), The Sea, 4. Wiley-Interscience, New York, pp. 53–84.

Lundin, E.R., Doré, A.G., 2017. The Gulf of Mexico and Canada Basin: Genetic Siblings on Either Side of North America. GSA Today, 27, 4–11.

Maher Jr., H.D., 2001. Manifestations of the Cretaceous High Arctic large igneous province in Svalbard. J. Geol. 109, 91–104.

Mahoney, J.J., Fitton, J.G., Wallace, P.J., et al., 2001. Site 1184. Proc. ODP, Init. Repts. 192. College Station, TX (Ocean Drilling Program). doi:10.2973/odp.proc.ir.192.2001.

Mair, J.A., Forsyth, D.A., 1982. Crustal structures of the Canada Basin near Alaska, the Lomonosov Ridge and adjoining basins near the North Pole. Tectonophysics 89, 239–253.

Mann, P., Hempton, M.R., Bradley, D.C., Burke, K., 1983. Development of pull-apart basins. Journal of Geology 91, 529–554.

Mayer, L.A., Armstrong, A.A., 2008. U.S. Law of the Sea cruise to map the foot of the slope and 2500-m isobath of the US Arctic Ocean margin report for 2008. Center for Coastal and Ocean Mapping. Paper 1258, 179 pp.

Mayer, L.A., Armstrong, A.A., 2011. U.S. Law of the Sea cruise to map the foot of the slope and 2500-m isobath of the US Arctic Ocean margin. Center for Coastal and Ocean Mapping. Paper 1253, 235 pp.

Mayer, L.A., Calder, B., 2016. U.S. Law of the Sea cruise to map and sample the U.S. Arctic Ocean margin, Healy 1603. Center for Coastal and Ocean Mapping, 135 pp.

Miller, E.L., Verzhbitsky, V., 2009. Structural Studies in the Pevek region, Russia: implications for the evolution of the East Siberian Shelf and Makarov Basin of the Arctic Ocean. Stephan Mueller Publication Series 4, 223–241.

Miller, E.L., Soloviev, A., Kuzmichev, A., Gehrels, G.E., Toro, J., Tuchkova, M., 2008. Jurassic and Cretaceous foreland basin deposits of the Russian Arctic: separated by birth of Makarov Basin? Norw. J. Geol. 88, 201–226.

Miller, E.L., Meisling, K.E., Akinin, V.V., Brumley, K., Coakley, B.J., Gottlieb, E.S., Hoiland, C.W., O'Brien, T.M., Soboleva, A. and Toro, J., 2017. Circum-Arctic Lithosphere Evolution (CALE) Transect C: displacement of the Arctic Alaska–Chukotka microplate towards the Pacific during opening of the Amerasia Basin of the Arctic. In: Pease, V., Coakley, B.J. (Eds.), Circum-Arctic Lithosphere Evolution: Geol. Soc., London, Special Publications 460, https://doi.org/10.1144/SP460.9.

Minakov, A., Faleide, J.I., Glebovsky, V.Y., Mjelde, R., 2012. Structure and evolution of the northern Barents-Kara Sea continental margin from integrated analysis of potential fields, bathymetry and sparse seismic data. Geophys. J. Int. 188, 79–102.

Mjelde, R., Raum, T., Myhren, B., Shimamura, H., Murai, Y., Takanami, T., Karpuz, R., Næss, U., 2005. Continent ocean-transition on the Vøring Plateau, NE Atlantic, derived from densely sampled ocean bottom seismometer data. J. Geophys. Res. 110, 1–19.

Moran, K., Backman, J., Brinkhuis, H., Clemens, S.C., Cronin, et al., 2006. The Cenozoic palaeoenvironment of the Arctic Ocean. Nature 441, 601–605.

Morozov, A.F., Petrov, O.V., Shokalsky, S.P., Kashubin, S.N., Kremenetsky, A.A., Shkatov, M.Yu, Kaminsky, V.D., Gusev, E.A., Grikurov, G.E., Rekant, P.V., Shevchenko, S.S., Sergeev, S.A., Shatov, V.V., 2013. New geological data are confirming continental origin of the central Arctic rises. Reg. Geol. Metallog. 53, 34–55 (in Russian).

Mosher, D.C. (Ed.), 2012. 2011 Canadian High Arctic seismic expedition: CCGS Louis S. St-Laurent expedition report, Geological Survey of Canada, Open File 7053, 290 pp.

Mosher, D.C., Shimeld, J., Hutchinson, D.R. (Eds.), 2009. 2009 Canada Basin seismic reflection and refraction survey, western Arctic Ocean: CCGS Louis S. St-Laurent expedition report, Geological Survey of Canada, Open File 6343, 266 pp.

Mosher, D.C., Shimeld, J., Hutchinson, D., Chian, D., Lebedova-Ivanova, N., Jackson, H.R., 2012. Canada Basin revealed. Arctic Technology Conference OTC 23797.

Mosher, D.C., Chapman, C.B., Shimeld, J., Jackson, H.R., Chian, D., Verhoef, J., Pederson, R., 2013. High Arctic marine geophysical data acquisition. Lead. Edge 32, 524–536.

Mosher, D.C., Shimeld, J.W., Hutchinson, D.R., Jackson, H.R., 2016. Canadian UNCLOS Extended Continental Shelf Program seismic data holdings (2006–2011), Geological Survey of Canada, Open File 7938, 1 .zip file. doi:10.4095/297590

Mudie, P.J., Blasco, S.M., 1985. Lithostratigraphy of the CESAR cores. In: Jackson, H.R., Mudie, P.J., Blasco, S.M. (Eds.), Initial Geological Data Report on CESAR, The Canadian expedition to study the Alpha ridge, Arctic Ocean. Geological Survey of Canada, Ottawa, Geological Survey of Canada Paper 84-22, pp. 59–99.

Nafe, J. E., Drake, C. L., 1961. Physical properties of marine sediments, Tech. Rep. 2, Lamont-Doherty Geol. Observ., Palisades, N.Y., 29 p.

Naryshkin, G. 2001. Bottom relief of the Arctic Ocean, bathymetric contour map. Russian Academy of Sciences, St Petersburg.

Nikishin, A.M., Malyshev, N.A., Petrov, E.I., 2014. Geological Structure and History of the Arctic Ocean. European Association of Geoscientists and Engineers (EAGE) Publications, Houten, Netherlands.

Nikishin, A.M., Petrov, E.I., Malyshev, N.A., Ershova, V.P., 2017. Rift systems of the Russian Eastern Arctic shelf and Arctic deep water basins: link of geological history and geodynamics. Geodyn. Tectonophys. 8, 11–43.

Noda, A., 2013. Strike-slip basin – its configuration and sedimentary facies. In: Itoh, Y. (Ed.), Mechanism of sedimentary basin formation – multidisciplinary approach on active plate margins. InTech, pp. 28–57.

Oakey, G.N., Saltus, R.W., 2016. Geophysical analysis of the Alpha–Mendeleev ridge complex: Characterization of the High Arctic Large Igneous Province. Tectonophysics 691, 65–84.

Operto, S., Charvis, P., 1995. Kerguelen Plateau: A volcanic passive margin fragment?. Geology, 23, 137–140.

Osler, J.C., 1993. Crustal structure of the extinct spreading center in the Labrador Sea: Implications for dynamic models of flow beneath mid-ocean ridges. Unpublished Ph.D. thesis. Dalhousie University, Halifax, Nova Scotia, Canada, 220 pp.

Overton, A., 1982. A seismic reflection profile across the Lomonosov Ridge, Central Arctic Ocean. Society of Exploration Geophysicists, Technical Program Abstracts and Biographies, 52nd Annual Meeting, Dallas, 87-89.

Passey, S.R., Bell, B.R., 2007. Morphologies and emplacement mechanisms of the lava flows of the Faroe Island Basalt Group, Faroe Islands, NE Atlantic Ocean. Bulletin of Volcanology 70, 139–156.

Pease, V., 2011. Eurasian orogens and Arctic tectonics: an overview. In: Spencer, A.M., Embry, A.F., Gautier, D.L., Stoupakova, A.V., Sørensen, K. (Eds.), Arctic Petroleum Geology: Geol. Soc. London, Memoirs 35, pp. 311–324.

Pease, V., Chev, S., Stephenson, R., Zhang, X., Pease, V., Zhang, X., 2014. Arctic lithosphere — a review. Tectonophysics 628, 1–25.

Petrov, O., Morozov, A., Shokalsky, S., Kashubin, S., Artemieva, I.M., Sobolev, N., Petrov, E., Richard E.E., Sergeev, S., Smelror M., 2016. Crustal structure and tectonic model of the Arctic region. Earth Sci. Rev. 154, 29–71.

Pietsch, R., Uenzelmann-Neben, G., 2015. The Manihiki Plateau—A multistage volcanic emplacement history, Geochem. Geophys. Geosyst. 16, 2480–2498, doi:10.1002/2015GC005852.

Pollack, H.N., Hurter, S.J., Johnson, J.R., 1993. Heat flow from the Earth's interior: analysis of the global data set. Rev. Geophys. 31, 267–280.

Poselov, V., Butsenko, V., Chernykh, A., Glebovsky, V., Jackson, H.R., Potter, D.P., Oakey, G., Shimeld, J., Marcussen, C., 2013. The structural integrity of the Lomonosov Ridge with the North American and Siberian continental margins. In: Stone D., Clough J.G., Thurston D.H., Coakley B. (Eds.), ICAM VI proceedings. Geophysical Institute, University of Alaska Fairbanks, Fairbanks, AK, USA, pp. 233–258.

Rasmussen, R., Pedersen, L.B., 1979. End corrections in potential field modelling. Geophys. Prospect. 27, 749–760. http://dx.doi.org/10.1111/j.1365-2478.1979.tb00994.x.

Rowley, D.B., Lottes, A.L., 1988. Plate-kinematic reconstructions of the North Atlantic and Arctic: Late Jurassic to Present. Tectonophysics 155, 73–120.

Salisbury, M.H., Christensen, N.I., 1978. The seismic velocity structure of a traverse through the Bay of Islands ophiolite complex, Newfoundland, an exposure of oceanic crust and upper mantle. J. Geophys. Res. 83, 805–817.

Saltus, R.W., Miller, E.L., Gaina, C., Brown, P.J., 2011. Regional magnetic domains of the Circum-Arctic: a framework for geodynamic interpretation. In: Spencer, A.M., Embry, A.F., Gautier, D.L., Stoupakova, A.V., Sørensen, K. (Eds.), Arctic Petroleum Geology: Geol. Soc. London, Memoirs 35, pp. 49–60.

Shephard, G.E., Müller, R.D., Seton, M., 2013. The tectonic evolution of the Arctic since Pangea breakup: integrating constraints from surface geology and geophysics with mantle structure. Earth Sci. Rev. 124, 148–183. http://dx.doi.org/10.1016/j.earscirev.2013.05.012.

Sheriff, R.E., and Geldart, L.P., 1995. Exploration seismology. Cambridge University Press, 592 pp.

Shimeld, J., 2009. Chapter 5: Acquisition and processing of the seismic reflection data. In: Mosher, D.C., Shimeld, J.W., Hutchinson, D.R. (Eds.). 2009 Canada Basin seismic reflection and refraction survey, western Arctic Ocean: CCGS Louis S. St-Laurent expedition report, Geological Survey of Canada, Open File 6343, pp. 151–171.

Shimeld, J., 2011. Chapter 2: Acquisition and processing of the seismic reflection data. In: Mosher, D.C., Shimeld, J.W., Chapman, C.B. (Eds.). 2010 Canada Basin seismic reflection and refraction survey, western Arctic Ocean: CCGS Louis S. St-Laurent expedition report, Geological Survey of Canada, Open File 6720, pp. 49–68.

Shimeld, J., Li, Q., Chian, D., Lebedeva-Ivanova, N.N., Jackson, H.R., Mosher, D.C., Hutchinson, D.R., 2016. Seismic velocities within the sedimentary succession of the Canada Basin and southern Alpha-Mendeleev Ridge, Arctic Ocean: Evidence for accelerated porosity reduction?. Geophys. J. Inter. 204, 1–20.

Schlanger, S. O., Jackson, E. D., Boyce, R. E., Cook, H. E., Jenkyns, H. C., Johnson, D. A., et al., 1976. Site 317. Texas A & M University, Ocean Drilling Program, College Station, TX, United States. doi:10.2973/dsdp.proc.33.105.1976.

Smith, D.G., 1987. Late Paleozoic to Cenozoic reconstructions of the Arctic. In: Tailleur, I., Weimer, P. (Eds.), Alaskan North Slope Geology. Pac. Sect. Soc. Econ. Paleontol. Mineral. and Alaskan Geol. Soc., Bakersfield, California, pp. 785–794.

Sorokin, M. Y., Zamansky, Y. Y., Languinen, A. Y., Brekke, H., Sand, M., Sørenes, N.B., 1998. North Pole-28 ice drift seismic line. 3rd International Conference on Arctic Margins (*ICAM III*), Celle, Germany.

Sorokin, M., Zamansky, Y., Langinen, A., Jackson, R., Macnab, R., 1999. Crustal structure of the Makarov Basin, Arctic Ocean determined by seismic refraction. Earth Planet. Sci. Lett. 168, 187–199.

Srivastava, S.P., 1985. Evolution of the Eurasian Basin and its implication to the motion of Greenland along Nares Strait. Tectonophysics 114, 29–53.

Stanghellini, G., Bonazzi, C., 2002. Local-trace zeroing and spike zeroing: Two short automated noise-rejection routines to remove noise and spikes on seismic traces. Geophysics 67, 188–196.

Sweeney, J.F., Weber, J.R., Blasco, S.M., 1982. Continental ridges in the Arctic Ocean: LOREX constraints. Tectonophysics 89, 217–237.

Tailleur, I.L., 1973. Probable rift origin of Canada basin, Arctic Ocean. In: Pitcher, M.G. (Ed.), Arctic geology: American Association of Petroleum Geologists Memoir 19, pp. 526–535.

Taldenkova, E., Nikolaev, S., Rekant, P., Chistyakova, N., 2014. Pleistocene sediment sequence of the southern Lomonosov Ridge, Arctic Ocean: preliminary stratigraphic subdivision based on iceberg-rafted debris and benthic foraminiferal records. In STRATI 2013. Springer International Publishing, pp. 1321–1325.

Talwani, M., Worzel, J.L., Landisman, M., 1959. Rapid gravity computations for two-dimensional bodies with application to the Mendocino submarine fracture zone. J. Geophys. Res. 64, 49–59.

Taylor, P.T., Kovacs, L.C., Vogt, P.R., Johnson, G.L., 1981. Detailed aeromagnetic investigation of the Arctic Basin, 2. J. Geophys. Res. 86, 6323–6333.

Tegner, C., Storey, M., Holm, P. M., Thorarinsson, S. B., Zhao, X., Lo, C. H., Knudsen, M. F., 2011. Magmatism and Eurekan deformation in the High Arctic Large Igneous Province: 40Ar–39Ar age of Kap Washington Group volcanics, North Greenland. Earth Planet. Sci. Lett. 303, 203–214.

Todd, B.J., Reid, I., Keen, C.E., 1988. Crustal structure across the Southwest Newfoundland Margin. Can. J. Earth Sci. 25, 744–759.

Trettin, H.P., 1991. Silurian—Early Carboniferous deformational phases and associated metamorphism and plutonism, Arctic Islands. In: Trettin, H.P. (Ed.), The Geology of the Innuitian Orogen and Arctic Platform of Canada and Greenland, Geological Survey of Canada, Ottawa, Vol. 3. pp. 295–341.

Van Wagoner, N.A., Williamson, M.-C., Robinson, P.T., Gibson, I.L., 1986. First samples of acoustic basement recovered from the Alpha Ridge, Arctic Ocean: New constraints for the origin of the ridge. J. Geodyn. 6, 177–196.

Vogt, P.R., Taylor, P.T., Kovacs, L.C., Johnson, G.L., 1979. Detailed aeromagnetic investigations of the Arctic Basin. J. Geophys. Res., 84, 1071–1089.

Vogt, P.R., Taylor, P.T., Kovacs, L.C., Johnson, G.L., 1982. The Canada Basin: aeromagnetic constraints on structure and evolution. Tectonophysics 89, 295–336.

Vogt, P.R., Jung, W.-Y., Jakobsson, M., Mayer, L., Williamson, M., 2006. The Alpha-Mandeleev magmatic province, Arctic Ocean– a new synthesis. Eos Trans. AGU 87 (Abs.), 36.

Weber, J.R., 1979. The Lomonosov Ridge experiment: LOREX '79. Eos Trans. AGU 60, 715–721.

Weber, J.R., 1980. Exploring the Arctic sea floor. Geos 9 (3), 2–7.

Weber, J.R., 1986. The Alpha Ridge: gravity, seismic and magnetic evidence for a homogenous, mafic crust. J. Geodyn. 6, 117–136.

Weber, J.R., 1990. The structures of the Alpha Ridge, Arctic Ocean and Iceland-Faeroe Ridge, North Atlantic; comparisons and implications for the evolution of the Canada Basin. Marine Geology 93, 43–68.

Weber, J.R., Sweeney, J.F., 1985. Reinterpretation of morphology and crustal structure in the central Arctic Basin. J. Geophys. Res. 90, 663–677.

Weber, J.R., Roots, E.F., 1990. Historical background; Exploration, concepts, and observations. In: Grantz, A., et al. (Eds.), The Arctic Ocean Region, Vol. L. Geological Society of America, The Geology of North America, Boulder, pp. 5–36.

Weigelt, E., Jokat, W., 2001. Peculiarities of roughness and crustal thickness of oceanic crust in the Eurasian Basin, Arctic Ocean. Geophys. J. Int. 145, 505–516.

Weigelt, E., Franke, D., Jokat, W., 2014. Seismostratigraphy of the Siberian Arctic Ocean and adjacent Laptev Sea Shelf. J. Geophys. Res. 119, 5275–5289. http://dx.doi.org/10.1002/2013JB010727.

White, R.S., Mackenzie, D., O'Nions, R.K., 1992. Oceanic crustal thickness from seismic measurements and rare earth element inversions. J. Geophys. Res. 9 (B13), 19,683–19,715.

Wilkens, R.H., Fryer, G.J., Karsten, J., 1991. Evolution of porosity and seismic structure of upper oceanic crust: importance of aspect ratios. J. Geophys. Res. 96, 17,981–17,995.

Wilson, J.T., 1963. Hypothesis of earth's behaviour. Nature, 198, 925–929.

Wu, J., McClay, K., Whitehouse, P., Dooley, T., 2009. 4D analogue modelling of transtensional pull-apart basins. Mar. Pet. Geol. 26, 1608–1623.

Zamansky, Y.Y., Zatsepin, Y.N., Langinen, A.Y., Sorokin, M.Y., 1999. Seismic model of the earth's crust on the geotraverse in the central part of the Arctic Ocean. Investigation and Protection of Bowels 7–8, 38–41 (in Russian).

Zamansky, Y.Y., Ivanova, N.N, Langinen, A.E., Sorokin, M.Y., 2002. Seismic investigations in the 'Arctic-2000' Expedition, Physics of the Earth 6, 21–31 (in Russian).

Zelt, C.A., 1994. Software Package ZPLOT. Bullard Laboratories, University of Cambridge.

Zelt, C.A., Smith, R.B., 1992. Seismic traveltime inversion for 2-D crustal velocity structure. Geophys. J. Int. 108, 16–34.

APPENDIX A

Below, previous seismic experiments from the Arctic Ocean and their salient results pertinent to this thesis are described (refer to Fig. A.1 for locations).
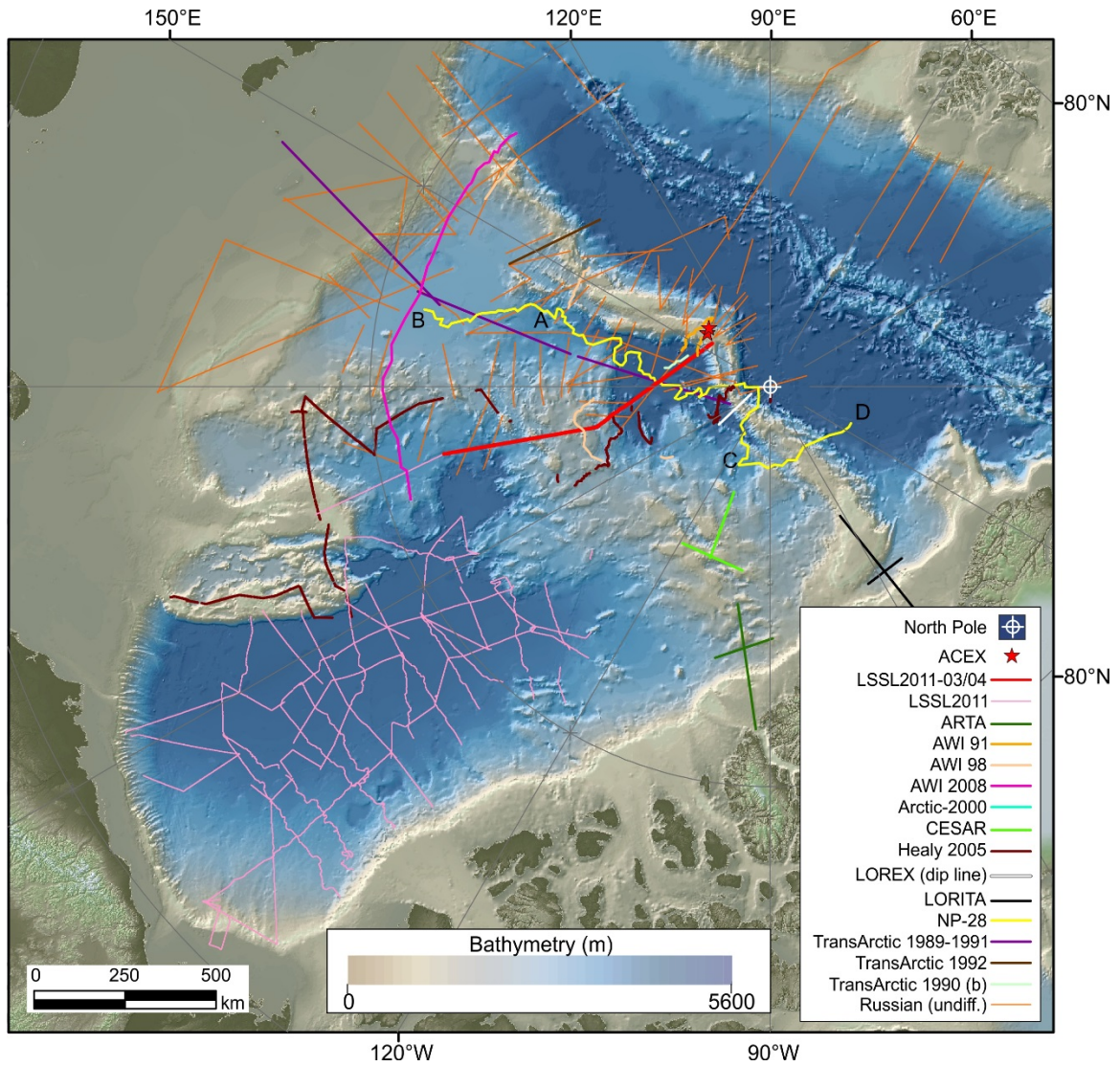
Fig. A.1. A coloured elevation map of the Arctic Ocean. Seismic transects shown in this figure are: LSSL2011-03/04 (Evangelatos and Mosher, 2016; Evangelatos et al., 2017), LSSL2007 to LSSL2011 (Mosher et al., 2016), ARTA (Funck et al., 2011), AWI 91 (Jokat et al., 1992, 1995), AWI 98 (Jokat 2003; 2005), AWI 2008 (Weigelt et al., 2014; Jokat and Ickrath, 2015), Arctic-2000 (Lebedeva-Ivanova et al., 2006), CESAR (Jackson et al., 1985), Healy 2005 (Bruvoll et al., 2010; 2012; Dove et al., 2010), LOREX (Forsyth and Mair, 1984), LORITA (Jackson et al., 2010), TransArctic 1989–1991 (Lebedeva-Ivanova et al., 2011), TransArctic 1992 (Poselov et al., 2011), NP-28, TransArctic 1990 (b) (Langinen et al., 2009) and other undifferentiated Russian lines (Kaminsky, 2017). ACEX refers to drill sites of IODP Expedition 3002 (Backman et al., 2006). Bathymetry and topography are from the IBCAO version 3.0 grid (Jakobsson et al., 2012).

Lomonosov Ridge Experiment (LOREX)

In Spring 1979, the Government of Canada undertook a large-scale scientific expedition to Lomonosov Ridge and adjacent basins, Makarov and Amundsen basins (Weber, 1979). Scientific investigations were supported by drifting ice stations. As part of this project, wide angle reflection/refraction profiles were acquired across and along strike of the ridge. Seismometers were positioned every 10 km along the profiles. Explosive charges lowered ~100 m beneath the sea ice were used as seismic sources. The dip line (perpendicular to Lomonosov Ridge) comprised six shots with reversed ray-coverage and extended over a composite length of ~130 km (Mair and Forsyth, 1982; Forsyth and Mair, 1984). Due to wide recorder spacing, resolution of the sedimentary cover was not possible. As such, a P-wave velocity of 2.7 km s^{-1} and a thickness of < 1 km were assigned to the sedimentary layer as part of velocity modelling. The upper crust was modelled using 4.7 km s^{-1} and a thickness of ~4 km in the basin and up to 6 km for Lomonosov Ridge. A velocity of 6.6 km s^{-1} is modelled for the lower crust. The base of this layer, i.e., Moho, changes from 14 km beneath Makarov Basin to 26–27 km under Lomonosov Ridge before rising to 17 km beneath Amundsen Basin. Weber (1980) and Sweeney et al. (1982) presented density models along the dip profile. Honouring seismic constraints for the depth of Moho in Amundsen Basin necessitated a dense 3000 kg m^{-3}

block in the upper crust and an unusually dense lower crust (3100 kg m^{-3}). Recognizing

that these values were inconsistent with young (<56 Ma) oceanic crust, Weber and

Sweeney (1985) revised the density model along the LOREX dip line (Fig. A.2). While

maintaining the same crustal density as with Makarov Basin (2.85 kg m^{-3}), these authors

fit the observed gravity field by reducing the depth of Moho for Amundsen Basin by ~2–

4 km. In addition to the wide angle reflection/refraction seismic data, single-channel

seismic reflection data were acquired along the drift track of the main ice station

(Overton, 1982; Weber and Sweeney, 1985). In Makarov Basin, these data reveal a thick

sedimentary package (down to at least ~7 s TWTT) situated between buried basement

highs and the Amerasian flank of Lomonosov Ridge.
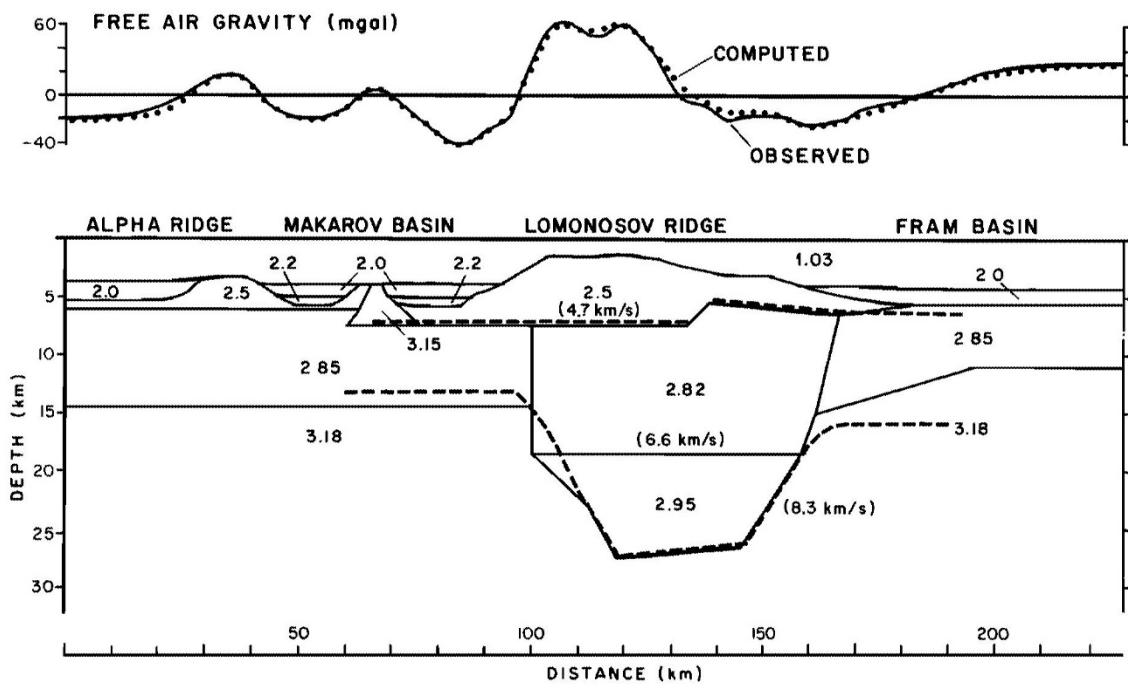
Fig. A.2. Two-dimensional crustal density model along LOREX (dip) line (Fig. A.1) from Weber and Sweeney (1985). Densities are in megagrams per cubic meter. Dashed lines represent seismic refraction results (from Mair and Forsyth, 1982) with an upper crustal velocity of 4.7 km s^{-1}, a lower crustal velocity of 6.6 km^{-1}, and an upper mantle velocity of 8.3 km^{-1}.

Canadian Expedition to Study the Alpha Ridge (CESAR)

Conducted in 1983, the Canadian Expedition to Study the Alpha Ridge (CESAR) operated out of an ice station (Jackson et al., 1985). To acquire wide-angle reflection/refraction seismic data over central Alpha Ridge, seismic receivers were deployed on sea ice. Receiver spacing varied from 2.8 to 15 km depending on the line. The seismic sources for CESAR were 54 to 630 kg GEOGEL charges detonated 100 to 200 m below sea ice. Four wide-angle reflection/refraction seismic lines with reversed ray-coverage were acquired. Resulting velocity models included a 0.4 km thick sedimentary cover with a P-wave velocity range of 1.8–2.4 km s^{-1}. The estimate for sedimentary thickness is consistent with observations from single-channel seismic reflection data acquired at the main CESAR camp (Jackson, 1985; Jackson et al. 1990). Results from seismic velocity modelling were published in Forsyth et al. (1986a, b) and Asudeh et al. (1988). The upper crust was modelled using thicknesses of 4.5–6.3 km and P-wave velocities of 5.0–6.5 km s^{-1}. The thicknesses of mid-crustal layers are estimated at 8 to 16 km thick with a range in velocities from 6.5 to 7.0 km s^{-1}. The lower crust is modelled with velocities of ~6.9 to 8.0 km s^{-1}. The depth of Moho is constrained to 24–40 km directly beneath Alpha Ridge, and 21–25 km on its Makarov Basin-facing flank. The juxtaposition of an 8.0 km s^{-1} velocity block adjacent to a 7.3 km s^{-1} block on the "strike line" is suspect (Fig. A.3), as such a dramatic contrast is not supported by gravity modelling. In addition to seismic acquisition, rock dredging, and piston and gravity cores were acquired as part of CESAR (Jackson et al., 1985). Of particular importance is CESAR core 6, a piston core that recovered laminated diatom ooze of late Campanian–early Maastrichtian age (76–69 Ma; Mudie and Blasco, 1985; Davies et al., 2009). This

date is considered an upper limit on the latest age of magmatism related to the Alpha

Ridge (Dove et al., 2010). Basaltic samples were dredged from the steep wall of a major

graben. The bulk geochemistry of these rocks is consistent with alkaline basalts (Van

Wagoner et al., 1986); however, due to extensive alteration, radiometric dating was

unfeasible. Based on geological and geophysical results from CESAR, Jackson et al.
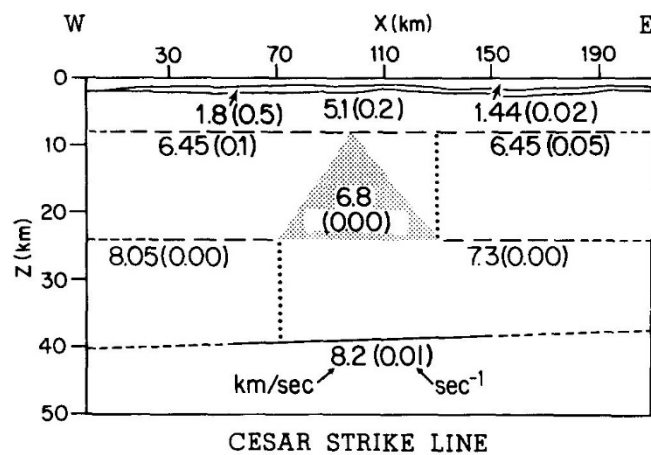
(1986) concluded that Alpha Ridge is an oceanic plateau.

Fig. A.3. P-wave velocity model along CESAR (strike) line from Forsyth et al. (1986b). Each boundary in the model is identified by a P-wave velocity (km s^{-1}) and velocity gradient (s^{-1}) shown in parentheses. When no gradient is shown the velocity is approximately constant for the entire block. Thick solid lines show reflecting interfaces, thick dashed lines shown those parts of the model well constrained by the data, thin dashed lines show regions sampled and dotted lines separate laterally varying structures.

Soviet/Russian North Pole Expeditions

Soviet/Russia ice station expeditions to the Arctic Ocean extend back to the late

1930s (references and short descriptions of surveys included in Weber and Roots [1990]

and Kristoffersen and Mikkelsen [2004]). These efforts produced large volumes of

geoscientific data that remain largely inaccessible outside of the Russian Federation;

however, bathymetric charts (e.g., Naryshkin, 2011) and scientific publications, mostly in

Russian journals, have been publically released.

The "North Pole" expeditions were conducted from ice stations and mostly operated over multiple years (Weber and Roots, 1990). From 1987-1989, ice station North Pole-28 (NP-28) drifted from Podvodnikov Basin, across Geophysicist Spur, continued into Makarov Basin, criss-crossed Lomonosov Ridge three times then drifted across Amundsen Basin and was finally abandoned around Fram Strait (Sorokin et al., 1999). The seismic profile totals ~4000 km in length. Reflection data acquired from this experiment relied on two 545 m arrays that crossed perpendicular to each other. Receivers were spaced 50 m apart along each of the two arrays. The source consisted of 3–5 electric caps placed at the cross point of the arrays. The 2–4 h firing interval resulted in data spacing of approximately 0.5–1 km. Langinen et al. (2009) rely on these data to correlate seismo-stratigraphies between Lomonosov Ridge, Marvin Spur and Amundsen and Makarov basins. Ages are constrained via jump-correlations to the ACEX core. Although the ice station data are extensive and penetrate into underexplored areas of the Arctic Ocean, resolution of the seismic image from this study is restricted to the upmost 1–1.5 s TWTT below seafloor (even in a sedimentary setting). Consequently, changes in seismic facies in the deeper successions are not apparent. Figs. A.4 and A.5 show two separate section of the NP-28 line.
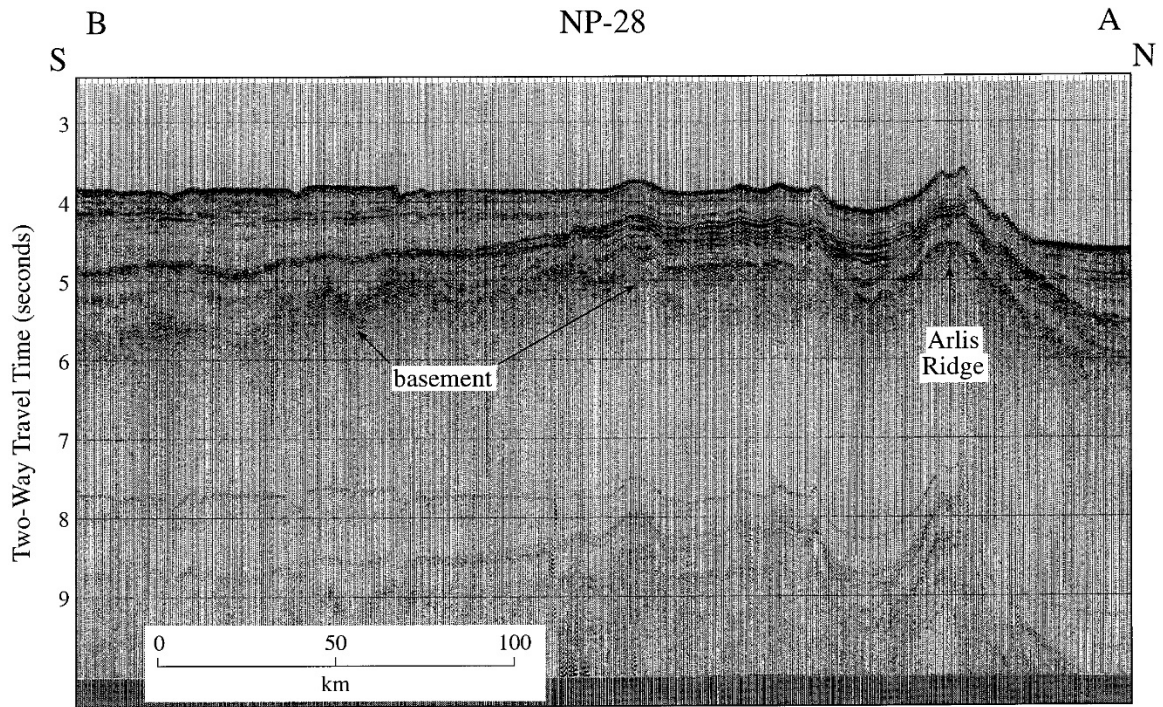
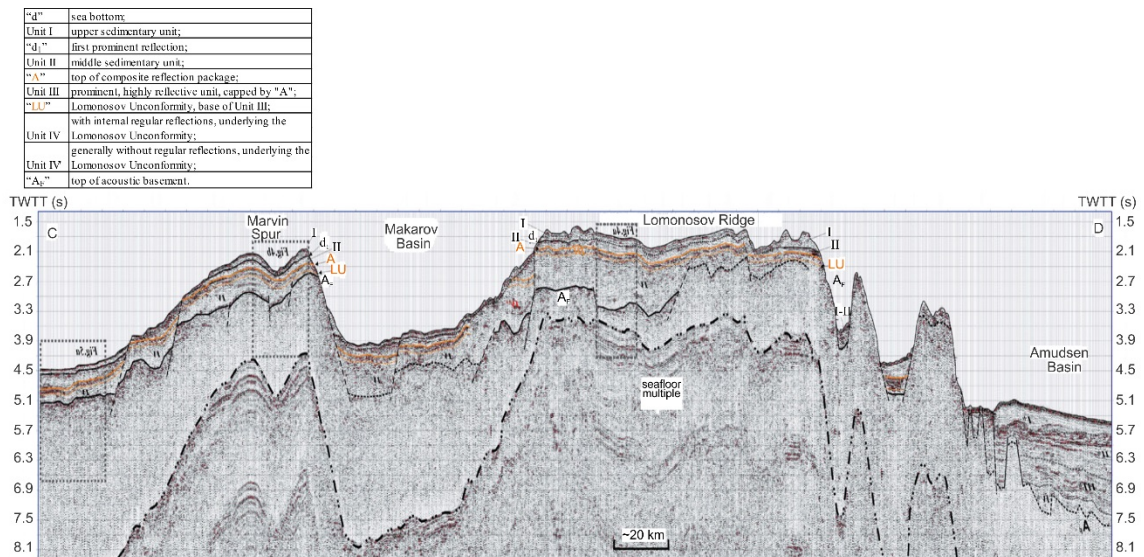Fig. A.4. A TWTT section between points B and A (Fig. A.1) of the NP-28 track (from Sorokin et al., 1999).

"d"	sea bottom;
Unit I	upper sedimentary unit;
"d₁"	first prominent reflection;
Unit II	middle sedimentary unit;
"A"	top of composite reflection package;
Unit III	prominent, highly reflective unit, capped by "A";
"LU"	Lomonosov Unconformity, base of Unit III;
Unit IV	with internal regular reflections, underlying the Lomonosov Unconformity;
Unit IV	generally without regular reflections, underlying the Lomonosov Unconformity;
"A_F"	top of acoustic basement.

Fig. A.5. A TWTT section between points C and D (Fig. A.1) of the NP-28 track. The main, reflections are marked as unbroken lines. Short-dashed lines indicate correlated reflections; long-dashed lines mark faults; letters d₁ and AF (acoustic basement) refer to the inferred surfaces of the main reflection boundaries within the sedimentary cover, "A" is the top of the composite reflection package; the base of which is the

Lomonosov Unconformity (LU), marked by a dotted line. Roman numerals refer to the main stratigraphic units (modified from Langinen et al., 2009).

Soviet/Russian TransArctic Expeditions

The TransArctic (a.k.a. TRA or Transarktika) experiments, conducted between 1989 and 1992, were a separate series of Soviet/Russian geophysical experiments conducting in the Arctic Ocean. The primary objective of these surveys was to acquire wide angle reflection/refraction seismic data to investigate deep crustal structures. Seismometers were deployed on ice and their spacing varied from 7 to 14 km for the different experiments (Lebedeva-Ivanova et al., 2011). Seismic sources consisted of explosive charges detonated ~50 m below water level and at 30 to 60 km intervals along the arrays (Sorokin et al., 1999). Lebedeva-Ivanova et al. (2011) modelled the P-wave velocity structure of a composite profile from this series, TransArctic 1989-1991 (Fig. A.6). This line extends 1487 km from the De Long Islands and across the East Siberian margin to Marvin Spur in Makarov Basin. As a consequence of the wide trace spacing, the velocity structure of the Upper Mesozoic–Cenozoic sedimentary successions (1.7–3.8 km s^{-1}) for Makarov and Podvodnikov basins is not well resolved. The underlying layer (5.0–5.4 km s^{-1}) is interpreted as older sedimentary successions possibly interbedded with mafic volcanic rock. Crustal thickness is 8–20 km for Podvodnikov Basin, and 8–12 km for Makarov Basin. Upper (5.9–6.5 km s^{-1}) and lower (6.7–7.3 km s^{-1}) crustal layers are interpreted as stretched continental crust; however, the abyssal part of Makarov Basin is "probably composed of oceanic crust" (Lebedeva-Ivanova et al., 2011). The TransArctic 1992 line is also part of this series (Poselov et al., 2012). This line extends 280 km from Podvodnikov Basin, across Lomonosov Ridge and into Amundsen Basin. Geophones were spaced 4–6 km apart. Due to the setup of the experiment, raypaths are

confined to the flanks of Lomonosov Ridge (i.e., there is no information on velocity structure directly beneath the ridge). Velocities interpolated between the flanks show upper, middle and lower crustal velocities of 5.3–5.4 km s^{-1}, 6.1–6.3 km s^{-1} and 6.6–6.7 km s^{-1}, respectively (Poselov et al., 2012).

Astafurova et al. (2006) modelled the gravity field of TransArctic 1989-1991, TransArctic 1992 and Arctic-2000 based on the earlier seismic velocity models of Zamansky et al. (1999), Ivanova et al. (2002) and Zamansky et al. (2002). In contrast to many gravity studies that employ uniform mantle densities (e.g., Oakey and Saltus, 2016), Astafurova et al. (2006) varied the density of the mantle (3.2–3.3 kg m^{-3}) in their density models. They thus fit the long wavelength signal of the observed gravity field while maintaining the constraints on boundary layers imposed by the velocity models.
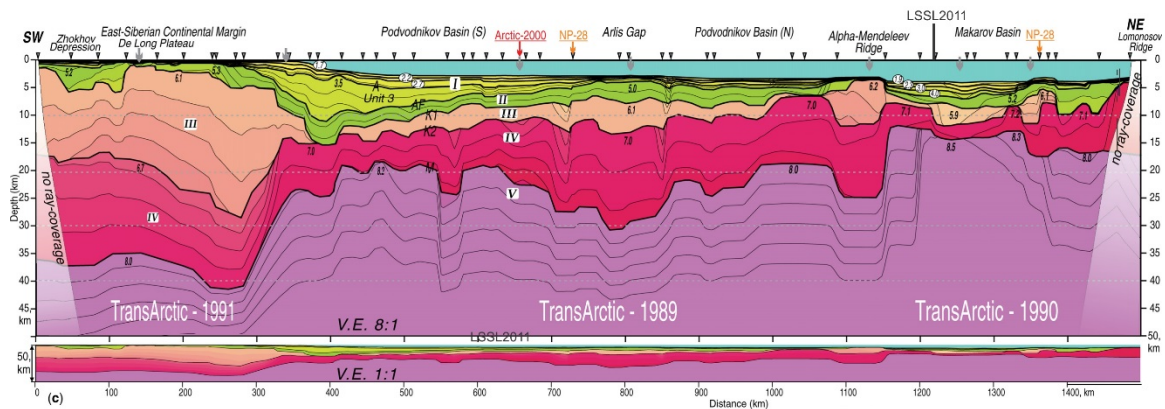
Fig. A.6. Seismic velocity model along transect TransArctic 1989–1991 (modified from Lebedeva-Ivanova et al., 2011). Cross-points with Arctic–2000, NP-28 and LSSL2011 profiles are indicated. Thick lines show seismic boundaries; thin lines are velocity isolines with intervals of 0.1 km s^{-1}. Roman numerals mark the sedimentary cover and layers of the consolidated crust; letters mark the seismic boundaries; triangles show the locations of shot points. Arabic numbers in ovals are velocities in sediments derived from TRA(b) reflection seismic data; other Arabic numbers are velocities at the top of seismic layers derived from refraction seismic data.

Alfred Wagner Institute 1991 and 1998 Expeditions

With the aid of icebreaker F/S *Polarstern*, scientists from the Alfred Wagner Institute (AWI) conducted multiple expeditions to the central Arctic Ocean with the aim of acquiring multi-channel seismic reflection data, refraction data from sonobuoys and sediment sampling from shallow cores. With respect to this thesis, cruises conducted in 1991 (Fütterer, 1992) and 1998 (Jokat, 1999) are relevant (Fig. A.1). The experimental setup was similar for all cruises. Seismic receivers consisted of a streamer towed behind the *Polarstern*. For the AWI 91 and AWI 98 lines, the active section of the streamer was 300 m with 12 channels and 200 m (originally 350 m) with 32 channels, respectively. The seismic source was an airgun array with a total volume of 24 L.

Using the AWI 91 seismic data, Jokat et al. (1992, 1995) published a seismic stratigraphy for Lomonosov Ridge with corresponding modelled P-wave velocities for the Cenozoic sedimentary drape (1.51–2.2 km s^{-1}) and older sedimentary successions (4.5–6.2 km s^{-1}). Their work described the prograding slope face of the Amerasian margin of Lomonosov Ridge, which contrasts with the fault-bounded half-grabens noted on the Eurasian side of the central part of the ridge (Figs. A.7 and A.8). Using seismic data from the AWI 98 cruise, Jokat (2003) broadly divides the sedimentary section of Alpha Ridge into Cretaceous syn-rift and Cenozoic post-rift deposits (Fig. A.9). Modelled P-wave velocities from sonobuoy records are 1.6–2.7 km s^{-1} for sedimentary layers and 4.3–6.7 km s^{-1} for the upper crust. Velocities above 4 km s^{-1} are "interpreted to represent the uppermost basaltic layer of oceanic crust". A sedimentary corer fortuitously recovered basalt interpreted as basement rock (site PS51/040-1; Jokat, 1999). Tentatively classified as alkaline basalt (Jokat, 2003), the bulk chemistry of these samples was later revealed to be tholeiitic (Jokat et al., 2013). Further, ^{40}Ar/^{39}Ar radiometric

dating of plagioclase yields an age of 89 ± 1 Ma (Jokat et al., 2013). During this same expedition, multiple traverses across Lomonosov Ridge were executed (Jokat, 1999). Based on the internal seismic reflection geometries and velocity information from sonobuoys, Jokat (2005) divided the sedimentary section into a Cenozoic drape (P-wave < 3.0 km s^{-1}) and Upper Cretaceous/Lower Cenozoic faulted section (P-wave > 3.0 km s^{-1}) that "may represent basement". The author speculates that an inferred erosional unconformity from central Lomonosov Ridge (Jokat et al., 1995) plausibly disappears closer to the Laptev Sea, which is consistent with the greater water depths.
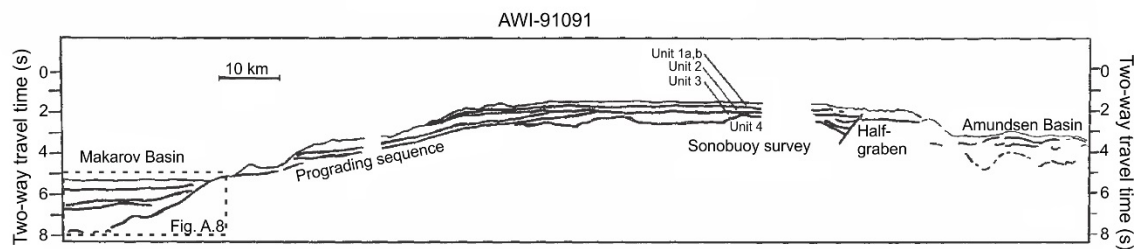
Fig. A.7. Interpretation of main features of line AWI-91091 from Jokat et al. (1992). Box outlines portion of line shown in Fig. A.8.
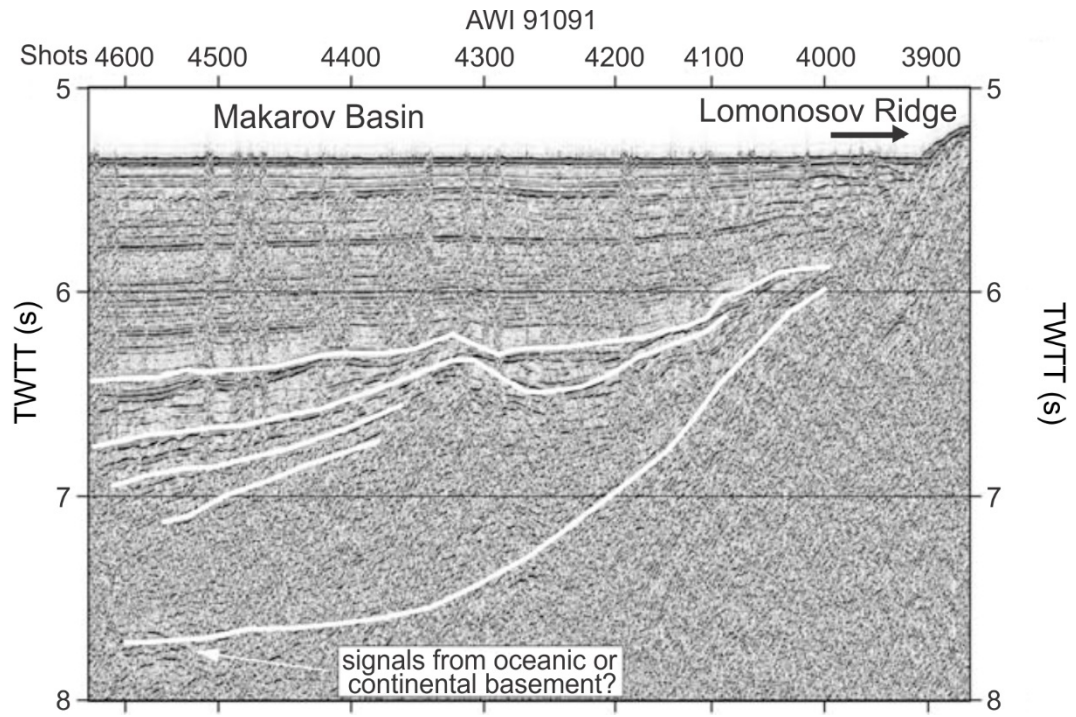
Fig. A.8. Part of profile AWI-91091 focused on Makarov Basin (Jokat, 2005). Refer to Fig. A.7 for location.
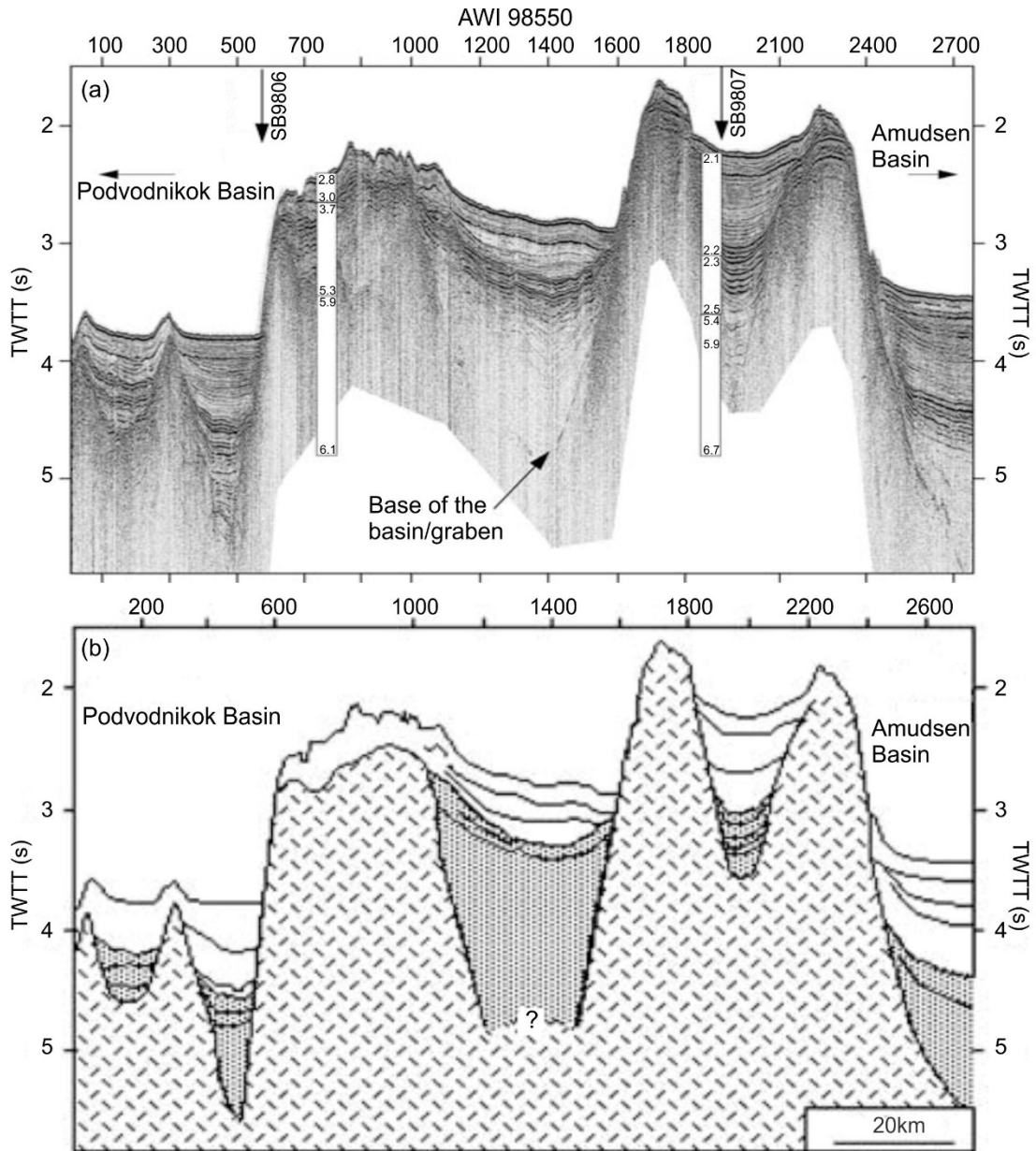
Fig. A.9. (a) The stacked seismic section of line AWI 98550 across the Lomonosov Ridge at 84°30' N. The line is 145 km long. The deployment locations of the sonobuoys and the velocity functions are indicated. (b) Interpretation of line AWI 98550. The grey shaded section indicates syn-rift sediments. The separation of the sedimentary column is based on reflection strength. Figures modified from Jokat (2005).

Arctic-2000 Expeditions

The Arctic-2000 line aligns approximately with 82° N from Nautilus Basin to

Podvodnikov Basin across the northern end of Mendeleev Ridge (Zamansky et al., 2002;

Lebedeva-Ivanova et al., 2006). The line is 485 km long. Unlike previous major Soviet/Russian Arctic geophysical expeditions, this experiment was supported by an icebreaker vessel. The experiment was configured with seismic recorders spaced ~5 km apart on ice and shots (explosive charges set 70–100 m below water level) fired about every 40 km. This configuration benefitted from reversed ray-coverage and long offsets up to 125 km. A P-wave velocity model by Lebedeva-Ivanova et al. (2006) is shown in Fig. A.10. The sedimentary cover is modelled using three layers (*I* to *III*) with velocities of 1.7 km s^{-1}, 2.3–2.6 km s^{-1} and 3.2–3.6 km s^{-1}, respectively. Along the line, total sedimentary thickness for these three layers is 2.5–3.0 km on the Nautilus Basin-facing flank of Mendeleev Ridge and 3.5 km thick in Podvodnikov Basin. The underlying layer (*layer IV*) is modelled with velocities of 5.0–5.7 km s^{-1} and tentatively interpreted as high velocity sedimentary rock (e.g., carbonates) or highly fractured/altered oceanic layer 2. *Layer V* has velocities of 5.9–6.5 km s^{-1} and a thickness of 1 to 4 km. The lower crust (*layer VI*) thickens from 5–7 km below the flanks of Mendeleev Ridge to 19–21 km thick below its crest. Modelled velocities are 6.7–7.3 km s^{-1}. Finally, the velocity model of Lebedeva-Ivanova et al. (2006) includes a high-velocity lower crust, beneath Mendeleev Ridge, with velocities intermediate between the lower crust and mantle (7.4–7.8 km s^{-1}). Funck et al. (2011) challenged the need for this layer, arguing that wide trace spacing, limited offsets and a reverberative source signature possibly inhibited the identification of a P_mP phase in the traveltime data. Seismic reflection data acquired during the Arctic-2000 experiment does resolve sedimentary structures; however, the overall resolution is coarse (Lebedeva-Ivanova et al., 2006).
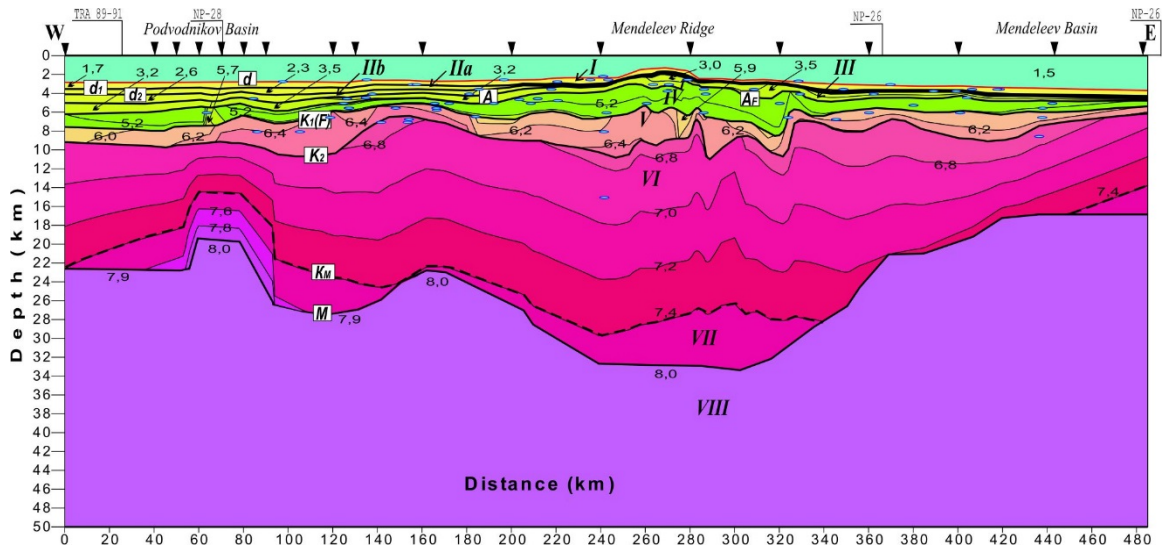
Fig. A.10. Seismic model along transect Arctic-2000 (from Lebedeva-Ivanova et al., 2006). Thick lines show seismic boundaries; thin lines are velocity isolines with intervals of 0.2 km s^{-1}; the dotted line is the inferred upper boundary of the crust–mantle mixed layer. Roman numerals mark the seismic sequences of the sedimentary cover and layers of the consolidated crust; letters mark the seismic boundaries; triangles show the locations of explosions. Cross-points with Arctic–2000, NP-28 and LSSL2011 profiles are indicated. Cross-points with TransArctic 1989–1991 (TRA 89–91), NP-28 and NP-26 are indicated.

Integrated Ocean Drilling Program Arctic Coring Expedition (IODP ACEX)

Integrated Ocean Drilling Program (IODP) Expedition 302 focused on coring the central part of Lomonosov Ridge (Backman et al., 2006). The expedition was realized in August 2004 and five holes were drilled across three sites all within 15.5 km from each other. Drilling reached down to 428 below seafloor in water depths of about 1300 m. Backman et al. (2008) presented a composite core with age constraints from biostratigraphic, cosmogenic isotope, magnetostratigraphic and cyclostratigraphic data (Fig. A.11). The ACEX core is divided into separate units numbered 1 to 4 from shallowest to deepest. Unit 1, composed primarily of silty clay, is further subdivided into units 1/1 to 1/6. Backman et al. (2008) reported hiatuses within unit 1/3 (9.4–11.6 Ma) and between units 1/5 and 1/6 (18.2–44.4 Ma). O'Regan et al. (2008) asserted that global lowstand cannot explain the major hiatus (18.2–44.4 Ma) documented in ACEX. Instead,

the authors proposed that Lomonosov Ridge was uplifted in the mid-Cenozoic due to far-field compression and/or a regional decrease in sea level. Unit 2 is primarily composed of mud containing biosiliceous ooze. Core recovery was less than 50% for Unit 3 (Backman et al., 2006). Lithologically, clays and silty clays dominate this unit. Unit 4 is the final unit near the base of the core. It is highly disturbed (Backman et al., 2006). Moran et al. (2006) referred to Unit 4 as a "Cretaceous [Campanian] unit composed of sand, sandstone and mudstone" and lies beneath a regional unconformity (also referred to as the Lomonosov Unconformity). Langinen et al. (2009) remarked that P-wave velocities for these lithologies are < 3 km s^{-1}, while Jokat et al. (1992) reported velocities of 4.0–4.6 km s^{-1} for this section. As such, Langinen et al. (2009) rejected the claim that the ACEX drillhole sampled beneath the unconformity. Their interpretation implies that the minimum age of the unconformity is, therefore, ~80 Ma as Campanian microfossils were interpreted near the base of the ACEX core (Backman et al., 2008).

Ma	Chron	Epoch	1995	ACEX	Tectonic and paleoceanographic evolution

Ma / Chron / Epoch / 1995 columns:

- 0
- C1 — Plei. / Plioc.
- 1.81
- C2 — m. / l. / e. / m. (early)
- LR-6
- 5 — 5.33
- C3
- C4 — late
- 10 — Miocene
- C5 — middle — LR-5
- 15 — 14.5 Ma region
- 17.5 region — early
- 20 — C6
- 23.0
- C7 — Oligocene — late
- 25 — C8
- C9
- C10 — LR-4
- 30 — C11 — early
- C12
- 33.8
- C13 – C16 — late
- 35
- C17
- C18 — Eocene
- 40 — C19 — middle — LR-3
- C20
- 45 — C21
- C22 — early
- 50 — C23
- C24 — Erosion (hiatus)
- 55.0 — Paleocene — late
- 55 — C25
- C26

ACEX column:

- Unit 1/2
- Unit 1/3
- Hiatus
- Unit 1/3
- Unit 1/4
- Unit 1/5
- Hiatus
- Unit 1/6
- Unit 2
- Unit 3
- No recovery and hiatus

Tectonic and paleoceanographic evolution:

- Brown (above) to olive color transition (1.5 Ma); absence biogenic carbonate below
- Core-seismic integration suggests an age of 5.8 Ma for the base of LR-6
- Proposed opening of the Fram Strait in upper C5n (ca 10 Ma) (*Jokat et al.,* 1995) Hiatus in early late Miocene (9.36-11.56 Ma) inferred from beryllium data
- Olive (above) to brown color transition (14.5 Ma)
- Beginning of Neogene ventilated circulation (17.5 Ma); deep opening of Fram Strait Youngest black layer at 196.17 mcd (17.9 Ma) marks end of euxinic conditions Young end of hiatus at the base of Subunit 1/5 (18.2 Ma) in the late early Miocene (see *Jakobsson et al.,* 2007)
- Separation of Yermak Plateau and Morris Jesup Rise "before Chron 12" (*Brozena et al.,* 2003)
- Old end of hiatus at the top of Subunit 1/6 (44.4 Ma) in the middle Eocene Youngest biogenic silica (44.6 Ma) Oldest large (2 cm) ice-rafted dropstone (44.8 Ma) End of biosiliceous ooze (45.4 Ma)
- Episodic freshwater surface conditions (48.6-49.2 Ma) (*Brinkhuis et al.,* 2006) Beginning of biosiliceous ooze (49.7 Ma) Oldest preserved biosiliceous taxa (50.1 Ma)
- Paleocene Eocene Thermal Maximum: >23°C in the Arctic Ocean (*Sluijs et al.,* 2006)
- Oldest Cenozoic ACEX sediment (56.2 Ma)

Fig. A.11. Chronologic distribution of ACEX lithological units, including hiatuses (from Backman et al., 2008). Reflection seismic units LR-3 to LR-6 are from Jokat et al. (1995). Units are described in Backman et al. (2006) and Moran et al. (2006).

Healy 2005 Expedition

During the 2005 HLY 05-03 expedition, multi-channel seismic reflection, sonobuoy wide-angle, multi-beam swath bathymetry and other data sets were acquired aboard the US Coast Guard icebreaker *Healy* (Coakley et al., 2005). The experimental setup for the MCS experiment included a hydrophone streamer with a 300 m length. Of the original 24 active channels, only 12 were live during acquisition over Alpha Ridge. The seismic source consisted of two 4 L airguns. Due to very heavy ice conditions, resulting seismic transects are crooked and data relatively noisy. During processing, traces were binned into 25 m intervals. Sonobuoys recorded signal up to a maximum of ~15 km offset. Also, similar to other experiments in the High Arctic that rely on sonobuoys, there is no reversed ray-coverage on refraction records. Fig. A.12 shows a short section acquired over Alpha Ridge.

Using seismic data acquired during the HLY 05-03 expedition, Dove et al. (2010) modelled the velocity structure of a section acquired over Mendeleev Ridge. P-wave velocities modelled are limited to the sedimentary cover (1.5–2.3 km s^{-1}) and upper crust (3.5–6.4 km s^{-1}). Seismic information was used to model the density structure of this ridge. Based on similarities in velocity and density structures, Dove et al. (2010) concluded that the Alpha and Mendeleev ridges form a contiguous geological entity with a common origin. Using the same data, Bruvoll et al. (2010) distinguished an upper sedimentary sequence (pelagic drape) from a lower sequence characterized by strong reflections and truncated at the top. The total thickness for the sedimentary layers was

~0.6–0.8 s two-way travel time (TWTT). These authors matched similar reflections

patterns between Alpha, Mendeleev and Lomonosov ridges. Using these intra-ridge

correlations and the constraints imposed by ACEX data (see below), Bruvoll et al. (2010)

produced an age model for the sediments over the Alpha-Mendeleev ridge complex. In a

later article, Bruvoll et al. (2012) define three acoustic basement facies. They interpret

basement beneath the Alpha-Mendeleev ridge complex as "basalt flows and sills capping

voluminous tuff deposits and possible sediments". In addition, horst and graben

structures on Mendeleev Ridge post-date the latest phase of HALIP-related magmatism.
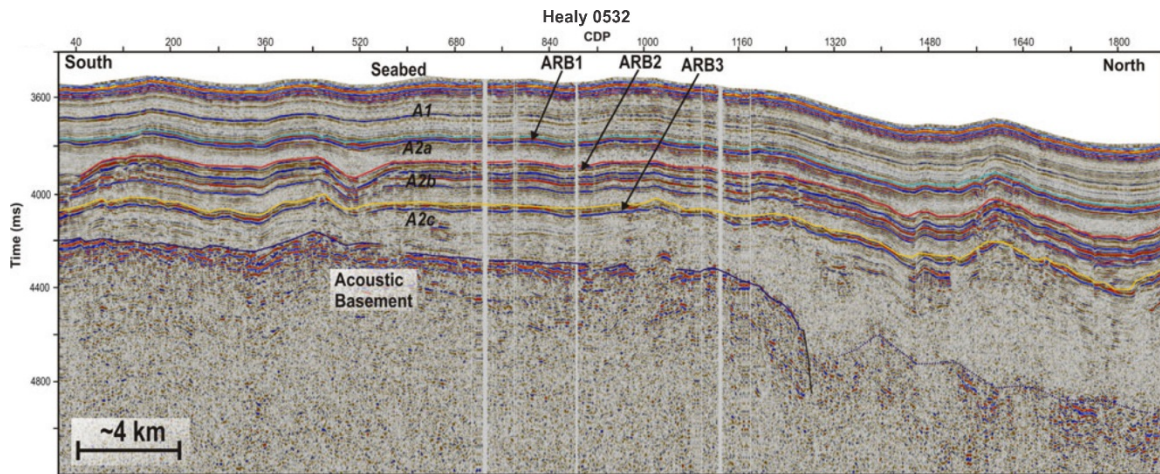
Fig. A.12. A section of profile H0532 traversing an undisturbed area of the Alpha Ridge (from Bruvoll et al., 2010). The turquoise line marks the boundary between Unit A1 and the more reflective Unit A2. This line also marks the top of subunit A2a. The red line marks the top of subunit A2b and the yellow line the top of subunit A2c. ARB1, ARB2 and ARB3 mark the Alpha Ridge reflection band 1, 2, 3, respectively. The dark blue line marks the acoustic basement (dotted line marks area where interpretation is less clear). For description of units and precise location of section, refer to Bruvoll et al. (2010).

Lomonosov Ridge Test of Appurtenance (LORITA)

The LORITA experiment was conducted on sea ice in Spring 2006 Dahl-Jensen et

al., 2007; Jackson and Dahl-Jensen, 2007). Long offset seismic reflection/refraction data

were acquired along two lines: 1) a "NS line" that extends 470 km from the Lincoln Sea

onto Lomonosov Ridge up to ~86.4° N (Fig. A.13), and 2) a shorter 120 km long "X line" that perpendicularly crosses the NS line at ~84.6° N. Geophones for the LORITA experiment were distributed 1.3–1.5 km apart. Explosives detonated beneath sea ice served as seismic sources for the long offset experiment. In addition, single-channel seismic reflection data were acquired over a distance of <340 km along the drift track of the ice camp.

The seismic data were used to produce a P-wave velocity model (Jackson et al, 2010). It is important to note the absence of seismometers north of 85.4 °N. Consequently, the experiment does not resolve the velocity structure of the sedimentary layers for the area north of the "plateau" on the southern end of Lomonosov Ridge and crustal layers are below the plateau are not well resolved. The meta-sedimentary and upper crustal layers were modelled using velocities of 5.2–5.7 km s^{-1} and 6.2–6.5 km s^{-1}, respectively, and have a combined thickness of about 10 km (Jackson et al., 2010). Beneath the plateau, a basement high with velocities of 6.0–6.2 km s^{-1} is modelled. The lower crust of the ridge has a velocity range of 6.5–6.7 km s^{-1}. The depth of Moho varies from 23 to 27 km beneath Lomonosov Ridge along the NS line.
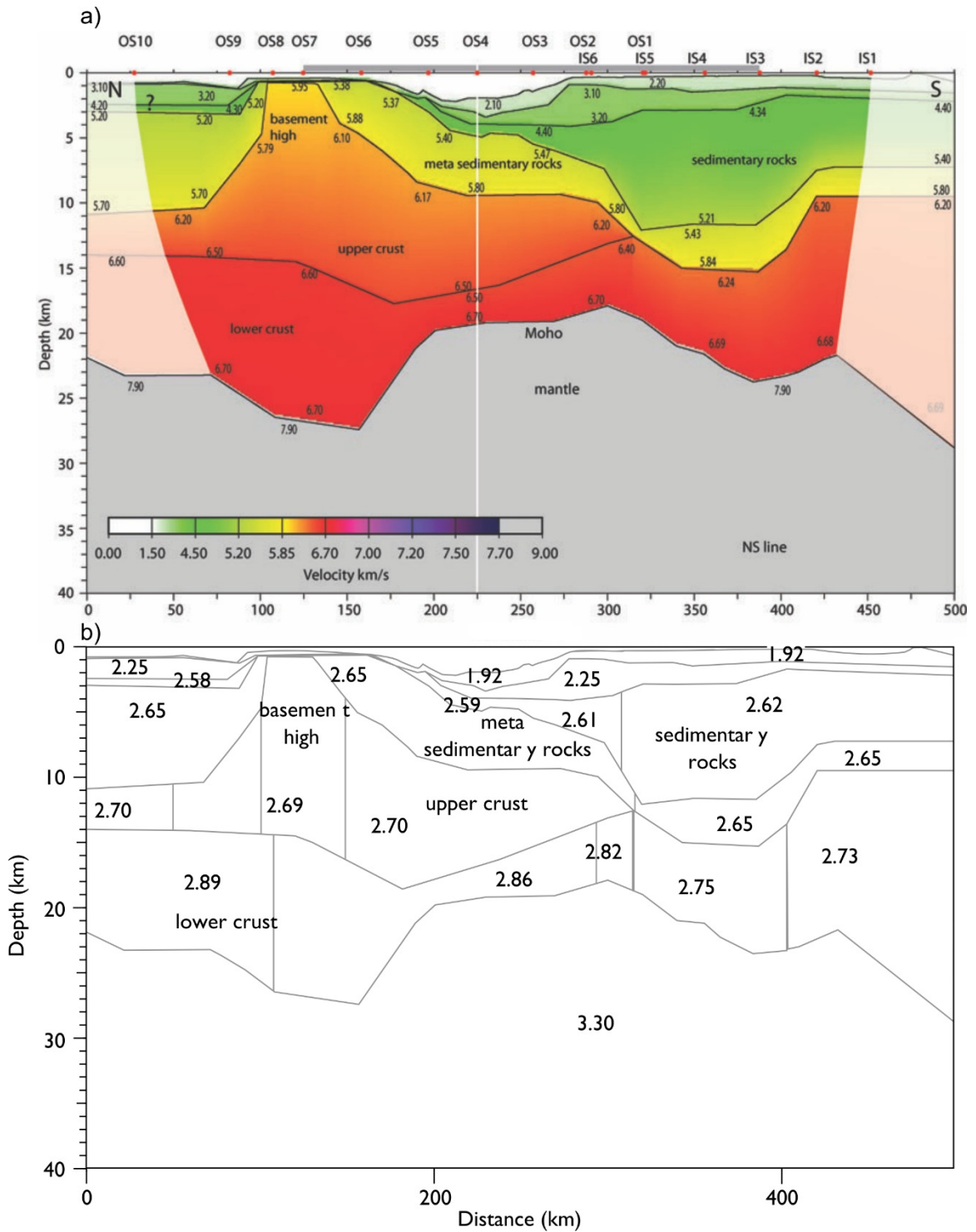
Fig. A.13. a) The velocity model on the LORITA (N-S) line, and b) gravity model along same line with velocities converted to densities (marked in g cm^3). Figures are from Jackson et al. (2010).

Alpha Ridge Test of Appurtenance (ARTA)

Initiated by the Government of Canada to address ECS requirements, the goal of the Alpha Ridge Test of Appurtenance (ARTA) 2008 seismic experiment was to determine if the Alpha Ridge is a "natural prolongation" of the adjacent Canadian Arctic shelf (Jackson and Potter, 2011). Acquisition of the seismic data entailed deployment of geophones and discharge of explosives directly on sea ice. The geophones were spaced 1.2 to 1.5 km apart. The seismic source consisted of explosives distributed at an interval of ~22 km. The ARTA experiment comprised a "Main" line (350 km distance) that extended from the continental shelf onto Alpha Ridge and a perpendicular "Cross" line (180 km distance) that intersected the Main line ~80 km seaward of the shelf break. Reverse ray-coverage was acquired along the lines and signal was recorded over long offsets (~150 km) with the intent of identifying P_n and P_mP phases. Although the principle data from this study were the wide angle reflections/refractions, short offset seismic reflection data were also acquired as part of ARTA (Funck et al., 2011). The reflection data chiefly show concordant reflections overlying acoustic basement. The velocity data were analyzed by Funck et al. (2011) using a forward and inverse raypath technique (RAYINVR), shown in Fig. A.14, and seismic tomography (JIVE3D). The authors reported P-wave velocities of 2.0–2.2 km s^{-1} for sediments on Alpha Ridge and a range in thickness from 0.4 to 1.5 km. The topmost layer in igneous crust (4.7–5.2 km s^{-1}) correlated to seismic facies in MCS profile interpreted as volcanic rock. Funck et al. (2011) noted the change in crustal velocity structure between the Canadian Polar margin and Alpha Ridge. The authors concluded that Alpha Ridge is underlain by thick igneous crust.
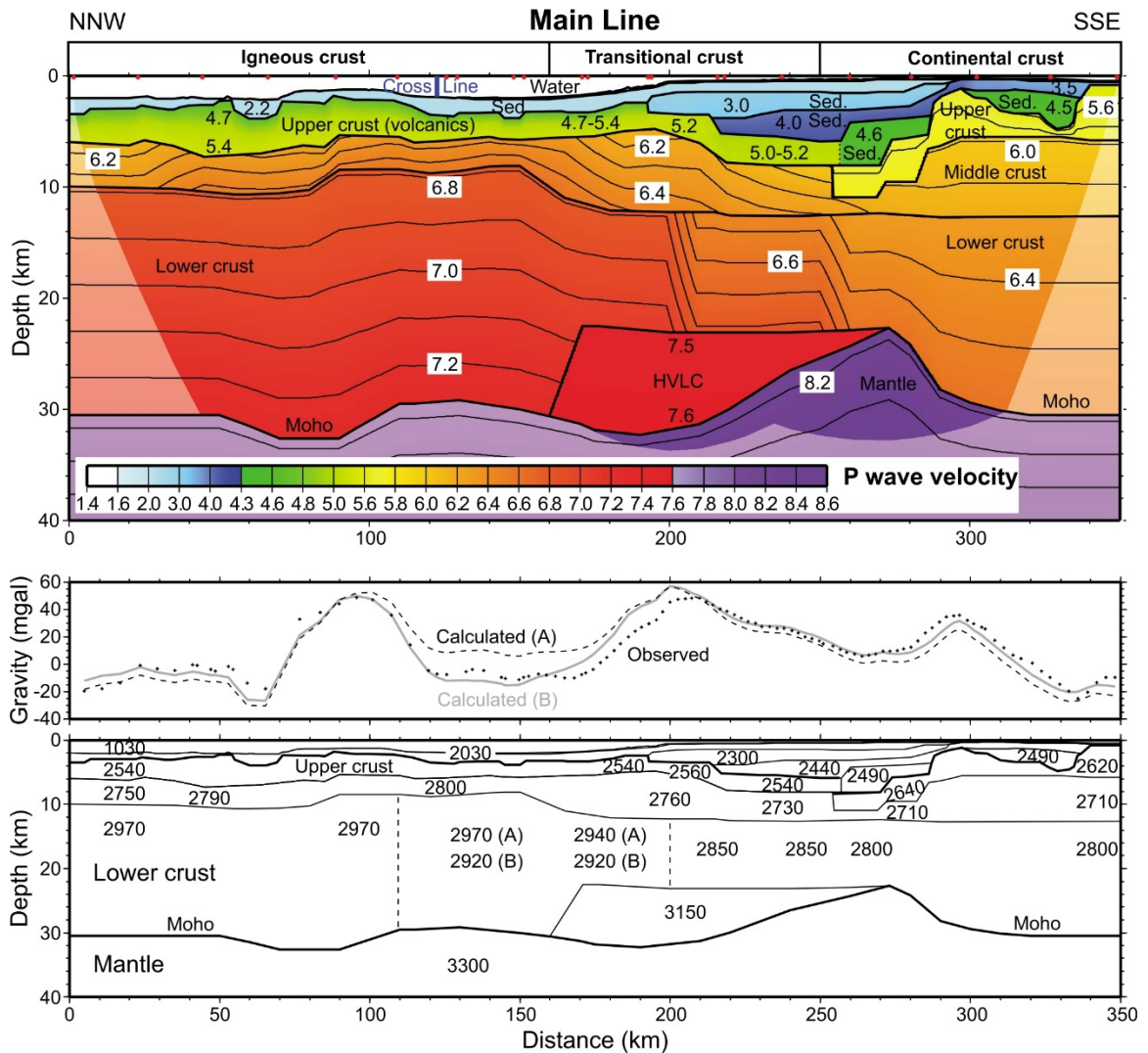
Fig. A.14. (Top panel) P-wave velocity model along ARTA (main) line. Numbers indicate velocity, in km^{-1}; the velocity contour interval is 0.1 km^{-1} (only shown for velocities >6.3 km^{-1}). The outer perimeter of the model with no ray coverage is shown in pale colours. Red circles mark the shot locations. Position of intersection with cross line is marked by a blue line. (Middle panel) Observed (crosses) and calculated gravity (grey lines). (Bottom panel) Densities in the model, given in kg m^{-3}. Model A is the original density model, whereas model B uses decreased lower crustal densities in the area between the two vertical dashed lines. Figures are from Funck et al. (2011).

Alfred Wagner Institute 2008 Expedition

In 2008, the experiment was upgraded by using a 300 m streamer with 48 channels and increasing the total volume of the airgun array to 32 L (Jokat, 2009). The multi-channel seismic data were sorted into 25 m bins. Sonobuoys were deployed coincident with the AWI seismic lines. Sonobuoys recorded signal up to a maximum

offset of 25 km, but typically < 15 km. Seismic transects are particularly crooked for lines acquired under heavy ice conditions above Alpha Ridge. Consequently, the MCS data are relatively noisy. In addition, sonobuoy records with reversed ray-coverage were not acquired. This line was coincident with 81°N and extends from Canada Basin, across Mendeleev Ridge, Podvodnikov Basin and Lomonosov Ridge, and ends in Amundsen Basin (Fig. A.15). This survey was used to establish the seismic stratigraphy of Podvodnikov Basin and adjacent areas (Weigelt et al., 2014). In addition, the seismic reflection profile revealed that 50% of Podvodnikov Basin is underlain by crust associated with Lomonosov Ridge (Jokat and Ickrath, 2015). Juxtaposed to the east of this thinned continental crust is the thick igneous crust of Mendeleev Ridge.
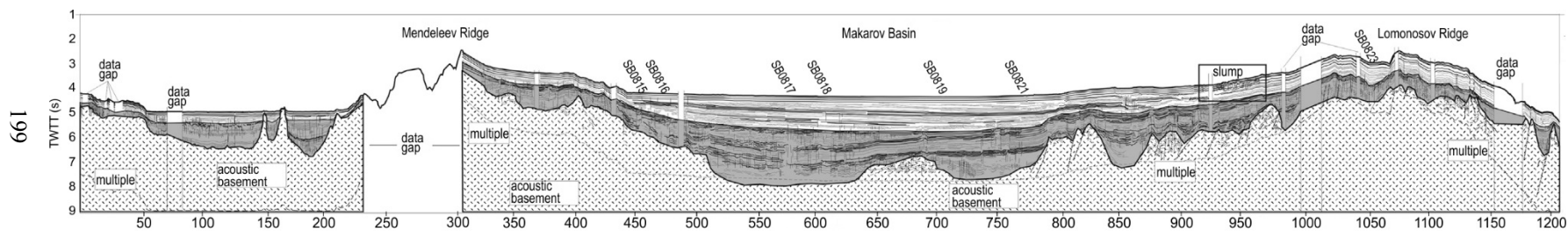
Fig. A.15. Line AWI-2008 (modified from Jokat and Ickrath, 2015). The grey shaded part of the sedimentary section is located below the Top Oligocene unconformity. The position of the sonobuoys is marked by their names.

APPENDIX B
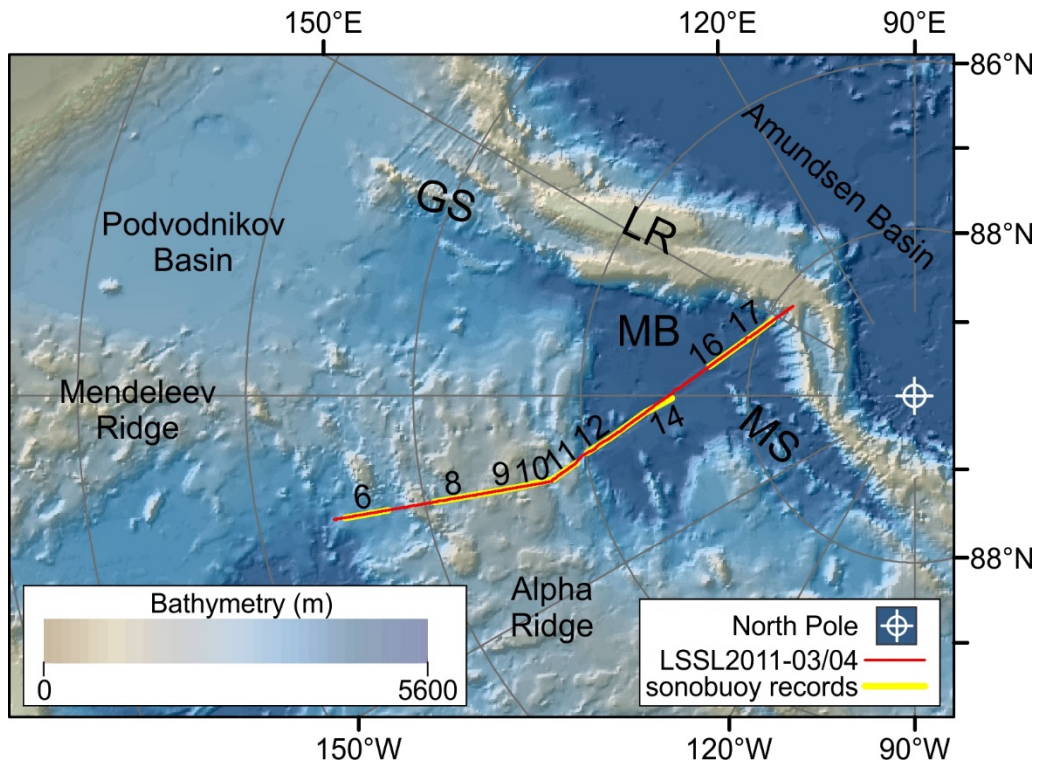
Fig. B.1. A coloured bathymetry map showing the location of sonobuoy records and seismic line LSSL2011-03/04 discussed in Chapter 3. Acronyms are GS – Geophysicist Spur, LR – Lomonosov Ridge, MB – Makarov Basin and MS – Marvin Spur. Bathymetry is from the IBCAO version 3.0 grid (Jakobsson et al., 2012).
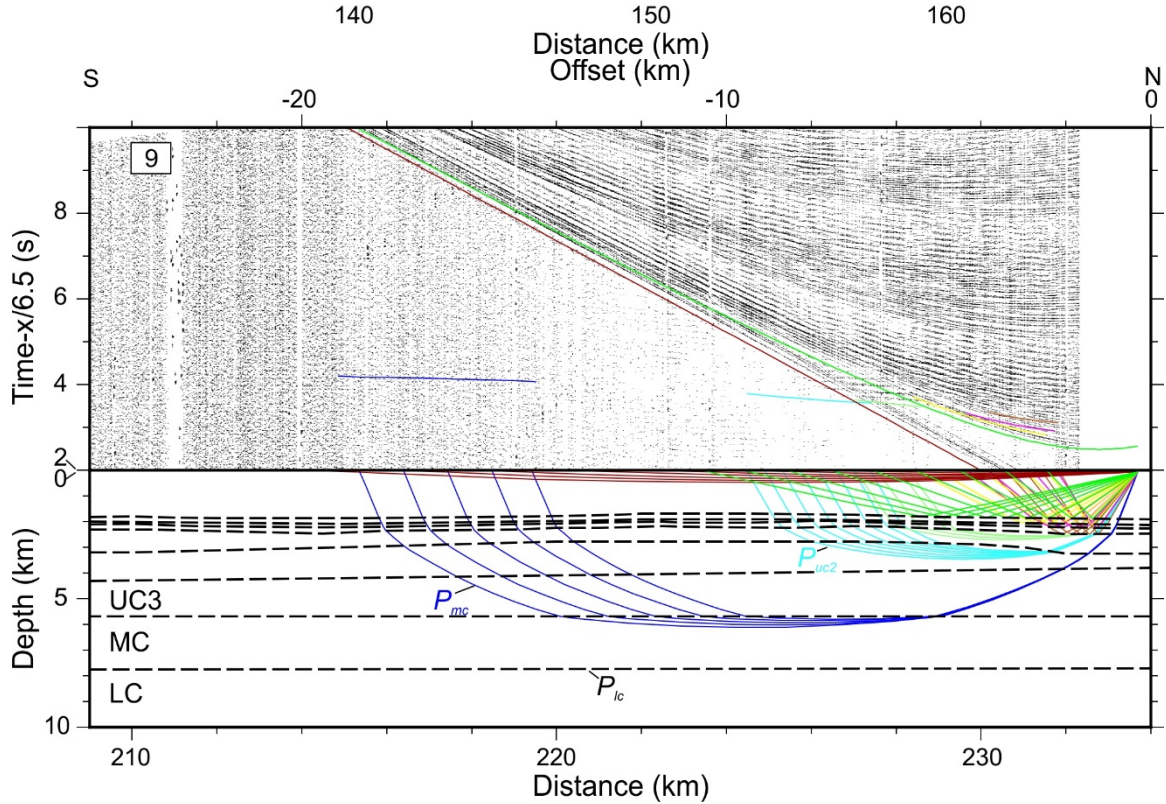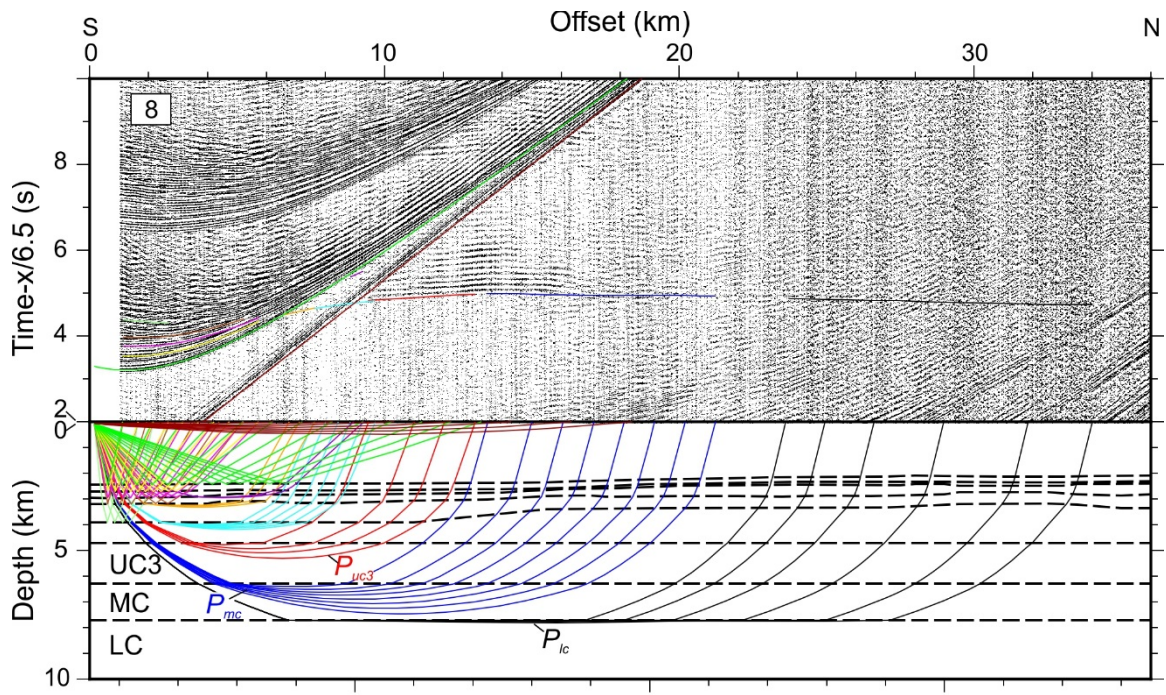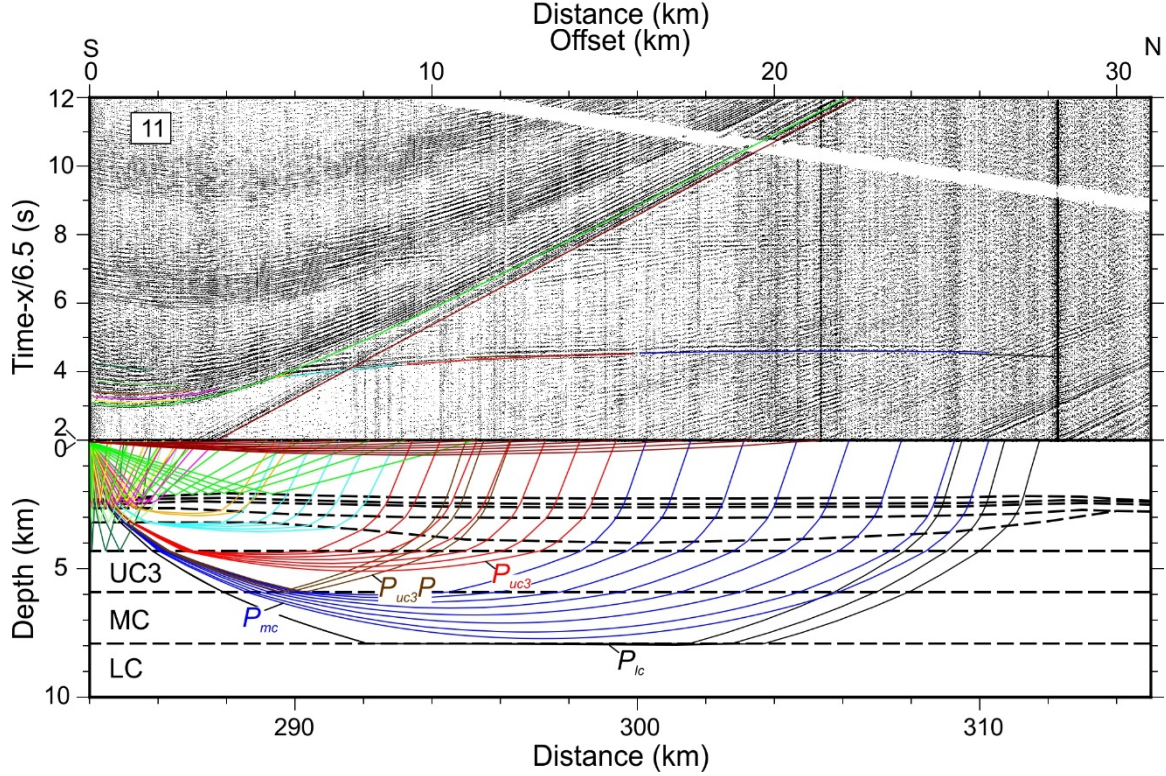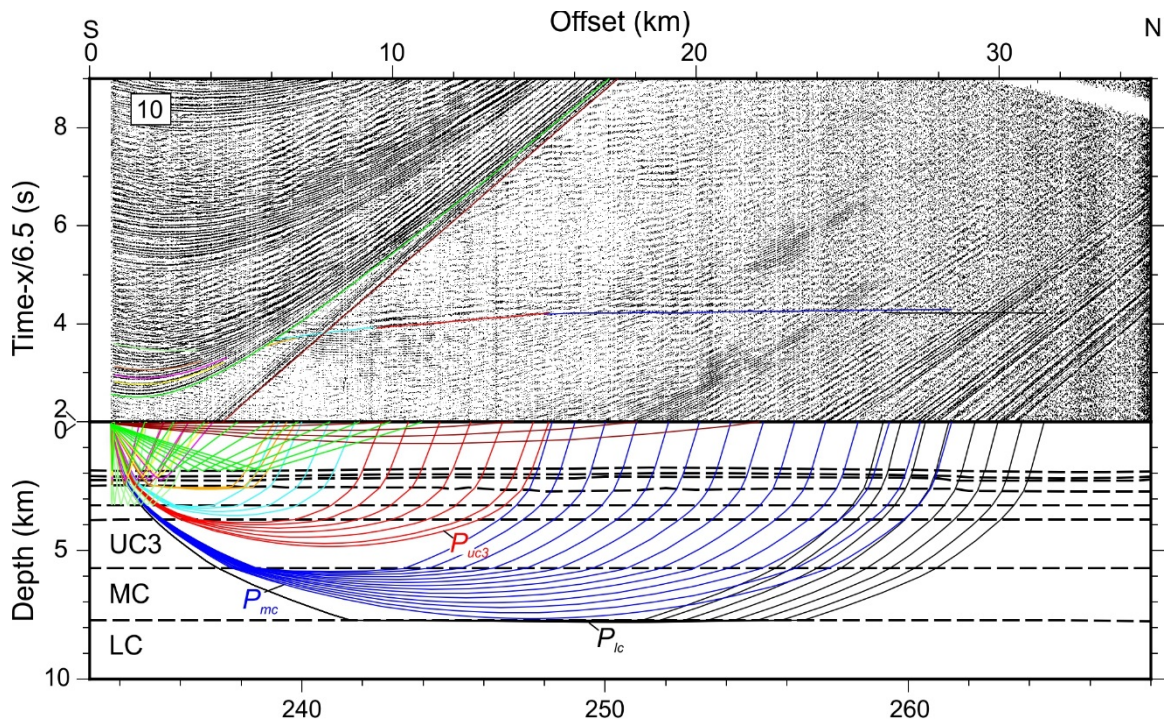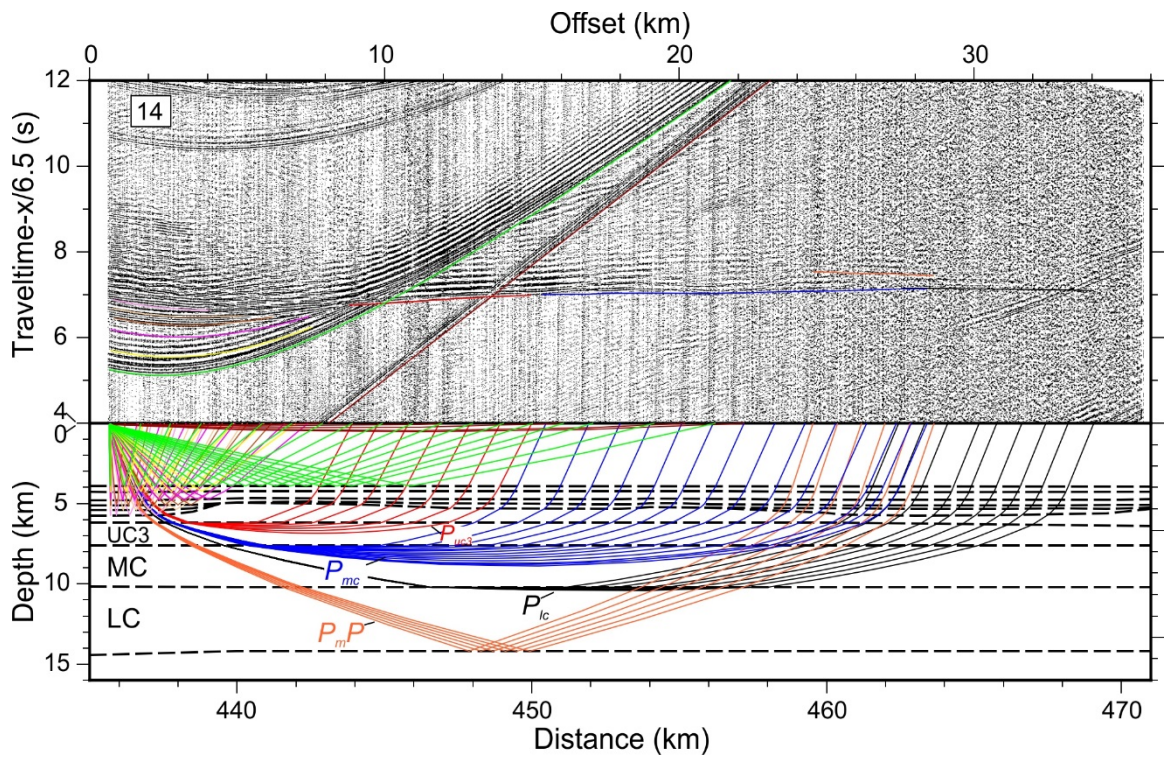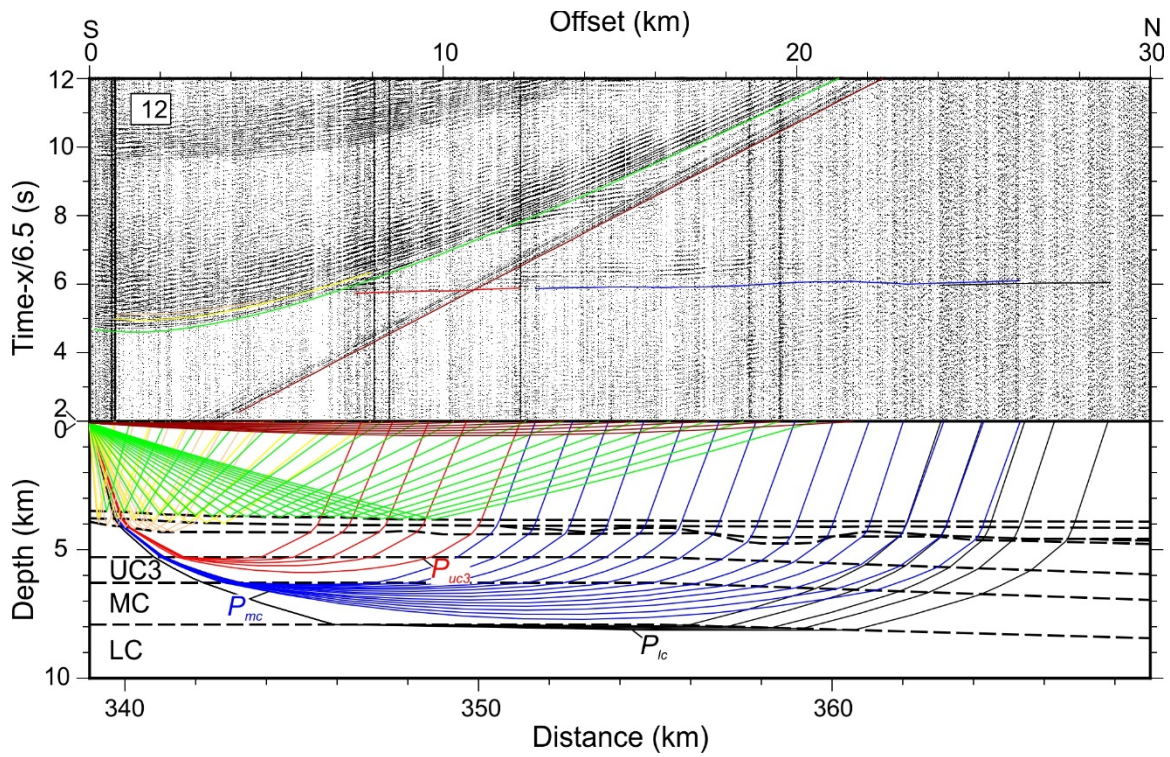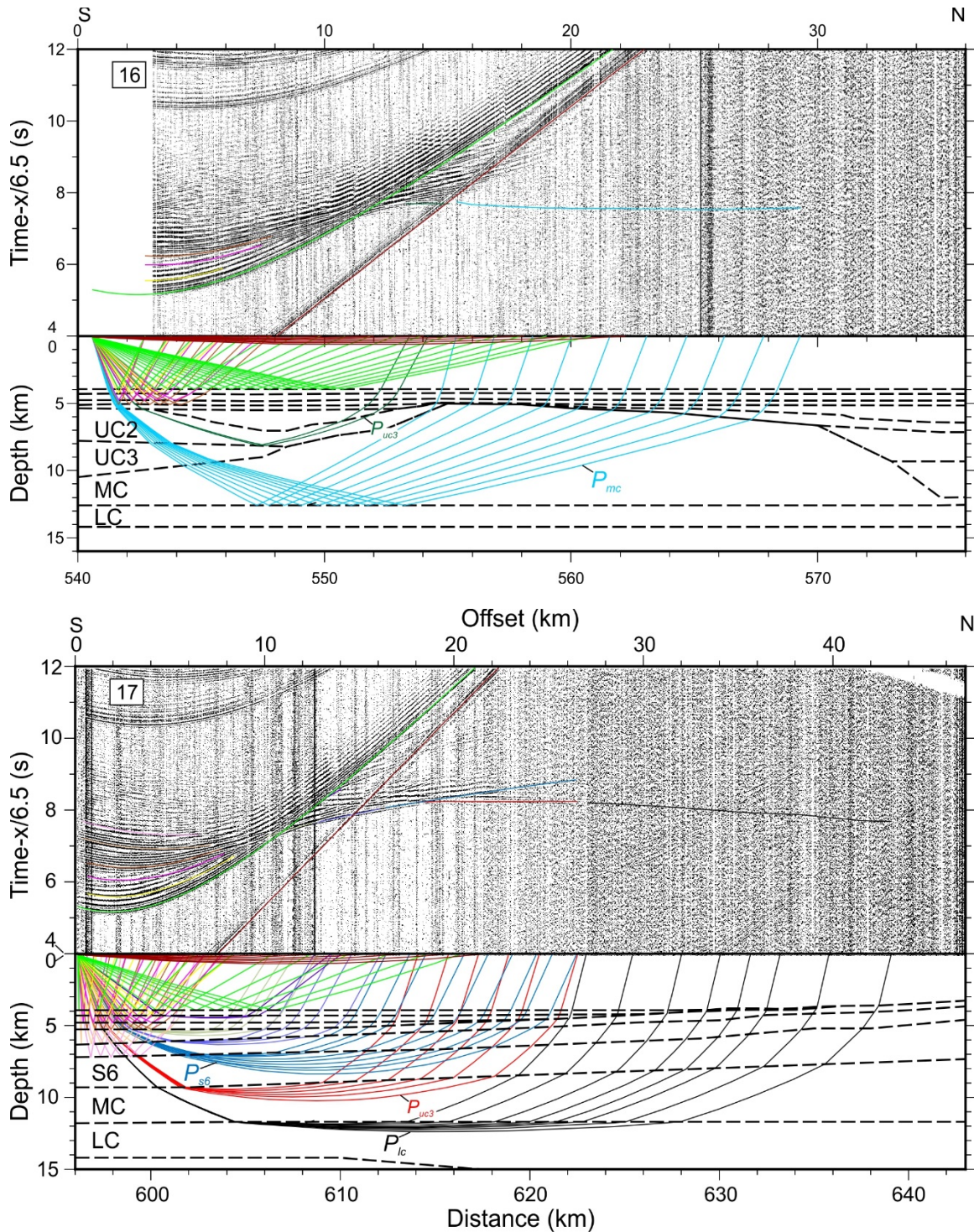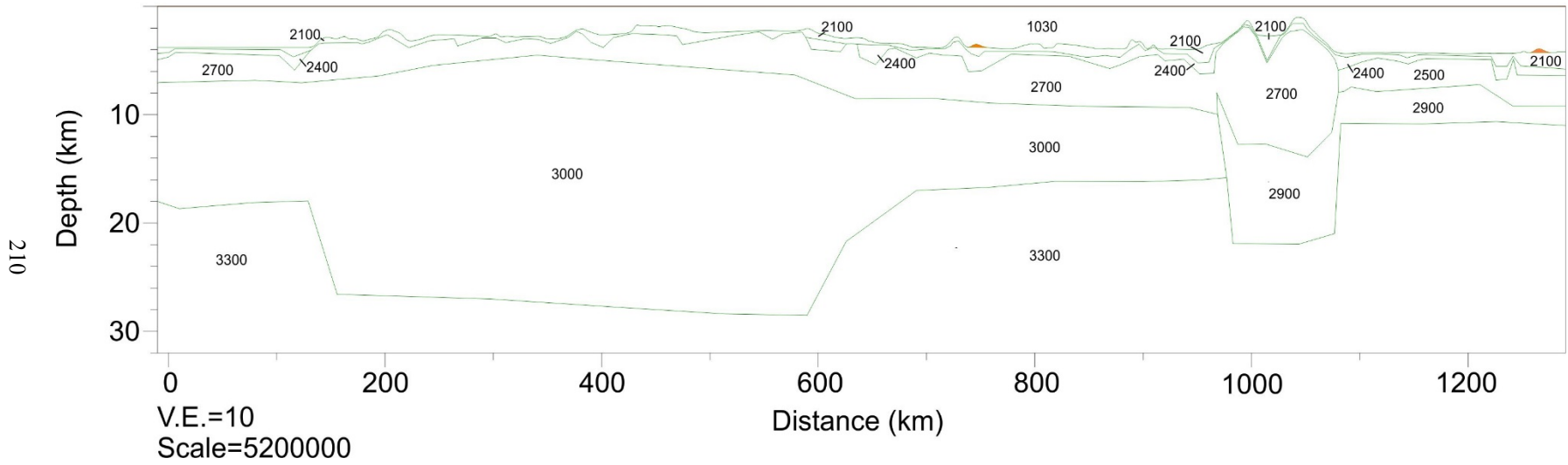
Fig. B.2. Records and modelling of sonobuoy stations 6, 7, 8, 9, 10, 11, 12, 14, 16 and 17 are depicted. The top panels show the seismograms with overlain calculated traveltimes, and the bottom panels outline the raypaths through the velocity model. Names and P-wave velocities (km s^{-1}) for select crustal phases and layers are labelled (refer to Chapter 3). Displayed seismic records were band-pass filtered between 4 and 20 Hz. Deployment positions are shown in Fig. B.1.

APPENDIX C
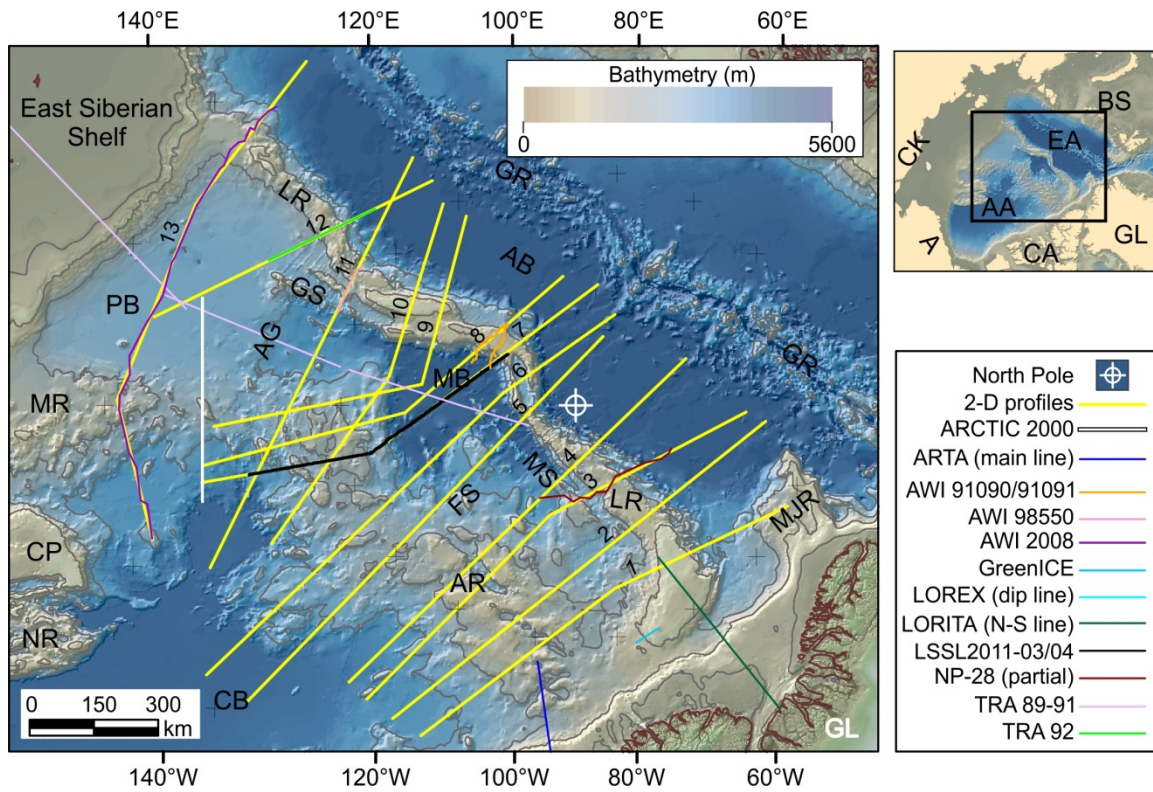
Fig. C.1. A coloured bathymetry map showing the location of gravity profiles discussed in Chapter 4. Acronyms are A – Alaska, AA – Amerasia Basin, AB – Amundsen Basin, AG – Arlis Gap, BS – Barents Shelf, CA – Canadian Polar margin, CB – Canada Basin, CK – Chukotka, CP – Chukchi Plateau, EA – Eurasia Basin, FS – Fedotov Seamount, GL – Greenland, GR – Gakkel Ridge, GS – Geophysicists Spur, LR – Lomonosov Ridge, MB – Makarov Basin, MR – Mendeleev Ridge, Morris Jesup Rise – MJS, MS – Marvin Spur, NR – Northwind Ridge, OS – Oden Spur and PB – Podvodnikov Basin. Bathymetry is from the IBCAO version 3.0 grid (Jakobsson et al., 2012).
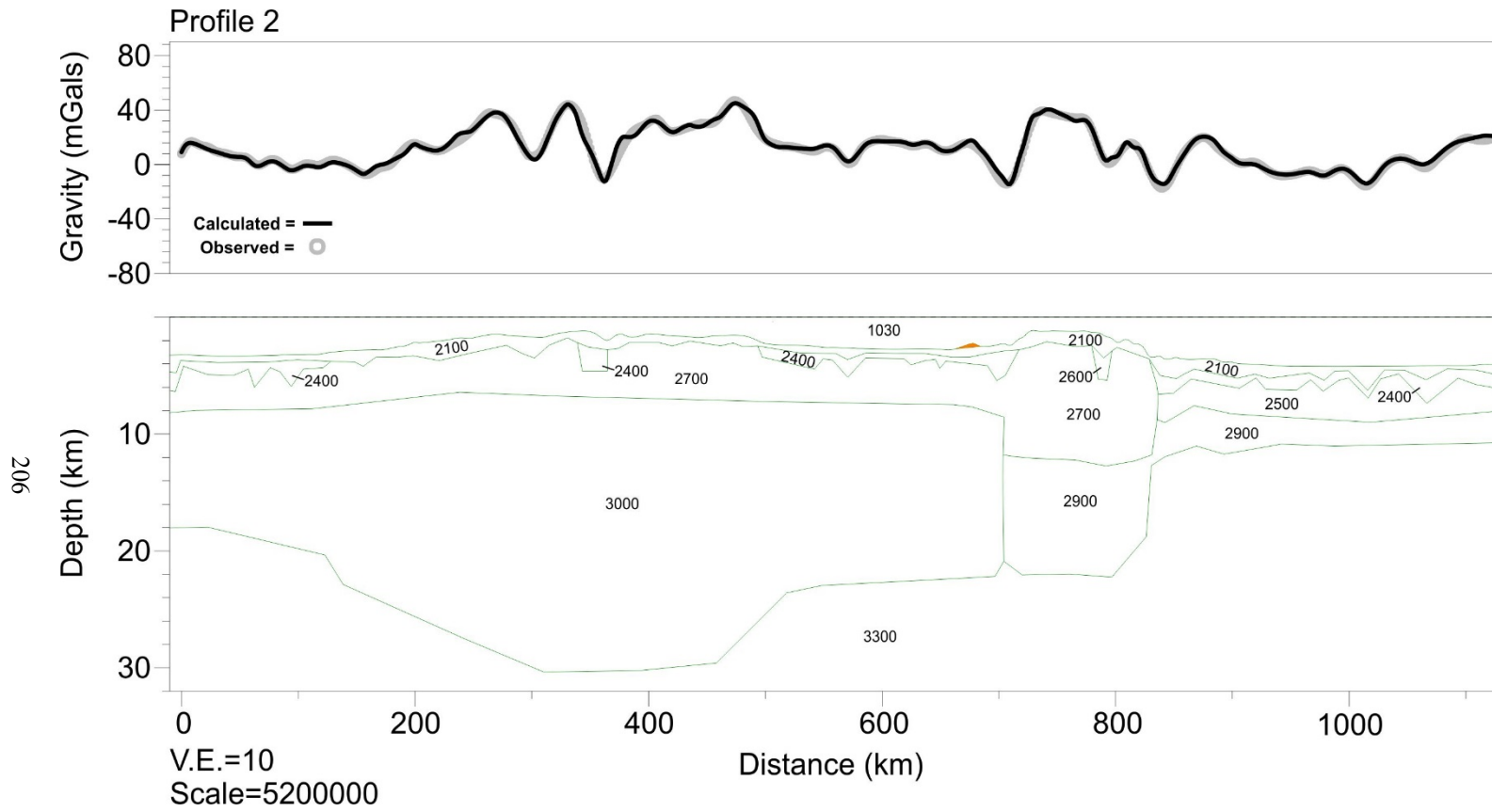
Profile 2

Profile 3

Profile 4

V.E.=10
Scale=5200000

Profile 5

V.E.=10
Scale=5200000

Profile 6

Profile 8

211

Profile 9

V.E.=10
Scale=5200000

Profile 10

Profile 11

Gravity (mGals)

Calculated =
Observed = ○

AWI-98550

2100
2400
2400
2400
1030
2400
2100
2600
2400
2400
2100
2400
2500
3000
3000
2700
2700
2900
3000
3000
2900
3300

Depth (km)

V.E.=10
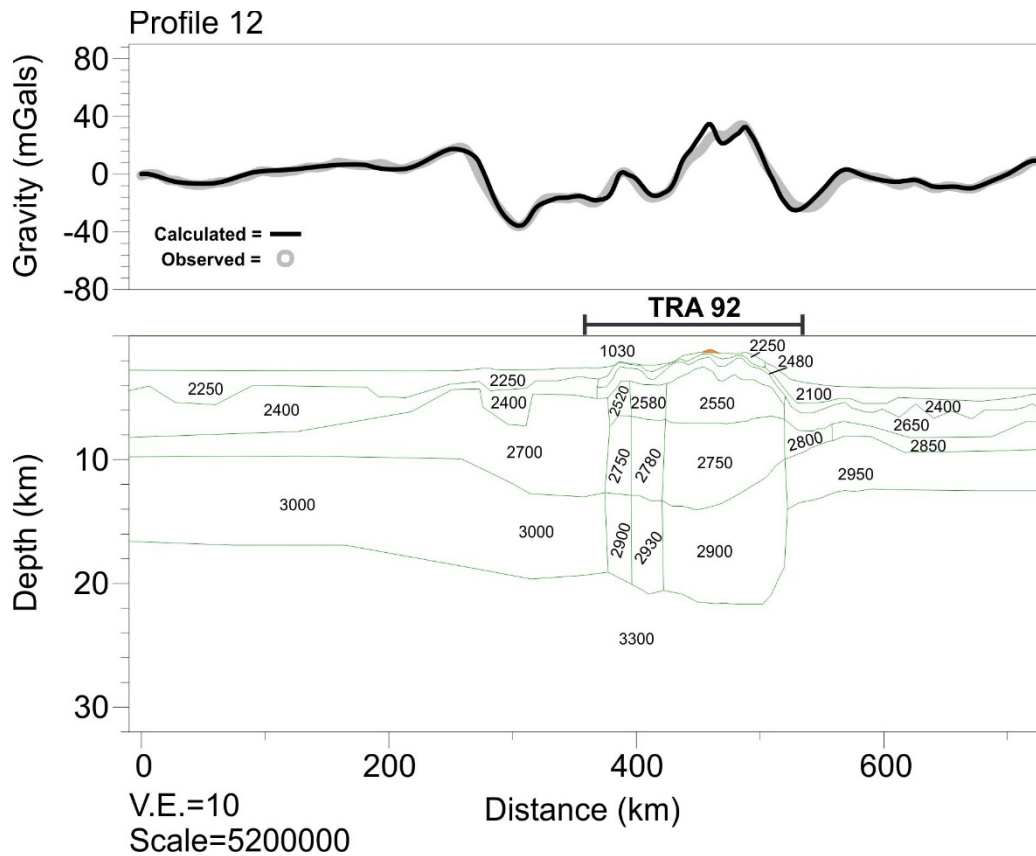Scale=5200000

Distance (km)

214
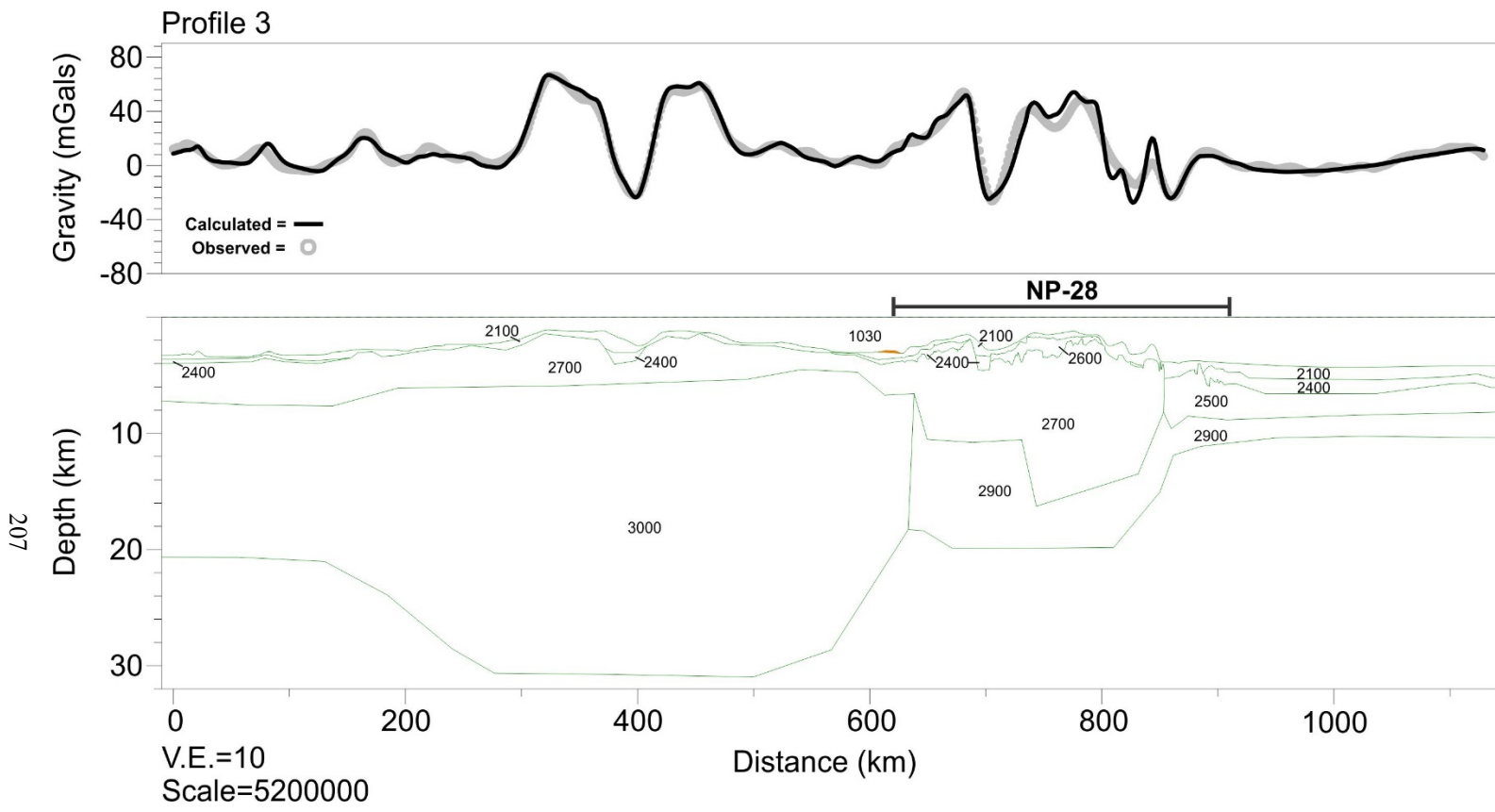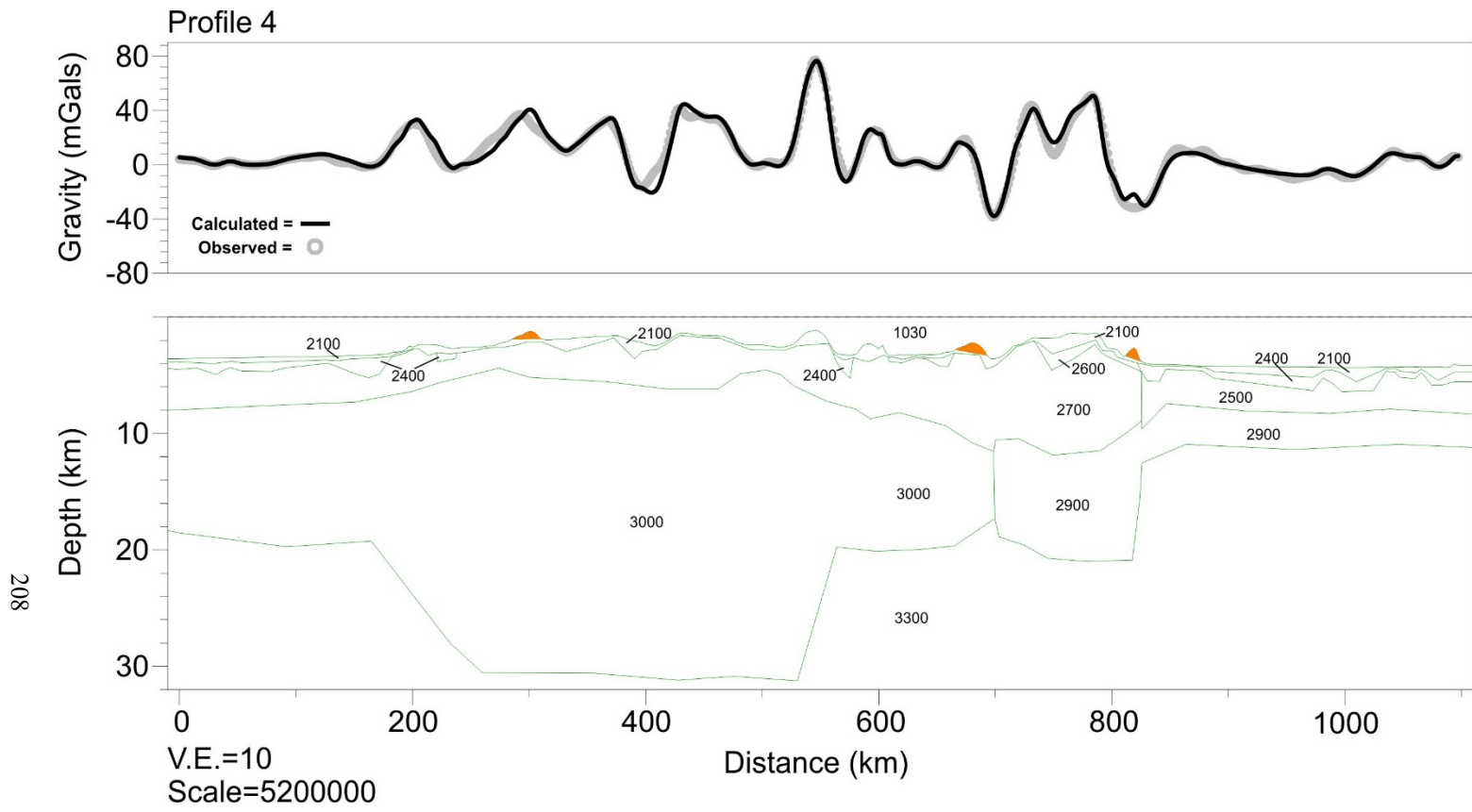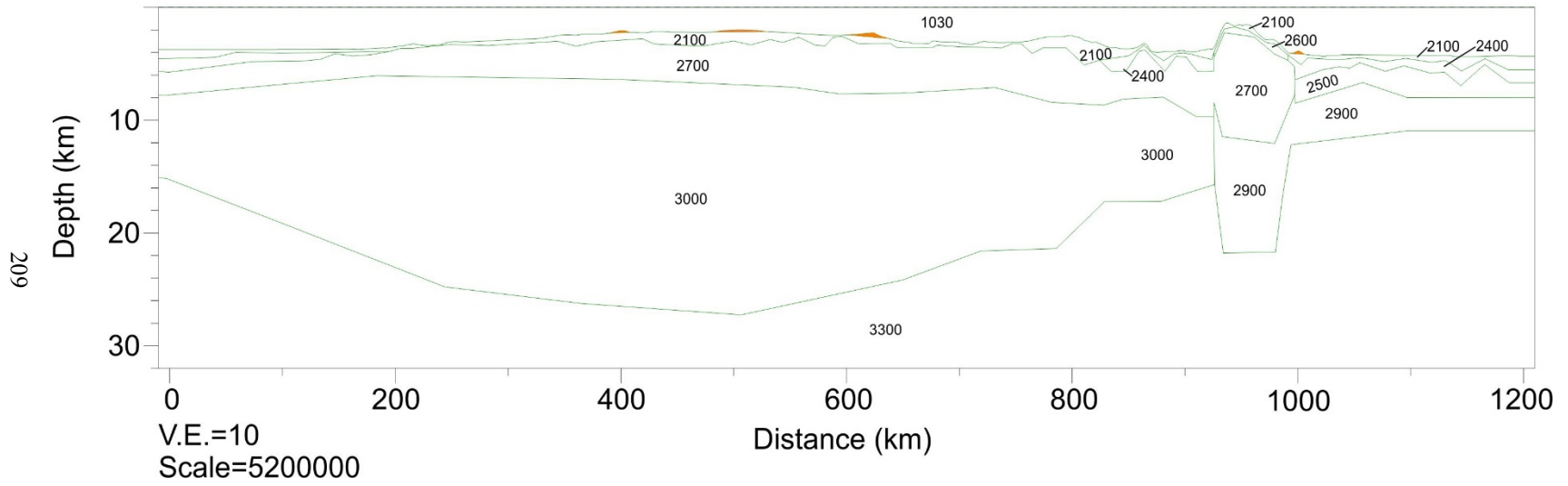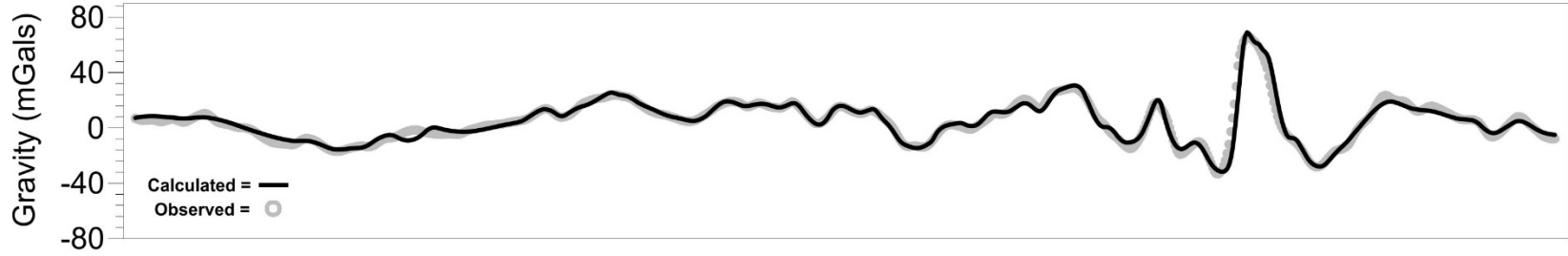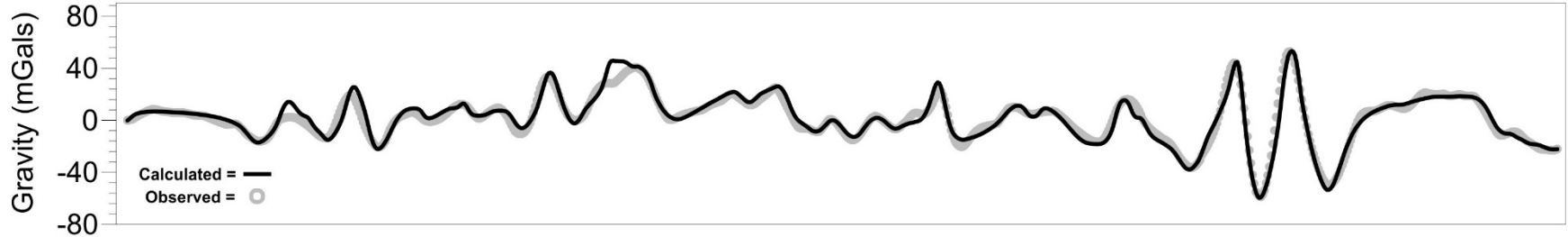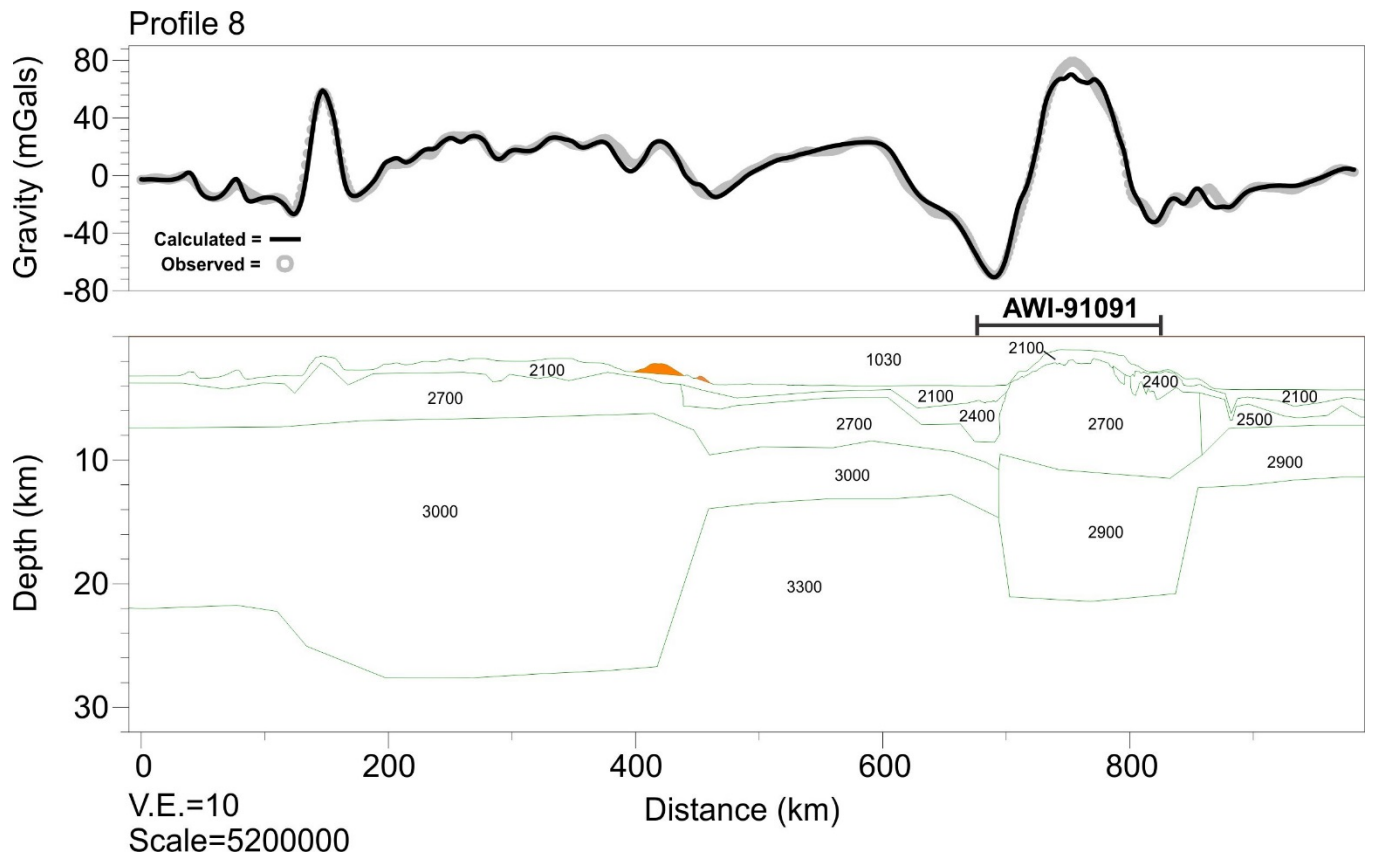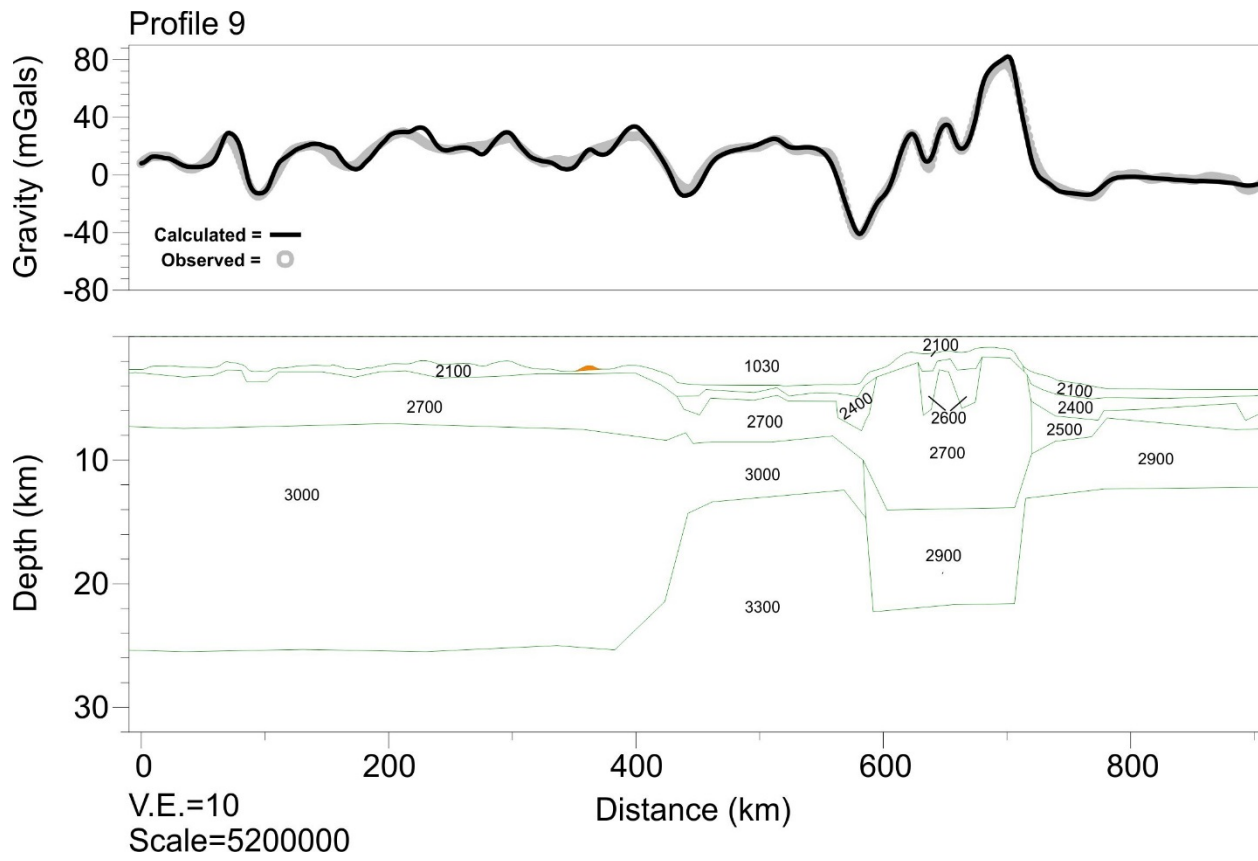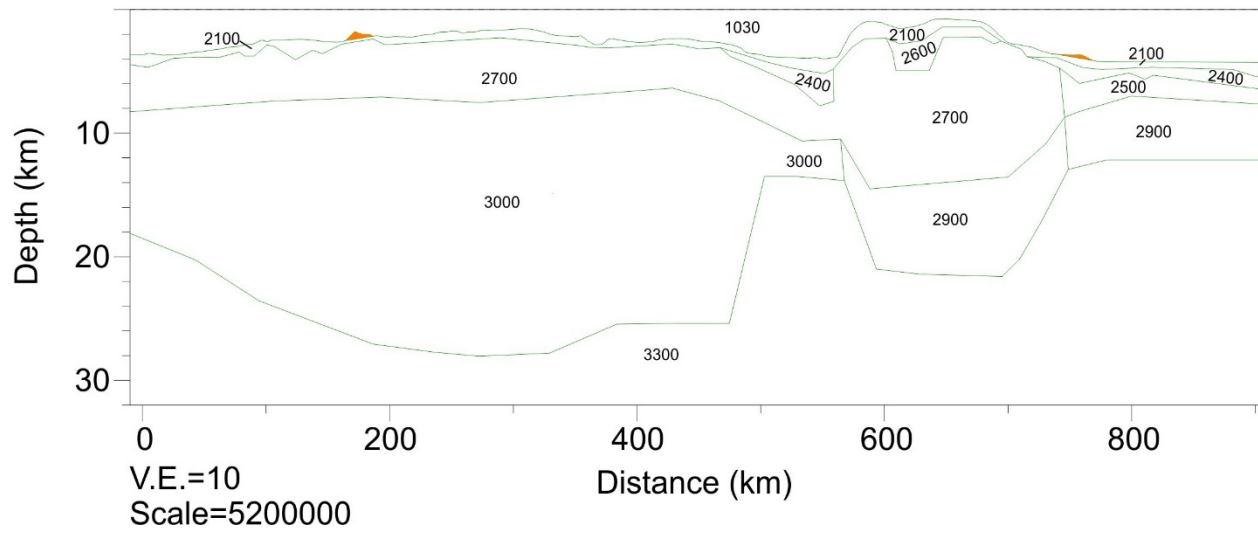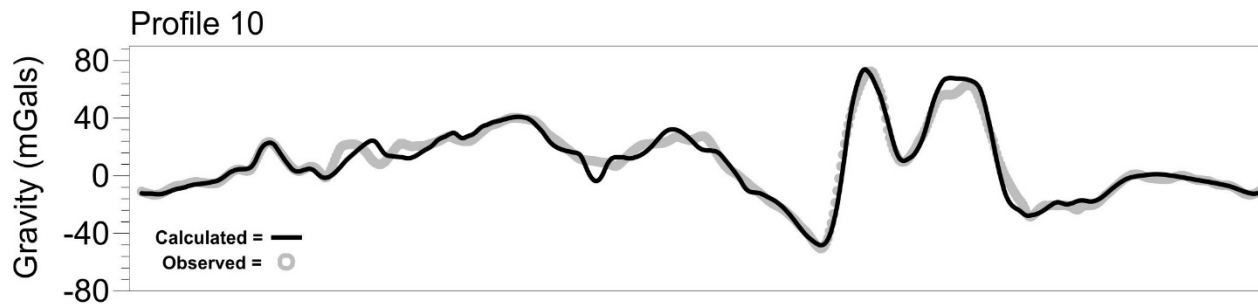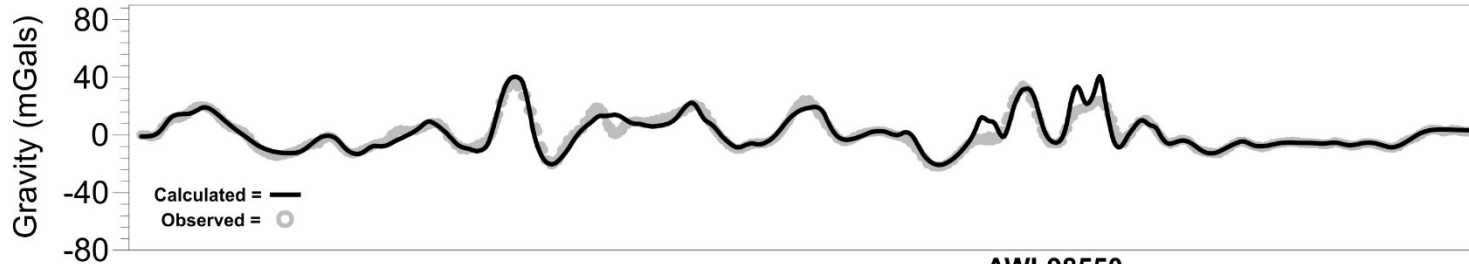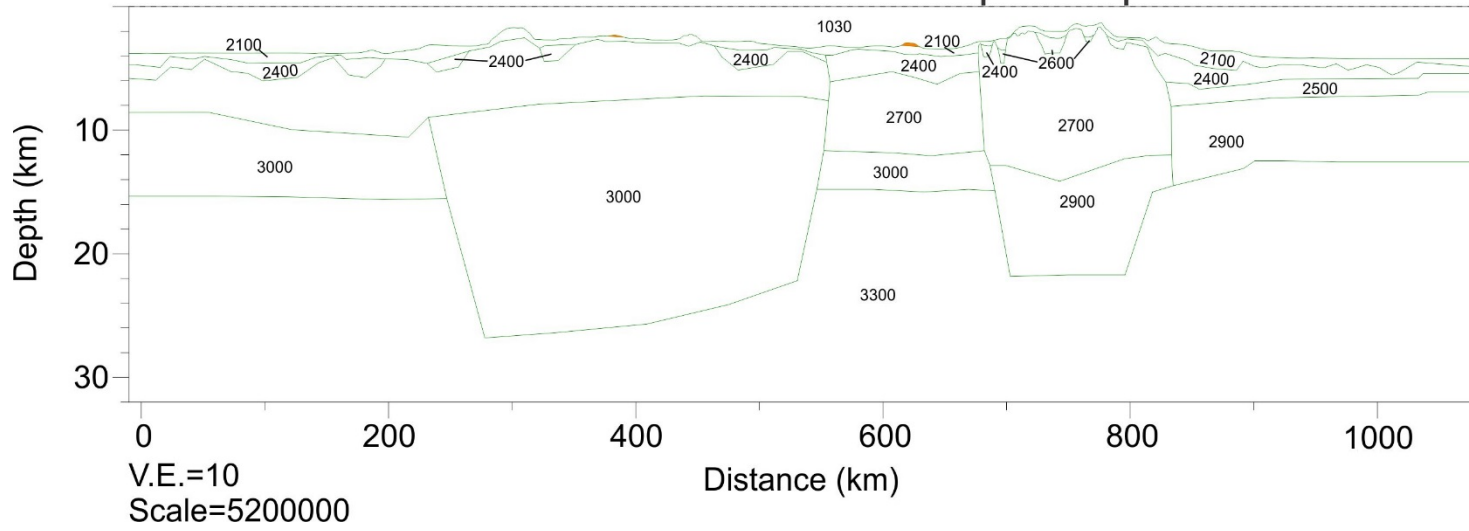
Fig. C.2. Two-dimensional gravity models for profiles shown in Fig. C.1 (except profiles 1, 7 and 13, which are introduced in Chapter 4). The top panel depicts the observed free-air gravity anomaly compared to calculated gravity (models 1A and 1B). The observed data was extracted from the compilation of Anderson et al. (2010). The bottom panel depicts the subsurface gravity model with densities specified in kg m^{-3}. Bathymetric highs that are coloured orange represent blocks with limited strike length (i.e., 2.5-dimensional blocks). Refer to Section 4.3.1 for descriptions of seismic data used to constrain certain models.